Stochastic dynamics of adhesion clusters under force

Stochastische Dynamik von Adhäsionsclustern unter Kraft

Dissertation
zur Erlangung des akademischen Grades
„doctor rerum naturalium”
(Dr. rer. nat.)
in der Wissenschaftsdisziplin „Theoretische Physik”

eingereicht an der
Mathematisch-Naturwissenschaftlichen Fakulät
der Universität Potsdam

angefertigt am
Max-Planck-Institut für Kolloid- und Grenzflächenforschung
in Potsdam-Golm

von
Thorsten Erdmann

Potsdam, im April 2005

Abstract

Adhesion of biological cells to their environment is mediated by two-dimensional clusters of specific adhesion molecules which are assembled in the plasma membrane of the cells. Due to the activity of the cells or external influences, these adhesion sites are usually subject to physical forces. In recent years, the influence of such forces on the stability of cellular adhesion clusters was increasingly investigated. In particular, experimental methods that were originally designed for the investigation of single bond rupture under force have been applied to investigate the rupture of adhesion clusters. The transition from single to multiple bonds, however, is not trivial and requires theoretical modelling.

Rupture of biological adhesion molecules is a thermally activated, stochastic process. In this work, a stochastic model for the rupture and rebinding dynamics of clusters of parallel adhesion molecules under force is presented. In particular, the influence of (i) a constant force as it may be assumed for cellular adhesion clusters is investigated and (ii) the influence of a linearly increasing force as commonly used in experiments is considered. Special attention is paid to the force-mediated cooperativity of parallel adhesion bonds. Finally, the influence of a finite distance between receptors and ligands on the binding dynamics is investigated. Thereby, the distance can be bridged by polymeric linker molecules which tether the ligands to a substrate.

Zusammenfassung

Adhäsionskontakte biologischer Zellen zu ihrer Umgebung werden durch zweidimensionale Cluster von spezifischen Adhäsionsmolekülen in der Plasmamembran der Zellen vermittelt. Aufgrund der Zellaktivität oder äußerer Einflüsse sind diese Kontakte normalerweise Kräften ausgesetzt. Der Einfluß mechanischer Kräfte auf die Stabilität zellulärer Adhäsionscluster wurde in den vergangenen Jahren verstärkt experimentell untersucht. Insbesondere wurden experimentelle Methoden, die zunächst vor allem zur Untersuchung des Reissverhaltens einzelner Moleküle unter Kraft entwickelt wurden, zur Untersuchung von Adhäsionsclustern verwendet. Die Erweiterung von einzelnen auf viele Moleküle ist jedoch keineswegs trivial und erfordert theoretische Modellierung.

Das Reissen biologischer Adhäsionsmoleküle ist ein thermisch aktivierter, stochastischer Prozeß. In der vorliegenden Arbeit wird ein stochastisches Modell zur Beschreibung der Reiss- und Rückbindedynamik von Clustern paralleler Adhäsionsmoleküle unter dem Einfluß einer mechanischen Kraft vorgestellt mit dem die Stabilität der Cluster untersucht wird. Im besonderen wird (i) der Einfluß einer konstante Kraft untersucht wie sie in zellulären Adhäsionsclusters angenommen werden kann und (ii) der Einfluß einer linear ansteigenden Kraft betrachtet wie sie gemeinhin in Experimenten angewendet wird. Besonderes Augenmerk liegt hier auf der durch die Kraft vermittelte Kooperativität paralleler Bindungen. Zuletzt wird der Einfluß eines endlichen Abstandes zwischen Rezeptoren und Liganden auf die Dynamik untersucht. Der Abstand kann hierbei durch Polymere, durch die die Liganden an das Substrat gebunden sind, überbrückt werden.

Contents

List of Symbols

β	tether energy in units of thermal energy, page 96
$\mathrm{E}\,(z)$	exponential integral, page 31
ℓ	separation of the rest lengths of tether and transducer springs, page 21
ℓ_b	rest length of tether springs, page 95
$\mathrm{erf}\,(x)$	error function, page 96
η	friction coefficient of the Brownian particle in Kramers' theory, page 16
Γ	Euler's constant $\gamma \simeq 0.5772$, page 32
γ	dimensionless single-bond on-rate, page 19
H_N	N^{th} harmonic number, page 39
κ	ratio of force constants of tether and transducer springs, page 21
$\kappa_N^3(\tau)$	third cumulant of the distribution $\{p_i(\tau)\}_{i=0}^{N_t}$, page 27
κ_T^3	third cumulant of the dissociation rate, page 73
k_BT	thermal energy, page 16
λ	dimensionless distance equilibrium resting positions of tethers and transducer, page 95
$\mathbb{W}$	W-matrix of the master equation, page 50
μ	dimensionless loading rate, page 22
ν_D	attempt frequency for barrier crossing in Kramers' theory, page 17
ω_{bd}, ω_{ts}	angular frequency of the undamped Brownian particle in at the bound state and at the transition state barrier, page 17
ϕ	tether force in units of the intrinsic force scale F_B, page 95
$\mathrm{pln}\,(x)$	product logarithm, page 48
$\psi^{(1)}(n+1)$	trigamma function, page 40
$\rho(x,t)$	time dependent spatial distribution of the Brownian particle in Kramers' theory, page 16

σ_T^2	variance of the dissociation rate, page 40
$\sigma_N^2(\tau)$	variance of the distribution $p_i(\tau)$, page 27
τ	dimensionless time, page 19
τ_1	crossover time, page 62
τ_c	time to reach the critical force at a loading rate $\mu = f_c/\tau_c$, page 81
ξ	dimensionless extension of tethers, page 96
ξ_b	dimensionless extensions of tethers that are bound to the transducer, page 95
$\zeta(n)$	Riemannian ζ-function, page 40
$D(\tau)$	dissociation rate: probability density for dissociation as function of time, page 25
$D(f)$	rupture force distribution: probability density for dissociation as function of force, page 25
$D(s)$	Laplace transform of the dissociation rate, page 45
E_{ts}	height of the transition state barrier, page 17
F	mean rupture force of a cluster, page 25
f	dimensionless force that is controlled during loading: $f = f_t$ for shared, $f = f_b$ for non-cooperative loading, page 19
F_B	intrinsic force scale for bond rupture, page 18
f_b	force exerted on a single bond, page 21
f_c	critical force for adhesion cluster stability, page 48
f_t	force exerted on the whole cluster through the transducer, page 21
F_{det}	deterministic rupture force, page 62
F_{max}	maximum of the rupture force distribution, page 25
$f_{wlc}(\xi)$	dimensionless force extension relation for the worm-like chain model, page 110
$F_{wlc}(x)$	force extension relation for the worm-like chain model, page 110
$g(i)$	functional form of the forward (rebinding) rate for the bonds in the adhesion cluster, page 23
$G(s,\tau)$	probability generating function, page 42
g_i	general expression for the forward (rebinding) rate for the bonds in the adhesion cluster, page 23
i	number of closed bonds in the adhesion cluster, page 21

k_0	Kramers' off-rate for a single bond, page 17
k_B	Boltzmann's constant, page 16
k_b	force constant of tether springs, page 20
k_t	force constant of transducer spring, page 20
k_{off}	force dependent single-bond off-rate, page 18
k_{on}	force independent single-bond on-rate, page 19
L	contour length of the worm-like chain, page 110
L_p	persistence length of the worm-like chain, page 110
M	mass of the Brownian particle in Kramers' theory, page 16
m	dimensional loading rate, page 22
$N(\tau)$	mean number of closed bonds and the deterministic value, page 26
N^*	minimum of the stationary probability distribution in the bimodal region, page 102
$N^b(\infty)$	average number of closed bonds in the bound state of an adhesion cluster for a bimodal distribution, page 103
$N^u(\infty)$	average number of closed bonds in the unbound state of an adhesion cluster for a bimodal distribution, page 103
N_0	initial number of closed bonds N_0 in the adhesion cluster, page 23
N_c	number of closed bonds in the stationary state at critical force, page 48
N_t	cluster size, page 20
N_{eq}	number of closed bonds in the steady state, page 41
$p_i^b(\infty)$	stationary state probability function in the bound state of an adhesion cluster for a bimodal distribution, page 102
$p_i^u(\infty)$	stationary state probability function in the unbound state of an adhesion cluster for a bimodal distribution, page 102
$p_i(\infty)$	stationary probability distribution, page 42
$p_i(\tau)$	state occupancy probability for state i with i closed bonds, page 23
$r(i)$	functional form of the reverse (rupture) rate for the bonds in the adhesion cluster, page 23
r_i	general expression for the reverse (rupture) rate for the bonds in the adhesion cluster, page 23
T	mean lifetime of a cluster, mean first passage time, page 25

$T_{\mu,\nu}$	mean first passage time from state μ to $\nu > \mu$, page 105
$T_{\nu,\mu}$	mean first passage time from state ν to $\mu < \nu$, page 105
T_{det}	deterministic cluster lifetime, page 31
T_{max}	maximum of the dissociation rate, page 38
$U(x)$	energy landscape for Kramers' theory, page 16
v	velocity of the Brownian particle along the reaction coordinate, page 16
x	reaction coordinate, position of the Brownian particle in Kramers' theory, page 16
x_B	reactive compliance: separation of bound state and transition state barrier, page 17
x_b	extension of the tether spring, page 21
x_t	extension of the transducer spring, page 21
x_{bd}	position of the bound state in $U(x)$, page 16
x_{ts}	position of the transition state barrier in $U(x)$, page 16
x_{ub}	position of the unbound state in $U(x)$, page 17
$Z(x_b)$	partition function for single tethers, page 96

Chapter 1

Introduction

1.1 Specific adhesion of biological cells

Life of multicellular organisms like humans is a concert of as many as 10^{13} individual cells which can be grouped into around 200 different cells types with distinct, specific functions [Alberts et al., 2002]. To enable accurate development of the young and reliable function of the adult organism, all cells have to coordinate their activity carefully and reliably in the noisy environment of neighbouring cells and subject to variable exterior conditions. To achieve this regulation in the absence of a central conductor, cells constantly have to react to signals from their immediate environment, i.e. from other cells or from the extracellular space.

An important class of stimuli regulating cell behaviour is of mechanical origin. Cells adhere to their environment, i.e. other cells or the extracellular matrix[1] (ECM), at specialised adhesion sites. Whether adhesion is possible at all is an important information in itself. Epithelial cells which usually are in contact to neighbouring cells normally undergo apoptosis ('programmed cell death') if no adhesion is possible. This is also the case for fibroblast cells which are mechanically very active cells abundant in connective tissue where they organise the collagen fibres of the ECM. Programmed cell death protects the organism from unruly cells. This mechanism is disturbed in cancer cells which enables these to travel through the body and form metastases. In general, the function of cell adhesion is twofold. The physical contact enables cells to resist and transmit mechanical forces and to maintain the integrity of tissues and the whole organism. Moreover, cells use adhesion sites like fingers which allow them to feel their environment and collect information about physical properties, such as the presence of binding sites and the presence of other cells, elasticity of substrates and strength of forces acting on the cells. In general, many processes such as embryonic development, cell migration or the immune response depend crucially on the specific adhesion of cells.

Adhesion of biological cells is based on clusters containing a large number of adhesion receptors which mediate contact to specific ligands either carried by other cells or attached to the ECM. Adhesion clusters are two-dimensional assemblies of transmembrane adhesion proteins which are held in the plasma membrane of the cell by hydrophobic interaction. On the cytoplasmic side (the inside of the cell) the receptors can be linked to the cytoskeleton. In many cases, an assembly of different accessory proteins ('cytoplasmic plaque') strengthens and regulates these links. A binding pocket on

[1] The extracellular matrix is the non-cellular component of an organism. It is a complex network of polysaccharides (e.g. hyaluronan acid) and proteins fibres (e.g collagen) which are secreted by cells and serve as structural elements in tissues [Alberts et al., 2002]. In bones, hard, mineralised material (e.g. calcium phosphate in form of hydroxyapatite crystals) is embedded in the fibrous part of the extracellular matrix which allows bones to resist not only tensile but also strong compressive forces.

the extracellular side allows specific interaction with appropriate ligands. Important types of receptors are selectins, cadherins and integrins [Alberts et al., 2002]. Selectins bind carbohydrate molecules and mediate contacts of white blood cells to the epithelial cells in the blood vessel wall. Selectin bonds associate and dissociate rapidly to facilitate transient adhesion and the rolling adhesion of white blood cells [Rossiter et al., 1997]. Cadherin receptors form homotypic (self-self) bonds to other cadherin molecules and thus mediate cell-cell adhesion between epithelial cells. They appear, e.g., in large clusters called adherens junctions. Integrin receptors mediate cell-ECM contacts. Integrin is a complex molecule which in mammalian cells exists in at least 24 different forms with different preferred ligands [Hynes, 2002]. Integrin is found e.g. in large adhesion clusters called focal adhesions which are similar in structure to adherens junctions and can contain as many as $\sim 10^5$ integrin receptors. Common to adherens junctions and focal adhesions is the tight linkage of the receptors to the actin cytoskeleton. This allows cells to transmit and resist tension of tissues and also to exert forces to the environment through adhesion clusters.

Biological adhesion bonds are usually non-covalent bonds with binding energies in the range of few units of thermal energy k_BT. They have finite lifetimes because they dissociate quickly by thermal activation. The large number of receptors in adhesion clusters and their dense arrangement in the vicinity of ligands facilitates rebinding of broken bonds and stabilises the clusters. This allows stable and long-lived cell adhesion sites to be formed by weak bonds and prevents disintegration of the organism. On the other hand, the use of many weak instead of a single strong (covalent) bond is an insurance against failure of individual bonds, increases the flexibility of the adhesion sites and allows rapid rearrangement of the contacts in response to external stimuli. The stability of adhesion clusters can be influenced by changes of the unbinding and rebinding probability through changes in the distance of receptor and ligand, through conformational changes of receptor or ligand which alter the affinity of the bonds or by changes in the number of receptors that may be controlled by transport processes. Also mechanical forces which can be exerted from outside or from within the cell, are known to influence bond dissociation. These control mechanisms allow for dynamic formation and destruction of adhesion clusters, for example during cell migration where adhesion clusters are formed at the leading edge of the cells and have to be disintegrated at the rear. In this work we will discuss the influence of forces on adhesion cluster stability.

Adhesion clusters are subject to mechanical forces in many situations. Deformation of tissue, for example of blood capillaries by pulsating blood or lung tissue during ventilation, leads to large strain and stress in the tissue which is transmitted from cell to cell through specific adhesion sites. White blood cells adhering to vessel walls are subject to hydrodynamic forces from the blood flow. In adherens junctions and focal adhesions, adhesion receptors are attached to the actin cytoskeleton so that cells can exert forces on the adhesion clusters actively by actomyosin contractility. The main component of the cytoskeleton are actin-filaments. These are often arranged into bundles which span the cell and terminate at adhesion clusters. The filaments in the bundles are cross-linked by myosin motor proteins which are able to ‘walk’ along the filaments and thereby displace them relative to each other and contract the bundle. These so-called stress fibres act like small muscles although they lack the strict, crystalline structure of muscle cells and can be dynamically rearranged.

Fig. 1.1a shows a light microscopic image of a fibroblast cell which adheres to a planar substrate. Stress fibres appear in green due to fluorescence labelling of actin filaments. The stress fibres terminate at focal adhesions which are stained in red and are distributed predominantly along the cell edge. A schematic view of an adhesion cluster connected to a stress fibre is shown in Fig. 1.1b. Integrin receptors assembled in the plasma membrane are bound to ligands on the planar substrate. On the inside of the cell, different proteins attach the integrin receptors to the actin filaments. Molecular motors are shown which slide actin filaments past each other in opposite direction and contract the stress

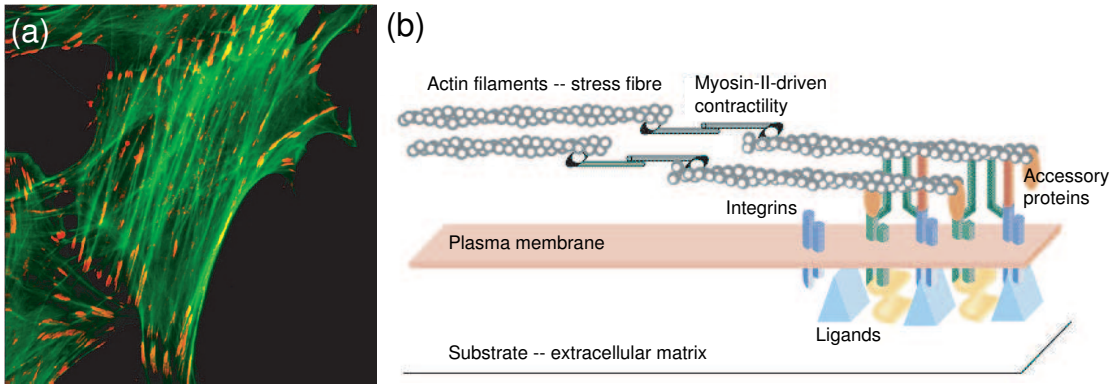

Figure 1.1: (a) Microscopic image of a fibroblast cell adhering to a planar, elastic substrate. Actin molecules are fluorescently labelled in green which makes the stress fibres visible. Stress fibres terminate at focal adhesions which are labelled in red and are distributed along the edge of the cell. (On the upper and the lower left edge of the picture two other cells are visible). (b) The sketch [Zamir et al., 2000] shows a schematic picture of an adhesion cluster with integrin molecules inserted in the plasma membrane and attached to ligand molecules and to a accessory proteins which connects the integrins to the stress fibres. Myosin motors lead to sliding motion of the actin fibres and thereby force is exerted on the receptor-ligand bonds.

fibres. In actual focal adhesions, the structure of the cytoplasmic side is much more complex with more than fifty different proteins involved [Geiger et al., 2001]. The precise structure and function of these, however, is not know yet.

The role of mechanical force in cell adhesion has attracted a lot of attention in recent years [Chicurel et al., 1998]. Traction forces of migrating cells have first been demonstrated qualitatively by observing the wrinkling of an elastic substrate [Harris et al., 1980]. Progress in substrate patterning techniques has allowed accurate measurements of forces on the level of single clusters for static cells. One approach used a continuous elastic substrate with a micro-pattern which was strained by cell traction [Balaban et al., 2001]. The strain pattern allowed to calculate the stress from the elastic properties of the substrate and revealed a close stress-area relation. Focal contacts of different cell types and under different conditions were found to be characterised by a similar stress constant of $5.5\,\mathrm{nN}\,/\,\mu\mathrm{m}^2$ [Balaban et al., 2001]. With approximately $10^3 - 10^4$ integrins per square micron, the force per integrin molecule was estimated to be in the range of pN. These findings for the relation between force and size were qualitatively confirmed in recent measurements [Tan et al., 2003]. Other studies on living cells have shown that force and contact size also correlate if force is applied externally [Riveline et al., 2001, Galbraith et al., 2002]. Exerting a force on an adhesion cluster of a cell induces growth of the cluster. The precise mechanism of this reinforcement is not understood yet [Geiger and Bershadsky, 2001] but it has been shown to depend on intracellular signalling pathways which convert a mechanical signal into a biochemical answer. Models explain this by the incorporation of additional material induced by lateral stretching of the cluster [Nicolas and Safran, 2004, Nicolas et al., 2004]. In this work we focus on passive adhesion clusters because at the current stage, the complexity of adhesion clusters is out of reach for modelling. In the following sections we describe physical properties of adhesion bonds and experimental methods to investigate them.

1.2 Physical properties of molecular adhesion bonds

Biological adhesion receptors are transmembrane proteins which are held in the plasma membrane by a hydrophobic domain. At their cytoplasmic tail they might bind to the cytoskeleton; on the extra-cellular side they have a binding site for ligand molecules which may either be proteins or other biomolecules such as carbohydrates. Interactions between receptor and ligand are mediated by non-covalent and typically short ranged forces such as hydrogen bonds, van der Waals forces and hydrophobic interactions. The binding energies are in the range of few units of thermal energies k_BT, where $k_BT \simeq 4.1\,\mathrm{pN\,nm}$ at physiological temperature $T \simeq 300\,\mathrm{K}$. These weak bonds can be disrupted by thermal activation and have finite lifetimes.

One of the most striking features of biological adhesion receptors is their tremendous specificity for ligands. This specificity is in part due to the shape of the binding site. Often it is formed as a binding pocket which excludes unsuitable ligands from binding right away. The corrugated surface of the binding site reveals complementary structures on ligand and receptor so that a very tight contact is possible with the native ligands. The major part of the specific interaction results from hydrogen bonds. These are contact interactions which form a characteristic pattern on the receptor which is recognised by ligands. Due to the short range and the orientation dependence of hydrogen bonds, there is a well defined ideal configuration of the two molecules which defines the ground state with the smallest energy. Small translations or rotations leads to an increase in energy because hydrogen bonds have to be disrupted. The specificity of the adhesion receptors depends crucially on their spatial structure. Proteins are thus ideal carriers for specific adhesion because they usually have a unique folded structure. Moreover, their sequence is conserved and can be optimised and adapted for specific ligands over evolutionary time-scales. Small changes in the linear amino acid sequence or misfolding of the proteins can deprive them of their function.

A classical equilibrium quantity to characterise adhesion bonds is their affinity. It reflects the free energy difference between the bound and the unbound state of the molecules. However, in biological adhesion clusters and under an applied force, adhesion bonds have to operate under non-equilibrium conditions. In many situations it is important that bonds associate and dissociate frequently on time-scales that are set by external processes, e.g. the flow velocity of blood for the rolling adhesion of white blood cells. To understand biological function of bonds it is thus important to take into account kinetic aspects that are quantified by the dissociation rate k_0 and the association rate k_{on}. The affinity measures the ratio k_{on}/k_0 but the absolute values are relevant for biological function. Bonds with the same affinity may be differently well suited for their function because they operate on different time-scales.

Biological bonds have been selected and optimised for their function as adhesion promoters. The structure of the complex adhesion molecules has evolved to facilitate rapid and reliable association and dissociation. Dissociation and association of biological bonds can often be described as proceeding along a one-dimensional pathway. All possible spatial configurations of the two molecules are projected onto a single reaction coordinate which represents the distance of the binding molecules. Steric repulsion constrains all movements in perpendicular directions. For bound molecules, dissociation is slowed down by an energy barrier which separates bound and unbound state. Therefore it is a slow process compared to the local dynamics of the molecules. For a given value of the reaction coordinate, the possible configurations of the bonds can be exhaustively explored. This allows to idealise the adhesion bond as a smooth energy landscape, although a binding site can contain as many as 100 hydrogen bonds [Bongrand, 1999] which rupture subsequently. An energy barrier in this landscape can be assigned to major translations or rotations of the molecules which requires simultaneous rupture of many hydrogen bonds or requires to overcome strong steric repulsion. In general there will be more

than a single barrier along the dissociation pathway. For example, for the unfolding of certain protein domains in the muscle protein titin, two barriers could be identified, one of which was assigned to the rupture of 2, the other to the rupture of 6 hydrogen bonds [Marszalek et al., 1999, Gao et al., 2001]. Moreover, there may be several parallel dissociation pathways as have been identified for the selectin bond [Evans et al., 2004]. A similar example for the emergence of a one-dimensional description of a higher dimensional process is protein folding. Although this proceeds in a three-dimensional energy landscape, the folding process can often be described as a sequence of events.

The rate of bond dissociation is determined mainly by the internal structure of the adhesion bond. For a one-dimensional energy landscape, the dissociation process can be modelled as thermally assisted escape from a potential well past a transition state barrier in the framework of Kramers' escape rate theory [Kramers, 1940, Hänggi et al., 1990]. The bond is described as a Brownian particle which is pushed by thermal impulses and finally moves past the energy barrier. This process can be described by a constant dissociation rate k_0 which is the inverse of the average time that a particle needs to cross the barrier from the bound to the unbound state. The transition rate is determined by the structure of the energy landscape, predominantly by the Arrhenius factor e^{-E_{ts}/k_BT}, where E_{ts} is the height of the energy barrier relative to minimum at the bound state. In a coarse grained picture, bond dissociation can be described as discrete transitions from bound to unbound state with the off-rate k_0 [Evans and Ritchie, 1997]. The index here indicates that the dissociation rate is taken in the absence of force. If there are several barriers along the pathway, unbinding can be described as a multi-step process with discrete transitions between neighbouring bound states [Evans, 2001]. Because backward steps are possible, the unbinding rate is reduced with respect to the single barrier picture. For parallel pathways, dissociation can proceed along several directions and dissociation is faster than for a single pathway. This behaviour is analogous to serial and parallel resistances in electric circuits.

In contrast to the dissociation rate, the association rate does not depend solely on the molecular structure but also on environmental conditions. How receptor and ligand find each other depends e.g. on the geometry of the system, electrostatic screening of interactions, and viscosity of the fluid surrounding. To separate the different influences, the binding process has been split into two steps: First, the unbound molecules encounter each other by diffusive motion and form a weakly bound complex, the so-called encounter complex. Weak, non-specific attachment allows the molecules to explore configurational space by rotations and small translations and to initiate the second, the actual binding step. Formation of the encounter complex can be described in the framework of Brownian motion. It has been applied to calculate the encounter rate for ligands and receptors in three as well as in two dimensions [Bell, 1978, Bongrand, 1999]. The rate for the second step depends mainly on the structure of the bond so that the picture separates environmental and structural properties. The total association rate is a function of these two rates. Depending on these rates, the process may either be diffusion limited (if the formation of the encounter complex is the slow process) or reaction limited (if the binding from the encounter complex is slow compared to diffusion). In biological adhesion clusters, binding is often facilitated by the dense arrangement of receptors in the clusters. The binding sites are held in close proximity with a separation of cell membrane of a few nm. Moreover, the two-dimensional diffusion in the plasma membrane is very slow and allows close by molecules to explore the binding site.

1.3 Dynamic force spectroscopy

Adhesion bonds in cells usually have to operate under force. To understand the behaviour of adhesion clusters it is thus vital to investigate bond failure under an applied force. These investigations also

allow to study the structure of adhesion molecules. Physical properties of single adhesion bonds cannot be investigated on living cells: cell adhesion is based on multiple bonds and single bond properties cannot be deduced from the multiple bond behaviour in a simple way [Merkel, 2001]. The complex elastic structure of the cell cytoskeleton with non-trivial stress-strain relation [Benoit et al., 2000] makes it difficult to exert force on adhesion sites in a controlled way. Moreover, active processes in living cells in reaction to force make controlled experiments difficult. Cells often contract in reaction to external stress and the structure of adhesion sites is regulated under the influence of an applied force [Riveline et al., 2001, Galbraith et al., 2002]. Therefore, biomimetic model systems have been developed to study physical properties of molecular adhesion bonds [Merkel, 2001]. These have defined mechanical properties so that the force on the adhesion site can be accurately controlled. Moreover they allow manipulation of single bonds. Single molecule experiments require observation methods with high spatial and temporal resolution.

Investigation of forced unbinding of single adhesion molecules has been pioneered in 1994 by Gaub and coworkers [Florin et al., 1994, Moy et al., 1994] with atomic force microscopy (AFM) experiments on biotin-avidin bonds. Avidin is a large, tetrameric molecule which can bind four biotin molecules with an unusually high binding energy of around $\sim 20 k_B T$. Using two of the binding sites the avidin was attached to the biotin-coated tip of an AFM-cantilever. The cantilever was brought into contact with a biotinylated agarose bead so that avidin could crosslink tip and bead. Retraction of the soft, elastic cantilever at a constant speed with piezo elements lead to a linear increase of force on the bond with separation. This experiment yielded a histogram of rupture forces for the biotin-avidin bond. The maximum of this histogram at around $160\,\mathrm{pN}$ was defined as the bond strength.

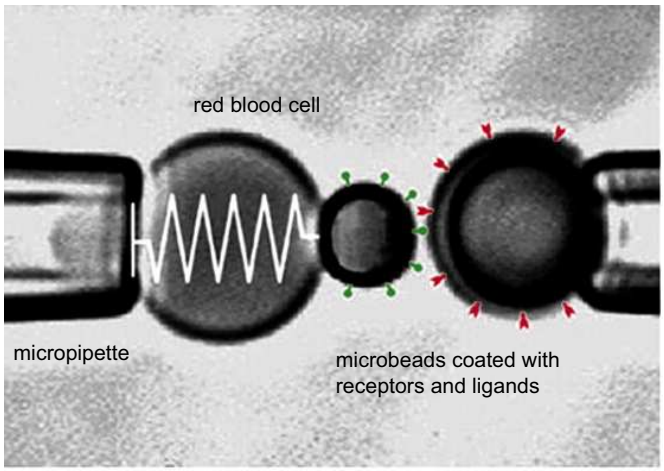

Figure 1.2: Setup of the biomembrane force probe [Evans et al., 2004]. The biotinylated red blood cell is a harmonic elastic element which carries a microbead to which the ligands are attached. The bead on the right is held by a second pipette and is functionalised with the receptors.

Apart from the atomic force microscopy, a number of different experimental techniques has been applied to exert forces on single molecules and investigate bond strengths, e.g. laser optical tweezers (LOT) [Kellermayer et al., 1997], magnetic tweezers [Smith et al., 1992] and the biomembrane force probe (BFP) [Merkel et al., 1999]. In LOT experiments the molecules are tethered to a dielectric bead which is trapped in the force field of the focus of a single laser beam. Force is exerted on the adhesion bond by moving the bead with the laser beam. This technique was applied to measure force-extension curves of the muscle protein titin [Kellermayer et al., 1997]. Magnetic tweezers use paramagnetic beads instead of dielectric ones which are held in a magnetic force field and used in the same way as optical tweezers. They have been applied, e.g. to investigate DNA elasticity [Smith et al., 1992]. In the biomembrane force probe, the molecules are carried by a functionalised microbead which is attached to a lipid vesicle or a red blood cell. The vesicle is aspirated in a micropipette at large aspiration

pressure. The ligands are carried by a second bead which is directly held by a pipette. Fig. 1.2 shows a micrograph of the BFP setup. The receptor and ligand molecules are sketched in colour on the microbeads. Single molecule binding is achieved by using a very small concentration of receptors. If a binding event occurs it is assumed that it stems from a single bond. The sketched spring indicates that the red blood cell is to a very good approximation a harmonic, elastic element. The force constant is determined by the tension of the vesicle which is directly determined by the aspiration pressure in the pipette [Simson et al., 1998, Merkel, 2001]. Common to all these techniques is that the force is applied to the adhesion bonds by the displacement of an elastic force transducer: the cantilever of the AFM, the force field of optical and magnetic tweezers or the red blood cell or vesicle in the BFP. In addition, receptor and ligands may be attached to their substrate through elastic tethers, usually polymeric linker molecules. For linear elasticity a linear relation between displacement and force on the bond results. The most common loading protocol is the linear ramp of force in which the transducer is retracted at constant speed and force increases linearly in time with a constant loading rate.

Theoretical studies of force induced bond rupture were initiated by steered molecular dynamics (SMD) simulations of the biotin-avidin bond [Grubmüller et al., 1996, Izrailev et al., 1997]. Steered molecular dynamics simulates in atomic detail the force induced unbinding process of the molecules. The setup is in principle the same as in the experiments: one end of the bond is trapped in a harmonic force field and the centre of this force field is moved outward at constant speed so that a linear force is exerted on the bond. The setup of SMD 'experiments' is illustrated in Fig. 1.3 in relation to the AFM technique. In SMD simulations it is possible to follow movements of the two molecules with high resolution. Single hydrogen bonds and their formation and rupture upon translation of rotation of receptor and ligand can be observed.

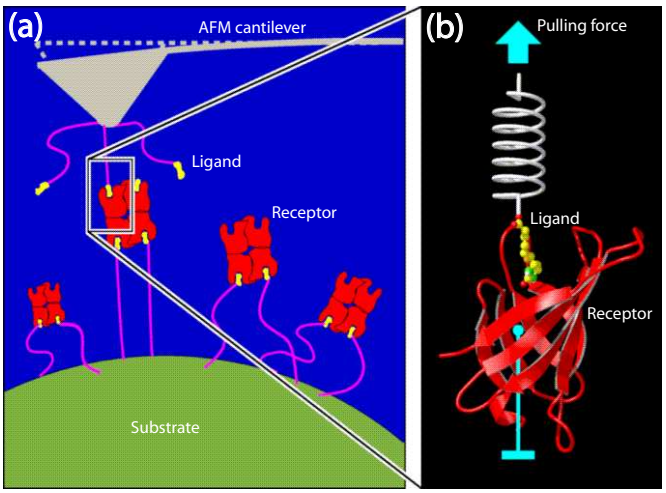

Figure 1.3: (a) Sketch of an AFM experiment on the forced unbinding of receptor-ligand bonds (biotin-avidin). (b) Picture of a single biotin-avidin bonds as it is modelled in steered molecular dynamics simulations. The structure of the avidin is shown as a ribbon model but it is simulated in atomic detail [Rief and Grubmüller, 2002].

A deeper understanding of early measurement of bond strength was only achieved after thorough theoretical analysis by Evans and Ritchie [1997]. Bond dissociation was described as thermally activated passage over an energy barrier in the framework of Kramers' theory. An applied force tilts the energy landscape and reduces the height of the barrier in proportion to the force and the separation of the bound state from the transition state barrier. In particular, it was pointed out that the rupture force is a stochastic variable with an intrinsic distribution which is not a result of experimental error. The most important message was that bond strength, commonly defined as the maximum of the rupture force histogram, is a dynamic quantity which depends on the speed of loading. For slow increase of force, thermal activation supports passage over the transition state barrier and the rupture force

is small. Since weak biomolecular bonds eventually will dissociate also under vanishing force, the rupture force vanishes for infinitely slow loading. For fast pulling, thermal activation is too slow as to assist dissociation which leads to larger rupture forces. For a single transition state barrier, Evans and Ritchie [1997] predicted a linear dependence of bond strength on the logarithm of the loading rate for transitions over a single barrier. An important assumption in the applications of Kramers' theory for time dependent energy barriers is that at any given time, the instantaneous dissociation rate for the given potential can be used. This 'adiabatic approximation' has been tested by Shillcock and Seifert [1998] by comparison of exact solutions for the mean first passage times in a time dependent energy landscape and the approximate expressions of Evans and Ritchie [1997]. It was shown that the approximation is applicable for a large range of loading rates.

Using the histogram of the fluctuating position for biotin-avidin from SMD simulations of Izrailev et al. [1997], Evans and Ritchie [1997] reconstructed an energy landscape. It displays two transition state barriers which hinder dissociation. For several barriers along the pathway unbinding could in principle be treated as a multi-step process between the minima. Due to the exponential dependence of the off-rate on barrier height, however, the largest barrier can be taken as rate limiting [Evans, 2001]. In the beginning of the loading process, this is the largest, outermost barrier but it is reduced most strongly by the linearly increasing force. Thus, in later stages, the inner barriers become rate limiting. A dynamic force spectrum, bond strength as function of the logarithm of loading rate, shows a sequence of linear regimes with increasing slopes. The increasing slope corresponds to the decreasing distance of the relevant barriers from the bound state.

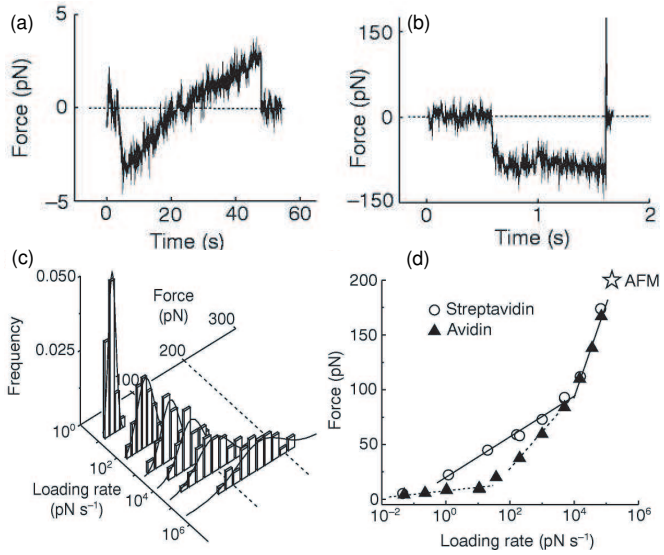

Figure 1.4: Results of dynamic force spectroscopy experiments with the biomembrane force probe [Merkel et al., 1999]. The typical time dependence of the force in a single experiment of bond rupture for (a) slow and (b) fast loading. (c) Histograms of bond rupture forces for increasing loading rate. (d) A dynamic force spectrum shows the bond strength as function of the logarithm of loading rate. The two and three linear regimes for biotin-avidin and biotin-streptavidin, respectively, show that there are two and three barriers, respectively, along the unbinding path of the adhesion bond.

Early measurements using LOT, BFP and AFM corresponded to a sequence of increasing loading rate and yielded increasing bond strength. These could be understood with the insight of Evans and Ritchie [1997] which induced the experimental field of 'dynamic force spectroscopy' (DFS): bond strength is measured for increasing loading rate to reveal structural properties of the energy landscape. Fig. 1.4 shows results of DFS experiments with the biomembrane force probe on biotin-avidin bonds and the structurally similar biotin-streptavidin bonds [Merkel et al., 1999] in which loading rate was changed over several orders of magnitude. Fig. 1.4a,b show the time dependence of the force in a typical experiment for small and large loading rates. Initially the binding sites are pressed together to facilitate binding. The pipette carrying the microbead with the ligands is retracted and force increases linearly until it vanishes as the bond breaks. The time-scale for bond rupture decreases with increasing

loading rate while the rupture force increases. The histograms in Fig. 1.4c show a sharp peak at small forces for slow loading and a broad distribution with a maximum at large forces for fast loading. The plot of the maximum as function of the logarithm of loading rate in Fig. 1.4d shows three and two linear regimes for biotin-avidin and biotin-streptavidin, respectively. This demonstrates to the presence of three and two energy barriers along the unbinding pathway, respectively.

Experiments with the biomembrane force probe have become very successful because they allow to explore a wide range of loading rates. This is possible by combining changes in vesicle tension and changes in retraction speed. The elasticity of the transducer and the linker molecules holding the adhesion bonds has an important influence on the interpretation of the results, because it determines the actual loading rate on the bond [Evans and Ritchie, 1999]. Conflicting results for the unfolding of titin with the AFM [Rief et al., 1997] and with LOT [Kellermayer et al., 1997] could be resolved in this way. In particular, the non-linear elasticity of strongly stretched polymers leads to a non-linear increase of force. DFS has been applied to many important biological bonds besides the biotin-avidin bond including integrin $\alpha_5\beta_1$ [Li et al., 2003], cadherin [Baumgartner et al., 2000, Perret et al., 2002] and selectins [Fritz et al., 1998, Evans et al., 2001, 2004]. The concept can also be applied to other biophysical systems. E.g. the formation of pores in lipid bilayers investigated under a ramp of increasing tension (the 'dynamic tension spectroscopy') allows to deduce values for the energy for pore formation and the line tension in lipid bilayers [Evans and Heinrich, 2003].

The binding properties of molecular bonds are also investigated with other experimental techniques. In flow chambers [Alon et al., 1995], the adhesion of white blood cells to a ligand coated wall is observed under the influence of hydrodynamic forces from a laminar shear flow. Using a very dilute concentration of ligands on the wall, allows to observe transient adhesion events which are mediated by single adhesion bonds [Alon et al., 1997]. Changing flow velocity or the viscosity of the fluid allows to change the force on these bonds. However, the calculation of the force on the bonds from the hydrodynamic flow is difficult for the elastic deformable leukocytes. Rigid microbeads coated with selectin are used for a better control of the experiment. The so-called photonic force microscopy [Rohrbach et al., 2004] is in spirit similar to the reconstruction of energy landscapes from SMD histograms. A dielectric bead is attached to the end of a molecular bond and held in an optical trap. The bead thus moves in the force field of the trap plus that of the adhesion bond. Tracking the bead position with high resolution allows to reconstruct the energy landscape of the adhesion site.

Dynamic force spectra as shown in Fig. 1.4d allow a partial reconstruction of the energy landscape: the slope of the linear segments allows to deduce the distance of the transition state barriers from the bound state. The crossover between the regimes is determined by the relative height of the barriers. Extrapolation of the linear curve corresponding to transitions over the outermost barrier to zero bond strength yields the off-rate k_0 for vanishing force. A general procedure for the reconstruction of energy landscapes from DFS data has been developed [Heymann and Grubmüller, 2000]. However, if several energy barriers are present in the unbinding pathway, the reconstruction of the landscape from the force spectra is not unique [Strunz et al., 2000]. If intermediate bound states are possible, landscapes with different numbers of transition state barriers can lead to identical force spectra [Derényi et al., 2004]. Existence of parallel pathways can make the behaviour of bonds under force even more complex [Bartolo et al., 2002]. In principle, receptor-ligand bonds may have evolved with even more peculiar behaviour, such as catch bonds for which the lifetime increases with increasing forces [Dembo et al., 1988]. A similar behaviour has been predicted for entropic ratchets [Cecchi and Magnasco, 1996] which consist of a branched energy landscape. Experimentally, catch bond behaviour was identified for P-selectin using a flow chamber [Marshall et al., 2003].

To overcome the difficulties in the reconstruction of the binding energy landscapes from DFS measurements, the detailed information from SMD simulations will be helpful to distinguish differ-

ent scenarios. Nevertheless, refined loading protocols for DFS experiments can give further insights. Recently a 'jump-ramp' mode in which force is first increased rapidly to a large value and then increased linearly has been used in experiments on P-selectin [Evans et al., 2004] and allowed to identify alternative unbinding pathways. A major theoretical breakthrough for the field of dynamic force spectroscopy was provided by Jarzynski's equality [Jarzynski, 1997a,b] which relates equilibrium and non-equilibrium properties of a system, namely the free-energy difference between two states and the work performed along a path connecting both states. On this path, the system may be driven arbitrarily far from equilibrium. On the basis of Jarzynski's equality, a method to reconstruct free energy landscapes from non-equilibrium single molecule pulling experiments has been conceived by Hummer and Szabo [2001]. This method was tested experimentally on RNA unfolding [Liphardt et al., 2002] and the quality of the free-energy estimate was investigated systematically by Gore et al. [2003]. It was concluded that the Jarzynski estimate will be superior for small numbers of trajectories and systems far from equilibrium. Jarzynski's equality is especially suited for measurements in molecular systems because the number of samples that are necessary for accurate averaging increases with the size of the system. Jarzynski's equality has been used to identify loading protocols which allow most efficient reconstruction of the energy landscape [Braun et al., 2004]. The periodic change of force proposed there, may be most suited for bistable systems, e.g. the un- and refolding of proteins such as titin [Braun and Seifert, 2004].

1.4 Modelling multiple adhesion bonds under force

Knowledge about single bond behaviour under force has to be integrated into an appropriate description of adhesion clusters of multiple bonds under force. For multiple bonds the environment becomes even more important for the derivation of an appropriate model. For single bond experiments it has already been demonstrated how the elasticity of the linker molecules determines the actual rate of loading and thus the off-rate [Evans and Ritchie, 1999]. For multiple adhesions one additionally has to deal with the problem of how the force is distributed on the force bearing adhesion bonds. The adhesion bonds are usually attached to a surface which acts as a force transducer. The distribution of the force is determined by the arrangement of the bonds, by the way the force is applied to the adhesion cluster and by the elastic properties of linkers and force transducer. In general, the distribution will not necessarily be homogeneous. While a fraction of bonds may be loaded, another fraction of bonds may be unloaded and make up a reservoir of spare bonds. Another difference of multiple adhesion sites compared to single bonds is that rebinding of broken bonds becomes important. In DFS experiments, receptor and ligand are usually retracted by an elastic recoil of the linker molecules and rebinding is impossible. In adhesion clusters, the remaining intact bonds keep the binding sites in close vicinity which facilitates the reformation of broken bonds. This fails as soon as the last bond breaks and rebinding from this completely dissociated state is impossible. The possibility of rebinding allows stable and long lived adhesions formed by weak bonds [Goldstein and Wofsy, 1996].

Equilibrium properties of the binding of lipid membranes decorated with specific adhesion bonds have been studied theoretically before [Bell et al., 1984, Zuckerman and Bruinsma, 1995, Lipowsky, 1996]. The specific interaction yields an additional attractive potential which helps to overcome the non-specific Helfrich-repulsion from the suppression of membrane fluctuations in the presence of another surface and can thus induce adhesion of the membrane [Weikl et al., 2000, Weikl and Lipowsky, 2001]. The soft membrane also mediates interactions between the mobile adhesion bonds. Fluctuations of the membrane are suppressed if it is anchored to the substrates by an adhesion bond and binding is thus disfavoured. This induces an effective attractive interaction of sticker molecules which

can lead to clustering. If two different species of adhesion bonds are present in the membrane, e.g. with different length, the membrane has to bend between two unlike adhesion bonds. This additional energy for bending can induce a phase separation between the different species of molecules [Weikl et al., 2002]. Non-equilibrium processes of vesicle unbinding have been investigates with pure membranes [Brochard-Wyart and de Gennes, 2003] and for membranes with mobile binders [Brochard-Wyart and de Gennes, 2002].

Adhesion receptors in cellular adhesion clusters are attached firmly to the cytoskeleton of the cell. Moreover the bonds are densely packed with distances in the range of nm so that the influence of membrane fluctuations is small. In BFP-experiments, the lipid vesicles are typically under strong tension. Often, the vesicles are only used as elastic force transducers while the bonds are attached to rigid microbeads. Therefore, effects of membrane fluctuations are small and can be neglected in the context of mature adhesion clusters. A deterministic model for the non-equilibrium dissociation of adhesion clusters under force has been introduced in a seminal paper by Bell [1978]. This model has been mainly used to study more specific problems, for example leukocyte rolling in shear flow [Hammer and Lauffenburger, 1987]. Recently, the deterministic Bell-model has also been extended to treat linear loading of a cluster of adhesion bonds, which usually is applied in dynamic force spectroscopy [Seifert, 2000, 2002]. A stochastic version of the Bell-model has been introduced, but studied only in the large system limit and for specific parameter values [Cozens-Roberts et al., 1990a,b]. Later the stochastic model has been treated with reliability theory in the special case of vanishing rebinding [Tees et al., 2001]. Other special cases of the stochastic model have been treated in order to evaluate specific experiments, for example the binding probability between ligands and receptors on opposing surfaces as a function of contact time [Chesla et al., 1998, Zhu, 2000]. In this work we will study the stochastic version of the Bell model from the point of view of theoretical physics.

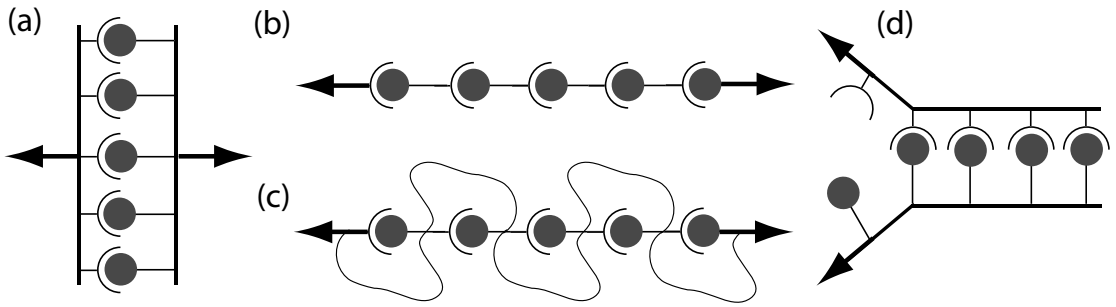

Figure 1.5: Different loading scenarios for multiple adhesion bonds. The arrows indicate the direction of the force. (a) parallel bonds, (b) serial bonds without and (c) with an additional linker which prevents chain rupture and (d) zipper-like arrangement with sequentially loaded bonds.

For multiple bonds, different loading scenarios can be distinguished in regard to the distribution of force between the bonds and the behaviour upon bond breakage. One-dimensional scenarios are shown schematically in Fig. 1.5. Parallel bonds as shown in Fig. 1.5a equally share the force applied to the cluster. Upon breakage of one bond the force is redistributed among the intact bonds but the cluster as a whole remains intact until the last bond breaks. Parallel loading can be assumed for cellular adhesion clusters and for many DFS-experiments on multiple bonds. Serial bonds as in Fig. 1.5b, are all subject to the force that is applied to the whole chain. Breakage of the first bond disrupts the whole chain as would be the case for protein filaments such as actin. With an additional link as in Fig. 1.5c, bond breakage only extends the chain and the loading process starts anew. This scenario may serve

as a model for loading of the muscle protein titin in which several folded protein domains unfold and extend upon loading. In a zipper-like arrangement as in Fig. 1.5d the whole force is exerted on the first bond in the chain and as soon as it breaks, the next bond is loaded. This arrangement can be used as a model for RNA or DNA unzipping [Liphardt et al., 2002, Bockelmann et al., 2002]. In general and in more dimensions, combined scenarios are conceivable. Pulling on a vesicle adhered to a planar substrate, for example, will put the largest force on the rim of the adhesion zone while the interior of this zone remains unloaded [Prechtel et al., 2002]. This corresponds to a combination of zipper-like and parallel arrangement.

Experiments on forced unbinding of adhesion clusters are still rare. The biomembrane force probe with a linearly increasing force was used to pull apart adhesion clusters of $\alpha_v\beta_3$ integrins which were expressed on epithelial cells [Prechtel et al., 2002]. Recently, a similar setup was used also for a constant force [Pierrat et al., 2004]. In the following we will discuss the dynamics of parallel adhesion clusters as a model for biological and biomimetic adhesion clusters. Dissociation and association dynamics of parallel adhesion clusters has first been discussed by Bell [1978]. Although it is clear that force leads to accelerated cluster dissociation, it is usually not known how it is distributed over the different closed bonds in different situations of interest. In many cases, most prominently in rolling adhesion, only few of the different bonds are loaded to an appreciable degree, thus dissociation occurs in a peeling fashion [Dembo et al., 1988, Hammer and Apte, 1992, Chang et al., 2000]. However, due to geometrical reasons, even in this case there will be a subset of bonds which are loaded to a similar extend. In the same vein, the loading situation at focal adhesions can also be expected to be rather complicated. Another problem with experiments in DFS is that the number of bonds in the cluster is typically not known. Thus, to analyse these experiments, one has to use an appropriate assumption over the binding process during contact of transducer and substrate and deduce some distribution of numbers of closed bonds.

1.5 Overview

In this work we investigate theoretically the stability of clusters of parallel adhesion bonds against dissociation under the influence of an applied force. In Chapter 2 we introduce the model used to describe adhesion cluster dynamics. We begin with a brief account of the calculation of single bond dissociation rates with Kramers' escape rate theory [Kramers, 1940, Hänggi et al., 1990] for thermally assisted dissociation of molecular bonds. The influence of a force is modelled by Bell's equation [Bell, 1978] which assumes an exponential increase of the dissociation rate with force. It can be understood in the framework of Kramers' theory. Since we are interested in generic properties of adhesion cluster stability we consider adhesion molecules with a unique unbinding pathway and a single transition state barrier. Multiple barriers or dissociation pathways can be included in the model straightforwardly.

Next, we discuss a model for the loading process on adhesion clusters consisting of N_t parallel bonds. The essence of the model is shown in Fig. 1.6; adhesion receptors are carried by a transducer while the ligands are tethered to the substrate. We assume that the bonds can either be in a closed or in an open state. Only in the closed state the bonds are able to carry load and provide attachment. A force f is applied to a transducer and is shared equally by all closed bonds. Transitions between the different states occur stochastically, driven by thermal activation. Closed bonds open with an off-rate k_{off} which increases exponentially with the force applied to the bond; open bonds close with a constant on-rate k_{on}. We will discuss two important limiting cases for the force transduction from transducer to bonds. For *shared loading*, the force exerted on the transducer is controlled and the i closed bonds are subject to the shared force f/i. For *non-cooperative loading*, the force on the closed

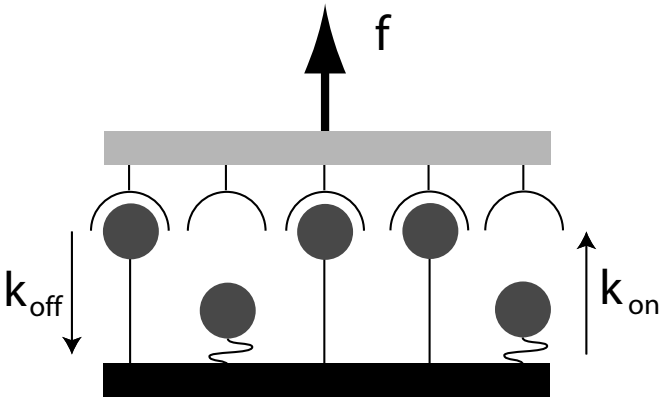

Figure 1.6: Model for loading of an adhesion cluster of $N_t = 5$ parallel adhesion bonds. The $i = 3$ closed bonds share the force equally so that each is subject to the force f/i. The closed bonds open with the off-rate k_{off} which increases exponentially with force and open bonds close with the constant on-rate k_{on}.

bonds is controlled directly and the force exerted on the cluster changes with the number of closed bonds.

Transducer and substrate are assumed to be rigid so that all adhesion bonds are subject to the same conditions. In particular, there is no horizontal spatial coordinate of relevance. The adhesion cluster is a localised arrangement of adhesion molecules that are subject to very similar conditions as in cellular focal adhesions where the adhesion clusters are forced by single stress fibres or at the contact zone of two microbeads in a BFP experiment. In a biological or biomimetic system, however, the actual distribution is unknown but most likely not ideally homogeneous. However, it can be assumed that at least a subset of bonds is subject to the same force. Effects from fluctuations of the plasma membrane are not taken into account in the model since we have in mind the firm attachment of adhesion bonds to the cytoskeleton of cellular adhesion clusters or the anchoring on fairly rigid microbeads as in DFS experiments. Even if immersed directly in the membrane of a vesicle as in some BFP experiments, the strong tension of the vesicles will suppress the influence of fluctuations [Merkel, 2001]. This is in accordance with previous treatments [Bell, 1978, Cozens-Roberts et al., 1990a, Seifert, 2000].

We then introduce a master equation that describes the stochastic dissociation and association dynamics of the adhesion bonds in the cluster. With a constant cluster size N_t, the state of the cluster is given by the number of closed bonds alone. For shared loading the force and thus the off-rate depends on the number of closed bonds and the master equation is non-linear while non-cooperativity is reflected by the linearity of the dynamic equations. From the master equation, a deterministic differential equation for the average number of closed bonds in the adhesion cluster can be derived which has been discussed before for constant loading by Bell [1978] and for linear loading by Seifert [2000, 2002]. For non-linear master equations, this is not an exact representation of the average number of closed bonds. Results from the deterministic description will be compared to solutions of the master equation. Stochastic versions of the model have been discussed before but in the limit of large clusters with applications to specific systems [Cozens-Roberts et al., 1990a,b] and for single bonds using concepts of reliability theory [Tees et al., 2001].

In Chapter 3 we discuss adhesion cluster stability for constant loading. The main focus of interest is on the cooperative effects due to shared loading. Results for this case were published before [Erdmann and Schwarz, 2004b,c]. For the non-linear master equation, analytic solutions are derived for several special cases. For vanishing rebinding one can use the fact that cluster dissociation corresponds to a unique sequence of unbinding events with constant rates which allows to construct a solution of the master equation. In the case of vanishing force the master equation is linear and can be solved for natural boundaries. For the experimentally important case of an absorbing boundary, we use an approximation valid for large clusters. For the general case of finite rebinding and force we

solve the master equation for small clusters. For larger clusters we use stochastic simulations with the Gillespie algorithm to solve the master equation numerically. The results for the average number of closed bonds are compared to numerical solutions of the deterministic model. An important measure for adhesion cluster stability is the mean lifetime before for dissociation from the initial bound state. This can be calculated for the general case in terms of the dissociation rates. It reveals that rebinding has an important impact for the stabilisation of large adhesion clusters. The linear master equations for non-cooperative loading can be solved by standard methods.

In Chapter 4 we discuss the case of linear loading of adhesion clusters. This is the situation in dynamic force spectroscopy experiments on multiple adhesions. A brief account of the main results has been given in Erdmann and Schwarz [2004a]. For this case, analytical solution for the case of shared loading are not found due to the time-dependence of the reverse rate. To derive approximations for adhesion cluster lifetime we use and extend a scaling analysis of the deterministic equation first presented in Seifert [2000]. The results for the scaling analysis are compared to numerical solutions of the master equation and the deterministic equation. For non-cooperative loading and for vanishing rebinding, the master equation can still be solved analytically. Also the mean lifetime is calculated exactly.

Finally, in Chapter 5 we include explicitly the dependence of binding and unbinding on the distance of ligands and receptors. In general, biomolecular bonds are tethered to their substrate by polymeric linker molecules. The distribution of ligand molecules above the substrate is thus a decreasing function of the distance from the substrate. On the other hand, the force needed to stretch the tethers and which pulls on the adhesion bonds increases with the distance. In Chapter 5 we do not exert a force from outside on the adhesion cluster but rather control the distance of the transducer from the equilibrium position of free tethers. We allow the binding of the tethers to pull the transducer closer by and thereby increase the rate of binding. In combination with cooperative loading, this gives rise to a rich behaviour of the dynamic equations. In particular we observe a region with a bimodal distribution of the number of closed bonds. In this region, the clusters switch frequently between a bound and an unbound state.

This work is entirely concerned with properties of passive adhesion clusters. All active processes as they are observed in living cells and which were described in the first section are not taken into account. For a direct comparison with experiments, biomimetic model systems will be most relevant. Here it will be necessary to analyse results of dynamic force spectroscopy on multiple bonds with an appropriate model. In particular since one ignores the number of initially closed bonds in these experiments, theoretical analysis has to support experiments. In biological adhesion clusters, active phenomena hide the aspects of passive adhesion. However, the results for passive adhesion will also be of relevance for biological adhesion clusters because active reinforcement has to outrun rupture of passive adhesions. In the long run, the results will have to be included in detailed models of biological adhesion clusters.

Chapter 2

Model for adhesion cluster dynamics

In this chapter we introduce a theoretical model to describe the stochastic dynamics of adhesion clusters. We first describe how the dissociation of single molecular bonds is modelled in the framework of Kramers' escape rate theory and introduce Bell's equation for the force dependence of the rate of dissociation. Next, we introduce a setup to integrate several bonds into a cluster. We derive a one-step master equation for the description of the stochastic cluster dynamics and a differential equation as an approximate treatment for the number of closed bonds in an adhesion cluster.

2.1 Modelling single bonds

2.1.1 Thermally activated dissociation of molecular bonds: Kramers' problem

Despite their intrinsic complexity, the dissociation of biomolecular bonds can be modelled successfully [Evans and Ritchie, 1997, Izrailev et al., 1997, Shillcock and Seifert, 1998] in the framework of Kramers' escape rate theory as thermally activated escape over a transition state barrier [Kramers, 1940, Hänggi et al., 1990]. The bond is described as a Brownian particle in a viscous environment which moves in a one-dimensional energy landscape. The energy landscape is determined by the structure of the binding pocket of the adhesion bond and the typical unbinding pathway. As described in the introduction, biological bonds have evolved pathways which can be described by a single coordinate to allow rapid and reliable dissociation and association. For complex bonds, one or several sequential energy barriers may exist along the pathway and limit dissociation. Besides a sequence of barriers along a preferred pathway there may also exist several parallel (but 1-dimensional) pathways for unbinding [Evans et al., 2001, Bartolo et al., 2002]. Which of the pathways is taken depends on the conditions for unbinding. In particular for force assisted unbinding the loading protocol can determine the unbinding pathway [Evans et al., 2004]. Experimentally, the different situations are difficult to distinguish. If multiple barriers and pathways exist, the reconstruction of the energy landscape from dynamic force spectra is not unique [Derényi et al., 2004, Bartolo et al., 2002]. Here, the detailed insight that is possible with steered molecular dynamics simulations will be helpful. Since we are interested in generic properties of adhesion clusters and do not aim to model a particular adhesion molecules, in the following we will use the simplest energy landscape with a single energy barrier and a single pathway. The conceptual framework can be straightforwardly generalised to more detailed models of adhesion bonds.

A qualitative sketch of a one-dimensional energy landscape $U(x)$ as a model for a molecular bond is shown in Fig. 2.1 as function of a reaction coordinate x which represents the distance between

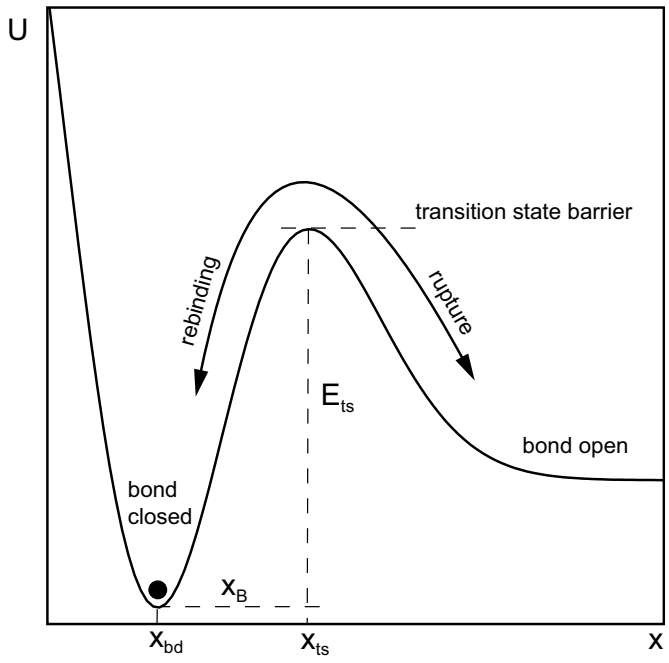

Figure 2.1: Energy landscape $U(x)$ on the one-dimensional reaction coordinate x as a model for a biomolecular adhesion bond. The bound state ('bond closed') at x_{bd} is separated by the transition state barrier at x_{ts} from the unbound state ('bond open'). Rupture and rebinding events correspond to transitions of the Brownian particle (black dot) over the transition state barrier.

receptor and ligand. The bound state is represented by a deep minimum at small distance $x = x_{bd}$. It is separated from the unbound state by a transition state barrier at $x = x_{ts} > x_{bd}$. The unbound state may be a minimum of free energy for particles that are trapped after dissociation or approach a constant value continuously for freely diffusing particles. The probability distribution $P(x, v, t)$ at time t for the coordinate x and the velocity v of a particle diffusing freely in the potential $U(x)$ satisfies the Klein-Kramers equation [Kramers, 1940, Hänggi et al., 1990, van Kampen, 2003]

$$M\frac{\partial}{\partial t}P(x,v,t) = -Mv\frac{\partial}{\partial x}P(x,v,t) + \eta\left\{\frac{U'(x)}{\eta}\frac{\partial}{\partial v} + \frac{\partial}{\partial v}v + \frac{k_BT}{M}\frac{\partial^2}{\partial v^2}\right\}P(x,v,t)\,. \qquad (2.1)$$

Boltzmann's constant is denoted by k_B, the unit of thermal energy is k_BT; η is the friction coefficient of the particle in the fluid and M its mass. The force exerted on the particle by the energy profile is $-U'(x) := -dU/dx$.

In the limit of large friction, $\eta \gg 1$, inertial terms can be neglected compared to thermal, Brownian forces and the velocity follows a Maxwell distribution $p(v) \sim e^{-Mv^2/2k_BT}$ which is independent of x. The Klein-Kramers equation for the full distribution is then replaced by the Smoluchowski equation

$$\eta\frac{\partial}{\partial t}\rho(x,t) = \frac{\partial}{\partial x}U'(x)\rho(x,t) + k_BT\frac{\partial^2}{\partial x^2}\rho(x,t)\,. \qquad (2.2)$$

for the spatial distribution $\rho(x, t)$ of overdamped Brownian motion in the external potential $U(x)$.

To calculate the transition rate over the barrier from bound to unbound, Kramers [1940] considered a quasi stationary state of the system in which $\rho(x, t)$ is localised in the bound state and locally in equilibrium. This situation could be maintained as a stationary, non-equilibrium state by removing particles from the system after they have crossed the barrier to the unbound state and adding new particles close to the bound state. In any case it is necessary that the time-scales for local equilibration and for establishing equilibrium between bound and unbound state, that is for transitions over the barrier, are sufficiently separated. This requires an energy barrier which is large compared to the thermal energy. The non-equilibrium situation results in a constant net flux over the barrier. The

transition rate k_0 for a single particle is given by the inverse of the mean first passage time from x_{bd} to the unbound state. Assuming a Boltzmann distribution for the particle inside the potential well, it can be calculated as [van Kampen, 2003]

$$\frac{1}{k_0} = \frac{\eta}{k_B T} \int_{x_{bd}}^{x_{ub}} \left\{ e^{U(x')/k_B T} \int_{-\infty}^{x'} e^{-U(x'')/k_B T}\, dx'' \right\} dx' \,. \tag{2.3}$$

Here, x_{ub} is a position of the unbound state which is assumed to be on the right of the barrier. The results are robust with the exact choice of x_{ub}. The integration over x'' gives a large contribution when the potential is small, i.e. around the bound state at x_{bd}. The integration over x' gives a large contribution only around the barrier x_{ts}. Around these positions, the potential $U(x)$ can thus be replaced by the parabolas $U(x) - U(x_{ts}) \approx U''(x_{ts})(x - x_{ts})^2/2$ and $U(x) - U(x_{bd}) \approx U''(x_{bd})(x - x_{bd})^2/2$, respectively; the range of integration can be extended to infinity. This saddle point approximation allows to solve the integrals and the expression for the dissociation rate reads

$$k_0 = \nu_D e^{-E_{ts}/k_B T} \,. \tag{2.4}$$

$E_{ts} = U(x_{ts}) - U(x_{bd})$ is the height of the barrier relative to the bound state. The prefactor ν_D has the dimension of an inverse time and is determined by the shape of the potential:

$$\nu_D = \frac{\omega_{bd}\omega_{ts}}{2\pi(\eta/M)} = \frac{\sqrt{U''(x_{bd})|U''(x_{ts})|}}{2\pi\eta} \,. \tag{2.5}$$

The curvature $U''(x_{bd}) > 0$ at the bound state and the curvature $U''(x_{ts}) < 0$ at the transition state barrier determine the squared angular frequencies $\omega_{bd}^2 := U''(x_{bd})/M$ and $\omega_{ts}^2 := |U''(x_{ts})|/M$ of undamped particles at the bound state and at the transition state, respectively. Thus, ν_D determines the time-scale for the diffusive motion in the potential and the dissociation rate (2.4) can be interpreted as the product of the frequency ν_D of attempts to cross the barrier reduced by the probability that enough energy is acquired to pass, which is the Arrhenius factor $e^{-E_{ts}/k_B T}$. Kramers' theory can be applied if $E_{ts} > k_B T$ so that the Arrhenius factor is very small. This implies a wide separation of the time-scale $1/\nu_D$ for local equilibration and $1/k_0$ for equilibration between bound and unbound state. For typical molecular bonds one estimates $\nu_D \sim 10^9/\,\mathrm{s}$ and with a barrier of $E_{ts} \sim 20 k_B T$ we get $k_0 \sim 1/\,\mathrm{s}$. In practice, bond lifetime varies from milliseconds for antibodies to hours for biotin-avidin, the strongest known non-covalent bond [Bongrand, 1999, Merkel, 2001]. For typical adhesion bonds such as integrins or selectins, lifetime is of the order of seconds. One important achievement of Kramers' theory is to derive the exact form of the prefactor ν_D and to show that for large friction it is independent of the barrier height E_{ts}. In the following, however, we will not use the exact form of the prefactor explicitly. Rather, the pure exponential dependence of the off-rate on barrier height will be exploited to describe the force dependence of the off-rate.

The Klein-Kramers equation (2.1) reduces to the Smoluchowski equation (2.2) for large friction η if the potential $U(x)$ and the distribution $\rho(x)$ are approximately constant on the thermal length scale $\sqrt{k_B T M}/\eta$ [Kramers, 1940, Hänggi et al., 1990]. In Brownian dynamics simulations a diffusion coefficient $D = k_B T/\eta \simeq 10^{-11}\,\mathrm{m}^2\,/\,\mathrm{s}$ has been used [Hummer and Szabo, 2001] to model typical AFM experiments. Thermal energy at physiological temperature is $k_B T \simeq 4.1\,\mathrm{pN\,nm}$ so that the friction coefficient is $\eta \simeq 4 \times 10^{-10}\,\mathrm{kg}\,/\,\mathrm{s}$. With a mass of a protein of about $M \simeq 100\,\mathrm{kDa} \simeq 1.7 \times 10^{-22}\,\mathrm{kg}$ the thermal length-scale is $\sqrt{k_B T M}/\eta \simeq 2 \times 10^{-12}\,\mathrm{m} \simeq 0.002\,\mathrm{nm}$ which is very small compared to the size of the binding pocket. For typical biomolecular bonds, the distance between the bound state and the transition state barrier – the so-called reactive compliance – is in the range of $x_B = 0.5\,\mathrm{nm}$ [Bell, 1978].

2.1.2 Force assisted bond dissociation: Bell's equation

In contrast to the situation in solution, biomolecular bonds in cell adhesion usually have to function under force. The influence of a mechanical force on the rupture kinetics of biomolecular bonds has been first discussed by Bell [1978]. In analogy to fracture mechanics of solids an exponential increase

$$k_{off}(F) = k_0 e^{F/F_B} \tag{2.6}$$

of the off-rate $k_{off}(F)$ under force with respect to the off-rate k_0 at vanishing force was put forward. The parameter F_B depends on the structure of the bond and determines the intrinsic force-scale for bond strength.

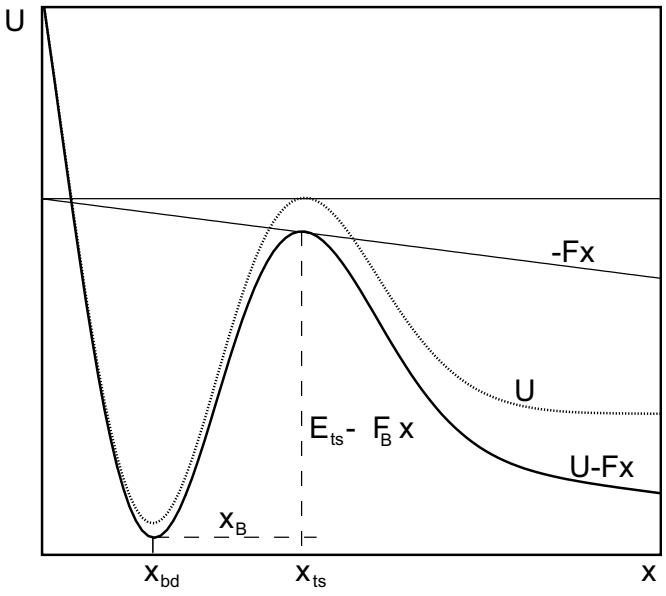

Figure 2.2: The applied force F induces the additional potential $-Fx$ and tilts the energy landscape of the adhesion bond.

Bell's equation can be understood in the framework of Kramers' escape rate theory. The force F adds $-Fx$ to the energy, $U(x;F) = U(x) - Fx$. If the barrier is very sharp, its height E_{ts} reduces in proportion to F and the reactive compliance $x_B = x_{bd} - x_{ts}$. As long as the barrier is large enough that Kramers' theory applies, the rupture rate can be inferred from (2.4) with the barrier height $E_{ts}(F) = E_{ts} - Fx_B$. The rupture rate under force is then given by

$$k_{off} = \nu_D e^{-(E_{ts}-Fx_B)/k_BT} = \nu_D e^{-E_{ts}/k_BT} e^{Fx_B/k_BT} = k_0 e^{F/F_B} \tag{2.7}$$

which has the form of Bell's equation. For barriers of finite width, the shape and the position of bound state and barrier changes with force. This leads to a algebraic force dependence of the prefactor ν_D and to corrections in the dependence of the barrier height on F [Evans and Ritchie, 1997, Shillcock and Seifert, 1998, Evans and Ritchie, 1999]. These corrections, however, are weak compared to the main influence of force on the barrier height which changes the off-rate exponentially. In the following we will therefore assume the form (2.6) for the force dependent off-rate.

The intrinsic force scale $F_B = k_BT/x_B$ is the force which is necessary to reduce the barrier by one unit of thermal energy k_BT. For molecular bonds one finds with a typical value of $x_B \simeq 0.5\,\mathrm{nm}$ and $k_BT \sim 4.1\,\mathrm{pN\,nm}$ that the intrinsic force scale is $F \simeq 8.2\,\mathrm{pN}$. Physiological loading has indeed been found to be in the pN-range, both for cell-matrix adhesion [Balaban et al., 2001, Schwarz et al., 2002, Tan et al., 2003] and rolling adhesion [Alon et al., 1995, 1997]. Values for k_0 and F_B have been

measured during recent years with dynamic force spectroscopy for different receptor-ligand systems, including integrin [Zhang et al., 2002, Li et al., 2003], cadherin [Baumgartner et al., 2000] and selectin [Fritz et al., 1998, Evans et al., 2001].

If molecular bonds are loaded dynamically with a time dependent force, Kramers' theory is not applicable in general, because there is no quasi stationary state. In this case the mean first passage time has to be determined for a time dependent potential. This has been done by Shillcock and Seifert [1998] who compared exact results to results of an 'adiabatic approximation'. This approximation assumes that the unbinding process – the crossing of the barrier – is fast compared to the change of the potential due to loading and that equilibration in the potential well is faster than changes of the potential. The results showed good agreement of the approximation with the exact results over a wide range of loading speeds. The adiabatic approximation allows to use expression (2.6) with a time-dependent force for the instantaneous rupture rate at a given time. This approach is commonly used in the analysis of dynamic force spectroscopy experiments [Evans and Ritchie, 1997, 1999].

In bonds with several sequential or parallel transition state barriers with different x_B and F_B, the exponential decrease of the off-rate with barrier height usually allows to treat one of these barriers as determining the off-rate. For sequential barriers the largest barrier limits the off-rate; for parallel barriers, the smallest one allows the fastest escape. With an applied force, the role of the different barriers changes because the outermost barriers are reduced most. This will lead to different regimes for the intrinsic force scale F_B when the dominating barrier changes from outer to inner (sequential) or inner to outer (parallel) upon an increase of loading. In dynamic force spectroscopy experiments, this is used to unveil the positions and relative height of the transition state barriers in an adhesion bond.

2.1.3 Association of molecular bonds

While the dissociation rate k_{off} depends mainly on the internal structure of a bond, the association rate k_{on} includes the formation of an encounter complex and therefore depends on the details of the situation under consideration. It is very difficult to determine k_{on} experimentally, especially in the case of cell adhesion, when the interacting molecules are anchored to opposing surfaces [Chesla et al., 1998, Zhu, 2000, Orsello et al., 2001]. In order to focus on the generic features of cluster stability, here we assume that k_{on} is a force-independent constant, in accordance with earlier theoretical work [Bell, 1978, Hammer and Lauffenburger, 1987, Cozens-Roberts et al., 1990a,b, Seifert, 2000]. In Chapter 5 we will refine this assumption to include in our model the effect of ligand receptor separation controlled by polymeric tethers on the binding rate.

For the following analysis, it is convenient to introduce dimensionless quantities. Forces will be measured in units of the intrinsic force scale F_B. We denote the dimensionless force by $f := F/F_B$. A typical time-scale is set by the force free unbinding rate k_0 and the dimensionless time is $\tau := k_0 t$. With the definitions of force and time, the dimensionless off-rate reads $k_{off}/k_0 = e^f$ and the dimensionless on-rate is denoted by $\gamma = k_{on}/k_0$.

2.2 Modelling multiple parallel bonds

The off-rate (2.6) is increased by the force exerted on the single molecular bond. To describe the stochastic rupture dynamics of molecular bonds in an adhesion cluster, it is necessary to specify the way in which the force exerted on the cluster is transduced to the individual molecular bonds. We use a simple spring model [Seifert, 2000] to describe general properties of force transduction. With this

information, the transition rates for molecular bonds in the cluster can be derived which then will be used in a master equation for the occupancy probabilities on the set of states of the cluster.

2.2.1 Harmonic force transducer

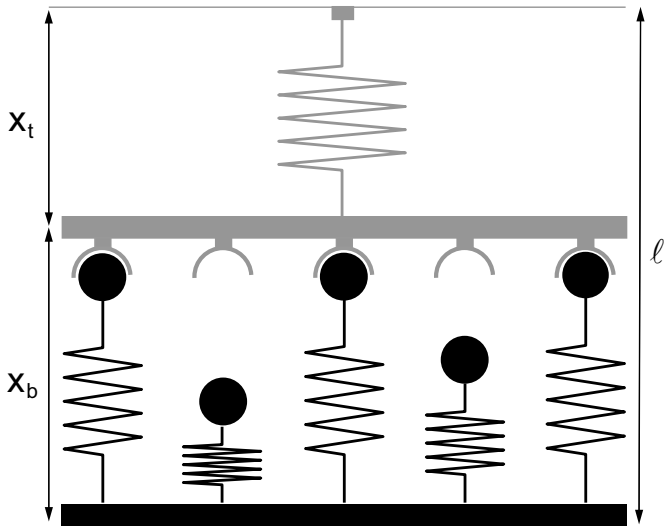

Figure 2.3: Spring model for force transduction at an adhesion cluster. The distance between the resting positions of transducer and tether springs is denoted by ℓ. It is the sum $\ell = x_b + x_t$ of the extension x_t of the transducer spring and x_b of the tether spring in a closed bond. The rest lengths of transducer and tethers are suppressed in the figure. The adhesion bonds in the cluster can be either open or closed. With a constant cluster size N_t, the state of the cluster is determined by the number of closed bond i (here $i = 3$).

The model that we use is shown in Fig. 2.3. We assume that the substrate and the transducer are rigid, planar and parallel to each other. The elastic part of the transducer is modelled as a harmonic spring with the force constant k_t. This is usually a good assumption for experimental setups [Merkel, 2001, Evans et al., 2004]. The polymer tethers are also modelled as harmonic springs with a force constant k_b, which is a valid assumption as long as the extension of the polymers is small compared to the contour length of the polymer backbone [Doi and Edwards, 1986]. The origin of this behaviour, however, is different from that for the transducer. While the deformation of the transducer requires elastic energy, the polymers act as entropic springs. Between substrate and transducer there are N_t molecular bonds which are either in an open or a closed state. If a bond is closed it is able to sustain force. All bonds are identical and immersed in the same environment. In particular, we do not consider the spatial coordinate parallel to the transducer.

If closed bonds exist in the adhesion cluster, a finite separation $\ell > 0$ between the resting positions of tethers and transducer leads to an extension x_b of the tether spring and x_t of the transducer spring with $\ell = x_b + x_t$. The forces required to extend the springs are $F_b = k_b x_b$ and $F_t = k_t x_t$. With i closed bonds, the balance of force $F_t = k_t x_t = k_t(\ell - x_b) = i k_b x_b = i F_b$ leads to the expression for tether extension as function of i

$$x_b = \frac{k_t \ell}{k_t + i k_b} \tag{2.8}$$

so that the force per bond is

$$F_b = k_b x_b = \frac{k_t k_b \ell}{k_t + i k_b} = \frac{k_b \ell}{1 + i\kappa}\,. \tag{2.9}$$

In the last expression, the ratio $\kappa := k_b/k_t$ of the force constants of tethers and transducer was introduced. The extension of the transducer spring is given by $x_t = \ell - x_b$ so that

$$x_t = \left(\ell - \frac{k_t \ell}{k_t + i k_b}\right) = \frac{i k_b \ell}{k_t + i k_b}\,. \tag{2.10}$$

The transducer force is

$$F_t = k_t x_t = \frac{i k_b k_t \ell}{k_t + i k_b} = \frac{i k_b \ell}{1 + i\kappa} = i F_b \,. \tag{2.11}$$

With the intrinsic force scale F_B introduced in Sec. 2.1.2, the dimensionless expressions for the force per bond and the force on the transducer are

$$f_b = \frac{F_b}{F_B} = \frac{(k_b \ell / F_B)}{1 + i\kappa} \quad \text{and} \quad f_t = \frac{F_t}{F_B} = \frac{i(k_b \ell / F_B)}{1 + i\kappa} = i f_b \,, \tag{2.12}$$

respectively. In the rest of the analysis, dimensionless expressions for the forces will be used. The dependence of the force per bond which determines the single bond off-rate introduces a non-trivial coupling between the otherwise independent closed bonds. A change in i through rupture or rebinding of one bond changes the rupture kinetics of the other bonds. This non-trivial coupling of cooperative adhesion bonds is one of the main points of interest of this work.

In the following we will discuss two important limiting cases for the relative stiffness κ of the springs. Both will be investigated in detail in the following chapters.

Soft transducer and shared loading

First we consider the limit of a 'soft transducer', in which the force constant of the transducer is small compared to that of the tethers, $k_t \ll k_b$. This corresponds to the regime of $\kappa \to \infty$.

In this limit, tether extension is small, $x_b \ll \ell$ whereas the transducer extension approaches the displacement of the transducer spring, $x_t \lesssim \ell$. The large stiffness of the tethers holds the transducer in a position close to the rest length of the tethers whereas the transducer spring is easily extended. In this case, the transducer force is directly proportional to the displacement, $F_t = k_t \ell$, or in dimensionless units

$$f_t = k_t \ell / F_B \,. \tag{2.13}$$

The force per closed bond is $f_b = f_t / i$, so that

$$f_b = (k_t \ell / F_B)/i = f_t / i \,. \tag{2.14}$$

When an adhesion cluster is loaded through a soft transducer, the displacement ℓ directly controls the force $f = f_t$ on the transducer, that is, the force on the cluster as a whole. The force per bond then depends on the number i of closed bonds which share the transducer force. For shared loading, the coupling of the closed bonds through force is most pronounced.

Stiff transducer and non-cooperative loading

The other extreme is the limit of the 'stiff transducer' for which the stiffness of the transducer spring exceeds that of the tethers acting together, $k_t \gg N_t k_b$. This limit corresponds to the regime $\kappa \to 0$.

In this case, the extension of the transducer spring almost vanishes, $x_t \ll \ell$, whereas the extension of the tethers approaches the displacement of the transducer from the tethers rest length, $x_b \lesssim \ell$. The force on each bond,

$$f_b = k_b \ell / F_B \,, \tag{2.15}$$

is directly controlled by the displacement ℓ. The force on the transducer is proportional to the number of closed bonds in the cluster,

$$f_t = i f_b = i(k_b \ell / F_B) \,. \tag{2.16}$$

The stiff transducer does not deform so that the tethers attached to the transducer are extended to the displacement ℓ. The force $f = f_b$ per closed bond is independent of i so that the individual bonds are fully uncoupled and non-cooperative.

The influence of the elastic properties of tethers and transducer on the actual force on a molecular bonds has been discussed for the case of a single bond [Evans and Ritchie, 1999]. In experiments, the displacement is usually controlled, rather than the force itself and it is important to take the elasticity into account. It should be noted, that the terms 'shared' and 'non-cooperative' loading do not refer to the relation between f_b and f_t which is always $f_t = if_b$. The distinction comes from whether $f = f_t$ or $f = f_b$ are controlled through the displacement ℓ of the transducer spring. Controlling the transducer force $f_t = f$ directly instead of ℓ would always result in shared loading, $f_b = f/i$, irrespective of the elasticity of tethers and transducer. For finite stiffnesses k_t and k_b, the general expression (2.12) shows that both f_b and f_t depend on i and are not directly determined by ℓ. In Chapters 3 and 4, both limits of shared as well as non-cooperative loading will be investigated. The case of general stiffnesses will be addressed in Chapter 5.

Constant and linear loading

Experimentally and theoretically, different 'loading protocols' for single and multiple bonds are used [Tees et al., 2001]. The most basic protocol is *constant loading*; in this case, the displacement of the transducer spring is kept constant which results in a constant force $f = f_t$ for shared and $f = f_b$ for non-cooperative loading. Constant forces are not usually used in single bond experiments but were applied in experiments with multiple bonds recently [Pierrat et al., 2004]. The other common loading protocol is *linear loading* in which the displacement is increased at a constant speed, $\ell(\tau) = vt$. For the linear elasticity as in the model of Fig. 2.3, this leads to a linearly increasing force $F_b(t) = m_b t$, where m_b is the (dimensional) loading rate. With the general expression (2.9) for the force per bond we have

$$F_b(t) = m_b t = \frac{k_b v t}{1 + \kappa i} \tag{2.17}$$

In dimensionless units, using k_0 as a scale for the time, we get the dimensionless force for linear loading

$$f_b(\tau) = \frac{k_b v / k_0 F_B}{1 + \kappa i} k_0 t = \mu_b \tau \,. \tag{2.18}$$

The dimensionless loading rate per closed bond, $\mu_b = (k_b v/k_0 F_B)/(1 + \kappa i)$, is related to m_b by

$$\mu_b = m_b / k_0 F_B \,. \tag{2.19}$$

where m_b depends on i. For the limiting case of shared loading we get

$$f_b(\tau) = \frac{k_t v / k_0 F_B}{i} k_0 t = \frac{\mu \tau}{i} = \frac{f(\tau)}{i} \,, \tag{2.20}$$

where the *loading rate of the whole cluster* is $\mu = k_t v/(k_0 F_B)$. For non-cooperative loading, the force is

$$f(\tau) = f_b(\tau) = \frac{k_b v}{k_0 F_B} k_0 t = \mu \tau \,, \tag{2.21}$$

where the *loading rate per bond* is $\mu = k_b v/(k_0 F_B)$.

2.2.2 Master equation for cluster dynamics

Thermally activated rupture and rebinding of single molecular bonds are stochastic events which implies that the dynamics of adhesion clusters has to be described as a stochastic process. We assume that every bond in the adhesion cluster is either open or closed at any given time. The total number of bonds in the cluster is denoted by N_t and is taken as a constant, $N_t = \mathrm{const}$. All bonds are assumed to be identical so that the state of the adhesion cluster is fully characterised by the number of closed bonds i (the number of open bonds is $N_t - i$). A stochastic process on the discrete set of states $0 \leqslant i \leqslant N_t$ can be described by a master equation for the probability distribution $\{p_i(\tau)\}_{i=0}^{N_t}$. The state probability function $p_i(\tau)$ is the probability that state i is occupied (or that i bonds are closed) at time τ.

Every bond in the adhesion cluster closes stochastically with the dimensionless on-rate γ and opens with the dimensionless off-rate $e^{f_b(i)}$, in which $f_b(i)$ is the dimensionless force per bond. The rate for a transition of any one of the molecular bonds in the adhesion cluster is given by the single bond rates times the number of candidates for the respective transition. Hence, the forward (or rebinding) rate g_i for closing one of the $N_t - i$ open bonds and the reverse (or rupture) rate for opening one of the i closed bonds are

$$g_i = g(i) := \gamma(N_t - i) \quad \text{and} \quad r_i = r(i) := i e^{f_b(i)}\,, \tag{2.22}$$

respectively. In general, the force per bond $f_b(i)$ may depend on time. If it depends on the number of closed bonds as in the general expression (2.12) or for shared loading (2.14), the reverse rate is a non-linear function of i. In the following we will refer to the single bond transition rates as on-rate and off-rate. The transition rates in the cluster are called forward (rebinding) and reverse (rupture) rate, respectively.

The transition of a single bond in the adhesion cluster changes the state i of the cluster to $i \pm 1$. Within a short time interval $\Delta\tau$ such a transition takes place with probability $(r_i + g_i)\Delta\tau$. The probability for two transitions in the same time interval is proportional to the square $(\Delta\tau)^2$. This defines a one-step process (also known as 'birth-death process') [van Kampen, 2003, Honerkamp, 1993] for which only transitions involving single bond transitions between neighbouring state are relevant. With a given probability distribution $\{p_i(\tau)\}_{i=0}^{N_t}$ at a time τ, the state probability $p_i(\tau+\Delta\tau)$ at time $\tau + \Delta\tau$ follows from the Chapman-Kolmogorov equation [van Kampen, 2003]:

$$p_i(\tau + \Delta\tau) = \{1 - (g_i + r_i)\Delta\tau\}\, p_i(\tau) + r_{i+1}\Delta\tau p_{i+1}(\tau) + g_{i-1}\Delta\tau p_{i-1}(\tau)\,. \tag{2.23}$$

The term in curly brackets is the probability that no transition takes place in the interval $\Delta\tau$ and the cluster stays in state i. The other terms are the probabilities to enter state i from one of the neighbouring states. Taking the limit for $\Delta\tau \to 0$ leads to the one-step master equation

$$\frac{d}{d\tau} p_i = r_{i+1} p_{i+1} + g_{i-1} p_{i-1} - \{r_i - g_i\}\, p_i\,. \tag{2.24}$$

It is a system of coupled, linear differential equations for the state probability functions $p_i(\tau)$. The initial condition is a δ-distribution $p_i(0) = \delta_{i,N_0}$ that is localised at the initial number of closed bonds N_0. If transitions with more than a single step in the interval $\Delta\tau$ had been included in (2.23), they would have vanished in the limit $\Delta\tau \to 0$. Because of the non-linear reverse rate, (2.24) is generally a *non-linear* one-step master equation[1]. Moreover, the reverse rate may depend on time if a time dependent force is assumed.

[1] A master equation is by definition a linear differential equation for the $p_i(\tau)$. In the particular case of a one-step process, the master equation is referred to as (non-)linear if the transition rates can be written as (non-)linear functions of i.

Because the set of states is finite, the boundaries of the system have to be specified. At the upper boundary (the completely bound state) at $i = N_t$, the forward rate vanishes, $g(N_t) = 0$. An initial condition with $N_0 \leqslant N_t$ leaves the states $i > N_t$ unoccupied. Hence, the completely bound state is a natural, reflecting boundary[2]. When the initial condition is chosen from the interval $0 \leqslant N_0 \leqslant N_t$, this reflecting boundary constrains the system naturally to states in the range $i \leqslant N_t$ and it does not need to be taken into account explicitly in a solution of the master equation.

The lower boundary (the completely dissociated state) at $i = 0$ requires more care. First, we have to require that the reverse rate r_0 vanishes, so that states with $i < 0$ remain unoccupied. This is not the case for shared loading where $f_b(i) = f/i$ and $r(i)$ diverges for $i = 0$. Here, the functional form (2.22) for the reverse rate cannot be used and $r_0 = 0$ imposes an artificial boundary condition at the dissociated state. Second, the definition (2.22) implies that the forward rate $g(0) = \gamma N_t$ is positive unless the on-rate itself vanishes. Therefore, broken bonds can close anew and the dissociated state is a reflecting boundary. However, in most experimental situations of interest, formation of new bonds is prevented by an elastic recoil of the transducer once the last bond is broken. This implies to use an absorbing boundary at $i = 0$ for which we have to set $g_0 = 0$. For $\gamma > 0$, this absorbing boundary is always an artificial boundary.

Shared loading

For shared loading of an adhesion cluster, the force per bond is given by $f_b = f/i$, where f is the force on the adhesion cluster. The transition rates are then given by

$$g_i = g(i) = \gamma(N_t - i) \quad \text{and} \quad r_i = r(i) = ie^{f/i} \tag{2.25}$$

for $0 < i \leqslant N_t$ and $r_0 = g_0 = 0$. The force dependent reverse rate is a strongly non-linear function of i. The non-linear master equation for shared loading is explicitly given by

$$\frac{d}{d\tau}p_i = (i+1)e^{f/(i+1)}p_{i+1} + \gamma(N_t - i + 1)p_{i-1} - \left\{ie^{f/i} + \gamma(N_t - i)\right\}p_i\,. \tag{2.26}$$

The transition rates may depend on time via a variable force $f(\tau)$. As described in the previous paragraph, the upper boundary at $i = N_t$ is a natural, reflecting boundary. The lower boundary is always artificial for $f > 0$ because $r_0 = 0$ has to be used. An absorbing boundary condition at the dissociated state is implemented by using $g_0 = 0$.

Non-cooperative loading

For non-cooperative loading, the force per bond is directly controlled so that $f_b = f$ enters the reverse rate. The transition rates are then given by

$$g(i) = \gamma(N_t - i) \quad \text{and} \quad r(i) = ie^{f}\,. \tag{2.27}$$

Both transition rates are linear so that the master equation for non-cooperative loading is also linear,

$$\frac{d}{d\tau}p_i = (i+1)e^{f}p_{i+1} + \gamma(N_t - i + 1)p_{i-1} - \left\{ie^{f} + \gamma(N_t - i)\right\}p_i\,. \tag{2.28}$$

[2]If the transition rates for a one-step process are given as functions of i, a boundary is referred to as a *natural* boundary if the functional definition applies also at the boundary and no additional constraints on the state functions p_i have to be imposed. An *artificial* boundary, on the other hand, requires a special value of the transition rates at the boundary. An example is the artificial absorbing boundary at $i = 0$ which is discussed next. In this case either $r_0 = 0 \neq r(0)$ and $g_0 = 0 \neq g(0)$ has to be used or, alternatively, $p_0 = 0$ could be required as a constraint.

Because $r(0) = 0$, the dissociated state is a natural boundary for a reflecting boundary. Requiring an absorbing boundary by setting $g_0 = 0$ we again have an artificial boundary. For a time dependent force, the reverse rate depends on time as well.

For shared and non-cooperative loading our model contains only three parameters: cluster size N_t, on-rate γ and force f. For shared loading, f is the force exerted on the transducer whereas for non-cooperative loading it is the force exerted on each of the bonds. For linear loading discussed in Chapter 4, the force is replaced by the loading rate μ as a parameter of the model. For a finite value of κ a fourth parameter would enter the model. This case will be studied in Chapter 5 where the model will be extended to include a distance dependent rebinding rate.

2.2.3 Dissociation rate and average lifetime of adhesion clusters

An adhesion cluster dissociates when the last closed bond breaks. The probability density of the stochastic dissociation time – or 'lifetime' – of an adhesion cluster is the dissociation rate

$$D(\tau) := \frac{d}{d\tau} p_0(\tau) = r_1 p_1(\tau)\,. \tag{2.29}$$

The second equality follows from the master equation (2.24) for p_0 with absorbing boundary condition $g_0 = 0$. The mean lifetime T of the adhesion cluster is the first moment of the distribution of dissociation times,

$$T := \langle \tau \rangle = \int_0^\infty \tau D(\tau)\, d\tau\,. \tag{2.30}$$

Higher moments $\langle \tau^n \rangle$ are calculated analogously. In the language of stochastic processes, $D(\tau)$ is the distribution of first passage time from the initial state $i = N_0$ to the detached state $i = 0$ and T is the mean first passage time. The mean first passage time alone can also be calculated without a solution for the master equation, that is, without calculating $D(\tau)$ explicitly [van Kampen, 2003].

For a time dependent force $f(\tau)$, the distribution of rupture forces is given by

$$D(f) = \frac{1}{df/d\tau} D(\tau(f))\,, \tag{2.31}$$

where $\tau(f)$ is the time at which a certain force is reached which is unique for a strictly monotonous increase of force. The average rupture force F is

$$F = \int_0^\infty f D(f)\, df = \int_0^\infty f(\tau) D(\tau)\, d\tau\,. \tag{2.32}$$

For a force increasing linearly in time, $f = \mu\tau$, the mean rupture force is given through the mean lifetime as $F = \mu T$. In dynamic force spectroscopy experiments, 'bond strength' is often defined as the maximum F_{max} of $D(f)$ [Evans and Ritchie, 1997, Merkel et al., 1999], i.e., by the condition

$$\left.\frac{d}{df} D(f)\right|_{f=F_{max}} = 0\,. \tag{2.33}$$

In the discussions of the following chapters we will focus on dissociation rate and average lifetime as characteristics for the dissociation process.

2.2.4 Deterministic approximation

A quantity of special interest is the average number of closed bonds

$$N(\tau) := \langle i \rangle := \sum_{i=0}^{N_t} i p_i(\tau) \,, \tag{2.34}$$

the first moment of the probability distribution $\{p_i(\tau)\}_{i=0}^{N_t}$. From the master equation (2.24) it follows that the time derivative of N is given by [van Kampen, 2003]

$$\frac{d}{d\tau} N = \sum_{i=0}^{N_t} i \frac{d}{d\tau} p_i = \langle g(i) - r(i) \rangle = \langle g(i) \rangle - \langle r(i) \rangle \,. \tag{2.35}$$

For linear transition rates, (2.35) leads to an ordinary differential equation for N:

$$\frac{d}{d\tau} N = g(\langle i \rangle) - r(\langle i \rangle) = g(N) - r(N) \,. \tag{2.36}$$

This equation allows to access the first moment of the probability distribution directly without solving the master equation. This makes it tempting to use it also for non-linear transition rates as it was done by Bell [1978] for constant shared loading and by Seifert [2000] for linear shared as well as non-cooperative loading. In the following (2.36) is referred to as the *deterministic equation* for the average number of closed bonds. This mean field description for N replaces the average over an ensemble of stochastic adhesion cluster trajectories by the single deterministic trajectory of a 'representative' adhesion cluster. It is exact for linear transition rates.

In principle, (2.36) is not valid for non-linear transition rates. However, for a localised distribution, forward and reverse rate can be expanded in a Taylor series around the average $N(\tau) = \langle i \rangle$ with $i = N + (i - N)$ as

$$h(i) = \sum_{n=0}^{\infty} \frac{h^{(n)}(N)}{n!} (i - N)^n \tag{2.37}$$

where $h(N)$ stands for the forward and reverse rate and $h^{(n)}(N) := d^n h(N)/dN^n$ denotes the n^{th} derivative. Inserting this expansion in (2.35) leads to

$$\frac{d}{d\tau} N = g(N) - r(N) + \sum_{n=2}^{\infty} \frac{g^{(n)}(N) - r^{(n)}(N)}{n!} \langle (i - N)^n \rangle \,. \tag{2.38}$$

The first order vanishes because $\langle i - N \rangle = 0$.

The time dependence of the averages $\langle (i - N)^n \rangle$ also follows from the master equation in analogy to (2.35). For example, the variance $\sigma_N^2 := \langle (i - N)^2 \rangle = \langle i^2 \rangle - \langle i \rangle^2$ is determined by [van Kampen, 2003]

$$\frac{d}{d\tau} \sigma_N^2 = \langle g(i) + r(i) \rangle + 2 \langle (i - N)(g(i) - r(i)) \rangle \,. \tag{2.39}$$

Inserting the expansion (2.37) of the transition rates, this becomes a differential equation for the variance which is coupled to the one for $N(\tau)$. For linear transition rates, this procedure leads to a hierarchy of coupled differential equations in which $\langle (i - N)^n \rangle$ is coupled only to those $\langle (i - N)^m \rangle$ with $m < n$. This allows to calculate the average deviations $\langle (i - N)^n \rangle$ recursively up to a given

order. For non-linear transition rates all differential equations are coupled to all other equations and the recursion is impossible. For the variance, (2.39) leads to

$$\frac{d}{d\tau}\sigma_N^2 = g(N) + r(N) + \sum_{n=2}^{\infty}\left\{\frac{g^{(n)}(N) + r^{(n)}(N)}{n!} + 2\frac{g^{(n-1)}(N) - r^{(n-1)}(N)}{(n-1)!}\right\}\langle(i-N)^n\rangle\,. \tag{2.40}$$

Solving the set of infinitely many coupled differential equations is impossible and one has to truncate the hierarchy at some order n and neglect all higher orders. Unlike the case of linear transition rates, this introduces an error in the differential equation which is on the order of magnitude of $\langle(i-N)^{n+1}\rangle$.

Taking only the first two orders of the expansion, the average and the variance, into account amounts to solving the pair of differential equations

$$\begin{aligned}\frac{d}{d\tau}N &= g(N) - r(N) + \frac{1}{2}\sigma_N^2\{g''(N) - r''(N)\}\\ \frac{d}{d\tau}\sigma_N^2 &= g(N) + r(N) + \sigma_N^2\left\{2(g'(N) - r'(N)) + g''(N) + r''(N)\right\}\,.\end{aligned} \tag{2.41}$$

Through the transition rates, these differential equations will in general be non-linear in N but are always linear in the higher order terms. The error in the differential equation is of the order of magnitude of the third cumulant $\kappa_N^3 = \langle(i-N)^3\rangle$. Typically, the ratio $\langle(i-N)^n\rangle/N^n$ decreases with increasing order n so that the corrections can be supposed to be small. A more thorough and elaborate expansion of the master equation in terms of the system size is demonstrated by van Kampen [2003].

In principle, a finite set of differential equations (2.41) can be solved numerically which allowed to construct the probability distribution of the number of closed bonds. Using only N and σ_N^2, the first two cumulants of the distribution, this approximate distribution is a Gaussian. Although fluctuations could be included in the deterministic description in this way, it is more instructive to solve the master equation directly. This solution contains fluctuations of all orders whereas the deterministic treatment has to be cut off at some finite order to become tractable. Moreover, the deterministic, mean field description can only use the transition rates in the functional form of (2.22), that is, it can treat only natural boundaries. However, the experimentally important case of an absorbing boundary requires an artificial boundary at $i = 0$.

Shared loading

For shared loading, the force per bond is f/i, where f is the force exerted on the whole cluster. The transition rates are given in (2.25), where the reverse rate $r(i)$ is a non-linear function of i. The deterministic equation (2.36) for shared loading reads

$$\frac{d}{d\tau}N = \gamma(N_t - N) - Ne^{f/N}\,. \tag{2.42}$$

This non-linear differential equation has first been studied for constant loading by Bell [1978] and later for linear loading by Seifert [2000]. Although only an approximation to the actual behaviour for the average, it allows valuable insight into generic features of the stochastic model as we will see in Chapters 3 and 4.

As our stochastic model, (2.42) contains three parameters, N_t, γ and f. But using the fraction $n(\tau) := N(\tau)/N_t$ of closed bonds allows to write the deterministic equation (2.42) in the form

$$\frac{d}{d\tau}n = \gamma(1-n) - ne^{(f/N_t)/n}\,, \tag{2.43}$$

which contains only two parameters: the on-rate γ and the ratio of force and cluster size, f/N_t. Solutions for $N(\tau)$ with different N_t are thus identical apart from a linear scaling with N_t. Quantities derived from N which do not involve an absolute measure for cluster size will be functions of γ and f/N_t only.

The differential equations (2.41) for the corrections of second order to the non-linear differential equation (2.42) explicitly read

$$\begin{aligned}\frac{d}{d\tau}N &= \gamma(N_t - N) - Ne^{f/N} - \sigma_N^2 e^{f/N}\frac{f^2}{2N^3} \\ \frac{d}{d\tau}\sigma_N^2 &= \gamma(N_t - N) + Ne^{f/N} - 2\sigma_N^2\left\{\gamma + e^{f/N}\left(1 - \frac{f}{N} - \frac{f^2}{4N^3}\right)\right\}\end{aligned} \tag{2.44}$$

A finite variance tends to reduce the average because the curvature of the reverse rate is negative. For small forces and large numbers of closed bonds, $f \ll N(\tau)$, the corrections due to σ_N^2 are small. They vanish for $f = 0$ because the master equation is linear and an exact, linear deterministic equation for N emerges from (2.44). For large forces and small clusters, the corrections grow and even diverge as $N \to 0$. The error imposed by using the deterministic equation (2.42) instead of the stochastic average over the distribution $\{p_i(\tau)\}_{i=0}^{N_t}$ will be large whenever large forces are exerted on small numbers of closed bonds. For finite force, $f > 0$, the reverse rate diverges for $N \to 0$ so that the number of closed bonds will become negative eventually. This is prevented in the stochastic description by using $r_0 = 0$. The variance σ_N^2 in (2.44) increases due to the first two terms which are linear in the transition rates. The additional contribution proportional to σ_N^2 is negative for sufficiently small $f/N \ll 1$. As long as the number of closed bonds is large, the increase in the variance can be balanced. If a cluster decays and N becomes very small, the variance grows with no bounds.

The corrections in (2.44) which result from the second derivative of $r(i)$ are proportional to f^2/N^3 and do not show scaling with f/N_t alone. They can only be neglected if $f \ll 1$, that is when the non-linearity is weak. Using N/N_t and σ_N^2/N_t as variables in (2.41) does not lead to the scaling with f/N_t alone. This reflects the fact that also the master equation cannot be treated in such a way.

Non-cooperative loading

For non-cooperative loading, the force f per bond is directly controlled. The transition rates for this case are given in (2.27). They are both linear in functions of N. The deterministic equation

$$\frac{d}{d\tau}N = \gamma(N_t - N) - Ne^f \tag{2.45}$$

is thus an exact equation for the average number of closed bonds. In particular, we see that N cannot become negative because the reverse rate now vanishes at $N = 0$. Also the variance of the distribution is determined exactly by the differential equation

$$\frac{d}{d\tau}\sigma_N^2 = \gamma(N_t - N) + Ne^f - 2\sigma_N^2\left\{\gamma + e^f\right\}, \tag{2.46}$$

in which the solution $N(\tau)$ from (2.45) enters. This equation does not diverge for $N \to 0$ so that the variance approaches a finite value. For the fraction of closed bonds $n = N/N_t$ and the variance in relation to the system size, $s_N^2 := \sigma_N^2/N_t$, the pair of differential equations is given by

$$\begin{aligned}\frac{d}{d\tau}n &= \gamma(1 - n) - ne^f \\ \frac{d}{d\tau}s_N^2 &= \gamma(1 - n) + ne^f - 2s_N^2\{\gamma + e^f\}\,.\end{aligned} \tag{2.47}$$

The solutions are fully determined by the two parameters γ and f. Not only the average but also the fluctuations scale linear in N_t for all orders n. The relative standard deviation scales as $\sigma_N/N \sim 1/N_t$ with system size.

2.3 Solutions of the dynamic equations

In the following we derive analytical solutions of the master equation (2.24) for several special cases. Analytical solutions for linear master equations can be derived via a generating function. This is the case for vanishing and non-cooperative constant loading. The use of the generating function is described in detail in Appendix A where solutions of (2.24) for vanishing force are given. For the case of vanishing rebinding, $\gamma = 0$, an analytical solution can be constructed also for shared loading using a recursive relation between the state probability functions. For small clusters with $N_t = 2$ an eigenvalue and eigenstate analysis is possible and allows to construct solutions.

In the general case, we use Monte Carlo simulations to solve the master equation numerically. In detail, for each set of parameter values N_t, f and γ, we generate an ensemble of 10^4 to 10^7 trajectories following the number of closed bonds i in an adhesion cluster over the course of time. To generate the trajectories, we use the Gillespie algorithm for exact stochastic simulations [Gillespie, 1976, 1977]. By cumulating the different simulation trajectories into a histogram, we obtain the desired probability distribution $\{p_i(\tau)\}_{i=0}^{N_t}$ as the relative frequency with which trajectories pass state i during a small time interval around τ. In general, it is also rather instructive to study single simulation trajectories, because their specific features are expected to be characteristic also for experimental trajectories. The Gillespie algorithm and its application to the master equation (2.24) is described in detail in Appendix B. The algorithm was originally developed for exact simulation of the stochastic dynamics of coupled chemical reactions. Applied to our case, open and closed bonds correspond to two different species of molecules and the transitions between these two species, that is rupture and rebinding, correspond to chemical reactions. The Gillespie algorithm is very efficient because it generates jumps between subsequent reactions rather than to discretise time in small steps. The basic quantity underlying the Gillespie algorithm is the waiting time distribution $w_\mu(\tau, \tau_0)d\tau$ which is the probability that the next reaction occurs in the time interval $[\tau_0+\tau, \tau_0+\tau+d\tau]$ and is of type μ under the condition that at time τ_0 the system has entered the current state. In our case, μ has only two values corresponding to rupture and rebinding, and the state of the system is completely described by the number of closed bonds i. For constant transition rates, w_μ depends only on the time interval between subsequent events. For time dependent rates as for linear loading, also the absolute time t_0 of the last transition becomes relevant. The detailed expressions and the method of implementation is described in Appendix B. This algorithm is exact in the sense that the only sources of inaccuracy lie in the choice of the random number generator and the finite number of trajectories used to calculate probability distribution. In particular, no additional inaccuracy due to the use of a finite time step is introduced.

The deterministic equation (2.36) for N is also solved if it is linear, that is, in cases where the master equation is solved by the generating function. For finite force and non-linear reverse rate but vanishing rebinding $\gamma = 0$, an implicit solution for $\tau(N)$ can be derived which has to be inverted numerically. Further analytical progress can be made with a scaling analysis of (2.36). Numerical solutions for the general case are obtained by integrating the deterministic equation with a standard integrator for ordinary differential equations. Specifically we use a fourth-order Runge-Kutta method ('Cash-Karp Runge-Kutta', [Press et al., 2002]). To determine the lifetime, the equation is integrated until only one last bond exists, that is, until $N = 1$ is reached.

Chapter 3

Constant loading

Constant loading in cell adhesion may be assumed as an approximation in situations where the environment of the adhesion site does not change much during the lifetime of the adhesion cluster. This includes, for example, adhesions of static cells or the adhesion of white blood cells when they have been arrested in the bloodstream. Experimentally, constant forces are difficult to access because the transducer position has to be controlled accurately. Theoretically, a constant force is the most basic loading protocol which also is the starting point for analysing the case of a time-dependent force.

In this chapter, we investigate adhesion cluster dynamics under constant force by analysing the master equation (2.26) and the deterministic equation (2.42). We begin with the simplest case of vanishing rebinding, $\gamma = 0$. Here, the decay of adhesion clusters follows a unique sequence which facilitates the analysis. Next, we discuss the dynamics of reversible clusters with $\gamma > 0$ but with vanishing force $f = 0$. In this case, the dynamic equations are linear. We close the chapter by the discussion of the general case with finite rebinding and finite force.

3.1 Vanishing rebinding

3.1.1 Deterministic analysis

We start our analysis with the case of vanishing rebinding, $\gamma = 0$. Then the deterministic equation (2.42) for shared loading reads

$$\frac{d}{d\tau}N = -Ne^{f/N}\,, \tag{3.1}$$

with $f = \mathrm{const}$. In principle, the total number of bonds N_t is irrelevant in this case. However, it is reintroduced through the initial condition $N_0 = N(0) = N_t$. Then (3.1) is solved implicitly by [Bell, 1978]

$$\tau(N) = \mathrm{E}\left(\frac{f}{N_t}\right) - \mathrm{E}\left(\frac{f}{N}\right) \tag{3.2}$$

where $\mathrm{E}(z) := \int_z^\infty (e^{-z'}/z')\,dz'$ is the exponential integral. Unfortunately, the inversion for $N(\tau)$ is not possible in general.

In the deterministic description, cluster lifetime T_{det} can be identified with the time $\tau(N = 1)$ at which only one last bond exists. Setting $N(T_{det}) = 1$ in (3.2) gives

$$T_{det} = \mathrm{E}\left(\frac{f}{N_t}\right) - \mathrm{E}(f)\ . \tag{3.3}$$

From this result, we can extract three different scaling regimes. For small force, $f \ll 1$, we use the small argument expansion of the exponential integral [Gradshteyn and Ryzhik, 1994], $\mathrm{E}\,(z) \approx -\,\Gamma - \ln z$ (where $\Gamma \simeq 0.5772$ is Euler's constant), and find

$$T_{det} \approx \ln N_t\,. \tag{3.4}$$

This corresponds to the familiar case of radioactive decay, when the differential equation $dN/d\tau = -N$ (Eq. (3.1) for $f = 0$) leads to an exponential decrease $N(\tau) = N_t e^{-\tau}$. This time dependence can also be extracted from (3.2). Replacing both exponential integrals by their small argument expansion leads to the expression

$$\tau(N) \approx -\ln\left(\frac{f}{N_t}\right) + \ln\left(\frac{f}{N}\right) = -\ln\left(\frac{N}{N_t}\right) \tag{3.5}$$

for the time as function of the number of bonds. Inverting this expression for $N(\tau)$ yields the exponential decay

$$N(\tau) = N_t e^{-\tau}\,. \tag{3.6}$$

This solution scales linearly with N_t as expected from the deterministic differential equation (2.43) for the fraction $N(\tau)/N_t$ of closed bonds. The lifetime, however, does not depend on the scaling variable f/N_t but on the absolute cluster size N_t, because the condition $N(T_{det}) = 1$ introduces a measure for the absolute size of the cluster in the equation (3.3) for the lifetime[1].

For intermediate force, $1 < f \ll N_t$, we can rewrite (3.3) for the cluster lifetime as the sum of two integrals,

$$T_{det} = \int_{f/N_t}^{1} \frac{e^{-z}}{z}\,dz + \int_{1}^{f} \frac{e^{-z}}{z}\,dz\,. \tag{3.7}$$

The second integral is bounded from above by $1/e$, because

$$\int_{1}^{f} \frac{e^{-z}}{z}\,dz < \int_{1}^{f} e^{-z}\,dz = e^{-1} - e^{-f} < e^{-1}\,. \tag{3.8}$$

In the first integral, we can expand the integrand for small arguments, leading to

$$\int_{f/N_t}^{1} \frac{e^{-z}}{z}\,dz \approx \int_{f/N_t}^{1} \frac{1-z}{z}\,dz \approx \ln\left(\frac{N_t}{f}\right)\,. \tag{3.9}$$

Since $N_t \gg f$ was assumed, the second integral in (3.7) can be neglected and we have

$$T_{det} \approx \ln\left(\frac{N_t}{f}\right)\,. \tag{3.10}$$

Because $f \ll N_t$, both exponential integrals in (3.2) can be replaced by the small argument approximation as long as $f \lesssim N(\tau)$. Thus, cluster decay will proceed exponentially in its initial phase until the for per bond reaches $f/N(\tau) \lesssim 1$. When $f/N(\tau) > 1$ exceeds the intrinsic force scale of the adhesion bonds, cluster dissociation will be faster than exponential due to the destabilising effect of force.

[1] Since $f/N_t = 0$, the lifetime has to be constant for different N_t. Without any numerical parameter at hand, this would imply either $T_{det} = 0$ or $T_{det} = \infty$. Since the lifetime has to be larger than zero, lifetime would be infinite without the condition $N(T_{det}) = 1$.

For large force, $f \gg N_t$, the second term in (3.3) can be neglected and we can use the large argument approximation for the exponential integral, $\mathrm{E}(z) \approx e^{-z}/(1+z)$, leading to [Bell, 1978]

$$T_{det} \approx \frac{e^{-f/N_t}}{1+f/N_t}\,. \tag{3.11}$$

Therefore cluster lifetime decreases faster than exponential with f/N_t in this regime. The small argument approximation is not applicable to either of the two terms in (3.2) and the decrease in N will be faster than exponential over the whole range of time .

In summary, the analysis of the deterministic equation (3.1) allows to identify three scaling regimes of small, intermediate and large force. For intermediate and large forces, the expressions for the lifetime depend only on the ratio f/N_t. The condition $N(T_{det}) = 1 =: N_{dis}$ for cluster dissociation is unimportant in these regimes due to the fast super-exponential decrease of N in the late stages of decay. For small force the trajectories are exponential throughout the decay process and the finite dissociation threshold becomes important (e.g. for $N_t = 1$ the lifetime is $T_{det} = 0$). The choice of this threshold is arbitrary. Although a different numerical value for N_{dis} leads to a logarithmic correction $\ln(N_t/N_{dis})$ in the result for the lifetime, it yields the same scaling with N_t as (3.4). To get rid of this arbitrariness the threshold has to be set to zero. This was done previously [Cozens-Roberts et al., 1990a,b], but for vanishing force it leads to an infinite deterministic lifetime which does not compare well to the stochastic result for the average lifetime, which is necessarily finite. Since N is supposed to be an estimate for the average number of bonds, using $N_{dis} = 0$ as a condition for cluster dissociation is misleading because it corresponds to the time when the last cluster in an ensemble dissociates.

3.1.2 Stochastic analysis

For finite force, $f > 0$, the reverse rate $r(i)$ in (2.25) is a non-linear function of i and the boundary at $i = 0$ is artificial. Therefore the master equation in general cannot be solved with standard techniques. However, in the case of vanishing rebinding, $\gamma = 0$, one can use the fact that the decay of the cluster corresponds to a unique sequence of events, with the number of closed bonds decreasing monotonously from N_t to 0. The transition from state i (with i closed bonds present) to the state $i-1$ (with one more broken bond) is a Poisson process with the time independent rate r_i. If i bonds are present at time τ, the probability that the next bond ruptures at time $\tau + \tau'$ is given by

$$p_{i\to i-1}(\tau') = r_i e^{-r_i\tau'}\,. \tag{3.12}$$

The state probability p_{i-1} is related to the state probability p_i and the transition probability $p_{i\to i-1}$ by the recursive expression

$$p_{i-1}(\tau) = \int_0^\tau p_i(\tau')p_{i\to i-1}(\tau-\tau')\,d\tau' = r_i e^{-r_i\tau}\int_0^\tau p_i(\tau')e^{r_i\tau'}\,d\tau'\,, \tag{3.13}$$

which uses the fact that the state $i-1$ can be reached only through the state i. This scheme is solved by

$$p_i(\tau) = \left\{\prod_{j=i+1}^{N_t} r(j)\right\}\sum_{j=i}^{N_t}\left\{e^{-r(j)\tau}\prod_{\substack{k=i\\k\neq j}}^{N_t}\frac{1}{r(k)-r(j)}\right\} \tag{3.14}$$

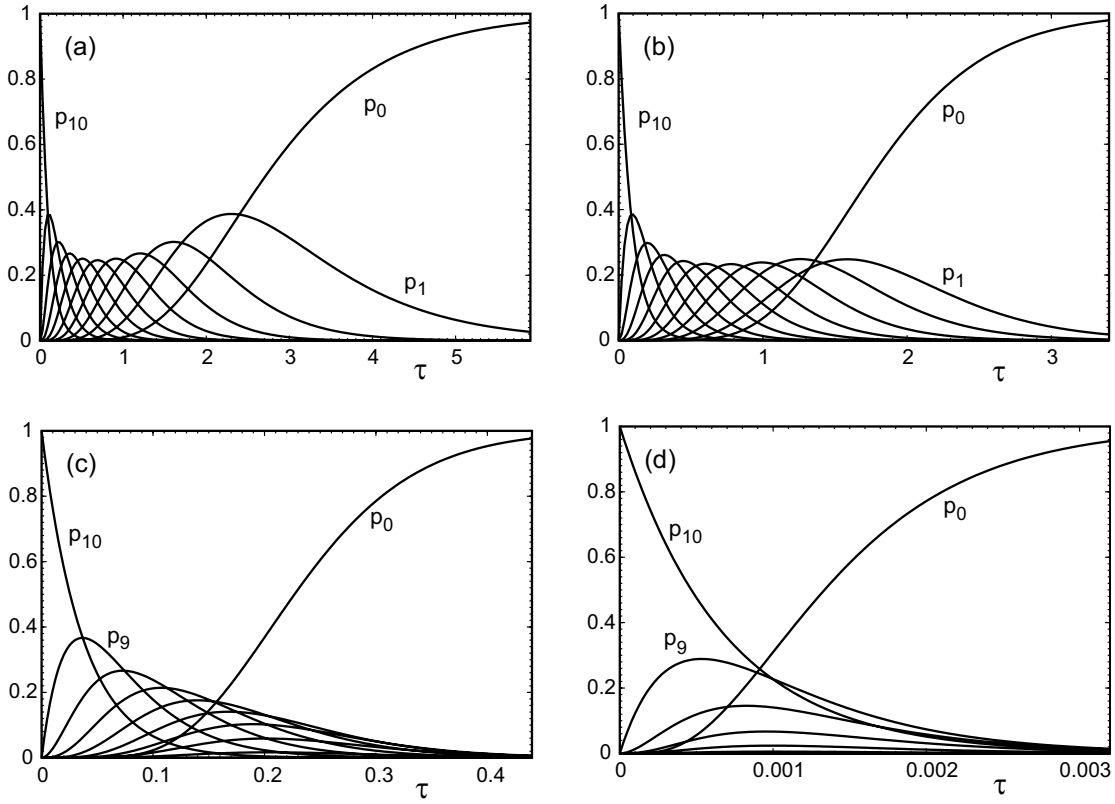

Figure 3.1: The state probability $p_i(\tau)$ is the probability that i bonds are closed at time τ ($0 \leqslant i \leqslant N_t$). Here, the p_i are plotted as a function of time τ for a cluster of initial size $N_t = 10$ for $\gamma = 0$ and (a) $f = 0$, (b) $f = 1$, (c) $f = 10$ and (d) $f = 50$. The force free decay in (a) corresponds to a stochastic 'radioactive decay' of N_t particles with constant rate.

as can be shown by induction . The properties of this expression follow from the properties of the reverse rate $r(i) = ie^{f/i}$, which for finite force, $f > 0$, is a non-monotonous function of i. It diverges for $i \to 0$, has a minimum at $i = [f]$ (the integer closest to f) and grows as i for $i \to \infty$. In the unlikely case that the value of f is such that $r(j) = r(k)$ for $j \neq k$, the limit of the expression in (3.14) for $r(k) \to r(j)$ has to be taken carefully. In order to treat this case properly, one has to replace (3.14) by

$$p_i(\tau) = \left\{ \prod_{j=i+1}^{N_t} r(j) \right\} \sum_{j=i}^{N_t} \left\{ e^{-r(j)\tau} \prod_{\substack{k=i \\ r(k)\neq r(j)}}^{N_t} \frac{1}{r(k) - r(j)} \prod_{\substack{k=i \\ r(k)=r(j) \\ k\neq j}}^{N_t} \frac{\tau}{2} \right\}, \tag{3.15}$$

where we have used

$$\lim_{\Delta \to 0} (1 - e^{-\tau\Delta})/\Delta = \tau \quad \text{with} \quad \Delta = r(i) - r(k) \tag{3.16}$$

for the factors $1/(r(i) - r(k))$ which appear with opposite sign in two terms of the sum in (3.14). In Fig. 3.1 we plot the full solution to the master equation, that is the state probabilities $p_i(\tau)$ from

(3.14), for $N_t = 10$ and four different values of force f. The case $f = 0$ gives the stochastic version of the radioactive decay with the binomial distribution $p_i = \binom{N_t}{i}(1 - e^{-\tau})^{N_t - i} e^{-i\tau}$. For small force, all states are appreciably occupied during the decay, that is, each of the curves is a maximum of the set of curves during a certain period of time. In the long run, p_0 approaches unity and all other p_i disappear, because without rebinding, the cluster has to dissociate eventually. For increasing force, the shape of the curves changes considerably. Now the lower states (with small number of closed bonds i) hardly become occupied during the decay process. For very large force, the maximum occupancy changes directly from the initial state N_t over to the detached state 0.

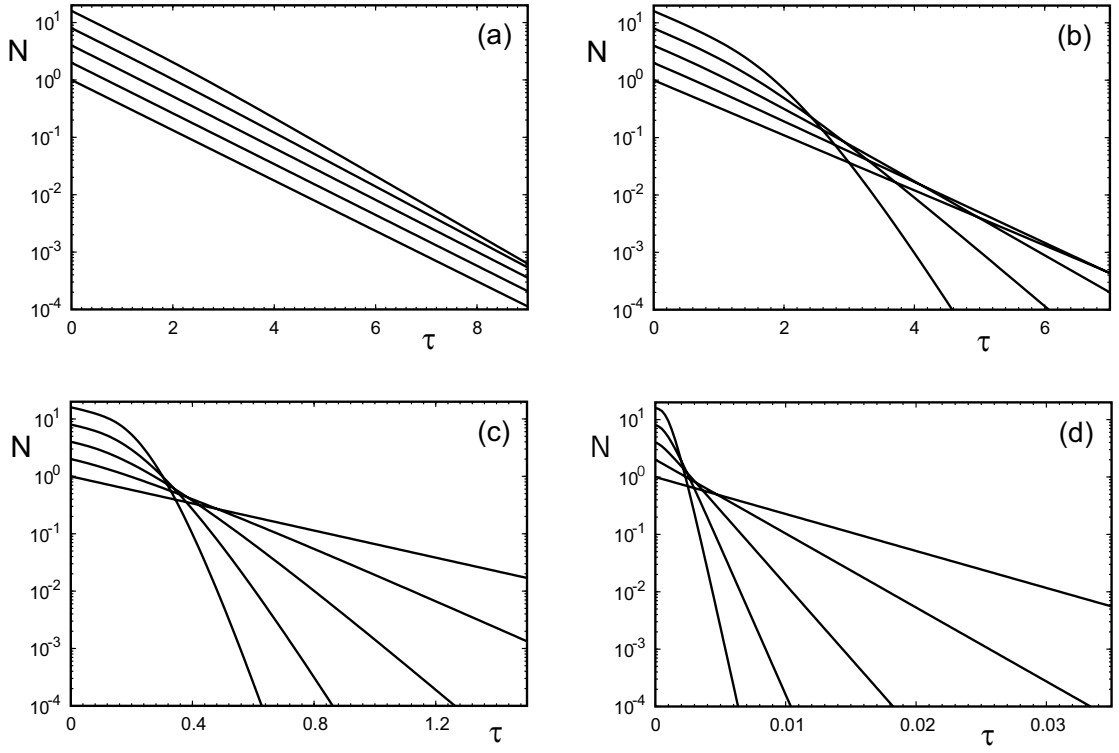

Figure 3.2: Average number of closed bonds N as a function of time τ for different cluster sizes $N_t = 1, 2, 4, 8$ and 16. (a) $f/N_t = 0.01$, (b) $f/N_t = 0.1$, (c) $f/N_t = 1.0$ and (d) $f/N_t = 5.0$.

With the exact solution (3.14), any quantity of interest can now be calculated. One quantity of large interest is the average number $N(\tau) = \langle i \rangle = \sum_{i=1}^{N_t} i p_i$ of closed bonds at time τ. For a single bond, N is simply the probability p_1 that the bond is attached,

$$N(\tau) = p_1(\tau) = e^{-e^f \tau} . \tag{3.17}$$

For a two-bond cluster we have

$$N(\tau) = p_1(\tau) + 2p_2(\tau) = \frac{2}{2 - e^{f/2}} \left\{ e^{-e^f \tau} + \left(1 - e^{f/2}\right) e^{-2e^{f/2}\tau} \right\} . \tag{3.18}$$

For increasing N_t, the corresponding expressions become increasingly cumbersome. In general, $N(t)$ is a sum of N_t exponentials with the different relaxation rates $r(i)$ with $1 \leqslant i \leqslant N_t$. For small force, $f \ll 1$, $r(i) \approx i$ and the smallest rate corresponds to $i = 1$, that is, $N \sim e^{-\tau}$ on large time-scales.

In this case where the influence of force could be neglected, clusters of any size decay with the same slope as single bonds and the difference between single and multiple bond rupture lies in the prefactor, not in the time-scale of average decay. For intermediate force, $1 < f \ll N_t$, and large time-scales, decay is dominated by $i = [f]$, that is $N \sim e^{-fe\tau}$. Thus the absolute value of force governs the long time behaviour, with different sizes showing up only in the prefactor. For large force, $f \gg N_t$, decay at large time-scales is dominated by $i = N_t$, that is $N \sim e^{-N_t e^{f/N_t}\tau}$. This implies that for a given force f, the largest clusters show the slowest decays in the long run. However, if one controls f/N_t rather than f, the cluster with the smallest size will decay the slowest, since it is subject to the smallest absolute force. In Fig. 3.2 we plot $\log N$ as a function of time τ for different values of cluster size N_t and force per initial bond, f/N_t. The initial behaviour is described by $N \simeq N_t e^{-\tau e^{f/N_t}}$ so that the initial slope in the logarithmic plot is identical for given f/N_t with different N_t . For small forces, decay stays exponential for almost all times. The larger force, the earlier decay crosses over to the late stage regime described above.

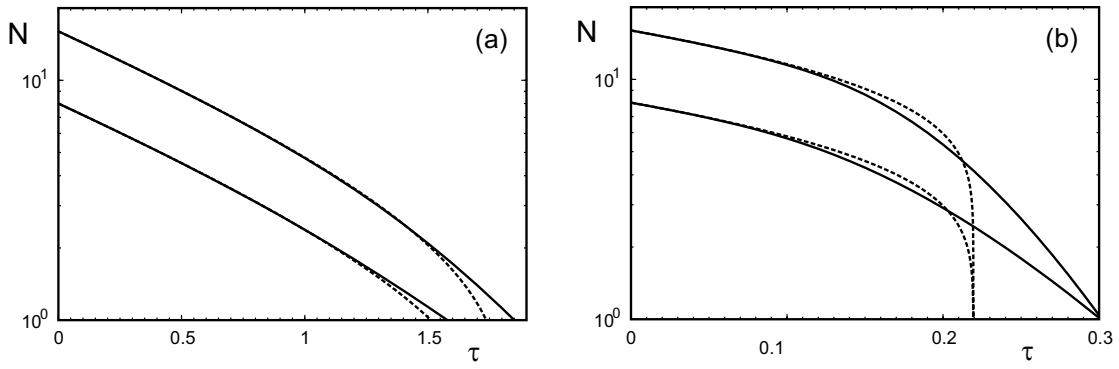

Figure 3.3: Average number of closed bonds N as a function of time τ for $N_t = 8$ and 16 and (a) $f/N_t = 0.1$ and (b) $f/N_t = 1$. Solid and dashed lines are stochastic and deterministic results, respectively.

As noted in Sec. 2.2.2, due to the non-linear form of $r(i) = ie^{f/i}$ for $f > 0$, the first moment $N(\tau)$ of the stochastic solution (3.14) is not identical with the function $N(\tau)$ obtained from the deterministic equation (3.1). In Fig. 3.3, results for $N(\tau)$ derived from the deterministic and the stochastic description are compared to each other. For a small but non-zero force, the non-linearity is small and the agreement between the two results is good in the initial phase of the decay. Towards the end of the decay strong deviations are observed. Here, the force on each bond grows strongly and the non-linearity of the transition rates is large. For increasing force, deviations appear also in earlier stages of decay. The deterministic results in Fig. 3.3b show a very steep breakdown since $r(N)$ and with it $dN/d\tau$ diverges for $N \to 0$. Because of the scaling with f/N_t alone, the time-point of breakdown, the deterministic lifetime T_{det}, is identical for both curves. The same divergence is present for the small forces but the cutoff at $N(T_{det}) = 1$ leads to the different lifetimes for different N_t. The stochastic results show a much smoother decrease of $N(\tau)$, especially for small clusters. Only the curves for large clusters approach the deterministic result. The stochastic results for $N(\tau)$ show no scaling with f/N_t alone because the solutions of the master equation include all moments of the probability distribution $\{p_i(\tau)\}_{i=0}^{N_t}$.

In Fig. 3.4a and b the result for the mean number of closed bonds $N(\tau)$ is compared to single simulation trajectories for small and large forces, respectively. The trajectories are generated with the

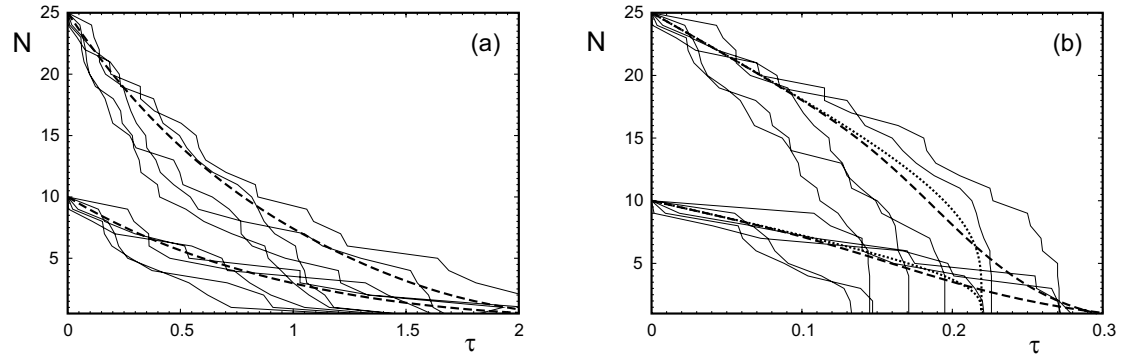

Figure 3.4: Single simulation trajectories (solid lines) compared with the average number of closed bonds $N(\tau)$ (dashed lines) for $N_t = 10$ and 25 and (a) $f/N_t = 0.1$ and (b) $f/N_t = 1$. In (b), in addition the deterministic results are plotted as dotted lines.

Gillespie algorithm which is described briefly in Sec. 2.3 and in detail in Appendix B. The single simulation trajectories are expected to resemble experimental realisations for the time evolution of the number of closed bonds. The figure shows that for small force, the trajectories decay in a similar way as does the average. For large force, the decay of the trajectories is strongly accelerated towards the end of the decay process. A decrease of i initiates a runaway process, since force is increasingly focused on less and less bonds due to shared loading. This type of rupture process is similar to avalanches or cascading failures in highly connected systems. Although rupture is rather abrupt, its time-point is widely distributed, leading to the smooth decrease of $N(\tau)$ observed in the average. In the large force case in Fig. 3.4b, we also show the deterministic results for $N(\tau)$ (for the small force case in Fig. 3.4a, they hardly differ from the stochastic results). These curves show that the typical shape with a rather abrupt decay of the single simulation trajectories at large force is reflected by the deterministic description, compare Fig. 3.3. This had to be expected because the deterministic equation describes a representative yet single trajectory.

The probability for dissociation of the overall cluster (that is for rupture of the last bond) was defined in (2.29) by $D(\tau) = \dot{p}_0(\tau) = r_1 p_1(\tau)$. It follows from (3.14) with the reverse rate r_1 from (2.25). The resulting formula has been given in Tees et al. [2001]. For a single bond it is simply $D(\tau) = e^f e^{-e^f \tau}$. For $N_t = 2$ we have

$$D(\tau) = \frac{2e^f}{2 - e^{f/2}} \left\{ e^{-e^f \tau} - e^{-2e^{f/2}\tau} \right\} . \tag{3.19}$$

In the special case $f = 2 \ln 2$, the two rates $r(1)$ and $r(2)$ are equal and we have

$$D(\tau) = 16 \tau e^{-4\tau} . \tag{3.20}$$

In general, as for $N(\tau)$, $D(\tau)$ is a sum of exponentials $e^{-r(i)\tau}$ and the decrease on long time-scales is governed by the exponential which decreases the slowest. In Fig. 3.5 we plot $D(\tau)$ for different values of N_t and f/N_t (by controlling f/N_t rather than f, the curves have comparable averages). The case $N_t = 1$ is a Poisson process with simple exponential decay. For $N_t > 1$, $D(0) = 0$, because instantaneous rupture of all bonds at $\tau = 0$ is a higher order process. For large times, all curves decay exponentially. For vanishing force, $f = 0$, the curves are very similar, with the same slope at large times. The maxima of the cluster dissociation rates for $f = 0$ are described by $T_{max} = \ln N_t$, in

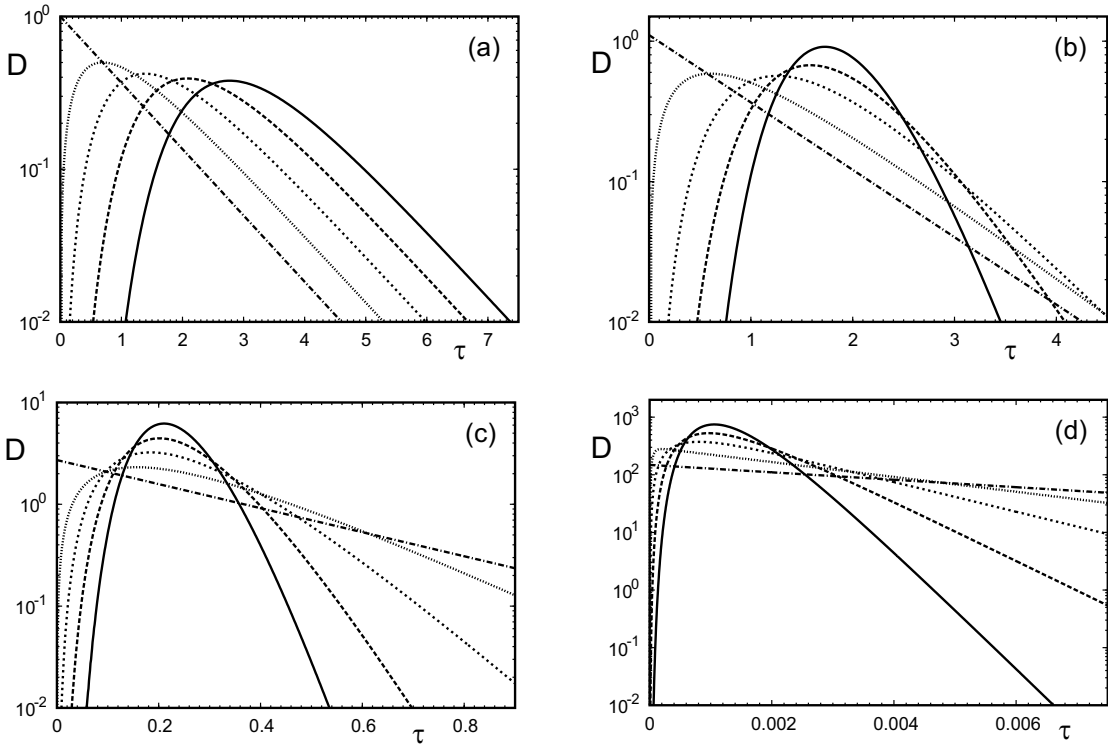

Figure 3.5: Probability for dissociation of the whole cluster D as a function of time τ for $N_t = 1, 2, 4, 8$ and 16 (left to right in (a)) for (a) $f/N_t = 0.0$, (b) 0.1, (c) 1.0 and (d) 5.0.

agreement with the result (3.4) from the deterministic description. For small f/N_t, the distributions are Gauss-like with small asymmetry and variance. For large f/N_t, they become Poisson-like, that is they develop a strong asymmetry with a maximum close to zero and a pronounced long-time tail. The reason is that in this case, decay is dominated by rupture of the first bond, that is, we are effectively back to a single bond system (except that $D(0) = 0$ as always for multiple bonds).

The average cluster lifetime can in principle be calculated as the first moment of the overall dissociation rate

$$T = \int_0^\infty \tau \, D(\tau) \, d\tau \, . \tag{3.21}$$

In practice, for $\gamma = 0$, it has a simple form which can be derived without using the probability distribution (3.14). The waiting time spent in state i before the transition into state $i-1$ is a stochastic variable characterised by the distribution function (3.12). Its average is given by the inverse transition rate $1/r(i)$. Since the decay process is a sequence of such independent Poisson processes, we simply have

$$T = \sum_{i=1}^{N_t} \frac{1}{r(i)} \, . \tag{3.22}$$

For $f = 0$ we get [Goldstein and Wofsy, 1996, Tees et al., 2001]

$$T = \sum_{i=1}^{N_t} \frac{1}{i} = \mathrm{H}_{N_t} \tag{3.23}$$

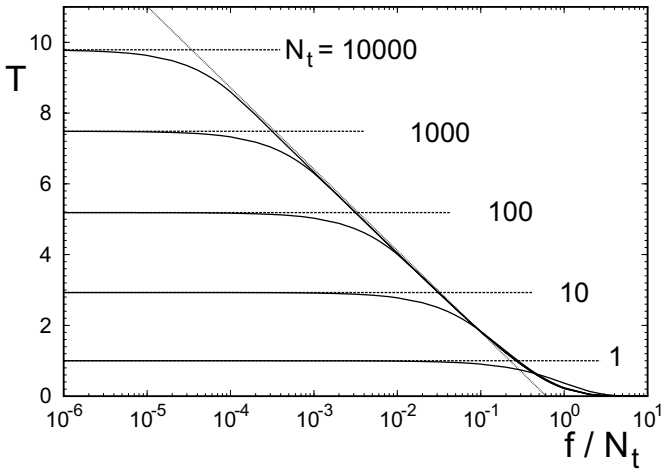

Figure 3.6: Average adhesion cluster lifetime T as a function of f/N_t for cluster sizes $N_t = 1, 10, 10^2, 10^3$ and 10^4. The dashed horizontal curves are the harmonic numbers, which are good approximations in the small force regime, $f \ll 1$. The dotted curve is the approximation $T = \ln(0.61 N_t/f)$ for the intermediate force regime, $1 < f \ll N_t$.

which are the harmonic numbers. The lifetime of a two-bond cluster is increased by a factor $3/2 = 1.5$ with respect to the single bond, that of the three-bond cluster by $11/6 = 1.8$, and so on. For large N_t one can write [Goldstein and Wofsy, 1996]

$$T \approx \ln N_t + \frac{1}{2N_t} + \Gamma \tag{3.24}$$

where $\Gamma \simeq 0.5772$ is Euler's constant. In fact this approximation is very good already for small values of N_t. The weak (logarithmic) dependence for large N_t means that for large adhesion clusters, size matters little since the bonds decay independently of each other and on the same time-scale. This result differs from the deterministic one for small force, (3.4), by the constant Γ and the additional contribution $1/2N_t$, which vanishes for large clusters. For small force, $f \ll 1$, (3.24) is a good approximation for cluster lifetime T. For intermediate force, $1 < f \ll N_t$, the reverse rate grows rapidly for states with $i < f$, whereas for states with $i > f$, $r(i)$ remains close to i. Therefore we can approximate the average lifetime of a cluster as $\mathrm{H}_{N_t} - \mathrm{H}_f$. Using (3.24), we get

$$T \simeq \ln(N_t/f) \ . \tag{3.25}$$

Thus cluster size N_t is now replaced by an effective size N_t/f, as we have already found in the deterministic framework, compare (3.10). For large force, $f \gg N_t$, the only term which contributes to (3.22) is the one for the rupture of the first bond. Then

$$T \approx \frac{e^{-f/N_t}}{N_t} \tag{3.26}$$

and we deal essentially with a single bond effect: if the first bond breaks, all remaining bonds follow within no time ('domino effect'). This effect is also evident from the dissociation rate $D(\tau)$, which for very large force approaches a Poisson distribution, compare Fig. 3.5d. In (3.26), the numerator represents the probability for single bond rupture under force, while the denominator represents the probability that any one out of N_t identical bonds breaks first. Since $f \gg N_t$ in this regime, the first effect dominates and T increases with N_t. For a given f/N_t, on the other hand, the lifetime decreases with increasing N_t, due to the increase in absolute force. In contrast to the deterministic result, (3.11), the stochastic result (3.26) does not scale with f/N_t. In Fig. 3.6 we plot the average cluster lifetime T from (3.22) as a function of f/N_t for different values of N_t. For small force, $f \ll 1$, T plateaus at

the value given by the harmonic number H_{N_t} according to (3.23). In the regime of intermediate force, $1 < f \ll N_t$, all curves with sufficiently large N_t fall on the master curve $T = \ln(0.61(N_t/f))$, as predicted by (3.25). For large force, $f \gg N_t$, the scaling with f/N_t is lost, as predicted by (3.26). Although deterministic and stochastic predictions for cluster lifetime T have similar overall features, the deterministic result underestimates the plateau at small force and predicts an incorrect scaling with f/N_t at large force.

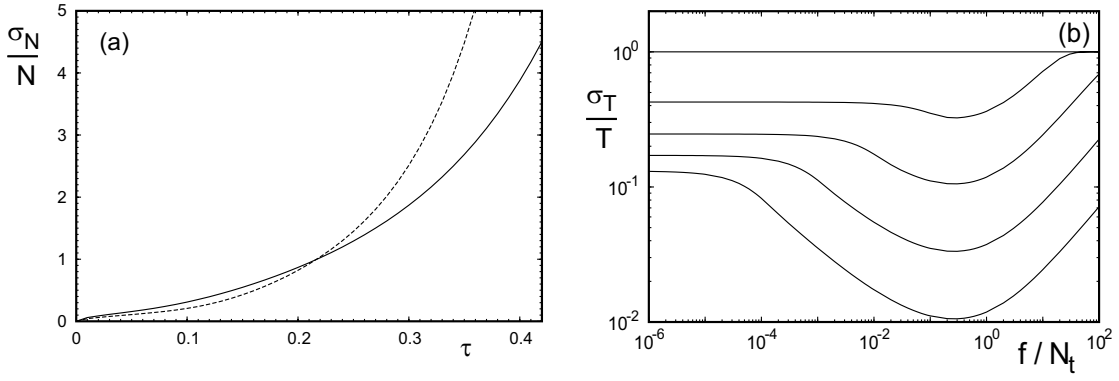

Figure 3.7: (a) Relative standard deviation σ_N/N for the number of closed bonds as function of time τ for $f/N_t = 1.0$ and $N_t = 8$ (solid) and 16 (dashed). (b) Relative standard deviation σ_T/T for cluster lifetime as a function of f/N_t for $N_t = 1, 10, 10^2, 10^3$ and 10^4.

Higher cumulants of the various distributions provide information about the effect of fluctuations. For the number of closed bonds at time τ, the width of the distribution is described by the variance, defined by $\sigma_N^2(\tau) = \langle i^2 \rangle - \langle i \rangle^2$. In Fig. 3.7a, we plot the relative standard deviation, $\sigma_N(\tau)/N(\tau)$, calculated by summation over the distribution (3.14) for cluster sizes $N_t = 8$ and $N_t = 16$. It is zero initially due to the initial condition and diverges for large times. In regard to the distribution of cluster lifetime, the variance σ_T^2 can be calculated in the same way as the average lifetime, because for a sequence of independent stochastic processes, all cumulants simply add up. The variance of the Poisson process (3.12) is $1/r^2(i)$. Therefore the variance for cluster lifetime is

$$\sigma_T^2 = \sum_{i=1}^{N_t} \frac{1}{r^2(i)} \,. \tag{3.27}$$

For vanishing force this expression reads

$$\sigma_T^2 = \sum_{i=1}^{N_t} \frac{1}{i^2} = \zeta(2) - \psi^{(1)}(N_t + 1) \,, \tag{3.28}$$

where $\psi^{(1)}(N_t + 1)$ is the trigamma function and ζ the Riemannian ζ-function [Gradshteyn and Ryzhik, 1994]. For increasing N_t, the variance converges to a finite value. For zero force, this limit is the well-known relation [Aigner and Ziegler, 2004]

$$\sigma_T^2 = \sum_{i=1}^{\infty} \frac{1}{i^2} = \zeta(2) = \frac{\pi^2}{6} \,. \tag{3.29}$$

This result is an upper limit for the variance in general, because the reverse rate increases with increasing force, $r(i) \geqslant i$. The relative standard deviation σ_T/T of cluster dissociation is always smaller than unity, since $(\sum x)^2 \geqslant \sum x^2$. For single bond rupture, we have a single Poisson process and it becomes exactly unity. For vanishing force and large clusters, it scales as $\sim 1/\ln N_t$. Although it decreases with increasing N_t, it does so in a different way than the Gauss process, which decreases as $\sim 1/N_t^{1/2}$. The reason is that the contributions from the different subprocesses are not constant, but decrease as rupture proceeds. For large forces, $f \gg N_t$, cluster dissociation becomes a Poisson process governed by the rupture of the first bond. Then the first term dominates in (3.22) and (3.27). Therefore the relative standard deviation $\sigma_T/T \approx 1$ again. In Fig. 3.7b, we plot σ_T/T as a function of f/N_t as it crosses over between the cases of vanishing and very large force, with a minimum around $f/N_t \approx 0.3$, that is, in the intermediate force range. The narrow distribution at intermediate force is also evident in Fig. 3.5. Moreover, now $\sigma_T/T \sim 1/N_t^{1/2}$, because only the first $N_t - f$ subprocesses contribute, with roughly similar values, like in a Gauss-distribution. Fig. 3.7b also shows how the relative standard deviation decreases with increasing cluster size N_t. In general, the agreement between deterministic and stochastic description is best for large cluster size N_t and intermediate force $1 < f \ll N_t$. However, as noted above, the definition of deterministic lifetime is to a certain extent arbitrary, because a discrete cutoff has to be introduced in a continuum description. In particular for small clusters and small forces, the choice of the cluster size at which dissociation occurs will have a large influence on T.

3.2 Vanishing force

3.2.1 Deterministic analysis

We now turn to the case of vanishing force, $f = 0$. Then the deterministic equation (2.36) reads

$$\frac{d}{d\tau}N = \gamma(N_t - N) - N\,. \tag{3.30}$$

For the initial condition $N(0) = N_t$, its solution is

$$N(\tau) = \frac{\gamma + e^{-(1+\gamma)\tau}}{1+\gamma}N_t = \left\{1 + \frac{1}{\gamma}e^{-(1+\gamma)\tau}\right\}N_{eq}\,. \tag{3.31}$$

Thus, there is an exponentially fast relaxation from N_t to the equilibrium state with $N_{eq} = \gamma N_t/(1+\gamma)$ closed bonds. N_{eq} increases linearly with the rebinding constant γ from $N_{eq} = 0$ for $\gamma = 0$ and saturates at N_t for $\gamma > 1$. In the deterministic description, the lifetime of the cluster is infinite, because the completely dissociated state $N = 0$ is never reached.

3.2.2 Stochastic analysis

In the case $f = 0$, the reverse rate defined in (2.25) is linear in i and $r(0) = 0$ at $i = 0$. Natural boundary conditions imply $g(0) = \gamma N_t$, that is, a reflecting boundary at $i = 0$. A linear master equation with natural boundaries can be solved with standard techniques, namely by deriving a generating function. For general initial conditions, solutions were derived by McQuarrie [1963] and a collection can be found in Goel and Richter-Dyn [1974]. For the specific master equation (2.26), they are listed in Appendix A. For the initial condition $p_i(0) = \delta_{i,N_t}$, the generating function given in (A.18) by

$$G(s,\tau) = \sum_{i=0}^{N_t} s^i p_i(\tau) = \left[\frac{1 + s\gamma - (1-s)e^{-(1+\gamma)\tau}}{1+\gamma}\right]^{N_t}\,. \tag{3.32}$$

The state probabilities follow from the generating function as

$$p_i(\tau) = \frac{1}{i!}\,\frac{\partial^i}{\partial s^i} G(s,\tau)\bigg|_{s=0} = \binom{N_t}{i} \frac{\left[\gamma + e^{-(1+\gamma)\tau}\right]^i \left[1 - e^{-(1+\gamma)\tau}\right]^{N_t - i}}{(1+\gamma)^{N_t}}\,. \tag{3.33}$$

One can easily check that by setting $\gamma = 0$ in (3.33), one obtains the same result as by setting $f = 0$ in (3.14). Eq. (3.33) shows that the system relaxes to the stationary state on a dimensionless time-scale $1/(1+\gamma)$, thus the larger rebinding, the faster the system equilibrates. In the stationary state, the state probabilities follow a binomial distribution

$$p_i(\infty) = \binom{N_t}{i} \frac{\gamma^i}{(1+\gamma)^{N_t}} \tag{3.34}$$

because the bonds are independent and each bond is closed and open with probabilities $\gamma/(1+\gamma)$ and $1/(1+\gamma)$, respectively.

The generating function also allows to calculate all moments of the distribution using the relation (A.6) given in Appendix A. Since now $r(i)$ is linear in i, the first moment $N(\tau) = \langle i \rangle$ is identical to the solution (3.31) of the deterministic equation. In order to assess the role of fluctuations, we calculate the variance

$$\sigma_N^2(\tau) = \langle i^2 \rangle - \langle i \rangle^2 = \frac{1 - e^{-(1+\gamma)\tau}}{1+\gamma} N(\tau)\,. \tag{3.35}$$

This is also a solution of the deterministic equation (2.44) for σ_N^2 in the case $f = 0$. The relative standard deviation σ_N/N scales as $N^{-1/2}$ for all times, thus fluctuation effects decrease with increasing bond number in the usual way. The stationary state value is

$$\lim_{\tau\to\infty} \frac{\sigma_N(\tau)}{N(\tau)} = ((1+\gamma)N_{eq})^{-\frac{1}{2}} = (\gamma N_t)^{-\frac{1}{2}}\,. \tag{3.36}$$

Therefore, larger rebinding does not only increase the equilibrium number of bonds, but also decreases the size of the fluctuations around N_{eq}. This leads to a narrow distribution for large cluster under strong rebinding, with a small probability of coming close to the lower boundary.

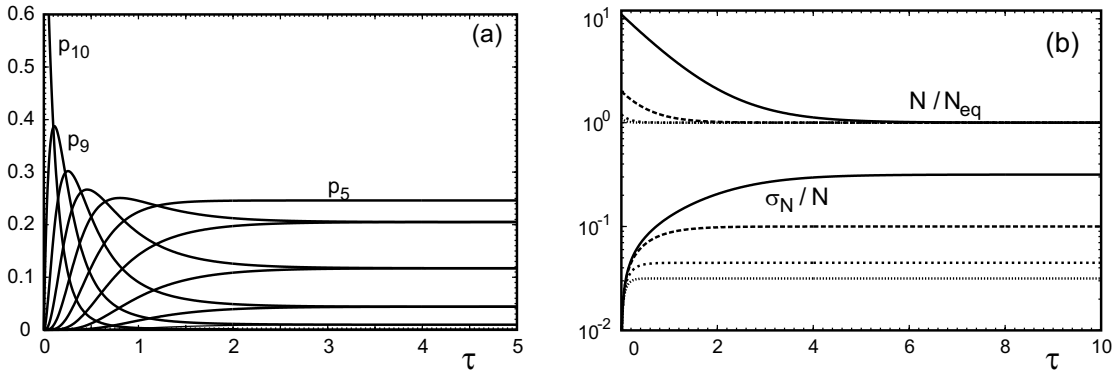

Figure 3.8: (a) State probabilities $p_i(\tau)$ from (3.33) for $N_t = 10$ with $f = 0$ and $\gamma = 1$ for a reflecting boundary at $i = 0$. (b) N/N_{eq} and σ_N/N for $N_t = 100$, $f = 0$ and $\gamma = 0.1$, 1, 5 and 10 (solid to finely dotted curves).

In Fig. 3.8a, we plot the state probabilities p_i from (3.33) for cluster size $N_t = 10$ and rebinding constant $\gamma = 1$. The system quickly relaxes to the equilibrium state. The only difference for different initial conditions is in the initial transient. In particular, for $N_0 = N_{eq}$, the average does not change in time, although the distribution initially spreads to the binomial one. For $\gamma = 1$, the stationary distribution is symmetric around the average. The width of the distribution for different γ is illustrated in Fig. 3.8b, which shows the average number of closed bonds normalised by the equilibrium number of bonds, that is N/N_{eq}, together with the relative standard deviation, σ_N/N, for different values of the rebinding constant γ. The curves for N are independent of N_t due to the normalisation. Fig. 3.8b shows that with increasing γ, relaxation becomes faster and the width of the distribution decreases.

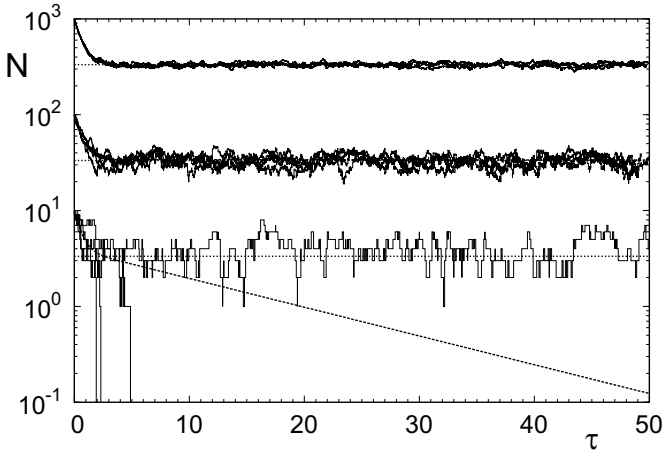

Figure 3.9: Single simulation trajectories for $f = 0$, $\gamma = 0.5$, $N_t = 10, 100$ and 1000 and an absorbing boundary at $i = 0$. Dashed lines are the average number of closed bonds N and dotted lines are the equilibrium number of closed bonds N_{eq}.

For the experimentally important case of an absorbing boundary at $i = 0$, it seems to be rather difficult to find a closed-form analytical solution for arbitrary cluster sizes. For the case $N_t = 2$, we will present such a solution in the next section. For arbitrary N_t, we use Monte Carlo simulations with the Gillespie algorithm. In Fig. 3.9, we show individual simulation trajectories for different parameter values of interest, in comparison to the average number of closed bonds for reflecting and absorbing boundaries at $i = 0$. The plots show that the number of closed bonds in a cluster first relaxes towards the steady state value, for which rupture and rebinding balance each other. Although for the absorbing boundary the number of closed bonds decreases with time in average, for individual realisations it stays roughly constant, until a large fluctuation towards the absorbing boundary leads to loss of this realisation. The time-scale for the decrease in N is thus determined by the probability for fluctuations from the steady state to the absorbing boundary.

Because a full analytical solution is not available for the case of an absorbing boundary, we now introduce an approximation for this case. It is similar to the local thermal equilibrium description introduced by Zwanzig [1995] for modelling protein folding dynamics. Our starting point is that for large clusters and strong rebinding, the absorbing boundary is a small perturbation to the solution for the reflecting boundary, (3.33), which in the following we will denote by $\{\bar{p}_i\}_{i=0}^{N_t}$. Since $g_0 = 0$ for the absorbing boundary, $\dot{p}_0 = r_1 p_1$ with $r_1 = 1$ and probability will accumulate in the completely dissociated state. Since p_0 is slaved to the other state probabilities and since we expect only a small perturbation for the states with $i \geqslant 1$, we assume that the different boundary only leads to a simple renormalisation caused by the 'leakage' into the absorbing state:

$$p_i(\tau) = \bar{p}_i(\tau)\,(1 - p_0(\tau)) \text{ for } i \geqslant 1 \quad \text{and} \quad p_0(\tau) = \int_0^\tau p_1(\tau')\,d\tau' \,. \tag{3.37}$$

Since relaxation to the steady state is faster than decay to the absorbing boundary, $\bar{p}_i(\tau)$ can be taken

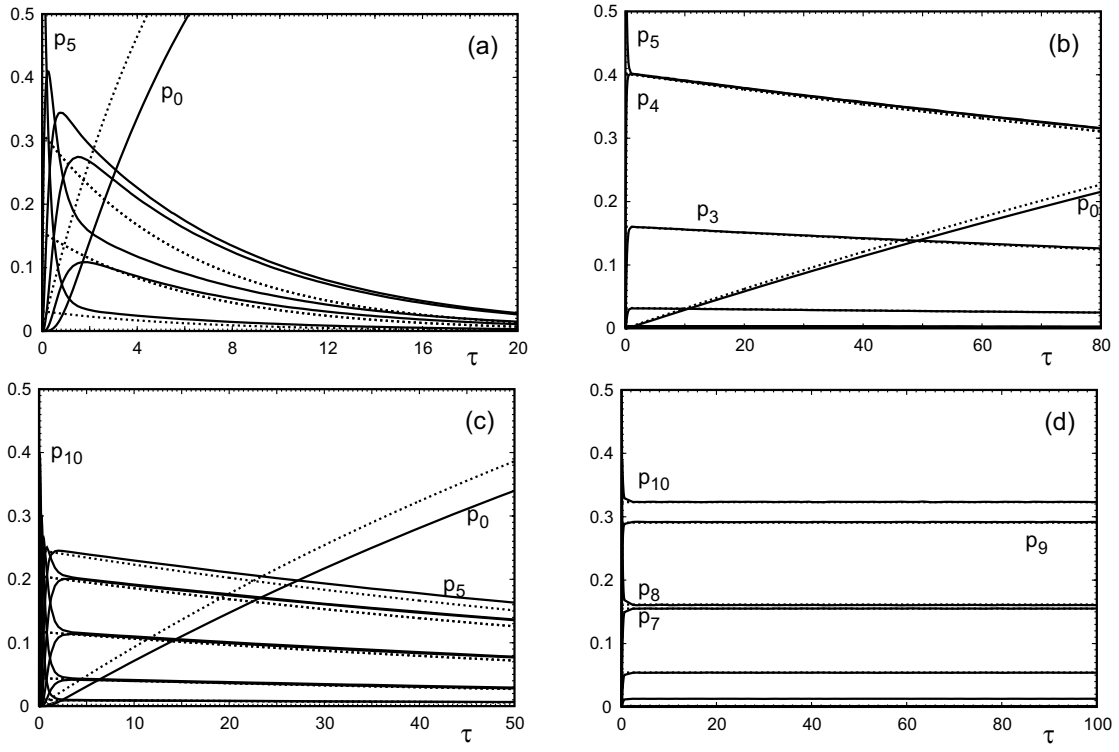

Figure 3.10: State probabilities p_i as a function of time τ for different cluster sizes $N_t = 5$ (a and b) and $N_t = 10$ (c and d) and for rebinding rates $\gamma = 1.0$ (a and c) and 5.0 (b and d). The numerical solutions (solid curves) are compared to the leakage approximation (3.39) (dashed curves).

to be the stationary value, that is the constant $\bar{p}_i(\infty)$ according to (3.34). Then

$$p_0(\tau) = \bar{p}_1(\infty) \int_0^\tau \big(1 - p_0(\tau')\big)\, d\tau' \,, \tag{3.38}$$

which is solved by $p_0(\tau) = 1 - e^{-\bar{p}_1(\infty)\tau}$. Therefore (3.37) simplifies to

$$\begin{aligned} p_i(\tau) &= \bar{p}_i(\infty) e^{-\bar{p}_1(\infty)\tau} \quad \text{for } i \geqslant 1, \\ p_0(\tau) &= 1 - e^{-\bar{p}_1(\infty)\tau} \,. \end{aligned} \tag{3.39}$$

We conclude that the solution decays exponentially on the time-scale $1/\bar{p}_1(\infty)$. In Fig. 3.10, we plot Monte Carlo solutions for the state probabilities in comparison to the approximation. For $\gamma = 1$, the approximation does not work well for $N_t = 5$, but it does so already for $N_t = 10$. For $\gamma = 5$, the approximation works well for both cluster sizes. Note that in this approximation, a term $\bar{p}_0(\infty) e^{-\bar{p}_1(\infty)\tau}$ is missing for proper normalisation $\sum_{i=0}^{N_t} p_i = 1$. This is a small error for large clusters and strong rebinding. In order to assess the validity of (3.39), we note that it presupposes that the time-scale for relaxation to the steady state, $1/(1+\gamma)$, is smaller than the time-scale for decay to the absorbing boundary, $1/\bar{p}_1(\infty) = (1+\gamma)^{N_t}/\gamma N_t$. Therefore, γ should be larger than $(N_{eq})^{1/N_t} - 1$. For large N_t and $1 \leqslant N_{eq} < N_t$ this number is close to 0.

It follows from (3.39) that the mean number of closed bonds decreases exponentially, $N(\tau) = N_{eq} e^{-\bar{p}_1(\infty)\tau}$. This is confirmed by Fig. 3.11a, which shows the corresponding simulation results. For

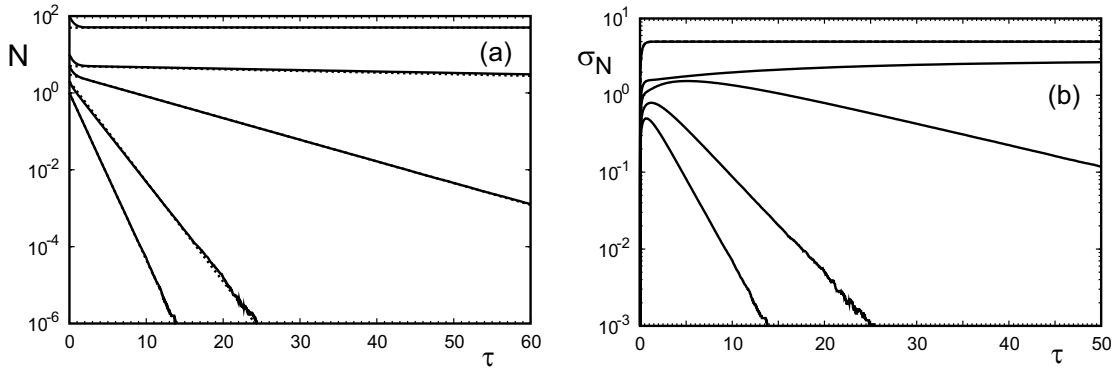

Figure 3.11: (a) Average number of closed bonds N obtained from stochastic simulations of the master equation for $\gamma = 1$ and $N_t = 1, 2, 5, 10$ and 100. (b) Variance σ_N of the cluster size distribution for the same parameters as in (a).

$N_t = 2, 5$ and 10, we have $\bar{p}_1(\infty) = 0.5, 0.16$ and 9.7×10^{-3}. Numerically we find $0.6, 0.13$ and 0.01, thus the approximation is rather good. In Fig. 3.11b, we plot numerical results for the standard deviation σ_N. The initial increase of σ_N is well described by (3.35) for the reflecting boundary, thus the boundary has little influence here. Large clusters stay close to the steady state during the time shown and the approximation is applicable. For small clusters, the variance grows larger than the steady state value before is decreases exponentially while the cluster size N approaches zero. The variance contains two time-scales. The second moment of the distribution decreases on the same time-scale as the average, while the square of the first moment decreases twice as fast. The long time exponential decrease of σ_N is thus described by twice the relaxation time as is was found for the average number of bonds.

Although an exact solution for the state probabilities seems to be impossible for the case of an absorbing boundary, more analytical progress can be made if one is only interested in the probability that the cluster dissociates as a whole. For the absorbing boundary, the cluster dissociation rate has been denoted by $D(\tau)$ before. In the context of the reflecting boundary, $D(\tau)$ can be identified as the probability that the state $i = 0$ is reached for the first time at time τ if the system has started in the state $i = N_t$ at time $\tau = 0$. This is a first passage problem which can be treated with Laplace techniques. Since the transition rates do not depend on absolute time, one can decompose the state probability for $i = 0$ in two parts:

$$p_0(\tau) = \int_0^\tau D(\tau') p_{0,0}(\tau - \tau')\, d\tau' \tag{3.40}$$

where $p_{0,0}(\tau)$ is the state probability for state $i = 0$ with initial condition $p_i(0) = \delta_{i,0}$. $p_{0,0}(\tau)$ can also be interpreted as the probability for having returned to the boundary after time τ. A Laplace transform of the equation leads to an algebraic relation between the Laplace transforms of the three functions:

$$D(s) = \frac{p_0(s)}{p_{0,0}(s)}\,. \tag{3.41}$$

Here, $h(s) = \int_0^\infty e^{-s\tau} h(\tau)\, d\tau$ denotes the Laplace transform of a function $h(\tau)$. The explicit form

of the probability $p_0(\tau)$ is given in (3.33):

$$p_0(\tau) = \left[\frac{1 - e^{-(1+\gamma)\tau}}{1+\gamma}\right]^{N_t} . \tag{3.42}$$

The probability $p_{0,0}(\tau)$ is also given in (A.23) of Appendix A:

$$p_{0,0}(\tau) = \left[\frac{1 + \gamma e^{-(1+\gamma)\tau}}{1+\gamma}\right]^{N_t} . \tag{3.43}$$

The Laplace transforms of the these two functions are given by

$$p_0(s) = \frac{1}{(1+\gamma)^{N_t}} \sum_{i=0}^{N_t} \binom{N_t}{i} \frac{(-1)^i}{s + i(1+\gamma)} \tag{3.44}$$

and

$$p_{0,0}(s) = \frac{1}{(1+\gamma)^{N_t}} \sum_{i=0}^{N_t} \binom{N_t}{i} \frac{\gamma^i}{s + i(1+\gamma)} , \tag{3.45}$$

so that the Laplace transformed first passage probability time distribution is

$$D(s) = \frac{\sum_{i=0}^{N_t} \binom{N_t}{i} \frac{(-1)^i}{s+i(1+\gamma)}}{\sum_{i=0}^{N_t} \binom{N_t}{i} \frac{\gamma^i}{s+i(1+\gamma)}} = \frac{\sum_{i=0}^{N_t} \binom{N_t}{i} (-1)^i \prod_{j\neq i}(s + j(1+\gamma))}{\sum_{i=0}^{N_t} \binom{N_t}{i} \gamma^i \prod_{j\neq i}(s + j(1+\gamma))} . \tag{3.46}$$

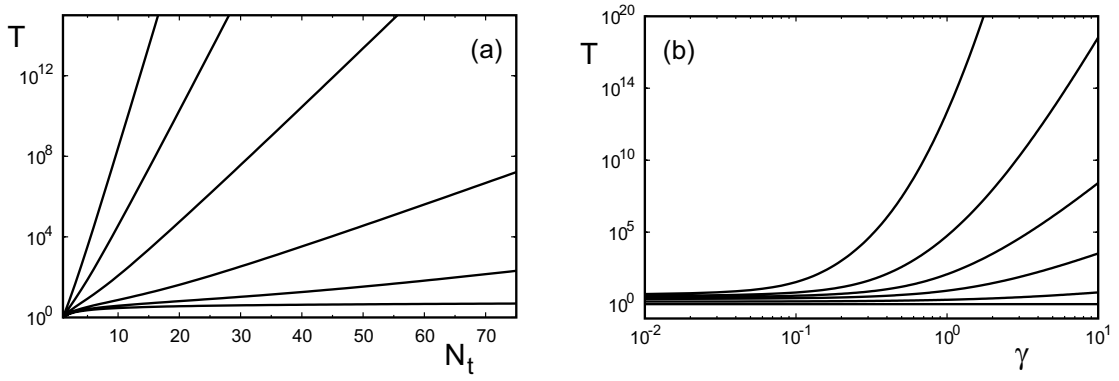

Figure 3.12: (a) Average lifetime T of adhesion clusters as function of cluster size N_t for rebinding rates $\gamma = 0.0, 0.1, 0.5, 1, 5$ and 10.0. (b) Average lifetime T as function of rebinding constant γ for cluster size $N_t = 1, 2, 5, 10, 20$ and 50.

Using the method of residues one might in principle calculate the inverse which will be a sum over N_t exponentials corresponding to the N_t possible zeros of the polynomial in the denominator. However, to derive a general, analytical expression for the backtransform of $D(s)$ seems to be impossible. Nevertheless, the mean first passage time can be extracted from this result, because it does not require the backtransform [van Kampen, 2003]:

$$T = \frac{d}{ds} D(s)\Big|_{s=0} = \frac{1}{1+\gamma} \left\{ \mathrm{H}_{N_t} + \sum_{n=1}^{N_t} \binom{N_t}{n} \frac{\gamma^n}{n} \right\} . \tag{3.47}$$

This equation is a polynomial of order $N_t - 1$ in γ. The zero order term is the harmonic number H_{N_t}, so for $\gamma = 0$ we recover the result from (3.23). The correction due to rebinding is a polynomial in γ of order $N_t - 1$. In Fig. 3.12, we plot (3.47) as a function of cluster size N_t and rebinding rate γ. As long as $\gamma < 1$, cluster lifetime grows only weakly (logarithmically) with cluster size (at least for not too large clusters). For $\gamma > 1$, the higher order terms in γ take over and the increase in T becomes effectively exponential, as shown in Fig. 3.12a. In Fig. 3.12b, it is shown explicitly that increasing γ to values larger than unity leads to a strong increase in lifetime. This effect is larger for larger clusters since the number of rebinding events in the dissociation path is larger.

3.3 Non-cooperative constant loading

In Sec. 2.2 we have introduced non-cooperative loading with a stiff force transducer. For a constant force, the linear master equation (2.28) is equivalent to the one for vanishing force discussed in this section. The solutions presented for $f = 0$, can be directly applied to non-cooperative loading with finite force, $f > 0$.

Non-cooperative loading with the force per bond $f_b = f = \mathrm{const}$ increases the off-rate e^{f_b} of the single bond, but it does not introduce a coupling between the bonds as in the case of shared loading. On the force dependent time-scale

$$\vartheta := \tau e^{f_b} , \tag{3.48}$$

the dimensionless off-rate equals 1 as in the force free case. Using the time-scale ϑ the dimensionless on-rate γ has to be replaced by the expression

$$\gamma_f := \gamma / e^{f_b} = k_{on}/k_0 e^{f_b} = k_{on}/k_{off} . \tag{3.49}$$

which decreases exponentially with force. It is the ratio of dimensional on-rate k_{on} and force dependent, dimensional off-rate $k_{off} = k_0 e^{f_b}$. Rewriting the master equation (2.28) and the deterministic equation (2.45) using ϑ instead of τ, leads to a form for the dynamic equations which is equivalent to the equations for vanishing force. The solutions can be transferred directly if τ and γ are replaced by ϑ and γ_f. Therefore, the effect of non-cooperative loading is two-fold: the rupture dynamics is accelerated exponentially with increasing force and the balance of rupture and rebinding is disturbed because only the off-rate increases while the on-rate stays constant.

For vanishing rebinding, $\gamma = 0$, the result is a radioactive decay for which the time-scale is reduced by the factor e^{-f_b}. This is the only effect of loading. The average lifetime is reduced to $e^{-f_b} \ln N_t$. Otherwise, the solutions are identical to the force free case. At any given time the distribution p_i is a binomial and with the same standard deviation as the for $f_b = 0$.

For finite rebinding, $\gamma > 0$, also the change of the balance between rebinding and unbinding is observed. The time-scale for the dynamics is shortened as before by e^{-f_b}. But now, the steady state is shifted to smaller numbers of closed bonds which increases the probability for fluctuations to the absorbing boundary. This leads to a non-linear effect of loading on the lifetime T, which was a polynomial of order $N_t - 1$ in $\gamma_f = \gamma e^{-f_b}$. This can also be understood in the leakage approximation. The rate of fluctuations is given by $1/e^{f_b} \bar{p}_1(\infty)$ which is also a polynomial of order $N_t - 1$ in e^{-f_b}.

The simple rescaling is possible for non-cooperative loading because the off-rate is independent of the number of closed bonds. Then, there are only two time-scales in the system which are determined by the on-rate γ and the off-rate e^{f_b}. For shared loading there are always $N_t + 1$ different time-scales which cannot all be brought into the form for $f_b = 0$.

3.4 Finite force and finite rebinding

3.4.1 Deterministic analysis

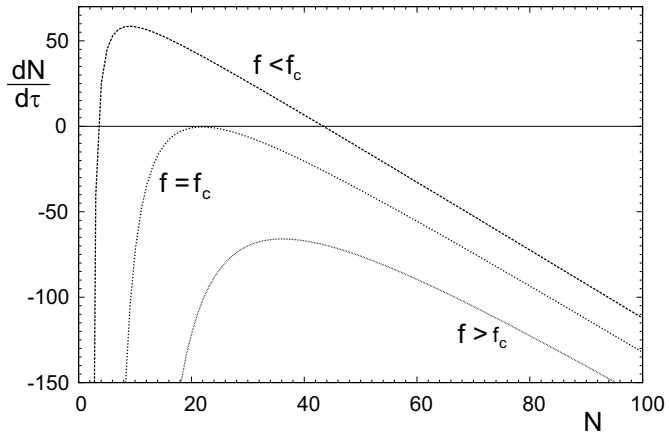

Figure 3.13: Time derivative $dN/d\tau$ of the number of closed bonds for forces below, at and above the critical force f_c. The two steady states that exist for $f < f_c$ merge at $f = f_c$. For $f > f_c$, no steady state exists.

Force destabilises the cluster, while rebinding stabilises it again. It has been shown by Bell [1978] in the framework of the deterministic equation (2.36) that, the cluster remains stable up to a critical force f_c. For the following it is helpful to revisit his stability analysis. The time derivative $dN/d\tau$ is plotted in Fig. 3.13 for forces below, at and above the critical force. In equilibrium, $dN/d\tau = 0$, we have the condition

$$N_{eq} e^{f/N_{eq}} = \gamma(N_t - N_{eq})\,, \tag{3.50}$$

for the fixed points N_{eq}. Exactly at critical loading the two roots of this equality – the two stationary states – merge and the slopes of the two terms become equal. This gives the additional equation

$$e^{f_c/N_c}\left(1 - \frac{f_c}{N_c}\right) = -\gamma\,. \tag{3.51}$$

These two equations allow to determine the critical values for cluster size and force:

$$f_c = N_t\,\mathrm{pln}\left(\frac{\gamma}{e}\right) \quad \text{and} \quad N_c = N_t \frac{\mathrm{pln}\left(\frac{\gamma}{e}\right)}{1 + \mathrm{pln}\left(\frac{\gamma}{e}\right)}\,, \tag{3.52}$$

where the product logarithm $\mathrm{pln}\,(a)$ is defined as the solution x of $xe^x = a$. For small forces, the unstable fixed point is very close to zero. This implies that the stable fixed point is an attractor for most initial conditions. Close to the critical force, the unstable fixed point is close to the stable one and only the initial conditions above N_c will reach the stable fixed point. As expected from the scaling of the deterministic equation (2.43) with N_t, the critical force and steady state (3.52) scale linearly with N_t (so that f_c/N_t and $N_{eq,c}/N_t$ are independent of N_t), but depend non-trivially on γ. For $\gamma < 1$, we have $f_c \approx \gamma N_t/e$. Thus the critical force vanishes with γ, because the cluster decays by itself with no rebinding. For $\gamma > 1$ and up to $\gamma \approx 100$, we have $f_c \approx 0.5 N_t \ln\gamma$. This weak dependence on γ shows that the single bond force scale set by F_B also determines the force scale on which the cluster as a whole disintegrates. Fig. 3.14a shows how f_c crosses over from linear to logarithmic scaling with increasing γ.

Eq. (3.50) is an implicit equation which cannot be inverted to give N_{eq} as a function of the model parameters N_t, f and γ. In general, N_{eq} decreases from $\gamma N_t/(1+\gamma)$ for $f = 0$ to N_c for $f = f_c$. For

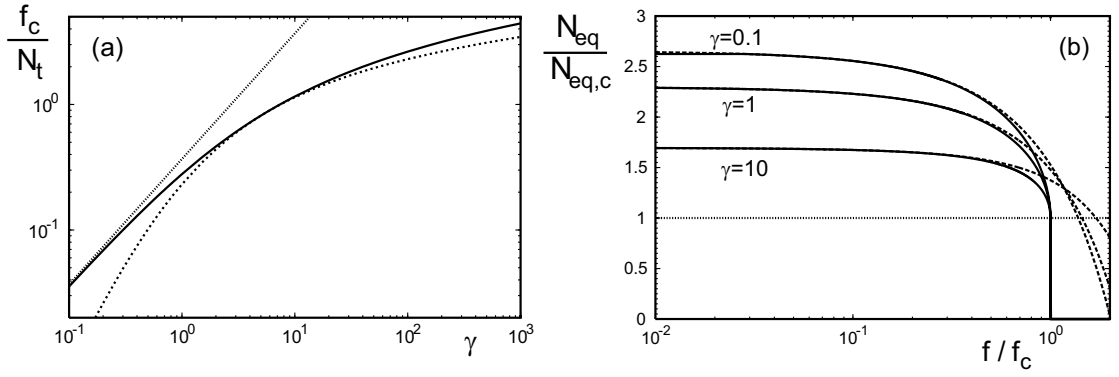

Figure 3.14: (a) Critical force (3.52) in relation to total cluster size, f_c/N_t, as function of the rebinding constant γ. It scales linearly (dotted curve) at small and logarithmically (dashed curve) for larger γ. (b) Stable steady value for number of closed bonds normalised by the critical value, $N_{eq}/N_{eq,c}$, for $\gamma = 0.1, 1$ and 10 (upper to lower curves) as function of force f/f_c for $N_t = 100$. Numerical results (solid lines) are compared to the approximation (3.53) (dashed lines). The horizontal line marks the smallest possible value at the critical force f_c.

small forces we can find an approximate solution by first expanding the exponential function in (3.50) to second order in f/N_{eq} and then expanding the resulting quadratic function for N_{eq} to second order in $f/\gamma N_t$:

$$N_{eq} \approx \frac{\gamma N_t}{1+\gamma}\left\{1 - \left(\frac{f}{\gamma N_t}\right) - \frac{\gamma+1}{2}\left(\frac{f}{\gamma N_t}\right)^2\right\}. \tag{3.53}$$

Fig. 3.14b shows numerical results for N_{eq}/N_c in comparison with the low force approximation (3.53) for different rebinding constants $\gamma = 0.1, 1.0$ and 10 as function of force f/f_c and for cluster size $N_t = 100$.

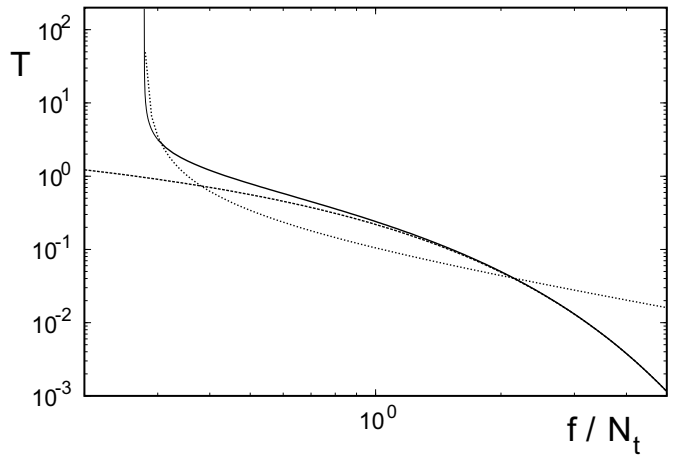

Figure 3.15: Deterministic mean lifetime T of a cluster of $N_t = 100$ bonds for $\gamma = 1$ as a function of the force-size ratio f/N_t. Numerical integration of the deterministic equation (solid line) is compared to the exact solution for vanishing rebinding (dashed line) and the inverse linear scaling (dotted line) predicted close to the critical force.

In the deterministic framework, cluster lifetime is infinite for $f \leqslant f_c$, because a stationary state exists at N_{eq}. For $f > f_c$, cluster lifetime is finite, but strongly varies as a function of N_t, f and γ. For $f \gg f_c$, we can neglect rebinding and use the results from Sec. 3.1, where we found for cluster

lifetime

$$T_{det} = \mathrm{E}\left(\frac{f}{N_t}\right) \approx \frac{e^{-f/N_t}}{1+f/N_t}\,, \tag{3.54}$$

compare (3.11). As force f is decreased towards the critical value f_c, rebinding becomes important again and cluster lifetime diverges. To understand this limit, we note that here the system will evolve very slowly, because it is still close to a steady state. Therefore we can expand the time derivative of N, compare (2.42), for small deviations from the critical state:

$$\frac{d}{d\tau}N \approx \frac{\partial}{\partial f}\left(\frac{d}{d\tau}N\right)\Big|_{f_c,N_c}(f-f_c) = -e^{f_c/N_c}(f-f_c) = -e^{1+\mathrm{pln}(\gamma/e)}(f-f_c)\,. \tag{3.55}$$

In this limit, the lifetime will be dominated by the time spent close to the critical state. The time for a significant change $\Delta N \simeq -1$ in N is

$$T \simeq \Delta\tau \simeq \frac{1}{f-f_c}e^{-(1+\mathrm{pln}(\gamma/e))}\,. \tag{3.56}$$

Therefore T_{det} diverges like the inverse of $f - f_c$. Fig. 3.15 shows the lifetime of an adhesion cluster derived from numerical integration of the deterministic equation for $\gamma = 1$ and $N_t = 100$ as a function of the force-size ratio f/N_t. The numerical results are compared to the approximation (3.54) for large forces and (3.56) for the divergence close to the critical point. Obviously both approximations work well for their respective limits. For different cluster sizes N_t, the plot remains basically unchanged (not shown), because the forces above f_c are already in the range where (3.3) predicts scaling with f/N_t alone. For different rebinding constants γ the results are qualitatively the same, only that the critical force is shifted to different values.

3.4.2 Stochastic analysis

In general, it seems to be difficult to find a closed-form analytical solution for the state probabilities $p_i(\tau)$ for general values of γ, f and N_t. In the following, we will derive such an analytical solution for the case $N_t = 2$ with an absorbing boundary. In principle, solutions can be constructed in the same way for a reflecting boundary or larger clusters, but for increasing cluster size, the analytical procedure quickly becomes intractable. For this reason, we will later use simulations to deal with the general case.

We start by rewriting the master equation (2.26) in matrix form:

$$\dot{\mathbf{p}} = \mathbb{W}\cdot\mathbf{p}\,. \tag{3.57}$$

For the case $N_t = 2$ with an absorbing boundary, $\mathbf{p} = (p_0, p_1, p_2)^\dagger$ and

$$\mathbb{W} = \begin{pmatrix} 0 & r_1 & 0 \\ 0 & -(r_1+g_1) & r_2 \\ 0 & g_1 & -r_2 \end{pmatrix}\,. \tag{3.58}$$

The master equation in matrix form is solved by [van Kampen, 2003]

$$\mathbf{p}(\tau) = e^{\mathbb{W}\tau}\cdot\mathbf{p}(0) = \mathbf{p}_\infty + \sum_{\lambda<0} c_\lambda e^{\lambda\tau}\mathbf{p}_\lambda \tag{3.59}$$

where $\mathbf{p}_\infty$ is the eigenstate with eigenvalue zero, that is the stationary state of the master equation. The other eigenvalues are negative and the corresponding eigenstates $\mathbf{p}_{\lambda<0}$ are transient states. The coefficients c_λ have to be determined from the initial condition

$$\mathbf{p}(0) = \mathbf{p}_\infty + \sum_{\lambda<0} c_\lambda \mathbf{p}_\lambda \,. \tag{3.60}$$

The stationary state with $\lambda_0 = 0$ is the absorbing state $\mathbf{p}_\infty = (1,0,0)^\dagger$ and guarantees normalisation of the probability distribution. The transient states give no net contribution to $\{p_i(\tau)\}_{i=0}^{N_t}$. The two negative eigenvalues can be written as

$$\lambda_{1,2} = -(\Omega \pm \omega) \tag{3.61}$$

with Ω and ω being defined as

$$\Omega = (r_1 + r_2 + g_1)/2 \quad \text{and} \quad \omega = \sqrt{\Omega^2 - r_1 r_2}\,. \tag{3.62}$$

Note that $0 < \omega < \Omega$ and hence $\lambda_{1,2} < 0$. The transient eigenstates are

$$\mathbf{p_1} = \frac{1}{g_1}\begin{pmatrix} \lambda_2 + r_1 \\ \lambda_1 + r_2 \\ g_1 \end{pmatrix} \quad \text{and} \quad \mathbf{p_2} = \frac{1}{g_1}\begin{pmatrix} \lambda_1 + r_1 \\ \lambda_2 + r_2 \\ g_1 \end{pmatrix}\,. \tag{3.63}$$

The three eigenstates $\mathbf{p}_\lambda$ are linearly independent and form a basis of the state space of the cluster. With the initial condition $p_i(0) = \delta_{i,N_t}$, i.e. $\mathbf{p}(0) = (0,0,1)^\dagger$, the coefficients c_λ follow from (3.60) as

$$c_{\lambda_1} = (\lambda_2 + r_2)/(\lambda_2 - \lambda_1) \quad \text{and} \quad c_{\lambda_2} = -(\lambda_1 + r_2)/(\lambda_2 - \lambda_1)\,. \tag{3.64}$$

The final result then can be written as

$$\begin{aligned} p_0(\tau) &= 1 - \left\{\cosh(\omega\tau) + \frac{\Omega}{\omega}\sinh(\omega\tau)\right\} e^{-\Omega\tau} \\ p_1(\tau) &= \frac{r_2}{\omega}\sinh(\omega\tau) e^{-\Omega\tau} \\ p_2(\tau) &= \left\{\cosh(\omega\tau) + \frac{\Omega - r_2}{\omega}\sinh(\omega\tau)\right\} e^{-\Omega\tau}\,. \end{aligned} \tag{3.65}$$

There is a competition between the hyperbolic terms, which grow on the time-scale $1/\omega$, and the exponential terms, which decrease on the time-scale $1/\Omega$. Since $\omega < \Omega$, the exponential terms will win and only the stationary state survives.

With the exact solution (3.65), one now can calculate any quantity of interest. For example, the mean number of bonds, $N(\tau) = p_1(\tau) + 2p_2(\tau)$, follows as

$$N(\tau) = \left\{2\cosh(\omega\tau) + \frac{r_1 + g_1}{\omega}\sinh(\omega\tau)\right\} e^{-\Omega\tau}\,. \tag{3.66}$$

The dissociation rate for the cluster as a whole as given by $D(\tau) = r_1 p_1 = \dot{p}_0$, resulting in

$$D(\tau) = \frac{r_1 r_2}{\omega}\sinh(\omega\tau) e^{-\Omega\tau}\,. \tag{3.67}$$

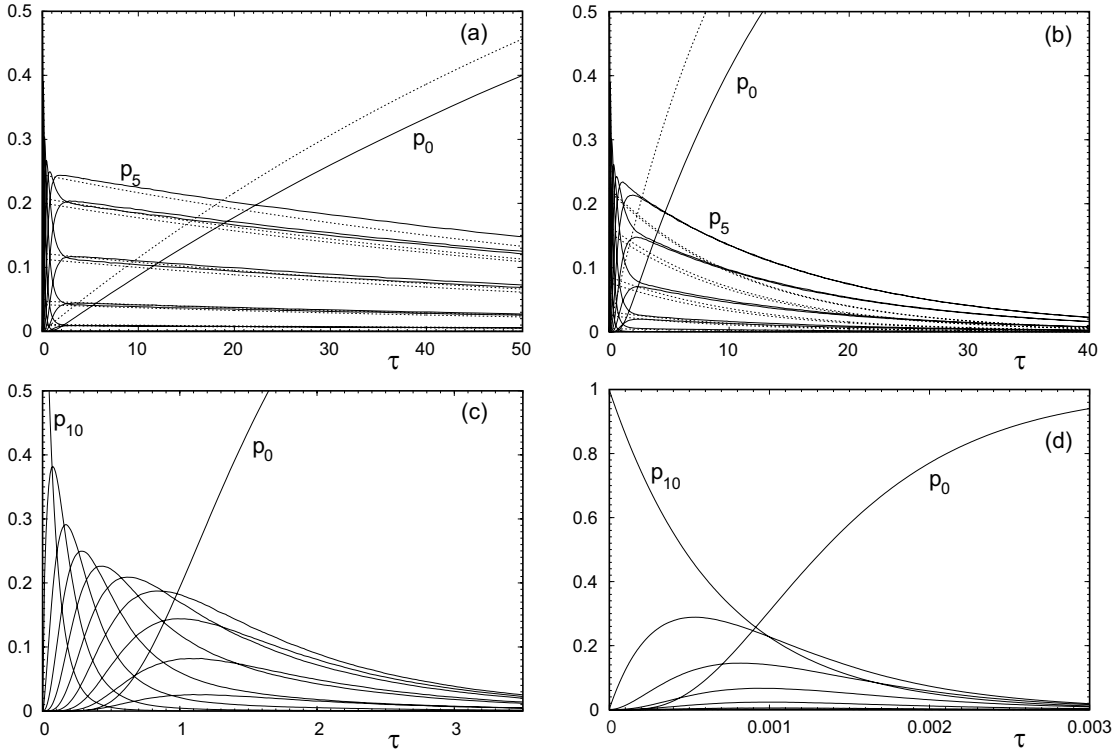

Figure 3.16: State probabilities p_i as a function of time τ for $N_t = 10$ with $\gamma = 1$ for force $f = 0.1, 1, 3$ and 10 (a - d). In (a), the numerical solution is compared with the leakage approximation (dotted lines). The intermediate force values are chosen below and above the critical force $f_c = 0.278 N_t$.

One easily checks that normalisation is correct, $\int_0^\infty D(\tau)\, d\tau = 1$. Mean cluster lifetime T now follows as

$$T = \int_0^\infty \tau D(\tau)\, d\tau = \frac{1}{2}\left\{2e^{-f} + e^{-f/2} + \gamma e^{-3f/2}\right\} . \tag{3.68}$$

As shown in the preceding sections for special cases, force leads to exponentially decreased lifetimes, while rebinding leads to polynomial terms in γ of order $N_t - 1$.

In Appendix C, the general solution of a three state one-step master equation with arbitrary transition rates is derived. The results from above for constant shared loading emerge as a special case. Although the eigenvalue analysis can be used also for the general case of arbitrary cluster size, in this case it is more efficient to use exact stochastic simulations as they are described in Appendix B. In Fig. 3.16 numerical solutions of the state occupancy probabilities $\{p_i(\tau)\}_{i=0}^{N_t}$ are plotted for $N_t = 10$ with $\gamma = 1$ for four different forces $f = 0.1, 1, 3$ and 50. This figure corresponds to Fig. 3.1 for vanishing rebinding and Fig. 3.10 for vanishing force. For small force, the numerical solutions compare well with the leakage approximation (3.39) introduced for vanishing force. Here, the steady state distribution for finite force had to be used. For constant rates, this can be calculated from the master equation (2.24) in terms of the transition rates for arbitrary one-step processes. For a one-step master equation, stationarity implies the detailed balance condition $g_i p_i(\infty) = r_{i+1} p_{i+1}(\infty)$. Iterating this

condition, the $p_i(\infty)$ are expressed in terms of $p_0(\infty)$ as

$$p_i(\infty) = p_0(\infty) \prod_{j=0}^{i-1} \frac{g(j)}{r(j+1)} \,. \tag{3.69}$$

The probability $p_0(\infty)$ is determined by the normalisation condition

$$1 = \sum_{i=0}^{N_t} p_i(\infty) = p_0(\infty) \left[1 + \sum_{i=1}^{N_t} \prod_{j=0}^{i-1} \frac{g(j)}{r(j+1)} \right] \tag{3.70}$$

so that

$$p_0(\infty) = \frac{1}{1 + \sum_{i=1}^{N_t} \prod_{j=0}^{i-1} \frac{g(j)}{r(j+1)}} \tag{3.71}$$

and the properly normalised stationary probability distribution is given by

$$p_i(\infty) = \frac{\prod_{j=0}^{i-1} \frac{g(j)}{r(j+1)}}{1 + \sum_{k=1}^{N_t} \prod_{j=0}^{k-1} \frac{g(j)}{r(j+1)}} \,. \tag{3.72}$$

The time-scale for fluctuations $1/r_1 p_1(\infty)$ is now given by

$$\frac{1}{r_1 p_1(\infty)} = \frac{1 + \sum_{k=1}^{N_t} \prod_{j=0}^{k-1} \frac{g(j)}{r(j+1)}}{r_1 (g_0/r_1)} = \frac{1}{g_0} \left\{ 1 + \sum_{k=1}^{N_t} \prod_{j=0}^{k-1} \frac{g(j)}{r(j+1)} \right\} = \frac{1}{g_0 p_0(\infty)} \,. \tag{3.73}$$

This expression has to be inserted into the local thermal equilibrium approximation of (3.39). For the smallest force $f/N_t = 0.01$, the leakage approximation can describe the solutions. For larger forces but still below the critical force the approximation breaks down. If force is increased beyond the critical force ($f_c = 2.78$ for $\gamma = 1$), a simple description is not available, because equilibration proceeds on the same or on a longer time-scale as the decay. For very large force, the behaviour of the adhesion cluster approaches that for vanishing rebinding, with the analytical solution (3.14).

Fig. 3.17 demonstrates that the decay process changes dramatically as force is increased above the critical value. It displays trajectories of individual clusters with $N_t = N_0 = 10, 100$ and 1000 bonds in comparison with the average number of bonds derived from a large number of these trajectories. Since $f_c = 0.278 N_t$ for $\gamma = 1$, Fig. 3.17a with $f = 0.25 N_t$ is below the critical value. For the largest cluster, the system equilibrates towards the steady state and then fluctuates around this value with very rare encounters of the absorbing boundary. For the smaller clusters, however, fluctuations towards the absorbing boundary frequently lead to loss of individual realisations. As a result, the average number of closed bonds decays exponentially on a much faster time-scale. Fig. 3.17b with $f = N_t$ is above the critical force and the behaviour is changed qualitatively. A steady state does not exist anymore and the clusters do not decay by fluctuations, but the size of each adhesion cluster is continuously reduced. Clusters of different size now decay on the same time-scale and rebinding events are very rare in comparison to rupture events.

Fig. 3.18 plots numerical results for the average number of closed bonds N as function of time τ for two different values of f/N_t and for cluster sizes $N_t = 1, 10, 10^2$ and 10^3. For $f = 0.25 N_t < f_c$, after initial relaxation all curves decay exponentially. For $f = N_t > f_c$, the larger clusters show a steep decrease in average cluster size at the end of the decay due to the effects of shared loading. For the small clusters, the average cluster size decreases slowly since cooperative effects are small.

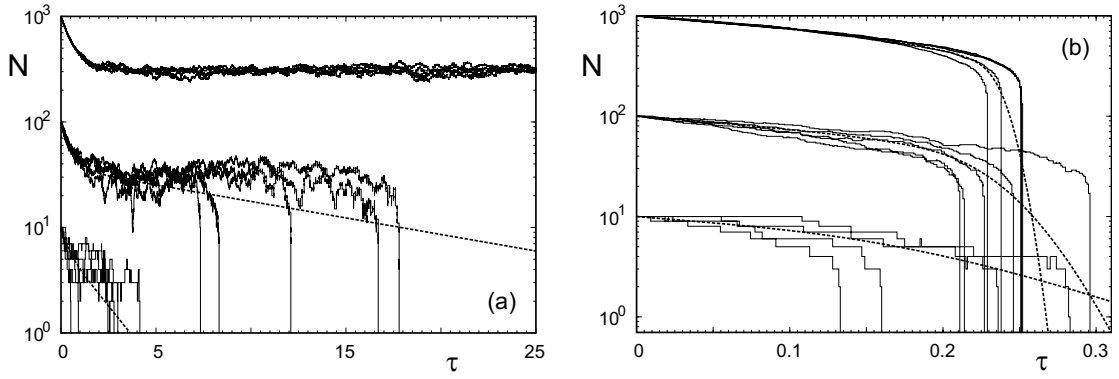

Figure 3.17: Single simulation trajectories for $N_t = 10, 100$ and 100 for $\gamma = 1$ and at two different forces (a) $f = 0.25N_t < f_c$ and (b) $f = N_t > f_c$. Representative trajectories are compared to the average number N of closed bonds resulting from averaging over a large number of such trajectories.

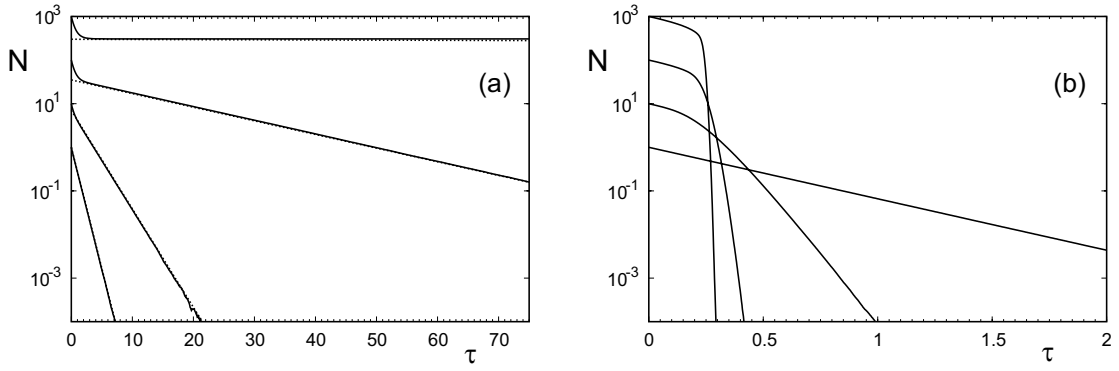

Figure 3.18: Average number of closed bonds N for $N_t = 1, 10, 10^2$ and 10^3, $\gamma = 1$ and (a) $f/N_t = 0.25$ and (b) $f/N_t = 1$. In (a), the numerical results are compared to exponentially decaying curves $\sim e^{-a\tau}$ (dashed lines) with $a = 1.28, 0.52, 0.072$ and 0.0009 for increasing bond number.

Fig. 3.19 plots the variance $\sigma_N(\tau)$ of the distribution p_i for the two force values used in the two previous figures. Below the critical force the behaviour is similar to that for vanishing force depicted in Fig. 3.11. The variance decreases exponentially after having traversed a maximum. For forces above the critical force, a different behaviour arises. After growing as expected in the initial phase, the variance displays a sharp peak. This effects becomes more pronounced the larger cluster size.

In Fig. 3.20 a comparison of the average number of closed bonds in the stochastic and the deterministic description is shown. $N(\tau)$ is plotted for cluster sizes $N_t = 10, 100$ and 1000 for the forces $f/N_t = 0.1$ and 1.0 and the rebinding rate $\gamma = 1.0$. For small forces $f < f_c$, the average number of closed bonds equilibrates towards the steady state and remains constant thereafter. The fluctuations occurring in the stochastic description lead to a slow exponential decrease of N. Above the critical force, the deterministic clusters decay as well, and in a more abrupt way than the stochastic average.

We now turn to the dissociation rate of the overall cluster as a function of the model parameters. For $\gamma = 1$ and $f = 0.25N_t$ and N_t, that is below and above the critical force, numerical results are plotted in Fig. 3.21. For a single bond, dissociation is a Poisson process with the maximum at $\tau = 0$

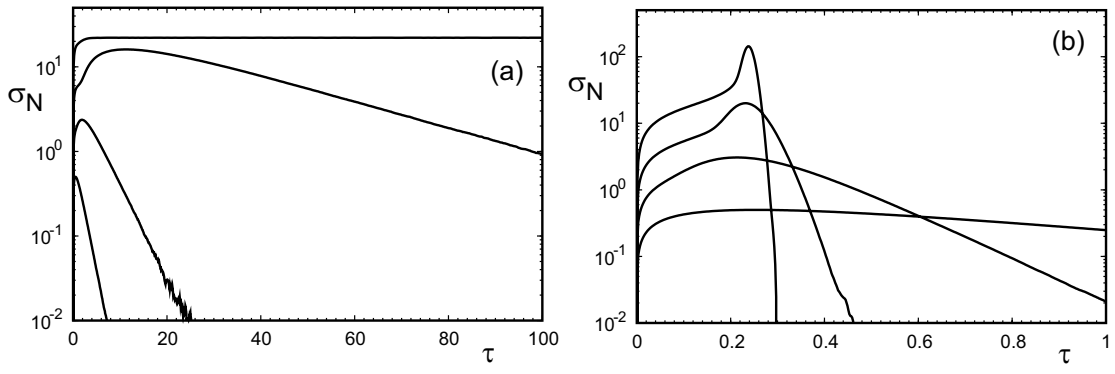

Figure 3.19: Variance σ_N for forces (a) $f = 0.25N_t$ and (b) $f = N_t$ for $\gamma = 1$ and $N_t = 1, 10, 10^2$ and 10^3 (lower to upper curves).

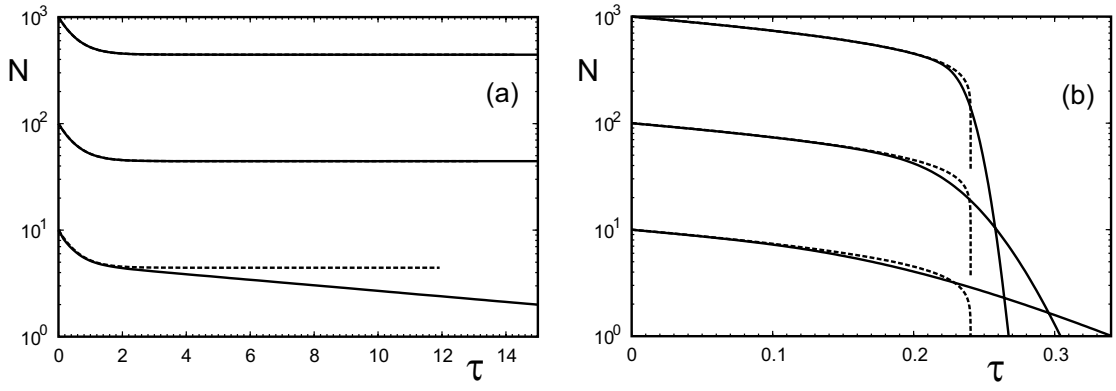

Figure 3.20: Comparison of stochastic and deterministic results for the average number of closed bonds N derived from numerical solutions of the master equation (solid lines) and from integration of the deterministic equation (dashed curves) for cluster sizes $N_t = 10, 10^2$ and 10^3 and forces (a) $f/N_t = 0.1$ and (b) 1.0. The rebinding rate is $\gamma = 1$.

and an exponentially decreasing dissociation rate $D(\tau) = r(1)p_1(\tau) = e^f e^{-e^f \tau}$. For larger clusters and below the critical force, fluctuations to the absorbing boundary determine the rate of dissociation, which vanishes at $\tau = 0$, goes through a maximum and then decreases exponentially with time. As explained above, exponential decay arises because decay proceeds by rare fluctuations from the steady state towards the absorbing boundary. Above the critical force, the dissociation rate for $N_t > 1$ becomes more sharply peaked and cannot be described with single exponential curves. A steady state does not exist anymore and dissociation does not proceed by fluctuations. The trajectories in Fig. 3.17 have shown that adhesion clusters decay fairly abrupt towards the end of the decay as a consequence of shared loading. This cooperative instability is the reason for the sharp dissociation distribution for large clusters under super-critical loading.

Whereas results for the dissociation rate have to be obtained numerically, the average lifetime can be calculated analytically. The basic idea here is to sum the average times for any possible pathway leading from the initial cluster size N_0 towards dissociation at the absorbing boundary $i = 0$ with its appropriate statistical weight. One can show that the lifetime T_{N_t,N_0} of a cluster with a total of N_t

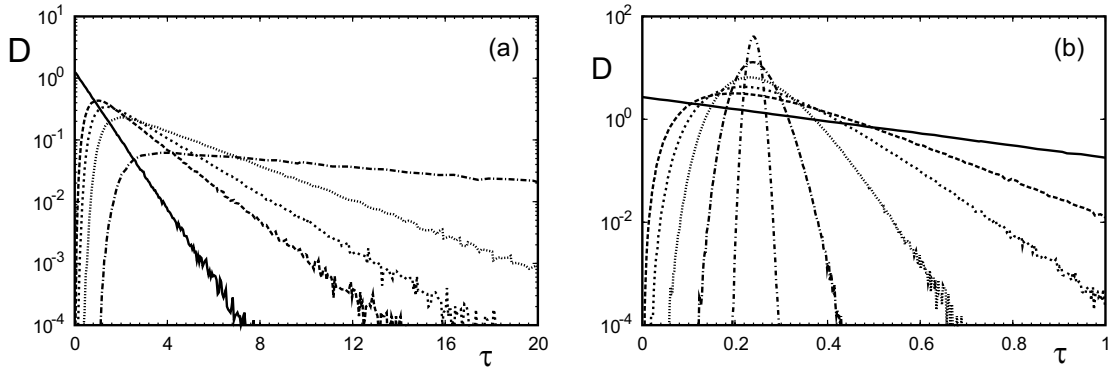

Figure 3.21: Dissociation rate D of the overall cluster for $\gamma = 1$ and $N_t = 1, 5, 10, 25, 10^2$ and 10^3. (a) $f = 0.25N_t$ and (b) $f = N_t$.

molecular bonds of which N_0 are closed initially satisfies the equation [van Kampen, 2003]

$$g(N_0)\,(T_{N_t,N_0+1} - T_{N_t,N_0}) + r(N_0)\,(T_{N_t,N_0-1} - T_{N_t,N_0}) = -1\,. \tag{3.74}$$

The left hand side can be considered to be the adjoint operator of the master equation acting on the average lifetime T_{N_t,N_0}. For the initial condition $N_0 = N_t$, the equation is solved exactly by

$$T = T_{N_t,N_t} = \sum_{i=1}^{N_t} \frac{1}{r(i)} + \sum_{i=1}^{N_t-1} \sum_{j=i+1}^{N_t} \frac{\prod_{k=j-i}^{j-1} g(k)}{\prod_{k=j-i}^{j} r(k)}\,, \tag{3.75}$$

where the first term is the result (3.22) for vanishing rebinding and the second term results in a polynomial of order $N_t - 1$ in γ. For $f = 0$, (3.75) is identical to the earlier result (3.47) obtained by Laplace transforms. Both expressions are polynomials of order $N_t - 1$ in γ, but in the general case from (3.75), the coefficients depend on force. For $N_t = 2$, we obtain the result from (3.68). For $N_t = 3$, we find

$$T = e^{-f} + \frac{e^{-f/2}}{2} + \frac{e^{-f/3}}{3} + \gamma\left(\frac{e^{-5f/6}}{6} + e^{-3f/2}\right) + \gamma^2\frac{e^{-11f/6}}{3}\,. \tag{3.76}$$

For $N_t = 2$ and 3, T can also be derived by explicitly summing over all possible dissociation paths. For larger N_t, direct summation becomes intractable and the results following from the general formula (3.75) become rather lengthy. In general, force always affects most strongly those terms of highest order in γ, thus for $\gamma > 1$, application of force is therefore an efficient way to reduce average lifetime T. For $\gamma < 1$, T is dominated by those terms of lowest order in γ, thus here the reduction of lifetime with increasing force is only weakly modulated by rebinding.

Fig. 3.22 shows the average lifetime of adhesion clusters of size $N_t = 1, 2, 5, 10, 15$ and 25 as a function of force-size ratio f/N_t for on-rates $\gamma = 0.1$ and $\gamma = 1.0$. For small forces, $f < 1$, the average lifetime plateaus at the value given by (3.47). For large forces, $f > N_t$, that is, when the force on each single bond is larger than the intrinsic force scale, the limit of vanishing rebinding applies. The critical forces for the given rebinding rates are $f_c = 0.0355N_t$ and $f_c = 0.278N_t$. In the intermediate force range, roughly around f_c, the lifetime is reduced from the zero force to the zero rebinding limit. This reduction is dramatic for large clusters ($N_t \geqslant 10$) with appreciable rebinding

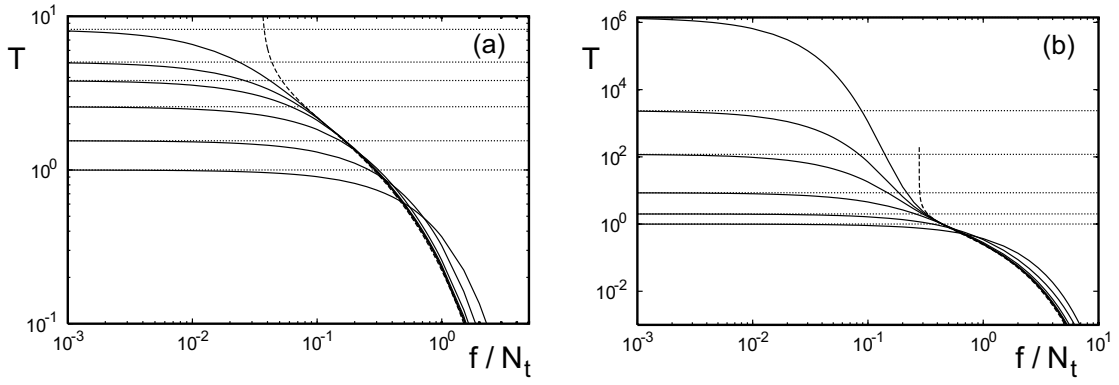

Figure 3.22: Average lifetime T according to (3.75) (solid lines) of adhesion clusters with $N_t = 1, 2, 5, 10, 15$ and 25 as a function of f/N_t for (a) $\gamma = 0.1$ and (b) $\gamma = 1$. The critical forces for these rebinding rates are $f_c/N_t = 0.0355$ and 0.278, respectively, where the deterministic results for the lifetimes (dashed lines) diverge.

($\gamma \geqslant 1$), where the lifetime is reduced by orders of magnitude. We also show the lifetime following from the deterministic framework. For large forces, it provides a lower limit for the stochastic lifetime, because here the largest clusters have the shortest lifetimes for a given force size ratio f/N_t. Below the critical force the deterministic lifetime is infinite and the stochastic curves approach the plateaus (3.47) determined by fluctuations towards the absorbing boundary.

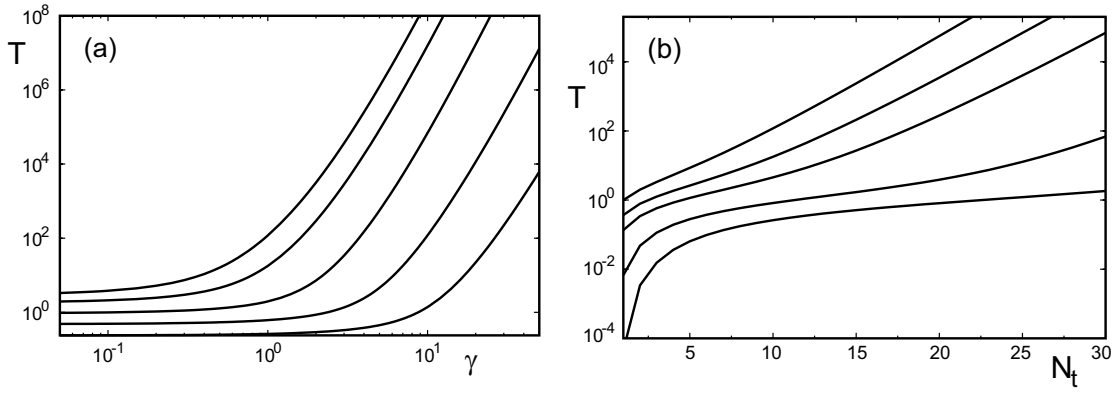

Figure 3.23: Average cluster lifetime T (a) as function of rebinding rate γ for $N_t = 10$ and $f/N_t = 0, 0.1, 0.3, 0.6$ and 1 and (b) as function of cluster size N_t for $\gamma = 1.0$ and $f = 0, 1, 2$ and 10.

Fig. 3.23a demonstrates the influence of rebinding on the average lifetime at different levels of force. Here we show average lifetime T as function of γ for $N_t = 10$ and for increasing values of force. For $f = 0$ the curves are as depicted in Fig. 3.12. Increasing force reduces the lifetime strongly and leads to an almost constant lifetime for different γ (compared the strong increase for $f = 0$). Only when rebinding is sufficiently strong that force is smaller than the critical force, $f < f_c$, lifetime begins to grow. The increase observed then is similar to that for vanishing force, only that the absolute value of lifetime is smaller. For example, for $f = 0.6N_t$, the cluster grows strongly for $\gamma \geqslant 5$ where

the critical force is $f_c = 0.82N_t$; for $f = N_t$ the strong increase is observed for $\gamma \geqslant 10$, for which the critical force is $f_c = 1.15N_t$. A similar effect is observed for the dependence of average lifetime on cluster size, see Fig. 3.23b. At small N_t, cluster lifetime grows strongly at large forces according to (3.22) due to shared loading. For larger N_t, lifetime grows slowly until N_t is large enough that $f_c \geqslant f$ is reached. Above this size, T grows on a rate comparable to that for vanishing or small force. For $\gamma = 0.1$, the increase of T with N_t is slow throughout the shown range of N_t.

3.5 Summary

In this chapter, we have presented a detailed analysis of the stochastic dynamics of adhesion clusters of size N_t under constant shared loading f and with on-rate γ. The corresponding master equation has been solved exactly for several special cases. For vanishing rebinding ($\gamma = 0$), the exact solution (3.15) could be constructed because cluster decay is a sequence of Poisson processes. For vanishing force ($f = 0$), we deal with a linear problem, which can be treated with standard techniques. In the case of natural boundaries (that is for a reflecting boundary at $i = 0$), the exact solution (3.33) follows with the help of a generating function. In the general case of finite force f and finite rebinding rate γ, for the case $N_t = 2$ and an absorbing boundary we used an eigenvalue analysis to derived the exact solution (3.65). In principle, the same method can also be applied for a reflecting boundary or for larger clusters, but this does not lead to simple analytical results.

For vanishing force ($f = 0$) and an absorbing boundary at $i = 0$, we introduced the 'leakage approximation' (also known as 'local thermal equilibrium description' in the theory of protein folding), which treats the absorbing boundary as a small perturbation to the exactly solved case of the reflecting boundary. The resulting formulae given in (3.39) work well if average cluster lifetime T is much larger than the internal time-scale $1/(1+\gamma)$ (that is for large clusters or strong rebinding). For finite force the time dependent solution is not known even for natural boundaries. Using the steady state distribution alone, the leakage approximation could also be used for the case of small, finite forces. All other cases have been treated with exact stochastic simulations using the Gillespie algorithm, which for large clusters is more efficient than the eigenvalue analysis. Moreover, the study of single simulation trajectories offers valuable insight into the typical nature of unbinding trajectories expected for experiments.

The case of non-cooperative loading with the force f on each closed bond was discussed shortly for comparison. In this case, the adhesion bonds are independent as for vanishing force but their rupture rate is increased by the factor e^f. The linear master equation for this case is equivalent to that for vanishing force $f = 0$. Because the bonds in the cluster lack any cooperativity, loading with a constant force only accelerates single bond rupture and thus changes the balance of rebinding γ and rupture e^f. With a reflecting boundary, this shifts the steady state to smaller values of i. With an absorbing boundary, the probability of fluctuations to the absorbing boundary that lead to a loss of realisations is increased. In the leakage approximation, this leads to a non-linear effect of e^f on the lifetime.

Once the master equation is solved, either exactly or numerically, all quantities of interest can be calculated. We focused on the mean number of closed bonds as a function of time, $N(\tau)$, and the dissociation rate for the overall cluster, $D(\tau)$. The first moment of $D(\tau)$ then gives the mean cluster lifetime T. We derived the exact solution $T = T(N_t, f, \gamma)$ from the adjoint master equation, see (3.75). For the special cases of vanishing rebinding and vanishing force, we also showed how the exact formulae for T can be derived via completely different routes. The result for $T = T(N_t, f)$ from (3.22) follows from the unique dissociation path without rebinding, while the result for $T = T(N_t, \gamma)$

from (3.47) can be derived with Laplace techniques as a mean first passage time for the case of a reflecting boundary. In order to assess the role of fluctuations, we also calculated the standard deviations σ_N and σ_T for the distributions of the number of closed bonds and cluster lifetimes, respectively.

A special interest of this chapter was a detailed comparison between the stochastic and deterministic treatment. Regarding mean cluster lifetime, the deterministic treatment is rather good in the case of vanishing rebinding, although it underestimates the plateau value for cluster lifetime at small force. In the presence of rebinding, the deterministic treatment fails, because it includes neither the effect of fluctuations nor the effect of an absorbing boundary. In particular, the deterministic treatment does not predict finite lifetime below the critical force f_c, when clusters decay due to fluctuations towards the absorbing boundary. Only at very large force, when rebinding becomes irrelevant, does the deterministic treatment work well again. Regarding the average number of closed bonds, the deterministic model fails because it does not correctly treat the non-linearity in the rupture rate. This effect is most evident for small clusters and at late stage of rupture. In general, the mean number of closed bonds in the stochastic model decay in a smoother way than in the deterministic model, which typically shows an abrupt decay in late stage. This abrupt decay in fact is typical for shared loading and shows up in the stochastic model when one studies single simulation trajectories. In this sense, the deterministic model makes an interesting prediction which should be confirmed in experiment, albeit not on the level of the first moment, as suggested by the deterministic model, but rather on the level of single trajectories, as suggested by the stochastic model.

Our results can now be used to evaluate a large range of different experimental situations. The stochastic dynamics of adhesion clusters under force can be quantitatively studied with many different techniques, including atomic force microscopy, optical tweezers, magnetic tweezers, the biomembrane force probe, flow chambers, and the surface force apparatus. In all of these cases, by measuring cluster lifetime T and two out of the three parameters N_t, f and γ, the third parameter can be estimated with the help of our exact results. In general, our exact results nicely show how mean cluster lifetime T varies with cluster size N_t, force f and rebinding rate γ. For example, if the single bond lifetime was one second ($k_0 = 1/\,\mathrm{s}$), for $f = 0$ and $\gamma = 0$ a cluster lifetime T of one minute could only be achieved with 10^{26} bonds, because in this case, cluster lifetime scales only logarithmically with cluster size. However, for a rebinding rate $\gamma = 1$ ($k_{on} = k_0$), only $N_t = 10$ bonds are necessary, because lifetime scales strongly with rebinding, $T \sim \gamma^{N_t - 1}$. Increasing force to $f = 10$ would decrease lifetime to $T = 0.05\,\mathrm{s}$, because T is exponentially decreased by f. To reach one minute again, cluster size or rebinding rate had to be increased such that $f < f_c$. This implies $N_t > 50$ or $\gamma > 10$. It is important to note that these predictions are based on the assumption of rigid force transducers. In many experimental situations of interest, the force transducer will be subject to elastic deformations or even to viscous relaxation processes, like for example when pulling on cells [Benoit et al., 2000]. In order to focus on generic aspects of adhesion clusters, here we only studied the minimal model for stochastic dynamics under force.

Our results can also be applied to experiments in cell adhesion. For example, the biomembrane force probe with linear loading has recently been used to study the decay of $\alpha_\nu\beta_3$-integrin clusters induced on the surface of endothelial cells [Prechtel et al., 2002, Erdmann and Schwarz, 2004a]. If one makes sure that the clusters do not actively grow during the time of dissociation, similar experiments could now be done also for constant loading [Pierrat et al., 2004]. Because in these kinds of experiments the exact cluster size is usually unknown, one had to convolute our results with a Poisson distribution for an estimated average number of bonds [Chesla et al., 1998, Zhu, 2000]. Recently, our result for the average cluster lifetime of two bonds under shared force and with rebinding, (3.68), has been applied to the analysis of flow chamber data on leukocyte tethering through L-selectin [Schwarz and Alon, 2004]. Since in this case force can be calculated as a function of shear flow, our formula

can be used to the estimate rebinding rate, which in this case turns out to be surprisingly large. This in turn explains why dissociation dynamics in L-selectin mediated leukocyte tethering appears to be first order: for large rebinding, the leakage approximation is rather good, and decay is exponential.

Our results can not be directly applied to adhesion clusters which compensate for force-induced decay by active growth, as it has been found experimentally for focal adhesions [Riveline et al., 2001]. Yet there are also interesting lessons for focal adhesions which can be learned from our model. For example, our stochastic analysis confirms the prediction from the deterministic stability analysis that cluster stability changes strongly around the critical value f_c (although small clusters tend to decay also at smaller force due to fluctuations towards the absorbing boundary). It is interesting to note that recent experiments measuring internally generated force at single focal adhesions suggest that f/N_t, the most important scaling variable of our analysis, is roughly constant for different cell types [Balaban et al., 2001, Tan et al., 2003]. It is therefore tempting to speculate that focal adhesions (or subsets of focal adhesions) are regulated to be loaded close to the critical value $f_c/N_t = \mathrm{pln}\,(\gamma/e)$ from (3.52). In this way, cells could quickly increase force on single bonds by small changes in actomyosin contractility. Large force on single closed bonds in turn might trigger certain signalling events in focal adhesions, possibly by mechanically opening up certain signalling domains [Isralewitz et al., 2001]. Our speculation provides a simple way to estimate the rebinding rate, which is very hard to measure experimentally. Using compliant substrates, it has been found that focal adhesions are characterised by a stress constant $\sim 5.5\,\mathrm{nN}\,/\,\mu\mathrm{m}^2$ [Balaban et al., 2001, Tan et al., 2003]. We do not know which of the many different proteins in focal adhesions defines the weak link which most likely ruptures under force, but we expect that it will have a similar area density as the integrin receptors, which are expected to have a typical distance between 10 and 30 nm, corresponding to 10^4 and 10^3 molecules per $\mu\mathrm{m}^2$, respectively. To obtain a lower estimate for γ, we therefore use $F_c = 5.5\,\mathrm{nN}$ and $N_t = 10^4$. For activated $\alpha_5\beta_1$-integrin binding to fibronectin, recent single molecule experiments obtained for the molecular parameter values $k_0 = 0.012\,\mathrm{Hz}$ and $F_B = 9\,\mathrm{pN}$ [Li et al., 2003]. Therefore the rebinding rate can be estimated to be at least $\gamma = 0.2$, that is $k_{on} = 0.002\,\mathrm{Hz}$ in dimensional units. Based on future experimental input, it would be interesting to extend our model of passive decay to active processes resulting in cluster growth under force.

Finally we want to comment that our model might also be applied to situations in materials science which are not directly related to biomolecular receptor-ligand pairs. One example is sliding friction, which recently has been modelled as dynamic formation and rupture of bonds under force [Filipov et al., 2004]. In general, we expect that many more cohesion phenomena in materials can be successfully modelled as dynamic interplay between rupture and rebinding.

Chapter 4

Linear loading

In many cases of interest, the force exerted on adhesion clusters is not a constant but varies in time. In the context of cell adhesion, time-dependent forces arise during the builup of force at newly formed contacts in migrating cells or during rolling adhesion of white blood cells. Experimentally, time-dependent forces are commonly used in dynamic force spectroscopy. The simplest possibility for a time-dependent force is a linear increase $f(\tau) = \mu\tau$ of force with the constant loading rate μ.

In this chapter we analyse the dynamic equations for adhesion cluster dynamics under linear loading. Results of the stochastic description will be compared to deterministic results. We begin with the case of vanishing rebinding, where we discuss shared as well as non-cooperative loading, before we turn to the general case of shared loading with finite rebinding and loading rate. For non-ccoperative loading the determnistic and the master equation are solved analytically. For shared loading we investigate the deterministic equation analytically using a scaling analysis for which the results of Chapter 3 are helpful and numerically by integration of (2.42) with the transition rates (2.25) for a linearly increasing force. The master equation is solved numerically to investigate the role of fluctuations.

4.1 Vanishing rebinding

4.1.1 Scaling analysis of the deterministic equation

In the deterministic framework, approximate analytic expressions for lifetime and rupture force of adhesion clusters and also for the time evolution of the number of closed bonds $N(\tau)$ can be found using a scaling analysis of the deterministic equation (2.42). In Chapter 3 we have applied this to the case of constant loading. For the more challenging case of linear loading, this analysis has been accomplished by Seifert [2000, 2002]. We will briefly recall this analysis for later use.

For $\gamma = 0$, the deterministic equation (2.42) reduces to

$$\frac{d}{d\tau}N = -Ne^{\mu\tau/N} \,. \tag{4.1}$$

To identify the most prominent contributions to this equation in different ranges of loading rate and for different times, it is convenient to replace the number of closed bonds $N(\tau)$ in (4.1) by the auxiliary variable $u(\tau) := \tau/N(\tau)$. Eq. (4.1) then becomes

$$\frac{d}{d\tau}u = u/\tau + ue^{\mu\tau} = u\left\{1 + 1/\tau\right\} + u\left\{e^{\mu u} - 1\right\} \,. \tag{4.2}$$

For small force per bond, $\mu u(\tau) \ll 1$ (i.e. $\mu\tau \ll N(\tau)$), the second term in (4.2) can be neglected, so that u satisfies the differential equation

$$\frac{d}{d\tau}u \approx u\left\{1 + 1/\tau\right\} . \tag{4.3}$$

The initial condition $N(\tau = 0) = N_t$ for $N(\tau)$ determines the time derivative of u at $\tau = 0$ as $(du/d\tau)|_{\tau=0} = 1/N_t$. With this initial condition (4.3) is solved by

$$u(\tau) = \tau e^{\tau}/N_t \, . \tag{4.4}$$

This solution corresponds to the force free exponential decay

$$N(\tau) = N_t e^{-\tau} \, . \tag{4.5}$$

For finite loading rate $\mu > 0$, the two parts of (4.2) will become equal at a 'crossover time' τ_1 which is implicitly defined through

$$e^{\mu u(\tau_1)} - 1 = 1 + \frac{1}{\tau_1} \, . \tag{4.6}$$

After the crossover, the exponential term dominates the differential equation (4.2) which can thus be replaced by

$$\frac{d}{d\tau}u \approx u\left\{e^{\mu u} - 1\right\} \approx u e^{\mu u} \, . \tag{4.7}$$

Additionally, the contribution of order unity has been neglected, which is allowed for $\mu u \gg 1$. Using separation of variables, this equation is solved implicitly by the expression

$$\tau_2 = \tau - \tau_1 = \mathrm{E}\left(\mu u(\tau_1)\right) - \mathrm{E}\left(\mu u(\tau)\right) = \mathrm{E}\left(\mu\tau_1/N(\tau_1)\right) - \mathrm{E}\left(\mu\tau/N(\tau)\right) \tag{4.8}$$

for the time τ_2 that has elapsed since the crossover at τ_1 when $u = u(\tau_1)$. The exponential integral $\mathrm{E}\,(z) = \int_z^\infty (e^{-z'}/z')\, dz'$ vanishes as $\mathrm{E}\,(x \to \infty) \sim e^{-x}/x$ for large arguments. Because $\tau_1/N(\tau_1) < T_{det}/N(T_{det})$ for $T_{det} > \tau_1$ and $N(T_{det}) \to 0$, the second exponential integral in (4.8) can be neglected to a good approximation. The lifetime T_{det} of the deterministic adhesion cluster can then be written as [1]

$$T_{det} = \tau_1 + \tau_2 = \tau_1 + \mathrm{E}\left(\mu u(\tau_1)\right) = \tau_1 + \mathrm{E}\left(\mu\tau_1/N(\tau_1)\right) \, . \tag{4.9}$$

This expression allows to extract the scaling behaviour of the lifetime T_{det} with loading rate and cluster size by estimating the crossover time τ_1 and the time τ_2 after crossover.

Slow loading, $\mu \ll 1$

For small loading rates, $\mu \ll 1$, the exponential solution in (4.5) applies until the decay of the cluster is complete and $N(T_{det}) = 1$. The lifetime of the cluster is

$$T_{det} \approx \ln N_t \, , \tag{4.10}$$

[1] For consistency we should use the condition $N(T_{det}) = 1$ for cluster dissociation as we have done for constant loading. The results will not differ much if $F_{det} = \mu T_{det} \gg 1$ and the number of closed bonds at crossover is large, $N(\tau_1) > 1$. In the following we will see that the rupture force is large unless $\mu \ll 1$ and that the number of intact bonds $N(\tau_1)$ at crossover approaches N_t for increasing loading rate.

as found in Sec. 3.2 for the force free decay of N_t independent molecular bonds. With $\mu \ll 1$, loading is too weak to affect bond rupture because the force per closed bond stays below the intrinsic force scale F_B of bond rupture throughout cluster decay, $\mu u(\tau) = \mu\tau/N(\tau) \ll 1$. If $\mu = 1$, the intrinsic force scale $f = 1$ is reached after the average, force free lifetime ($T = 1$) of a single adhesion bond. This would imply the stricter upper bound $\mu \ln N_t \ll 1$ for the scaling region to guarantee the validity of the force free description. However, even for large clusters the logarithm $\ln N_t$ is usually small. In general, deviations from exponential decay will be observed for $\mu \lesssim 1$.

Intermediate loading, $1 < \mu \ll N_t$

For intermediate loading rates, $1 < \mu \ll N_t$, the crossover time is smaller than $\ln N_t$ because $\mu \ln N_t > 1$ and the force per bond will exceed the intrinsic force scale during the final stages of cluster decay. On the other hand, the force per closed bond is small as long as $\tau \lesssim 1$ and the time $\tau \sim N_t/\mu \gg 1$ to reach the intrinsic force scale exceeds unity. Therefore, the crossover time will be larger than unity as well. This estimate is the better, the smaller the ratio μ/N_t is.

Crossover occurs when the force per bond, $\mu u(\tau)$, approaches unity so that $\mu u(\tau_1) < 1$ holds at crossover. Thus, to estimate the crossover time, the exponential on the left hand side of (4.6) can be expanded in a Taylor series to first order, $e^{\mu u} - 1 \approx \mu u$. Inserting the exponential solution (4.5) for u and neglecting the inverse $1/\tau_1$ of the crossover time leads to the relation

$$(\mu\tau_1/N_t)e^{\tau_1} = 1 + 1/\tau_1 \approx 1\,. \tag{4.11}$$

Multiplication with N_t/μ yields

$$\tau_1 \approx \mathrm{pln}\,(N_t/\mu) \simeq \ln(N_t/\mu)\ , \tag{4.12}$$

where the large argument approximation $\mathrm{pln}\, x \simeq \ln x$ for the product logarithm is used. The remaining time $\tau_2 = T_{det} - \tau_1$ after crossover is given by (4.9) as

$$\tau_2 = \mathrm{E}\,(\mu u(\tau_1)) \approx \mathrm{E}\,(\mu\tau_1 e^{\tau_1}/N_t) \approx \mathrm{E}\,(\ln(N_t/\mu))\ . \tag{4.13}$$

For $N_t \gg \mu$, the large argument approximation $\mathrm{E}\,(x) \approx e^{-x}/x$ for the exponential integral can be used and we have

$$\tau_2 \approx \frac{\mu/N_t}{\ln(N_t/\mu)} \ll \frac{1}{\ln(N_t/\mu)} = \frac{1}{\tau_1} = \frac{\tau_1}{\ln^2(N_t/\mu)} < \tau_1\,. \tag{4.14}$$

Since $\mu \ll N_t$, this time is very small compared to the inverse crossover time and because $\tau_1 > 1$ we have $\tau_2 \ll \tau_1$. The lifetime of the adhesion cluster scales like

$$T_{det} \approx \tau_1 \simeq \ln\frac{N_t}{\mu} \tag{4.15}$$

with the logarithm of the ratio of cluster size and loading rate. Obviously, this expression is valid only for $\mu > 1$. At $\mu = 1$ it equals the result for slow loading (4.10) but would yield a larger lifetime as for the force free decay for $\mu < 1$.

Fast loading, $\mu \gg N_t$

For fast loading with large loading rates, $\mu \gg N_t$, the two constant terms in (4.6) for the crossover time can be neglected and τ_1 is defined through

$$1 = \tau_1 e^{\mu u(\tau_1)} \approx \tau_1 \exp\left(\frac{\mu\tau_1}{N_t} e^{\tau_1}\right) , \tag{4.16}$$

where the exponential solution (4.3) was inserted for $u(\tau_1)$. Assuming that the crossover time will be sufficiently small ($\tau_1 \ll 1$), we can set $e^{\tau_1} \approx 1$ in the exponent in (4.16) and use

$$1 = \tau_1 \exp\left(\frac{\mu\tau_1}{N_t}\right) \quad \Leftrightarrow \quad \frac{\mu}{N_t} = \frac{\mu\tau_1}{N_t} \exp\left(\frac{\mu\tau_1}{N_t}\right) \tag{4.17}$$

to determine τ_1. Inserting $x := \mu\tau_1/N_t$ in the last equation leads to the solution for x as the product logarithm $x = \mathrm{pln}\,(\mu/N_t)$ so that the crossover time is

$$\tau_1 = \frac{N_t}{\mu} \mathrm{pln}\left(\frac{\mu}{N_t}\right) \simeq \frac{N_t}{\mu} \ln\left(\frac{\mu}{N_t}\right) . \tag{4.18}$$

In the last step, the large argument approximation $\mathrm{pln}\, x \simeq \ln x$ for the product logarithm has been used. The remaining time after the crossover is given by the exponential integral as in (4.9), that is

$$\tau_2 = T_{det} - \tau_1 \approx \mathrm{E}\left(\mu u(\tau_1)\right) \approx \mathrm{E}\left(\mu\tau_1 e^{\tau_1}/N_t\right) = \mathrm{E}\left(\ln\left(\mu/N_t\right)\right) \tag{4.19}$$

where (4.18) for the crossover time was inserted. Since $\mu/N_t \gg 1$ should hold the large argument approximation for the exponential integral, $\mathrm{E}\,(z) \approx e^{-z}/z$, can be used and

$$\tau_2 \approx \frac{N_t/\mu}{\ln\left(\mu/N_t\right)} = \frac{\tau_1}{\ln^2(\mu/N_t)} \ll \tau_1 . \tag{4.20}$$

Since $\tau_2 \ll \tau_1$, the lifetime of the adhesion cluster for fast loading is given by the crossover time

$$T_{det} \approx \frac{N_t}{\mu} \ln\left(\frac{\mu}{N_t}\right) . \tag{4.21}$$

Summary of the scaling regimes

The analysis has revealed three distinct scaling regimes for adhesion cluster lifetime with loading rate and initial cluster size. As in Seifert [2000, 2002], the scaling expressions for T_{det} and for the rupture force $F_{det} = \mu T_{det}$ are

$$T_{det} \begin{cases} \approx \ln N_t & \text{for } \mu \ll 1, \\ \simeq \ln\left(\frac{N_t}{\mu}\right) & \text{for } 1 < \mu \ll N_t, \\ \simeq \frac{N_t}{\mu} \ln\left(\frac{\mu}{N_t}\right) & \text{for } \mu \gg N_t \end{cases} \quad \text{and} \quad F_{det} \begin{cases} \approx \mu \ln N_t & \text{for } \mu \ll 1, \\ \simeq \mu \ln\left(\frac{N_t}{\mu}\right) & \text{for } 1 < \mu \ll N_t, \\ \simeq N_t \ln\left(\frac{\mu}{N_t}\right) & \text{for } \mu \gg N_t. \end{cases} \tag{4.22}$$

For slow loading, force does not yet affect bond rupture and the result for $\mu = 0$ applies with a slow, logarithmic increase of T_{det} with cluster size N_t. The force at rupture thus scales linearly with μ. For intermediate and fast loading, lifetime scales with the ratio μ/N_t alone, as expected from the deterministic equation (2.43) for the fraction of closed bonds which contains μ/N_t as the only parameter (when $\gamma = 0$). The lifetime is given by the time of the crossover from exponential to

super-exponential cluster decay. The time over which cluster decay proceeds exponentially becomes extremely short for large loading rates so that practically the whole cluster breaks down abruptly after the crossover and the condition $N(T_{det}) = 1$ for dissociation is irrelevant. For the rupture force $F_{det} = \mu T_{det}$, scaling with N_t/μ alone is lost. While for $\mu \ll 1$, the rupture force is $F_{det} \lesssim 1$, for intermediate and large loading, the rupture forces exceed $F_{det} > 1$ as it was assumed in the derivation of the expression for intermediate loading.

4.1.2 Numerical solutions of the deterministic equation

Due to the explicit time dependence of the deterministic equation, analytic solutions for $N(\tau)$ are not available. Instead, we use numerical integration of (4.1) to investigate the time dependence of $N(\tau)$ and test the assumptions and predictions of the scaling analysis. Moreover, lifetime and rupture force are calculated numerically and compared to the scaling results.

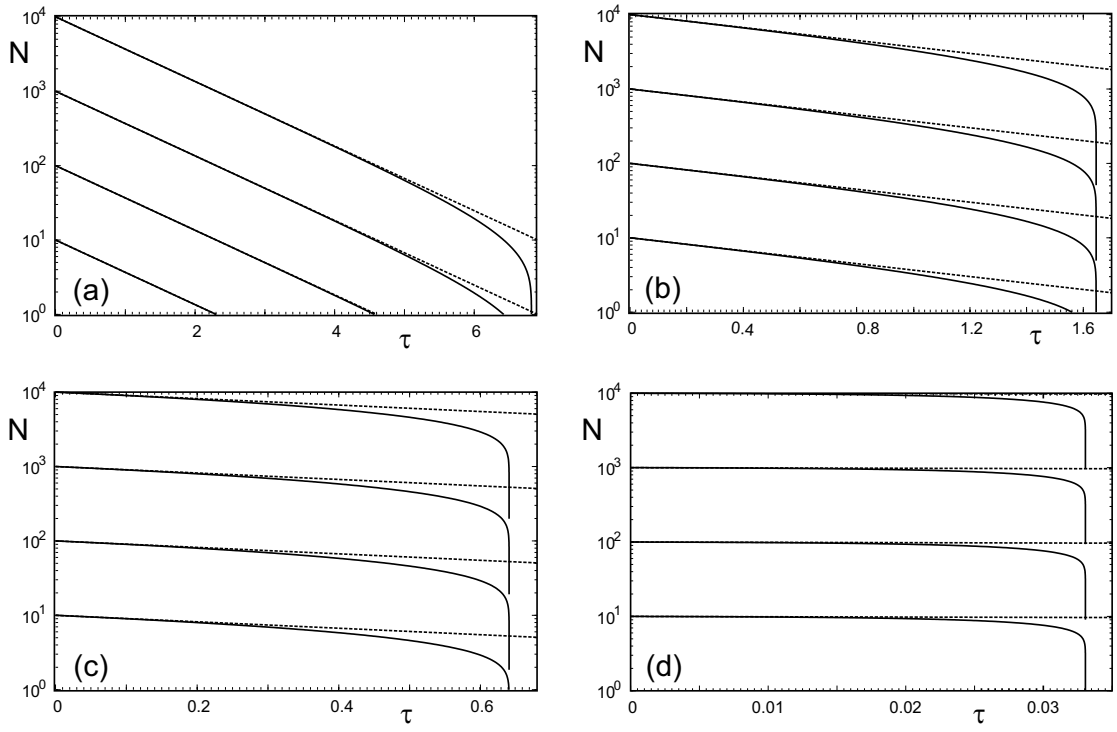

Figure 4.1: Solid lines: Numerical solutions of the deterministic equation (4.1) for the number of closed bonds $N(\tau)$ for the case of vanishing rebinding $\gamma = 0$ for the values $\mu/N_t = 10^{-4}$, 10^{-1}, 1 and 10^2 (a-d) of loading rate per initially closed bond and for $N_t = 10$, 10^2, 10^3 and 10^4 in each graph. Dashed lines: Force free exponential decay (4.5) plotted for comparison.

Fig. 4.1 plots results of numerical integration of the deterministic differential equation (4.1) for the number of closed bonds $N(\tau)$ in an adhesion cluster as function of time. The graphs show $N(\tau)$ for initial conditions $N_t = 10, 10^2, 10^3$ and 10^4. The ratio μ/N_t of loading rate and cluster size is the same for the different initial conditions in each graph. This means that the solutions are identical apart from the linear scaling with N_t. The numerical solutions for $N(\tau)$ are compared to the exponential approximations for times before the crossover time.

For the smallest value of $\mu/N_t = 10^{-4}$, the influence of force on cluster decay is weak and $N(\tau)$ follows closely the exponential approximation. Only for larger clusters with absolute loading rates of $\mu = 0.1$ and $\mu = 1$, the increasing force is able to accelerate cluster decay towards the end of the decay. The deviations from the exponential decay become large for small fractions of remaining bonds in the range of $N(\tau)/N_t \lesssim 100$. The force per bond reaches values of $0.5 \lesssim \mu\tau/N(\tau)$ which approaches the intrinsic force scale. For smaller N_t, these values were reached only below $N(\tau) = 1$. As described for constant loading in Sec. 3.1, the finite threshold $N(T_{det}) = 1$ then leads to scaling of the lifetime with $\ln N_t$.

For intermediate and fast loading, the initial cluster decay under small force can also be approximated by the force free exponential decay. As it was assumed in the scaling analysis, the crossover time after which the force becomes important and the decay becomes super-exponentially fast is usually close to the lifetime of the cluster. This assumption is best for very large loading rates where the lifetime becomes very short and the number of closed bonds hardly decreases during the exponential decay. At crossover, the fraction of intact bonds is

$$N(\tau_1)/N_t = e^{-\tau_1} \approx e^{(N_t/\mu)\ln(\mu/N_t)} = (N_t/\mu)^{N_t/\mu} \lesssim 1\,, \tag{4.23}$$

where the fast loading expression for $\tau_1 \approx T$ has been used. This fraction approaches unity for $\mu/N_t \to \infty$ since $N_t \ll \mu$ and $\lim_{x\to 0} x^x = 1$. The rest of the cluster breaks down completely within no time. The instability of adhesion clusters against a decrease of $N(\tau)$ under shared loading was observed already for constant force. For linear loading it is enhanced by the increasing force $f(\tau) = \mu\tau$. Because of the rapid breakdown of the cluster, the finite threshold becomes irrelevant for intermediate and fast loading and lifetime scales with μ/N_t alone.

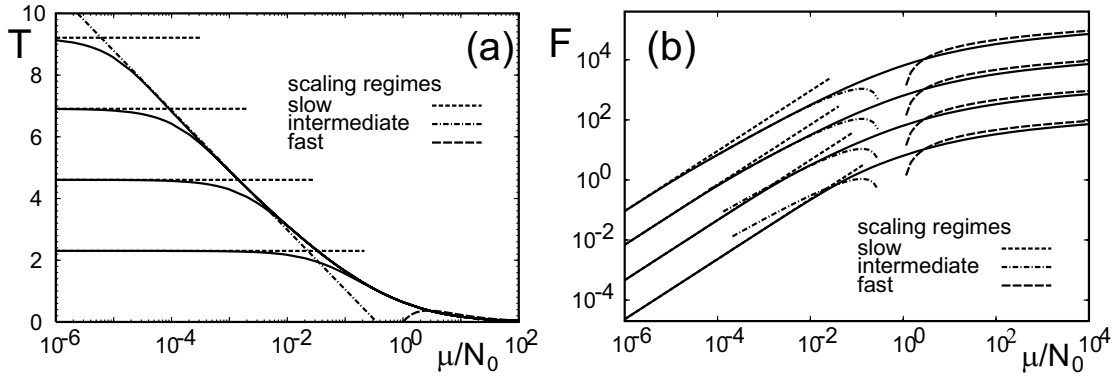

Figure 4.2: Solid lines: Deterministic, numerical results for (a) lifetime T_{det} and (b) rupture force $F_{det} = \mu T_{det}$ for the case of vanishing rebinding $\gamma = 0$ as function of μ/N_0 for $N_t = N_0 = 10$, 10^2, 10^3 and 10^4. Dashed lines: Curves for all three scaling regimes (4.22). For intermediate loading the expression $T = 0.83 \ln(0.38 N_t/\mu)$ is used.

The lifetime T_{det} is computed numerically by integrating the deterministic equation for $N(\tau)$ until $N(T_{det}) = 1$ is reached. Fig. 4.2 displays plots of (a) T_{det} and (b) F_{det} as functions of μ/N_t. Results are plotted for the initial conditions $N_t = 10, 10^2, 10^3$ and 10^4. The scaling expressions (4.22) are plotted in comparison. For slow and fast loading they describe the numerical results very well for all cluster sizes N_t. For intermediate loading we have used the expression $T_{det} \approx 0.83 \ln(0.38 N_t/\mu)$ for the scaling result. It can only be applied for large enough clusters for which $N_t \gg 1$ ($N_t \geqslant 100$ in

Fig. 4.2). For smaller clusters, a pronounced scaling regime does not exist due to the strong influence of the finite cutoff.

4.1.3 Stochastic analysis

For $\gamma = 0$, the forward rates $g(i)$ vanish especially at $i = 0$ and we do not need to distinguish between reflecting and absorbing boundary the detached state $i = 0$. The master equation (2.26) reduces to

$$\frac{d}{d\tau}p_i = r_{i+1}p_{i+1} - r_i p_i = (i+1)e^{\mu\tau/(i+1)}p_{i+1} - ie^{\mu\tau/i}p_i\,. \tag{4.24}$$

For finite force $\mu\tau > 0$, the reverse rate $r(0)$ diverges. Setting $r_0 = 0$ implies an artificial boundary. However, because $i = 0$ is an absorbing boundary, this is not relevant for the solution of (4.24) for the states $i > 0$. The occupancy of the detached state would be determined by the normalisation of the distribution.

Single bond rupture

For a single, irreversible bond, the master equation (4.24) can be solved analytically. In fact, the corresponding analysis by Evans and Ritchie [1997] lead to the new field of 'dynamic force spectroscopy', with subsequent experiments quickly corroborating the theoretical predictions. For $N_t = 1$, the master equation (4.24) reduces to the ordinary differential equation

$$\frac{d}{d\tau}p_1 = -e^{\mu\tau}p_1 \tag{4.25}$$

for p_1. The probability p_0 follows from integration of $dp_0/d\tau = r(1)p_1$ or through the normalisation of the distribution as $p_0 = 1 - p_1$. With the initial condition $p_1(0) = 1$, (4.25) is solved by

$$p_1(\tau) = e^{-(e^{\mu\tau}-1)/\mu} \quad \text{so that} \quad p_0(\tau) = 1 - p_1(\tau) = 1 - e^{-(e^{\mu\tau}-1)/\mu}\,. \tag{4.26}$$

Bond rupture proceeds exponentially with the exponentially increasing rupture rate $e^{\mu\tau}$. The average number of closed bonds is the probability that the bond is atached:

$$N(\tau) = p_1(\tau)\,. \tag{4.27}$$

The variance of the distribution is

$$\sigma_N^2 = \langle i^2\rangle - \langle i\rangle^2 = p_1 p_0 = p_1(1-p_1)\,. \tag{4.28}$$

It is zero initially, passes through a maximum at $p_1 = 0.5$ or $\tau = \ln(\mu\ln(2)+1)/\mu$ and then dies out on the same time-scale as the average. The relative standard deviation $\sigma_N(\tau)/N(\tau)$ thus diverges for large times. In general the average deviation $\langle(i-N)^n\rangle$ from the average is a polynomial of order $n-1$ in p_1. The leading term for long times is linear in p_1 so that the fluctuations die out on much longer time-scales than the average and $\langle(i-N)^n\rangle/N^n$ diverges.

The dissociation rate for the single bond follows from the solution of the master equation as

$$D(\tau) = \dot{p}_0 = e^{\mu\tau}p_1 = e^{\mu\tau}e^{-(e^{\mu\tau}-1)/\mu}\,. \tag{4.29}$$

Averaging τ with $D(\tau)$ yields the average lifetime T. The result can be written in terms of the exponential integral $\mathrm{E}(1/\mu)$ as

$$T = \int_0^\infty \tau D(\tau)\,d\tau = \frac{e^{1/\mu}}{\mu}\,\mathrm{E}\left(\frac{1}{\mu}\right)\,. \tag{4.30}$$

For slow loading $\mu \ll 1$, this expression approaches $T \approx 1$ because the prefactor of the exponential integral is the inverse of the large argument approximation for $E(1/\mu)$. For fast loading, $\mu \gg 1$, the average lifetime vanishes as $T \approx \ln(\mu)/\mu$.

The average rupture force is $F = \mu T = e^{1/\mu}\,\mathrm{E}\,(1/\mu)$ so that $F \approx \mu$ for slow loading, $\mu \ll 1$, and $F \approx \ln \mu$ for fast loading, $\mu \gg 1$. For slow loading, the average rupture force vanishes continuously. A finite 'critical loading rate' for bond strength arises only when the rupture force is defined as the maximum of the dissociation rate [Evans and Ritchie, 1997]. As a function of force, the dissociation rate reads

$$D(f) = \frac{1}{df/d\tau} D(\tau(f)) = \frac{1}{\mu} D(\tau(f)) = \frac{1}{\mu} e^f p_1(f) = \frac{1}{\mu} e^f e^{-\left(e^f - 1\right)/\mu}. \tag{4.31}$$

For $\mu \geqslant 1$, this expression has a maximum at $F_{max} = \ln \mu$. For $\mu \leqslant 1$, the maximum is $F_{max} = 0$ so that adhesion bonds decay with highest probability under no force. At the critical loading rate, $\mu = 1$, the dissociation rate has a horizontal tangent at $f = 0$. For $\mu > 1$, the expression for the maximum is identical to the fast loading limit for the average. For slow and intermediate loading, however, differences between average and maximum arise. In particular, the average is a smooth function for all $\mu > 0$.

The maximum dissociation time is $T_{max} = \ln(\mu)/\mu$ for $\mu \geqslant 1$. This is non-monotonous function of μ. It is zero at $\mu \leqslant 1$, increases with $\mu > 1$ up to a maximum at $\mu = e$ and decreases thereafter. The average, on the other hand, is a monotonous, decreasing function of μ. Using the maximum of the dissociation rate to define the rupture time thus leads to counterintuitive results [2].

Time evolution of adhesion clusters

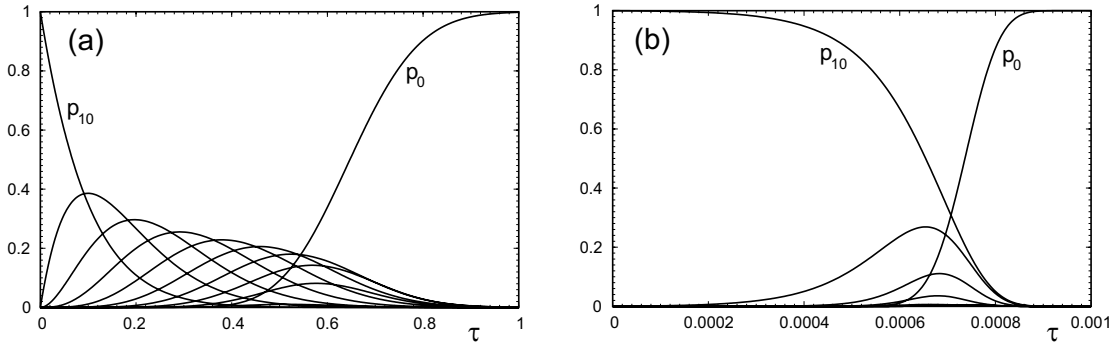

Figure 4.3: Time evolution of the probability distribution $\{p_i(\tau)\}_{i=0}^{N_t}$ for vanishing rebinding $\gamma = 0$ with initial number of closed bonds $N_t = 10$ and values (a) $\mu/N_t = 1$ and (b) $\mu/N_t = 10^4$ for the ratio of loading rate and cluster size, i.e., for loading rates $\mu = 10$ and 10^5.

For larger adhesion clusters the master equation for the probability distribution $\{p_i\}_{i=0}^{N_t}$ can only be solved numerically. Monte Carlo solutions of the master equation (4.24) are plotted in Fig. 4.3. The time evolution of the state probabilities p_i of an adhesion cluster with initial condition $p_i(\tau = 0) = \delta_{i,N_t}$ to the detached state $p_i(\infty) = \delta_{i,0}$ is shown for $N_t = 10$ and different values of μ/N_t.

[2] In particular, an increase of lifetime is typically associated with catch-bonds. Here, however, rupture rate increases with force and the increase in lifetime would be a mere artefact from the definition of the lifetime.

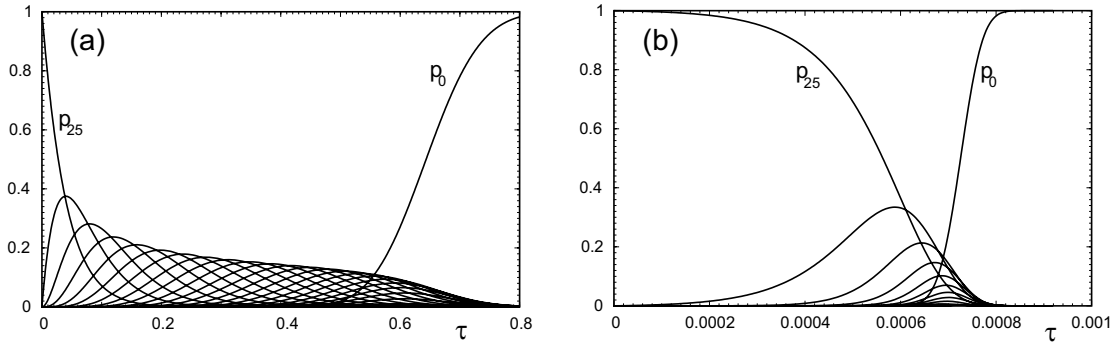

Figure 4.4: Time evolution of the probability distribution $\{p_i(\tau)\}_{i=0}^{N_t}$ for vanishing rebinding $\gamma = 0$ with initial number of closed bonds $N_t = 25$ and values $\mu/N_t = 1$ (a) and $\mu/N_t = 10^4$ (b) for the ratio of loading rate and cluster size, i.e.,for loading rates $\mu = 25$ and 2.5×10^5.

For very slow loading, $\mu \ll 1$ (not shown), the $p_i(\tau)$ are practically identical to the evolution under no loading, compare Fig. 3.1 in Sec. 3.1. For larger loading rates in the range of intermediate loading, cluster decay gradually accelerates which is demonstrated for $\mu = N_t$. Initially, decay proceeds in a similar way as for $\mu \ll 1$ by traversing all states from $i = 10$ to $i = 0$. The height of the maxima of subsequent state functions p_i decreases gradually due to the increasing force which facilitates fluctuations to the absorbing boundary and leads to a slow increase of p_0. Towards the end of the decay, the force per closed bond exceeds the intrinsic force scale, $f/i > 1$. Further decay is strongly accelerated and the occupancy of the detached state increases quickly. For very fast loading, $\mu \gg N_t$, the dissociation of the clusters proceeds very rapidly and the maximum of the distribution passes from the initial state directly to the detached state. However, because the force vanishes initially and cluster evolution is slow, lower states can still be occupied appreciably. This is unlike the case of constant force. The following transition to the detached state appears more rapid than for constant loading because the instability of adhesion clusters under shared force is combined with the increase of force with time.

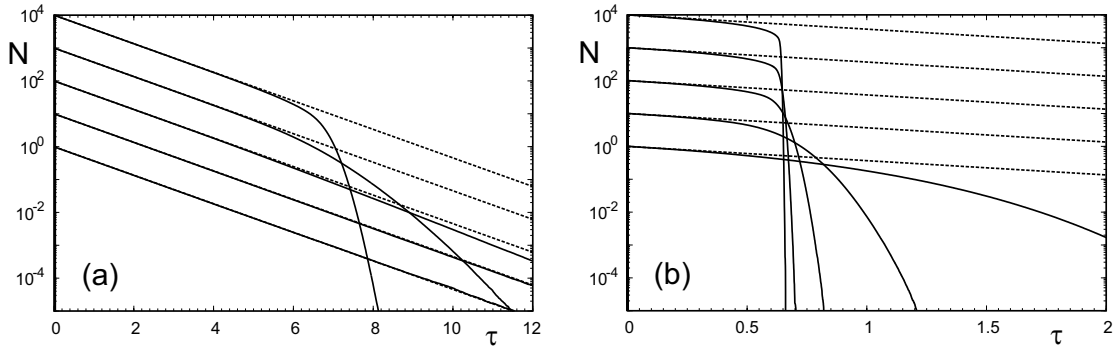

Figure 4.5: Solid curves: Results of Monte Carlo calculations for the average number of closed bonds $N(\tau)$ as a function of time for (a) $\mu/N_t = 10^{-4}$ and (b) $\mu/N_t = 1$. Each graph shows results for $N_t = 1, 10, 10^2, 10^3$ and 10^4. Dashed curves: Exponential approximation which is expected for $\mu = 0$. The single bond results are identical to the analytic expression (4.27).

Fig. 4.4 shows the time evolution of an adhesion cluster with $N_t = 25$. The values for μ/N_t are the same as in Fig. 4.3 to allow a direct comparison to the evolution of smaller clusters. Moreover, the dissociation times are comparable. The basic structure of the distribution seems to be identical. For intermediate loading, cluster evolution gradually accelerates before the final dissociation of the last bonds. For fast loading, several states close to the initial state become appreciably occupied before p_0 rises abruptly. In both cases, the final increase of p_0 is steeper than for smaller clusters in Fig. 4.3 because for a given $\mu\tau/N_t$, the force on the last bonds increases with N_t while the decay time was the same for different N_t.

Fig. 4.5 shows results of Monte Carlo calculations for the average number of closed bonds $N(\tau)$ with different initial condition and values for the ratio μ/N_t of loading rate to cluster size. The numerical results are compared to the exponential decay expected for small forces $\mu\tau \ll 1$. As it was found for the deterministic description, this is indeed a good approximation for slow loading. For $\mu/N_t = 10^{-4}$, deviations are observed for large clusters at a similar fraction of remaining closed bonds, $N(\tau)/N_t \lesssim 1/100$ and in a similar extent as for the deterministic results. For intermediate and fast loading, the exponential decay still describes the initial behaviour of $N(\tau)$. It decreases only slightly before it drops to zero rapidly as most clusters of the ensemble dissociate at the crossover time. Due to a larger influence of fluctuations and weaker cooperativity, the final decrease is smoother for smaller clusters. This means that for a given μ/N_t, the curves $N(\tau)$ as solutions of the master equation are not congruent and do not scale linearly with N_t as the deterministic result. The stochastic average contains all moments of the probability distribution that were neglected in the deterministic equation (4.1). The numerical result for the single bond $N_t = 1$ reproduces the analytical result (4.27).

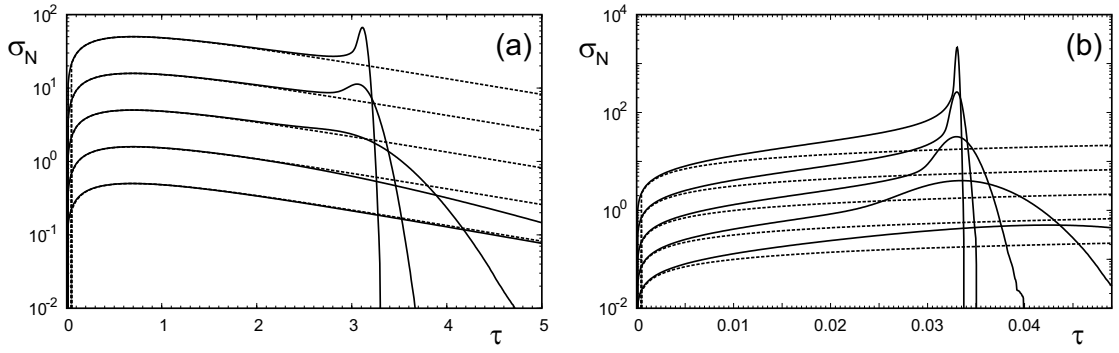

Figure 4.6: Standard deviation $\sigma_N(\tau)$ of the distribution $\{p_i\}_{i=0}^{N_t}$ as function of time for (a) $\mu/N_t = 10^{-2}$ and (b) $\mu/N_t = 10^2$ with initial conditions $N_t = 1, 10, 10^2, 10^3$ and 10^4. Solid curves: Monte Carlo results. Dashed curves: Analytic result (4.28) for $\mu = 0$ plotted for $N_t > 1$.

The width of the distribution $\{p_i\}_{i=0}^{N_t}$ is described by the variance $\sigma_N^2(\tau)$ which also gives information about the expected deviations of the deterministic result from the stochastic average which grow with $\sigma_N^2(\tau)$ in the lowest, non-vanishing order. For vanishing loading, $\mu = 0$, the analytical result for the variance of the radioactive decay process is (see (A.29) of Appendix A)

$$\sigma_N^2(\tau) = N(\tau)\left(1 - e^{-\tau}\right) = N_t e^{-\tau}\left(1 - e^{-\tau}\right) . \tag{4.32}$$

It scales linearly with N_t and decreases exponentially as $e^{-\tau}$ for large times. For the single bond, the variance was given in (4.28). Fig. 4.6 plots numerical results for the square root of the variance, the standard deviation σ_N, for finite loading rates $\mu/N_t > 0$. For $N_t = 1$, the analytical result is

reproduced. The approximation (4.32) for $\mu = 0$ describes the initial increase of σ_N^2 but deviations appear with growing force. For small clusters, the standard deviation decreases smoothly but faster than for $\mu = 0$ because cluster decay in general is accelerated. Larger clusters display a peak of the standard deviation immediately before the ultimate decay of $\sigma_N^2(\tau)$ and also $N(\tau)$. This peak becomes sharp for large clusters under fast loading, that is, under those conditions for which also the average showed a fast breakdown.

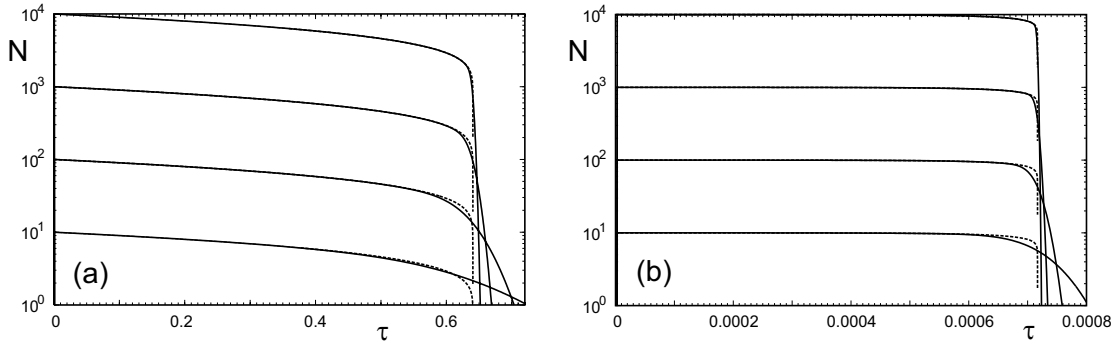

Figure 4.7: Comparison of stochastic and deterministic results for the average number of bonds $N(\tau)$. Solid lines: Results of Monte Carlo simulations of the master equation (4.24) for $\gamma = 0$ and the values (a) $\mu/N_t = 10^{-2}$ and (b) $\mu/N_t = 10^2$ of loading rate per initially closed bond and for initial conditions $N_0 = N_t = 10$, 10^2, 10^3 and 10^4 in each graph. Dashed lines: Results of numerical integration of the deterministic equation (4.1) for the given set of parameters.

Fig. 4.7 directly compares stochastic and deterministic result for the average number of closed bonds, $N(\tau) = \langle i \rangle$. As expected, the different results agree well in the initial phase which is approximately described by an exponential decay. Here, the non-linearity of the transition rates in the master equation is weak due to the small force $f(\tau) = \mu\tau$. Strong deviations appear after the crossover to the super-exponential decay. These are especially pronounced for small clusters and large loading rates. For increasing cluster size, the deviations are confined to a very small region around the breakdown of the cluster where the stochastic result is always smoother than the deterministic one. This is in agreement with the results for the variance for which the peak became sharper with increasing cluster size. For small clusters, stochastic fluctuations lead to a smooth decrease in $N(\tau)$. Initially, fluctuations from the average towards smaller values and to the absorbing boundary let $N(\tau)$ decrease faster than in the deterministic description. Later, rare realisations of clusters with long lifetimes let the stochastic average decrease more slowly than the deterministic one.

Dissociation rate and average cluster lifetime

For a single bond, the dissociation rate $D(\tau) = dp_0(\tau)/d\tau = r_1 p_1$ under finite linear loading $\mu > 0$ is given in (4.29). For larger clusters and vanishing loading, $\mu = 0$, the expression for the $p_i(\tau)$ is given in (A.27) of Appendix A and the dissociation rate follows as

$$D(\tau) = N_t e^{-\tau} \left(1 - e^{-\tau}\right)^{N_t - 1} . \tag{4.33}$$

For $N_t = 1$, the initial dissociation rate is finite and given by $D(\tau = 0) = 1$, independent of μ. For $N_t > 1$, cluster dissociation is a multistep process and the dissociation rate vanishes at $\tau = 0$.

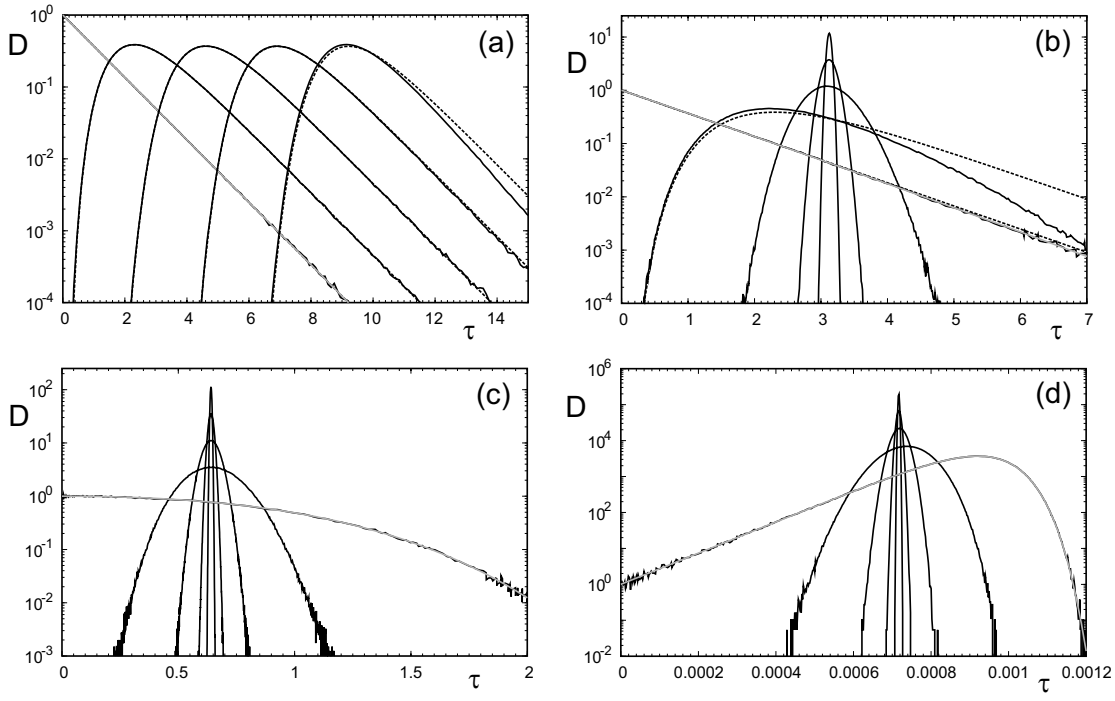

Figure 4.8: Solid black curves: Monte Carlo results for the dissociation rate $D(\tau)$ of adhesion clusters with initial conditions $N_t = 1, 10, 10^2, 10^3$ and 10^4 and $\mu/N_t = 10^{-6}, 0.1, 1.0$ and 10^4 (a-d). Grey curves: Analytical single bond result (4.29) superimposed on the numerical curves for $N_t = 1$. Dashed curves: Analytical results (4.33) for $\mu = 0$ are compared to numerical ones for $\mu/N_t = 10^{-6}$ and also for $\mu/N_t = 10^{-2}$ at $N_t = 1$ and 10.

As discussed in Sec. 3.1, the dissociation rate for vanishing rebinding and vanishing loading has a maximum at $T_{max} = \ln N_t$ and decreases as $D(\tau) \sim e^{-\tau}$ for large times. Fig. 4.8 plots results of stochastic simulations for the dissociation rate for different N_t and increasing values of μ/N_t. For slow loading with $\mu < 1$, (4.33) describes the dissociation rate very well. The small forces accelerates cluster in particular towards the end of the decay process and shifts the maximum to smaller times. For intermediate and fast loading and for a given μ/N_t the maximum hardly depends on N_t. Cluster size mainly determines the width of the distribution which decreases with increasing N_t. Moreover, width and asymmetry reduce with increasing loading rate. Unlike the case of constant force, the distributions do not approach a Poisson distribution. For large custers they remain Gauss-like with weak asymmetry. Because force vanishes initially, cluster dissociation is slow and the rupture of several bonds contributes to cluster dissociation. This has been observed in the plots of the state functions p_i. For the *single bond* the numerical result for $D(\tau)$ is well represented by the analytical result (4.29). For $\mu < 1$, the maximum of $D(\tau)$ is always $D(\tau = 0) = 1$. For $\mu = 1$ the slope at $\tau = 0$ vanishes and a maximum at finite times emerges. As described above, the position of the maximum first increases until $\mu = e$ and then decreases again. For large loading rates, $D(\tau)$ for the single bond is a strongly asymmetric function.

The mean lifetime $T = \int_0^\infty \tau D(\tau)\, d\tau$ of adhesion clusters with N_t bonds for vanishing loading and rebinding is given in (3.23) of Sec. 3.1. It can also be calculated from the expression (4.33) for

the dissociation rate and is given by the N_t^{th} harmonic number

$$T = \mathrm{H}_{N_t} \approx \ln N_t + \frac{1}{2N_t} + \Gamma \ . \tag{4.34}$$

It differs from the deterministic scaling result by the additional terms $(1/2N_t) + \Gamma$. Comparison of numerical results and the deterministic scaling expressions (not shown) reveals that the main difference is in the fluctuation dominated regime of slow loading. For intermediate and fast loading, where cluster decay is driven by force, there is a good agreement between stochastic and deterministic results and the scaling expressions can be applied. However, for fast loading, there is no scaling with μ/N_t alone but lifetime reduces with larger absolute loading rates. This is similar to the results found for constant loading.

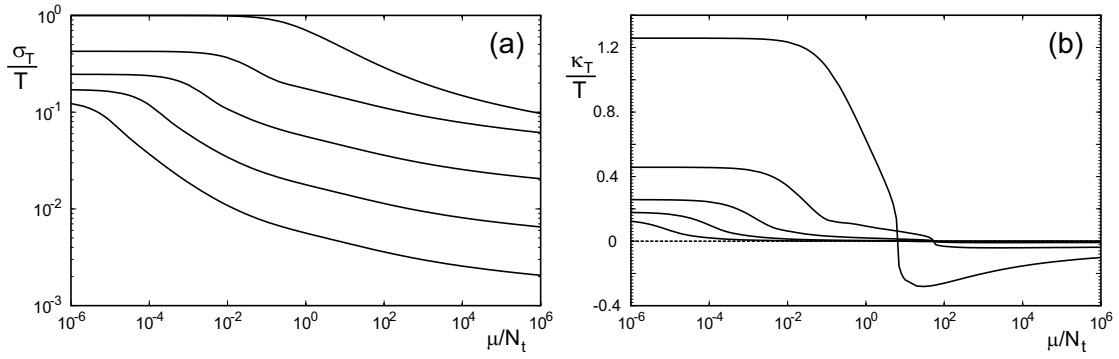

Figure 4.9: (a) Relative standard deviation σ_T/T and (b) the cubic root of third cumulant normalised with the lifetime, κ_T/T, of the dissociation rate $D(\tau)$ as function of μ/N_t for initial conditions $N_t = 1, 10, 10^2, 10^3$ and 10^4 (top to bottom at small μ/N_t).

The plots of $D(\tau)$ in Fig. 4.8 demonstrated qualitatively the influence of loading rate and cluster size on width and asymmetry of the dissociation rate. Quantitative measures are the variance σ_T^2 and the third cumulant κ_T^3 of $D(\tau)$. For vanishing force, we have

$$\sigma_T^2 = \zeta(2) = \sum_{i=1}^{N_t} \frac{1}{i^2} \quad \text{and} \quad \kappa_T^3 = \zeta(3) = \sum_{i=1}^{N_t} \frac{1}{i^3} \, , \tag{4.35}$$

for the sequence of Poisson processes as explained in Sec. 3.2. Fig. 4.9 plots the relative standard deviation σ_T/T and the cubic root of the third cumulant relative to the lifetime, κ_T/T, as function of μ/N_t for different initial cluster sizes. The standard deviation decreases monotonously from the zero force values with increasing μ/N_t. Unlike the case of large constant force the relative standard deviation does not reach $\sigma_T/T = 1$ for fast loading. Adhesion cluster dissociation under linear loading does not approach a Poisson process because initially the force is small and rupture proceeds slowly. The ratio κ_T/T is positive for $\mu \ll 1$ which reflects the exponential long time tail for slow loading. At intermediate loading $\mu/N_t \lesssim 1$ it becomes negative, that is, the dissociation rate is skewed towards small times, because cluster dissociation is accelerated by the rapidly increasing force.

4.2 Non-cooperative linear loading with vanishing rebinding

For non-cooperative *constant* loading it was shown in Sec. 3.3 that the dynamic equations (2.28) and (2.45) are equivalent to those equations for vanishing loading. The reason for this is that there are only two time-scales for cluster dynamics which are set by the on- and the off-rate. This is not the case for shared loading because the (single bond) off-rate depends on i so that there are $N_t + 1$ different transition rates and time-scales in the master equation. For non-cooperative loading, the *force per bond* $f(\tau) = \mu\tau$ is controlled directly so that it does not depend on i. The linear time-dependence introduces another time-scale $1/\mu$ for a change in the off-rate. In the following we will derive solutions for the master equation for non-cooperative linear loading in the case of vanishing rebinding, $\gamma = 0$. These allow a comparison of numerical and exact analytical results for the case of multiple bonds and time-dependent transition rates.

4.2.1 Transformation of the dynamic equations

For vanishing rebinding, $\gamma = 0$, the master equation (2.28) for non-cooperative linear loading reads

$$\frac{d}{d\tau}p_i = (i+1)e^{\mu\tau}p_{i+1} - ie^{\mu\tau}p_i\,. \tag{4.36}$$

The deterministic equation (2.45) for this case is

$$\frac{d}{d\tau}N = -Ne^{\mu\tau}\,. \tag{4.37}$$

The time-scale for cluster dynamics is given by the off-rate $e^{\mu\tau}$ which changes on a time-scale set by the loading rate. With a transformation $\vartheta(\tau)$ of time τ such that the off-rate is constant on ϑ, the dynamic equations become linear equations with *constant* transition rates and can be solved by standard methods. A transformation that achieves this is

$$\tau \to \vartheta = \left(e^{\mu\tau} - 1\right)/\mu\,. \tag{4.38}$$

The variable ϑ equals τ for $\mu = 0$, vanishes at $\tau = 0$ and increases strictly monotonic, but non-linearly, with τ. The time derivative is transformed to the derivative with respect to ϑ according to

$$\frac{d}{d\tau} = \frac{d}{d\tau}\vartheta\frac{d}{d\vartheta} = e^{\mu\tau}\frac{d}{d\vartheta}\,. \tag{4.39}$$

Inserting this into (4.37) and (4.36), respectively, eliminates the explicit time dependence from the dynamic equations. The master equation (4.36) for $\gamma = 0$ is transformed to

$$\frac{d}{d\vartheta}p_i = (i+1)p_{i+1} - ip_i \tag{4.40}$$

and the deterministic equation (4.37) takes the simple form

$$\frac{d}{d\vartheta}N = -N\,. \tag{4.41}$$

The differential equation (2.46) for the variance is

$$\frac{d}{d\vartheta}\sigma_N^2 = N - \sigma_N^2\,. \tag{4.42}$$

The equations (4.40) to (4.42) describe a 'radioactive' decay of independent molecular bonds in the variable ϑ. Solutions for these equations are given in Appendix A and can be applied directly to the present case of non-cooperative linear loading.

The simple variable transformation is successful because the reverse rates $r(i)$ all share the same time-dependence and the loading rate μ and the off-rate $e^{\mu\tau}$ define the only two time-scales in the system. This is a similar situation as for constant loading with finite on-rate $\gamma > 0$. Introducing finite rebinding for linear loading introduces a third time-scale and the dynamic equations could not be recast on the simple case of linear equations with constant transition rates.

4.2.2 Deterministic analysis

The solution of (4.41) is the exponential decay $N(\vartheta) = N_t e^{-\vartheta}$ of the number of closed bonds $N(\tau)$ with unit relaxation rate. In the force free time-scale τ, the solution reads

$$N(\tau) = N_t e^{-(e^{\mu\tau}-1)/\mu} \,. \tag{4.43}$$

Cluster decay is accelerated exponentially as $e^{\mu\tau}$ due to the increase in force $f = \mu\tau$ with time. The dissociation 'time' Θ_{det} at which $N(\vartheta = \Theta_{det}) = 1$ is given by $\Theta_{det} = \ln N_t$. The actual dissociation time is

$$T_{det} = \frac{1}{\mu} \ln\left(\mu\Theta_{det} + 1\right) = \frac{1}{\mu} \ln\left(\mu \ln N_t + 1\right) \,. \tag{4.44}$$

The corresponding result for the rupture force $F_{det} = \mu T_{det}$ is

$$F_{det} = \ln\left(\mu \ln N_t + 1\right) \,. \tag{4.45}$$

The results (4.44) and (4.45) for lifetime and rupture force of the deterministic adhesion cluster should be compared to the results of the scaling analysis presented by Seifert [2000]. There, two different scaling regimes for slow and fast loading, respectively, were identified. For slow loading, lifetime scaled with $\ln N_t$. This is indeed the limit of (4.44) for vanishing loading rate,

$$\lim_{\mu\to 0} T_{det} = \ln N_t \,. \tag{4.46}$$

For fast loading, lifetime was found to scale as $\ln(\mu)/\mu$. This is the limit of (4.44) for large μ since

$$\lim_{\mu\to\infty} T_{det} = \lim_{\mu\to\infty} \frac{\ln\ln N_t + \ln\mu}{\mu} = \lim_{\mu\to\infty} \frac{\ln\mu}{\mu} \,. \tag{4.47}$$

The scaling expressions for lifetime and rupture force of adhesion clusters, which are derived from (4.44) are

$$T_{det} \approx \begin{cases} \ln N_t & \text{for } \mu \ln N_t \ll 1 \\ \frac{\ln\mu}{\mu} & \text{for } \mu \ln N_t \gg 1 \end{cases} \quad \text{and} \quad F_{det} \approx \begin{cases} \mu \ln N_0 & \text{for } \mu \ln N_t \ll 1 \\ \ln\mu & \text{for } \mu \ln N_t \gg 1. \end{cases} \tag{4.48}$$

As for shared loading we may assume that $\ln N_t$ is roughly unity so that the scaling regimes are separated by $\mu = 1$. If the loading rate per closed bond is far below unity, loading does not affect rupture of adhesion bonds and the result for the force free decay applies. For large μ the initial number of closed bonds is irrelevant and the single bond result applies. There are only two different loading regimes whereas three different regimes were identified for linear *shared* loading. These regimes were separated by values of the loading rate (for the whole cluster) $\mu = 1$, for which the loading rate per bond, $\mu/N(\tau)$, reaches unity for the last bond and $\mu = N_t$, where the loading rate per bond is larger than unity from the start. Because force is not shared in the present case, the intermediate regime is absent for *non-cooperative* loading.

4.2.3 Stochastic analysis

The solution of the master equation (4.40) on the time-scale ϑ is the binomial distribution (3.33) which, on the time-scale τ, reads

$$p_i(\tau) = \binom{N_t}{i} \left[1 - e^{-(e^{\mu\tau}-1)/\mu}\right]^{N_t-i} e^{-i(e^{\mu\tau}-1)/\mu} . \tag{4.49}$$

Cluster evolution accelerates exponentially with time but the relative distribution of states at any given time is unchanged with respect to the force free decay.

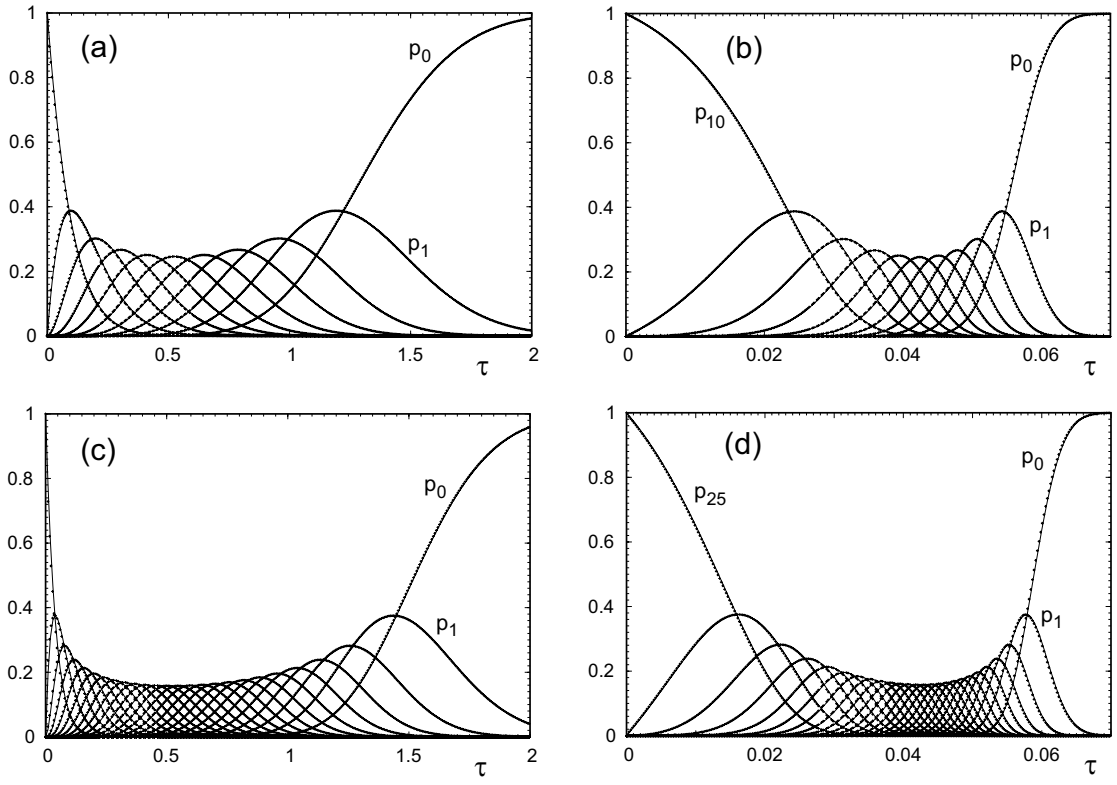

Figure 4.10: Probability distribution $\{p_i(\tau)\}_{i=0}^{N_t}$ as function of time τ for initial conditions $N_0 = N_t = 10$ (a and b) and $N_0 = N_t = 25$ (c and d) and the loading rates $\mu = 1$ (a and c) and $\mu = 100$ (b and d). Solid curves: Analytic solutions (4.49). Small symbols: Numerical results from stochastic simulations with the Gillespie algorithm for time-dependent transition rates.

The probability distribution $\{p_i\}_{i=0}^{N_t}$ from (4.49) is plotted in Fig. 4.10 for the initial number of bonds $N_t = 10$ and $N_t = 25$ and the loading rates $\mu = 1.0$ and 100.0. At any time of the decay process, the relations between the curves are the same as for $\mu = 0$ at the corresponding time $\vartheta(\tau)$. The accelerated decay for fast loading leads to a shorter overall time for dissociation and a relatively stretched initial time evolution with a quenched evolution of the final stages due to the larger force and larger bond rupture rates. The analytic solutions are compared to numerical results which coincide exactly with the analytic ones.

The probability distribution (4.49) yields the same result (4.43) as the deterministic description

for the average number of closed bonds. The variance is given by

$$\sigma_N^2(\tau) = N(\tau)\left(1 - e^{-(e^{\mu\tau}-1)/\mu}\right) = N_t e^{-(e^{\mu\tau}-1)/\mu}\left(1 - e^{-(e^{\mu\tau}-1)/\mu}\right) . \tag{4.50}$$

As always for linear master equations, this is a solution for the deterministic differential equation (2.46). The relative mean square deviation scales with the inverse of system size,

$$\frac{\sigma_i^2(\tau)}{N^2(\tau)} = \frac{1 - e^{-(e^{\mu\tau}-1)/\mu}}{N(\tau)} = \frac{e^{(e^{\mu\tau}-1)/\mu} - 1}{N_t} \tag{4.51}$$

For small times $\mu\tau \ll 1$, this width of the distribution increases linearly with time since $(e^{\mu\tau}-1)/\mu \approx \tau$ and $e^{\tau} \approx 1 + \tau$. For large loading rates and times the increase is exponential in the exponentially increasing reverse rate $e^{\mu\tau}$. The ratio diverges since the average number of bonds approaches zero faster than the variance.

According to the result (3.23) for the force free average cluster lifetime without rebinding, the average $\Theta := \langle\vartheta\rangle$ of the dissociation 'time' ϑ is the N_t^{th} harmonic number,

$$\Theta = \sum_{i=1}^{N_0} \frac{1}{i} = \mathrm{H}_{N_t} . \tag{4.52}$$

The average lifetime $T = \langle\tau\rangle$ cannot be derived directly from this since ϑ is a non-linear function of τ. Nevertheless, the approximation

$$\Theta = \frac{1}{\mu}\left(\langle e^{\mu\tau}\rangle - 1\right) \approx \frac{1}{\mu}\left(e^{\mu T} - 1\right) \tag{4.53}$$

may be used to find the estimate

$$T \approx \frac{1}{\mu}\ln\langle e^{\mu\tau}\rangle = \frac{1}{\mu}\ln\left(\mu\Theta + 1\right) . \tag{4.54}$$

for the average adhesion cluster lifetime. In fact, this expression imposes an upper bound for T since

$$\langle e^x\rangle \geqslant e^{\langle x\rangle} \tag{4.55}$$

for arbitrary probability distributions [Chandler, 1987]. Equality holds for a δ-distributed random variable x. With the result (4.52) for Θ, the estimate for the average lifetime of an adhesion cluster is

$$T \approx \frac{1}{\mu}\ln\left(\mu\,\mathrm{H}_{N_t} + 1\right) \approx \frac{1}{\mu}\ln\left(\mu\left\{\ln N_t + \frac{1}{2N_t} + \Gamma\right\} + 1\right) , \tag{4.56}$$

where the approximation $\mathrm{H}_{N_t} \approx \ln N_t + (1/2N_t) + \Gamma$ for the harmonic number has been used with Euler's constant $\Gamma \simeq 0.5772$. This result corresponds to the deterministic one where the logarithm $\ln N_t$ is replaced by the harmonic number H_{N_t}. Lifetime grows logarithmically with the logarithm of the initial number of closed bonds. The extremely weak influence of cluster size on the average lifetime results because the bonds are independent and decay simultaneously. The dependence is weaker than for vanishing force because rare events with long bond survival are suppressed by the increasing force.

The exact expression for the average cluster lifetime T is found by averaging τ with the dissociation rate $D(\tau) = dp_0/d\tau = r_1 p_1(\tau)$. With (4.49) for p_1 the dissociation rate reads

$$D(\tau) = e^{\mu\tau}p_1(\tau) = \frac{d}{d\tau}p_0 = \frac{d}{d\tau}\left[1 - e^{(1-e^{\mu\tau})/\mu}\right]^{N_t} \tag{4.57}$$

so that the average adhesion cluster lifetime is the integral

$$T = \int_0^\infty \tau \frac{d}{d\tau} p_0 \, d\tau = \int_0^\infty \tau \frac{d}{d\tau} \left[1 - e^{(1-e^{\mu\tau})/\mu}\right]^{N_t} d\tau \,. \tag{4.58}$$

Integrating by parts then leads to

$$T = \tau \left[1 - e^{(1-e^{\mu\tau})/\mu}\right]^{N_t} \Big|_0^\infty - \int_0^\infty \left[1 - e^{(1-e^{\mu\tau})/\mu}\right]^{N_t} d\tau \,. \tag{4.59}$$

Both parts in this expression diverge. They can be written as the limits

$$T = \lim_{a\to\infty} \left\{ \tau \left[1 - e^{(1-e^{\mu\tau})/\mu}\right]^{N_t} \Big|_0^a - \int_0^a \left[1 - e^{(1-e^{\mu\tau})/\mu}\right]^{N_t} d\tau \right\} \tag{4.60}$$

$$= \lim_{a\to\infty} \left\{ a \left[1 - e^{(1-e^{\mu a})/\mu}\right]^{N_t} - \int_0^a \left[1 - e^{(1-e^{\mu\tau})/\mu}\right]^{N_t} d\tau \right\} . \tag{4.61}$$

Inserting the binomial series for the power in the integral leads to

$$T = \lim_{a\to\infty} \left\{ \sum_{n=0}^{N_t} \binom{N_t}{n} (-1)^n \left[a e^{n(1-e^{\mu a})/\mu} - \int_0^a e^{n(1-e^{\mu\tau})/\mu} \, d\tau \right] \right\} \tag{4.62}$$

$$= \lim_{a\to\infty} \left\{ \left(a - \int_0^a d\tau \right) + \sum_{n=1}^{N_t} \binom{N_t}{n} (-1)^n \left[a e^{n(1-e^{\mu a})/\mu} - \int_0^a e^{n(1-e^{\mu\tau})/\mu} \, d\tau \right] \right\} . \tag{4.63}$$

The two diverging contributions in parentheses stem from $n = 0$ and cancel each other. The first term in brackets vanishes in the limit $a \to \infty$. The expression for the average cluster lifetime thus becomes

$$T = -\sum_{n=1}^{N_t} \binom{N_t}{n} (-1)^n \lim_{a\to\infty} \int_0^a e^{n(1-e^{\mu\tau})/\mu} \, d\tau = -\sum_{n=1}^{N_t} \binom{N_t}{n} (-1)^n \int_0^\infty e^{n(1-e^{\mu\tau})/\mu} \, d\tau \tag{4.64}$$

Changing the integration variable from $\tau \to x := n e^{\mu\tau}/\mu$ transforms the integral to

$$\int_0^\infty e^{n(1-e^{\mu\tau})/\mu} \, d\tau = e^{\frac{n}{\mu}} \int_0^\infty e^{-n e^{\mu\tau}/\mu} \, d\tau = \frac{e^{\frac{n}{\mu}}}{\mu} \int_{\frac{n}{\mu}}^\infty \frac{e^{-x}}{x} \, x = \frac{e^{\frac{n}{\mu}}}{\mu} \mathrm{E}\left(\frac{n}{\mu}\right) \tag{4.65}$$

where $\mathrm{E}(z)$ is the exponential integral so that the average lifetime can be written as the expansion

$$T = \sum_{n=1}^{N_t} \binom{N_t}{n} (-1)^{n+1} \frac{e^{\frac{n}{\mu}}}{\mu} \mathrm{E}\left(\frac{n}{\mu}\right) \tag{4.66}$$

in exponential integrals, which can be evaluated numerically. This generalises expression (4.30) for single to multiple, independent bonds. The average rupture force $F = \mu T$ follows from (4.66) as

$$F = \sum_{n=1}^{N_t} \binom{N_t}{n} (-1)^{n+1} e^{\frac{n}{\mu}} \mathrm{E}\left(\frac{n}{\mu}\right) . \tag{4.67}$$

To validate the scaling expressions (4.48) from the deterministic description, we compare it to the limits of (4.66) and (4.67) for slow and fast loading, respectively. For slow loading, $\mu \ll 1$, the

large argument approximation $\mathrm{E}\,(z \to \infty) \to e^{-z}/z$ for the exponential integral can be used and the average lifetime becomes

$$T = \sum_{n=1}^{N_t} \binom{N_t}{n} \frac{(-1)^{n+1}}{n} = \mathrm{H}_{N_t} \approx \ln N_t + \frac{1}{2N_t} + \Gamma \ . \tag{4.68}$$

This is the lifetime for vanishing loading that was encountered several times before. For fast loading, $\mu \gg N_t$, the small argument approximation $\mathrm{E}\,(z \to 0) \simeq e^{-z} \ln(1/z)$ inserted in (4.66) leads to the expression for the average cluster lifetime

$$T = \sum_{n=1}^{N_t} \binom{N_t}{n} (-1)^{n+1} \frac{\ln \mu - \ln n}{\mu} = \frac{\ln \mu}{\mu} - \frac{1}{\mu} \sum_{n=1}^{N_t} \binom{N_t}{n} (-1)^n \ln n \approx \frac{\ln \mu}{\mu} \, . \tag{4.69}$$

This is the scaling expression (4.48) found earlier this section. Summarising, the scaling expressions for average lifetime and rupture force $F = \mu T$ are

$$T \approx \begin{cases} \ln N_t & \text{for } \mu \ll 1, \\ \frac{\ln \mu}{\mu} & \text{for } \mu \gg 1 \end{cases} \quad \text{and} \quad F \approx \begin{cases} \mu \ln N_t & \text{for } \mu \ll 1, \\ \ln \mu & \text{for } \mu \gg 1. \end{cases} \tag{4.70}$$

These results are the same as those of (4.48) for the scaling analysis of the deterministic equation.

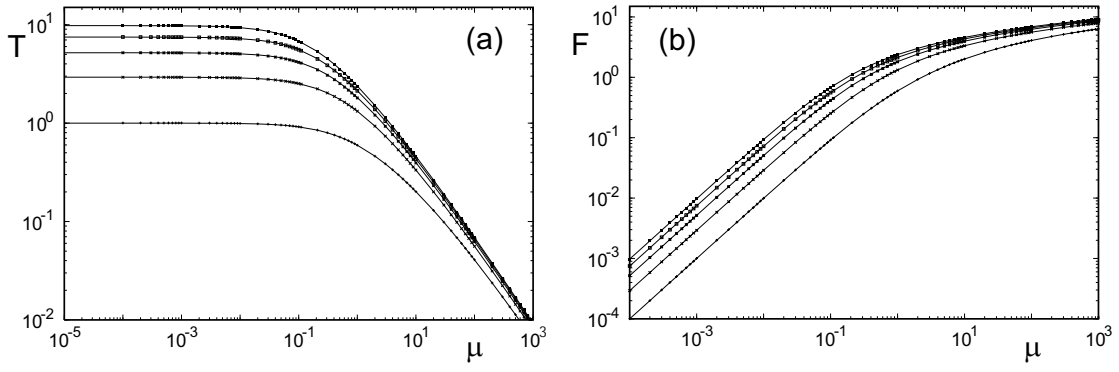

Figure 4.11: (a) Mean cluster lifetime T and (b) mean rupture force F as function of loading rate μ for initial conditions $N_t = 1, 10, 10^2, 10^3$ and 10^4. Solid curves: Exact analytical results (4.66) for $N_t = 1$ and 10 and approximations (4.56) for $N_t \geqslant 100$. Symbols: Numerical results from Monte Carlo simulations.

Fig. 4.11 shows the results of Monte Carlo calculations for the average lifetime and the average rupture force for different initial conditions as a function of loading rate μ in comparison with analytical results. For $N_t \geqslant 100$ the approximate expression (4.56) was used. For these cluster sizes the approximation is very accurate. For smaller clusters, the finite width of the dissociation rate $D(\tau)$ would lead to strong deviations. Therefore, the exact result (4.66) is used in Fig. 4.11 for $N_t \leqslant 10$ which exactly agrees with the numerical results.

In dynamic force spectroscopy, the maximum of the rupture force distribution is commonly used to characterise the strength of a molecular bond. Written in terms of force, the dissociation rate (4.57) reads

$$D(f) = \frac{1}{\mu} e^f p_1(f) = \frac{1}{\mu} N_t e^f e^{(1-e^f)/\mu} \left[1 - e^{(1-e^f)/\mu}\right]^{N_t - 1} \ . \tag{4.71}$$

The maximum F_{max} is determined by the condition $dD/df|_{F_{max}} = 0$ but an explicit analytical form seems to be inaccessible. However, the maximum of $D(\vartheta)$ as function of ϑ is found easily. The condition

$$\left.\frac{d}{d\vartheta} D\right|_{\Theta_{max}} = N_t \left[1 - e^{-\Theta_{max}}\right]^{N_t - 1} e^{-\Theta_{max}} = 0 \tag{4.72}$$

leads to $\Theta_{max} = \ln N_t$, which is identical to the deterministic result for the Θ_{det}. As before for the average, an approximation for the maximum of the force and the time distribution is obtained by solving $\mu\Theta_{max} = (e^{F_{max}} - 1)$ for the maximum force F_{max},

$$F_{max} = \ln\left(\mu\Theta_{max} + 1\right) = \ln\left(\mu \ln N_t + 1\right) \tag{4.73}$$

The results for the maximum Θ_{max} and the approximation for F_{max} are identical to the deterministic results for Θ_{det} and F_{det} (see (4.45)). The scaling behaviour is given in (4.48).

4.3 Cluster decay with rebinding

For finite rebinding, adhesion cluster dynamics is determined by all three parameters of the model: on-rate γ, loading rate μ and cluster size N_t. In principle, also the initial number of bonds N_0 is import. In practice we will usually fix N_0 to a reasonable value. Canonical choices are the cluster size, $N_0 = N_t$, or the number of closed bond in the force free steady state, $N_0 = N_{eq}$. Although rebinding can stabilise adhesion clusters, the unlimited increase of force will eventually lead to the dissociation of any adhesion cluster. Even in the deterministic description lifetime will be finite.

4.3.1 Scaling analysis of the deterministic equation

As in the previous sections we use a scaling analysis to find approximate expressions for the dependence of lifetime and rupture force on the model parameters; for $\gamma > 0$, the deterministic equation contains effectively two parameters, the on-rate γ and the ratio μ/N_t of loading rate and cluster size. A similar scaling analysis was performed before by Seifert [2000] (see also added comments in Seifert [2002]).

Again, it is convenient to use the auxiliary variable $u(\tau) = \tau/N(\tau)$ instead of $N(\tau)$. The deterministic differential equation (2.42) for $u(\tau)$ reads

$$\frac{d}{d\tau} u = u\left\{(1/\tau) + 1 + \gamma - \gamma N_t(u/\tau)\right\} + u\left\{e^{\mu u} - 1\right\}\,, \tag{4.74}$$

where the terms were rearranged and $0 = u - u$ has been added to facilitate the following analysis.

In the following we use the initial condition $N(\tau = 0) = N_0 = N_{eq}$, i.e. , we assume that the adhesion cluster equilibrates under force free conditions before loading starts at time $\tau = 0$. The influence of the initial condition on the results will be discussed. The initial condition for $N(\tau)$ implies the initial condition $(du/d\tau)|_{\tau=0} = 1/N_{eq}$ for the solution for $u(\tau)$. The initial change of $u(\tau)$ for $\tau = 0$ is determined by the first term, the inverse of time, in curly brackets in (4.74). All other terms taken together vanish at $\tau = 0$. The second derivative of u at time $\tau = 0$ is small for sufficiently large clusters. Therefore $u(\tau)$ initially increases linearly with constant slope as

$$u(\tau) \approx \tau/N_{eq}\,. \tag{4.75}$$

This solution corresponds to a constant number of bonds $N(\tau) = N_{eq}$. It neglects any influence of force on cluster evolution.

As cluster decay proceeds, the force per closed bond, $f(\tau)/N(\tau) = \mu u(\tau)$, increases and the exponential term in (4.74) will eventually determine $du/d\tau$ after the crossover time τ_1, which is defined by the equality

$$\frac{1}{\tau_1} + 1 + \gamma - \gamma N_t \frac{u(\tau_1)}{\tau_1} = e^{\mu u(\tau_1)} - 1 \,. \tag{4.76}$$

After the crossover, the full differential equation (4.74) can be replaced by

$$\frac{d}{d\tau} u \approx u \left\{ e^{\mu u} - 1 \right\} \approx u e^{\mu u} \,. \tag{4.77}$$

This is the same equation as found in Sec. 4.1.1 for vanishing rebinding. After the crossover, rebinding can thus be neglected. The solution for this differential equation is given implicitly in terms of the exponential integral,

$$\tau - \tau_1 = \mathrm{E}\left(\mu u(\tau_1)\right) - \mathrm{E}\left(\mu u(\tau)\right) \,. \tag{4.78}$$

The time between crossover and decay of the cluster is given by (compare (4.8))

$$\tau_2 = T_{det} - \tau_1 = \mathrm{E}\left(\mu u(\tau_1)\right) \,. \tag{4.79}$$

Slow loading, $\mu \ll 1$

The time-scale for an exponential relaxation of adhesion clusters towards the steady state at vanishing force is given by the inverse sum of on- and off-rate, $(1+\gamma)^{-1}$. For a finite, constant force, relaxation is even faster. For a continuously increasing force there is no steady state. But, if the time-scale $1/\mu$ for a change in force exceeds the relaxation time, that is if

$$\mu \ll 1 \leqslant (1 + \gamma) \,, \tag{4.80}$$

the adhesion cluster stays in a time-dependent, quasi steady state which is given by the stable steady state $N_{eq}(f)$ at a given force $f(\tau) = \mu\tau$. The force dependence of N_{eq} was calculated approximately in (3.53) and the exact, numerical results are plotted in Fig. 3.14b. N_{eq} vanishes above the critical force f_c. Thus, adhesion clusters are stable until $f = \mu\tau = f_c$ and dissociate quickly thereafter. The critical force is

$$f_c = N_t \,\mathrm{pln}\,(\gamma/e) \tag{4.81}$$

and the time it takes to reach f_c with the loading rate μ is

$$\tau_c = \frac{f_c}{\mu} = \frac{N_t}{\mu} \,\mathrm{pln}\left(\frac{\gamma}{e}\right) \,. \tag{4.82}$$

For a constant force larger than f_c rebinding can be neglected and the time for the decay of an adhesion cluster from $N_0 = N_t$ is approximately given by (3.11) as

$$\tau_2 \simeq \frac{e^{-f/N_t}}{1 + (f/N_t)} \simeq \frac{N_t}{f} e^{-f/N_t} \,. \tag{4.83}$$

It is usually smaller than τ_c. Inserting $f = f_c$ yields $\tau_2 \simeq e/\gamma$. Since $\mathrm{pln}\,(\gamma/e) \approx \gamma/e$ for $\gamma \ll 1$, the time τ_2 equals τ_c for $\gamma/e \approx \sqrt{\mu/N_t} \ll 1$. This on-rate is very small so that an approximation for vanishing rebinding might well apply. The lifetime of an adhesion cluster under slow linear loading with $\mu \ll 1$ can thus be identified with the critical time τ_c,

$$T_{det} = \tau_c = \frac{f_c}{\mu} = \frac{N_t}{\mu} \,\mathrm{pln}\left(\frac{\gamma}{e}\right) \tag{4.84}$$

It depends only on the ratio of loading rate and cluster size and on the on-rate. The condition for dissociation, $N(T_{det}) = 1$, has no influence on the result because the decay under super-critical loading is very fast. Since it was assumed that loading is much slower than equilibration, the choice of the initial condition has no influence on the result (4.84).

The rupture force is given by the critical force itself. It is independent of loading rate.

Intermediate loading, $1 < \mu \ll N_{eq}$

The estimate $\tau_2 \ll \tau_c$ depends only on the ratio of loading rate and cluster size, $\mu/N_t \ll 1$. The inequality $\mu \ll 1$ was only used to argue that the adhesion cluster follows a quasi steady state. Thus, the estimate for the lifetime remains valid also in an intermediate loading regime where $1 < \mu \ll N_t$. In this regime, however, the cluster cannot follow the change of the steady state due to the increasing force. The time for decay after the critical force is not strongly dependent on the initial condition so that the estimate for τ_2 remains valid and the scaling expression for the lifetime is given by (4.84).

Fast loading, $\mu \gg N_{eq}$

For fast loading, $\mu \gg N_{eq}$, the constant terms in Eq. (4.76) for the crossover time can be neglected. The condition then is

$$\tau_1 e^{\mu\tau_1/N_{eq}} = 1 \tag{4.85}$$

where again the solution for the initial behaviour of u was used. As in the previous section the crossover time is given in terms of the product logarithm

$$\tau_1 = (N_{eq}/\mu)\,\mathrm{pln}\,(\mu/N_{eq}) \simeq (N_{eq}/\mu)\ln(\mu/N_{eq}) \tag{4.86}$$

where the large argument approximation for the product logarithm was used. For the remaining time τ_2 after the crossover, the same arguments apply as in Sec. 4.1.1. It is negligible with respect to τ_1 and the lifetime of the cluster is

$$T_{det} \simeq \tau_1 \simeq \frac{N_{eq}}{\mu}\ln\left(\frac{\mu}{N_{eq}}\right). \tag{4.87}$$

Since the derivation of (4.87) neglected rebinding completely, using a different $N_0 \neq N_{eq}$ simply replaces N_{eq} by N_0 in (4.87). For a general initial cluster size the lifetime is thus given by

$$T_{det} \simeq \frac{N_0}{\mu}\ln\left(\frac{\mu}{N_0}\right), \tag{4.88}$$

which is the result for vanishing rebinding from Sec. 4.1.1.

Summary of the scaling regimes

The scaling analysis of the deterministic equation reveals the existence of two different scaling regimes of cluster lifetime with loading rate. They are distinguished by whether the loading rate per closed bond in the steady state N_{eq} (the initial state) is smaller or larger than the intrinsic force scale. Summarising, the scaling expressions for the lifetime and the rupture force $F_{det} = \mu T_{det}$ are

$$T_{det}\begin{cases}\approx \frac{N_t}{\mu}\,\mathrm{pln}\left(\frac{\gamma}{e}\right) & \text{for } \mu \ll N_{eq},\\ \simeq \frac{N_{eq}}{\mu}\ln\left(\frac{\mu}{N_{eq}}\right) & \text{for } \mu \gg N_{eq}\end{cases} \quad \text{and} \quad F_{det}\begin{cases}\approx N_t\,\mathrm{pln}\left(\frac{\gamma}{e}\right) = f_c & \text{for } \mu \ll N_{eq},\\ \simeq N_{eq}\ln\left(\frac{\mu}{N_{eq}}\right) & \text{for } \mu \gg N_{eq}.\end{cases} \tag{4.89}$$

Both scaling expressions for T depend on the on-rate γ and the ratio μ/N_{eq} alone. Loading destabilises adhesion clusters and reduces their lifetime. An increased on-rate, on the other hand, stabilises adhesion clusters. However, lifetime increases only weakly as the product logarithm of γ. In the slow loading regime, the rupture force is given by the critical force for cluster stability f_c. Thus, it depends only on cluster size N_t and on-rate γ but is independent of loading rate μ. For fast loading rebinding could be fully neglected and the scaling expressions are independent of the on-rate. It only enters the scaling expressions through the specific choice of the initial condition $N_0 = N_{eq}$.

4.3.2 Numerical solution of the deterministic equation

Number of closed bonds

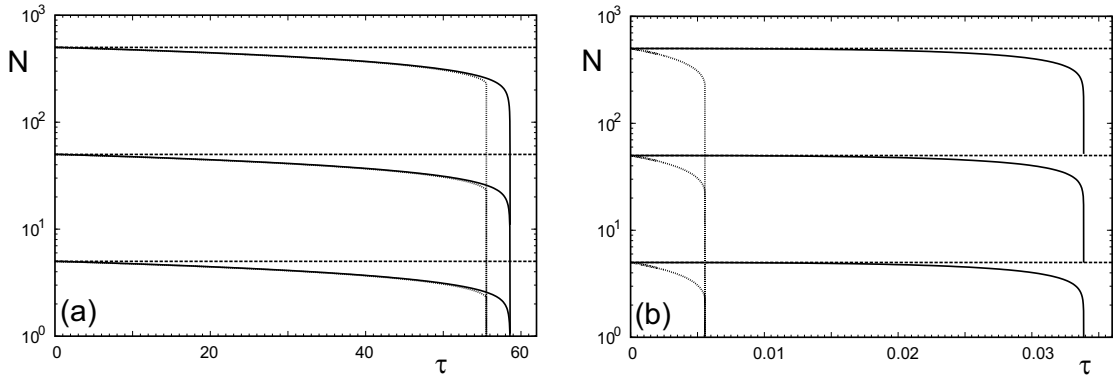

Figure 4.12: Solid curves: Number of closed bonds $N(\tau)$ obtained from numerical integration of the deterministic equation for the case $\gamma = 1$ and $N_t = 10, 10^2$ and 10^3 for the loading rates (a) $\mu/N_0 = 10^{-2}$ and (b) $\mu/N_0 = 10^2$. Initial condition is $N_0 = N_{eq} = \gamma/(1+\gamma)N_t$. Dashed curves: approximation of constant $N(\tau) = N_{eq}$. Dotted curves: Numerically determined, force dependent stationary state $N_{eq}(f = \mu\tau)$ (see Fig. 3.14 in Sec. 3.4).

Fig. 4.12 plots the number of closed bonds $N(\tau)$ obtained from numerical integration of the deterministic equation for the case $\gamma = 1$. The initial condition is $N_0 = N_{eq} = N_t/2$. The numerical results are compared to the time-dependent steady state $N_{eq}(f(\tau) = \mu\tau)$ and the constant $N = N_{eq} = \gamma N_t/(1+\gamma)$. Fig. 4.12a shows that for slow and intermediate loading the number of closed bonds $N(\tau)$ follows closely the quasi steady state. Only close to f_c, where $N_{eq}(f)$ decreases quickly towards the critical value N_c, equilibration is too slow and cluster decay is retarded. For slower loading than shown in the figure, the agreement becomes even better. With increasing loading rate, the trajectories of $N(\tau)$ deviate earlier from the quasi steady state and the retardation grows. For very fast loading as shown in Fig. 4.12b, the number of closed bonds remains nearly constant at the initial value $N_0 = N_{eq}$ before the whole cluster breaks down abruptly.

For general initial conditions $N_0 \neq N_{eq}$, cluster decay under linear shared loading with rebinding can proceed in three phases. First, the cluster equilibrates to the quasi steady state. Then it follows this state until the critical force is reached. Thereafter, the unstable cluster decays quickly under the super-critical force. In the regime of slow loading, $\mu \ll 1$, the equilibration is very fast so that the initial condition has no influence on the trajectories or the results for lifetime and rupture force. For fast loading, $\mu \gg N_{eq}$, rebinding was neglected and lifetime and rupture force were determined by

the initial number of closed bonds alone. An equilibration to a quasi steady state is not possible; the trajectories for fast loading are the same as in Fig. 4.12b but with a different initial condition $N_0 \neq N_{eq}$. In the intermediate region, the clusters cannot fully relax to the quasi steady state but still the time to reach the critical force is small compared to the time for cluster decay under super-critical force. Hence, the scaling expression for the lifetime is the same as for slow loading.

Cluster lifetime and rupture force

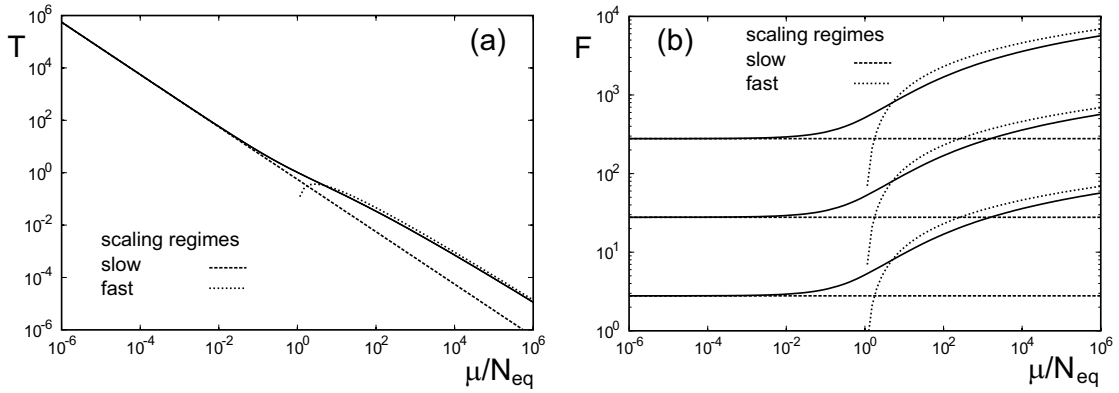

Figure 4.13: Solid curves: Numerical results for deterministic (a) lifetime T_{det} and (b) rupture force $F_{det} = \mu T_{det}$ as function of μ/N_0 for the case $\gamma = 1$ and $N_t = 10, 10^2$ and 10^3. Initial condition is $N_0 = N_{eq} = \gamma N_t/(1+\gamma) = N_t/2$. Lifetime is independent of N_t and the curves are identical. Dashed curves: Scaling expressions (4.89) for slow and fast loading for T_{det} and F_{det}.

Fig. 4.13a plots the deterministic adhesion cluster lifetime T_{det} as function of μ/N_{eq} for the case $\gamma = 1$ and cluster sizes $N_t = 10, 10^2$ and 10^3. The initial condition is $N_0 = N_{eq} = N_t/2$. The lifetimes for different cluster sizes are identical over the whole range of μ/N_{eq}. This confirms the findings of the scaling analysis that lifetime depends only on μ/N_{eq} and γ in both scaling regions. As illustrated by the numerical solutions for $N(\tau)$, this scaling behaviour arises because the clusters are stable for sub-critical forces and decay quickly for super-critical forces. The condition $N(T_{det}) = 1$ for dissociation is thus irrelevant as long as the critical cluster size is larger than $N_c = 1$. The independence of solutions for $N(\tau)$ on N_t together with the divergence of $dN/d\tau$ for $N \to 0$ leads to the independence of the lifetime on N_t, even for slow loading. For fast loading, this was observed before in the case of $\gamma = 0$ and for constant forces. The scaling expressions describe the lifetime very well in the respective scaling regions. In the range of $\mu \sim N_{eq}$ there is a small crossover region; an actual scaling regime for intermediate loading as put forward in Seifert [2000] is not observed. Fig. 4.13b plots the deterministic rupture force F_{det} as function of μ/N_{eq}. Now, the results scale linearly with cluster size N_t.

4.3.3 Stochastic analysis

The deterministic analysis has allowed to determine scaling expressions for lifetime and rupture force and provided insight into the qualitative behaviour of the trajectories $N(\tau)$. The numerical solutions of the deterministic equation have confirmed these findings. In this section we compare the deterministic results with solutions of the stochastic master equation. For finite rebinding $\gamma > 0$, the absorbing

boundary at $i = 0$ is artificial. The non-linear master equation with time-dependent rates for linear loading will be solved numerically and mean lifetime and rupture force are calculated.

Time evolution

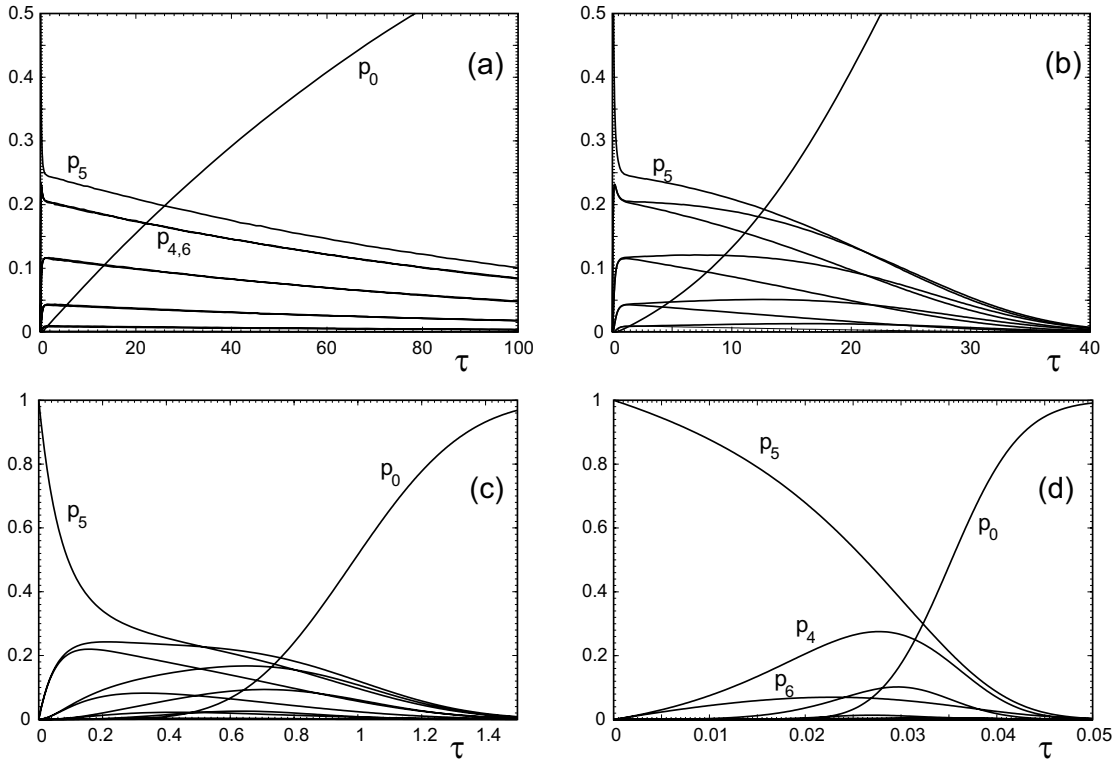

Figure 4.14: Numerical solutions obtained by stochastic simulations for the probability distribution $\{p_i(\tau)\}_{i=0}^{N_t}$ for the case $\gamma = 1$ and $N_t = 10$. Loading rate per initially closed bond is $\mu/N_0 = 10^{-4}$, 10^{-2}, 1 and 10^2 (a-d). Initial condition is $N_0 = N_{eq} = N_t/2 = 5$.

In Fig. 4.14 results of stochastic simulations for the probability distribution $\{p_i\}_{i=0}^{N_t}$ are plotted for the on-rate $\gamma = 1$ and the cluster size $N_t = 10$. The initial condition is $N_0 = N_{eq} = N_t/2$. The ratio of loading rate and initial number of closed bonds increases from $\mu/N_{eq} = 10^{-4}$ to 10^2. For the smallest loading rate in (a), the distribution equilibrates almost immediately to the steady state distribution for vanishing force. Thereafter, the probability for attachment decreases through fluctuations to the absorbing boundary but the distribution within the bound states does not change significantly. Force is irrelevant for cluster decay in this regime. For larger loading rates in the slow and intermediate loading regimes (b and c), adhesion clusters follow the quasi steady state after the initial equilibration. The distribution becomes asymmetric which is indicated by the opposite behaviour of the pairs of state functions $p_{5-i,5+i}$. Cluster decay accelerates as force approaches $f_c \simeq 0.278 N_t$. For $\mu/N_{eq} = 10^{-2}$ this is the case at $\tau_c \simeq 56$. Clusters decay before the critical force is reached because fluctuation to the absorbing boundary are still important. For $\mu/N_{eq} = 1$ the critical force is reached at $\tau \simeq 0.56$. Cluster decay is now driven mainly by loading with forces above f_c. For very fast loading, $\mu/N_{eq} = 10^2$, rebinding can be neglected and the state probabilities behave

as for the case of $\gamma = 0$.

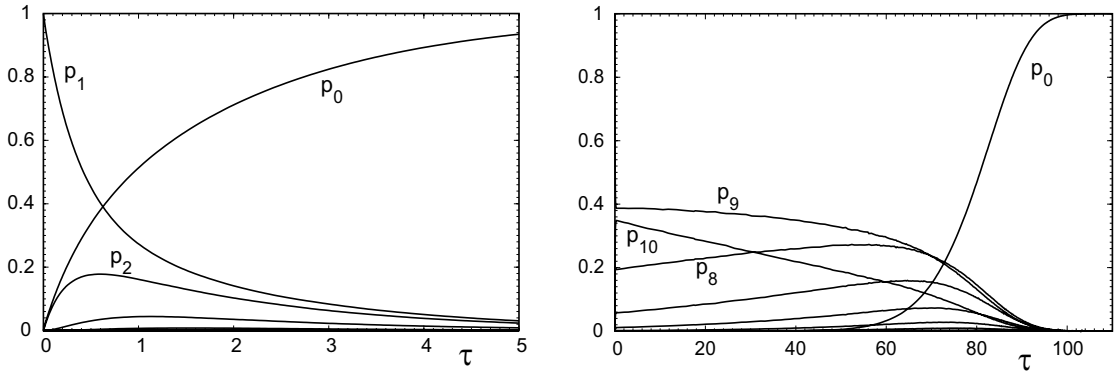

Figure 4.15: Solutions of the master equations from stochastic simulations for (a) $\gamma = 1/9$ and (b) $\gamma = 9$ with $N_t = 10$ and the loading rate per initially closed bond $\mu/N_0 = 10^{-2}$. Initial condition is $N_0 = N_{eq}$, i.e. , $N_{eq} = N_0 = 1$ and $N_0 = 9$, respectively, for the two different values of the on-rate.

Fluctuation and force driven cluster decay in the slow loading regime is further illustrated in Fig. 4.15. It shows solutions of the master equation for $N_t = 10$ and $N_0 = N_{eq}$ as in Fig. 4.14, but for the on-rates (a) $\gamma = 1/9$ and (b) $\gamma = 9$ (b) so that $N_0 = 1$ and $N_0 = 9$. The loading rate is $\mu/N_0 = 10^{-2}$ (i.e. slow loading). For weak rebinding adhesion clusters decay quickly from their initial state $N_0 = 1$ to the absorbing state. However, rebinding occurs and states with $i > N_{eq}$ are still occupied. The force per bond is very weak throughout the decay with $f(\tau) = \mu\tau \lesssim 0.05 \ll 1$ for $\tau \simeq 5$. For strong rebinding, the distribution evolves very slowly. Initially it is centred around the force free steady state N_{eq} and shifts gradually to smaller values with increasing force. Fluctuations to the absorbing state are rare and the probability for detachment stays small. Towards the end of the decay, the force reaches $f = N_{eq}\mu\tau \simeq 9$ which is close to the critical force $f_c \simeq 11$ for $\gamma = 9$. This induces large fluctuations and leads to fast dissociation of clusters. For clusters which are relatively stable against fluctuations, dissociation is induced by loading and the time-scale is set by the time to reach the critical force.

Fig. 4.16 plots the average number of closed bonds, $N(\tau) = \langle i \rangle = \sum_{i=1}^{N_t} i p_i$ for the on-rate $\gamma = 1$ for different cluster sizes between $N_t = 1$ and $N_t = 10^4$. The initial number of closed bonds is $N_0 = N_{eq}$. For the smallest loading rate shown, clusters of all sizes show an exponential decrease as for vanishing force. Here, rare fluctuations determine the lifetime and the dynamics of $N(\tau)$. For larger loading rates, the influence of fluctuations is reduced and large clusters decay abruptly if the critical force is exceeded at $\tau_c \simeq 56$ for $\mu/N_{eq} = 10^{-2}$. Small clusters decay earlier due to the influence of fluctuations and the decrease in $N(\tau)$ becomes smoother for smaller N_t. With a further increase of loading rate per cluster size, the importance of fluctuations is reduced also for smaller clusters and the lifetimes become comparable for different N_t. Moreover the final descent becomes steeper. An exception is $N_t = 2$; here, the initial number of closed bonds is $N_0 = 1$ and the very smooth decrease in typical for single bond dissociation.

Fig. 4.17 shows single simulation trajectories of the number of closed bonds i for slow and fast loading. For vanishing loading, the situation has been elucidated in Fig. 3.9 of Sec. 3.2. The number of realisation reduces only by rare fluctuations to the absorbing boundary. For slow linear loading the trajectories fluctuate around the force dependent steady state $N_{eq}(f)$ which follows from the deterministic description and is plotted for comparison. For the smallest clusters, fluctuations to $i = 0$ are

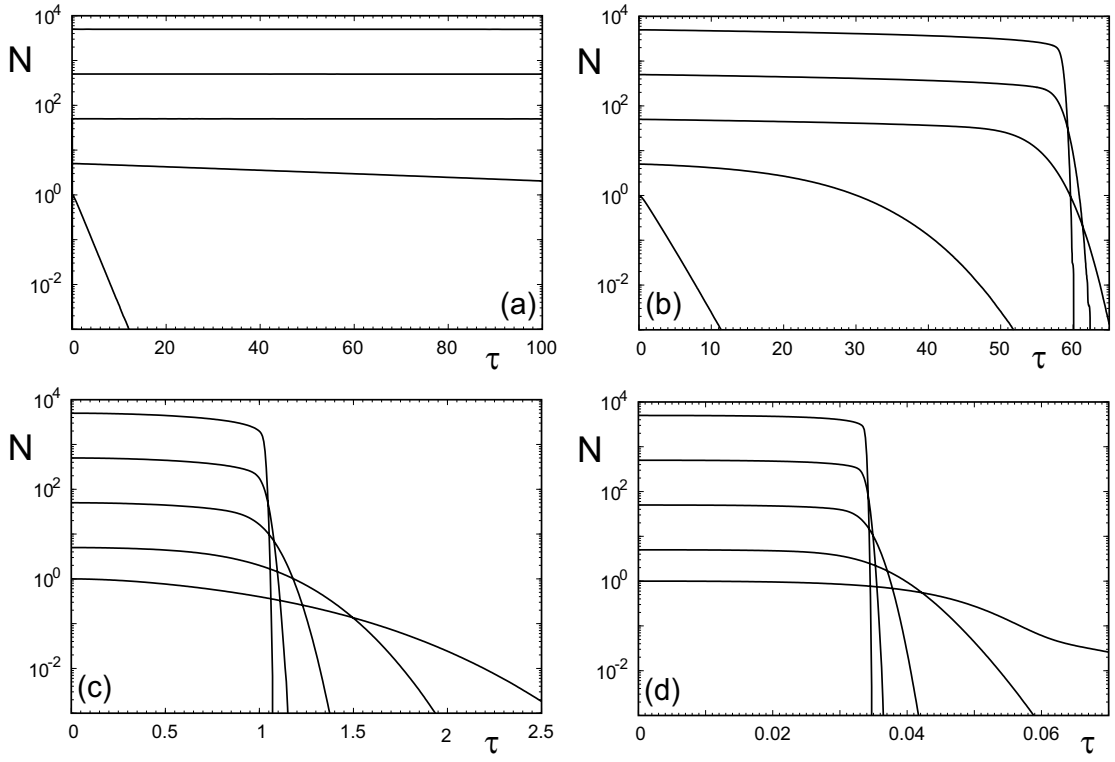

Figure 4.16: Average number of closed bonds $N(\tau)$ as function of time τ from stochastic simulations for the case $\gamma = 1$ and $N_t = 2, 10, 10^2, 10^3$ and 10^4. The initial condition is $N_0 = N_{eq} = N_t/2$. The value for the ratio of loading rate and initial number of closed bonds is $\mu/N_{eq} = 10^{-2}$, 10^{-1}, 1 and 10^2 (a-d).

frequent and the average $N(\tau)$ reduces faster than the steady state. For the larger clusters fluctuations become rare and most clusters dissociate around the deterministic critical force where the steady state vanishes and fluctuations are enhanced. This leads to the fast decrease of the average $N(\tau)$ close to f_c. For fast loading the critical force is reached very quickly and rebinding can almost completely be neglected. Cluster of all sizes decay quickly. Fluctuations mainly affect the moment at which the single trajectories dissociate. The distribution of these events is wider for small clusters which smoothes the curve of the average $N(\tau)$. As noted before for constant loading, the single trajectories with their abrupt breakdown very much resemble the deterministic curves. Averaging over many with different dissociation times leads to the smooth appearance of the averages.

Stochastic and deterministic results for $N(\tau)$ are compared in Fig. 4.18 for the case $\gamma = 1$ and $N_t = 10, 10^2, 10^3$ and 10^4 and for the values $\mu/N_0 = 10^{-2}$ and 10^2 The initial condition is $N_0 = N_{eq}$. For $N_t = 10$, the stochastic results with a reflecting boundary condition are given for comparison. The results coincide well for the initial evolution under small forces. Towards the end of the decay the force is large and strong deviations arise. For small clusters under slow loading, the deviations are large throughout the decay due to the frequent loss of realisations to the absorbing boundary. For a reflecting boundary the deviations are limited to the final stages of decay. For fast loading, fluctuations to the absorbing boundary are less relevant and results for absorbing and reflecting boundary do not differ significantly. The definition of large and small cluster depends on the parameters μ and γ. A

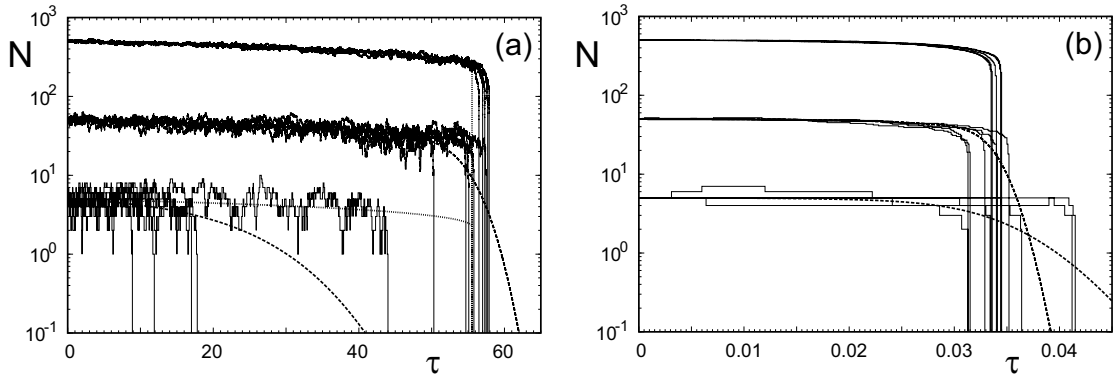

Figure 4.17: Solid curves: Single simulation trajectories for the number of closed adhesion bonds for the case $\gamma = 1$ and $N_t = 10, 10^2$ and 10^3 for loading rates (a) $\mu/N_0 = 10^{-2}$ and (b) $\mu/N_0 = 10^2$. Initial condition for the trajectories is $N_0 = N_{eq} = N_t/2$. Dashed curves: Average number of closed bonds calculated from a large number of trajectories. Dotted: Deterministic stationary state $N_{eq}(f = \mu\tau)$ for constant force (see Fig. 3.14 in Sec. 3.4) as function force at time τ. It vanishes when the critical force is reached at $\tau_c = f_c/\mu$

cluster is small as long as the time-scale for the fluctuations is smaller than that for the force driven decay τ_c.

Dissociation rates and average lifetime

In Fig. 4.19, the dissociation rate $D(\tau) = dp_0/d\tau = r_1 p_1$ is plotted for the case $\gamma = 1$ and for different cluster sizes $N_t = 2, 6, 10, 10^2, 10^3$ and 10^4. The initial condition is $N_0 = N_{eq}$ and the ratio of loading rate and initial cluster size ranges from and initial number of closed bonds, $\mu/N_0 = 10^{-2}$ to 10^2. The analytical result for the single bond dissociation rate is plotted for comparison. For loading rates slower than shown in the figure, the approximation for vanishing force can be applied (compare Fig. 3.21). After a fast initial increase from $D(0) = 0$ for $N_t > 1$, the dissociation rates decrease exponentially because cluster realisations are lost due to rare fluctuations to the absorbing boundary. The exponentials can be approximated by

$$D(\tau) \approx e^{-\tau/T}/T \tag{4.90}$$

where T is the average lifetime for vanishing loading (3.47).

For larger loading rates, the dissociation rate cannot be described by a single exponential. The distributions develop a pronounced maximum. For slow loading, the position of the maximum shifts to larger τ with increasing N_{eq}. For fast loading, however, it hardly depends on cluster size. The distributions become sharply peaked and rather symmetric as it was already observed for vanishing rebinding. One difference to the case $\gamma = 0$ is that rebinding is possible and occurs especially as long as the force is small. For $N_t = 2$ and $N_0 = 1$ this leads to 'bimodal' distribution. At short times, the dissociation rate is determined by the immediate rupture of the initial, single bond and is well described by the analytic curve (4.29) for the single bond dissociation rate. The fraction of clusters that first rebinds to get into state $i = 2$ dissociates on a longer time-scale which is seen in the shoulder of the curve at large times. Similar separation into subpopulations can be observed also for larger clusters at even larger loading rates.

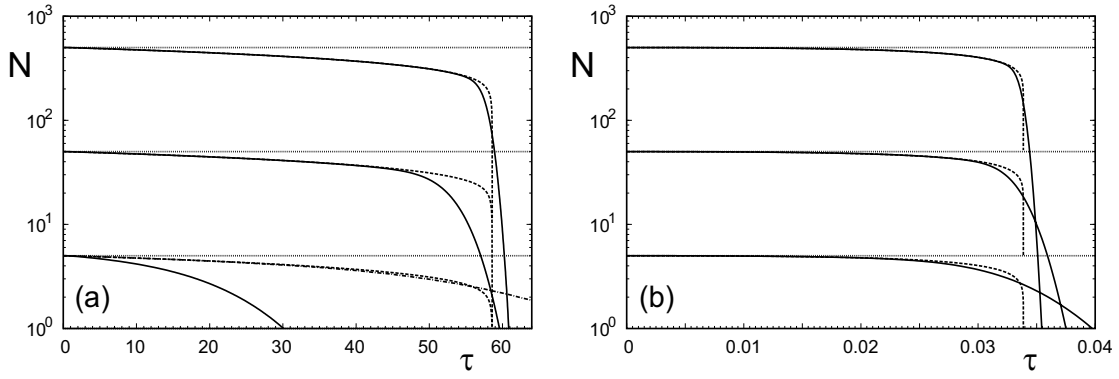

Figure 4.18: Comparison of stochastic and deterministic results for the average number of closed adhesion bonds $N(\tau)$ as function of time for the case $\gamma = 1$ and $N_t = 10, 10^2$ and 10^3 and for loading rates (a) $\mu/N_0 = 10^{-2}$ and (b) $\mu/N_0 = 10^2$. Initial condition is $N_0 = N_{eq} = N_t/2$. Solid curves: Stochastic results from Monte Carlo solutions of the master equation. Dashed: Deterministic results from numerical integration of the differential equation. Dash-dotted (for $N_t = 10$ and $\mu/N_0 = 10^{-2}$): Solution of the master equation with reflecting boundary condition at $i = 0$.

The discussion of the time evolution of adhesion clusters has shown that there are two different mechanisms for the decay at slow loading. *Ultra-slow loading* is present as long as the time-scale for fluctuations to the absorbing boundary is short compared to the time it takes to reach the critical force f_c. In this case, adhesion clusters are not affected by force and decay by fluctuations to the absorbing boundary. The mean lifetime can be approximated by that of an adhesion cluster under vanishing force which was calculated in Sec. 3.2. For the initial condition $N_0 = N_t$ it is given in (3.47) as

$$T_0 = \frac{1}{1+\gamma}\left\{\mathrm{H}_{N_t} + \sum_{i=1}^{N_t}\binom{N_t}{i}\frac{\gamma^i}{i}\right\}. \tag{4.91}$$

Since the relaxation to the steady state is fast, this expression can also be used for the initial condition $N_0 = N_{eq}$. The regime of ultra-slow loading is defined by loading rates $\mu \ll f_c/T_0 \ll N_{eq}$. For *slow loading* $f_c/T_0 \ll \mu \ll N_{eq}$, the critical force is reached before the cluster can decay by fluctuations. Because stochastic clusters decay quickly for forces above the critical force, lifetime is then given by $T = f_c/\mu$, i.e., the time it takes to reach the critical force f_c with a loading rate μ. These two regimes can only be observed if the time-scales can be separated. This requires that the time-scale for fluctuations is sufficiently large and $f_c/T_0 \ll N_{eq}$ holds. Because T_0 grows strongly with N_t and γ this is usually the case for large clusters or strong rebinding. Only for small clusters, the *slow loading* regime will be absent. For *fast loading* $\mu \gg N_{eq}$, fluctuations have a weak effect on cluster dissocation and the deterministic scaling result can be used to describe the average lifetime of stochastic adhesion clusters. In summary, we have three different scaling regimes for the stochastic mean lifetime T and rupture force $F = \mu T$. The scaling expressions are

$$T \approx \begin{cases} \frac{1}{1+\gamma}\left\{\mathrm{H}_{N_t} + \sum_{i=1}^{N_t}\binom{N_t}{i}\frac{\gamma^i}{i}\right\} & \text{for } \mu \ll f_c/T_0 \ll N_{eq}, \\ N_t\,\mathrm{pln}\,(\gamma/e)\,/\mu & \text{for } f_c/T_0 \ll \mu \ll N_t, \\ \frac{N_0}{\mu}\ln\left(\frac{\mu}{N_0}\right) & \text{for } N_t \ll \mu \end{cases} \tag{4.92}$$

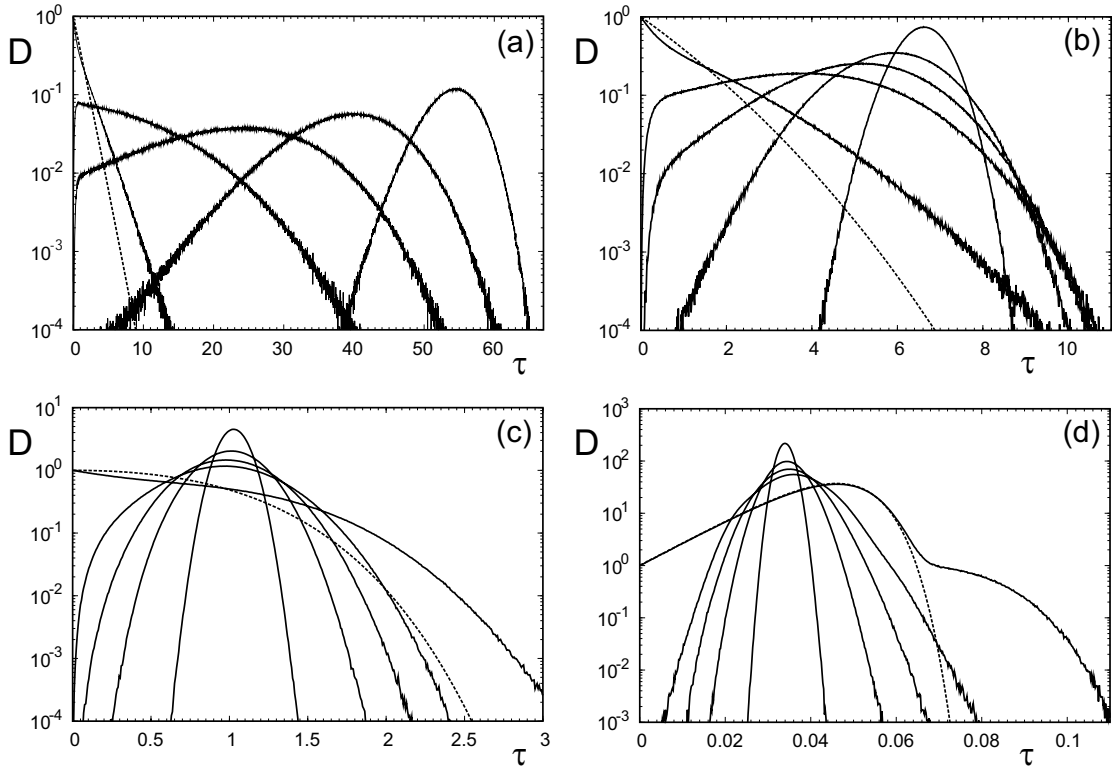

Figure 4.19: Numerical results for the dissociation rate $D(\tau)$ as function of the time τ for the case $\gamma = 1$ and $N_t = 2, 6, 10, 10^2$ and 10^3 and for loading rates are $\mu/N_0 = 10^{-2}$, 10^{-1}, 1 and 10^2 (a-d). The initial condition is $N_0 = N_{eq} = N_t/2$. Dashed line: Analytic result (4.29) for $N_t = 1$ with $N_0 = 1$.

for the lifetime and

$$F \approx \begin{cases} \frac{\mu}{1+\gamma}\left\{\mathrm{H}_{N_t} + \sum_{i=1}^{N_t}\binom{N_t}{i}\frac{\gamma^i}{i}\right\} & \text{for } \mu \ll f_c/T_0 \ll N_{eq}, \\ N_t \,\mathrm{pln}\,(\gamma/e)\,/\mu & \text{for } f_c/T_0 \ll \mu \ll N_{eq} \\ N_0 \ln\left(\frac{\mu}{N_0}\right) & \text{for } N_t \ll \mu \end{cases} \tag{4.93}$$

for the mean rupture force. In the ultra-slow loading regime, the lifetime is constant. The force at rupture thus increases linearly with loading rate. In the slow loading regime, the rupture force is constant and given by the critical force. The lifetime decreases with the inverse of loading rate. For fast loading the result for vanishing rebinding and fast loading arises which was discussed before. Lifetime essentially decreases inversely with the ratio of loading rate and initial number of closed bonds, μ/N_0 with a weak logarithmic correction. The rupture force increases logarithmically with loading rate.

Fig. 4.20 plots numerical results of stochastic simulations for the average lifetime T and the average rupture force F as function of μ/N_{eq} for the on-rate $\gamma = 1$ for the cluster sizes $N_t = 2, 10$, 10^2, and 10^3. The initial condition is $N_0 = N_{eq}$. In the range of loading rates shown, the lifetime of the two largest clusters are described by the scaling results for slow and fast loading. For very slow loading slight deviations are observed for $N_t = 100$ which indicates the transition to the ultra-slow

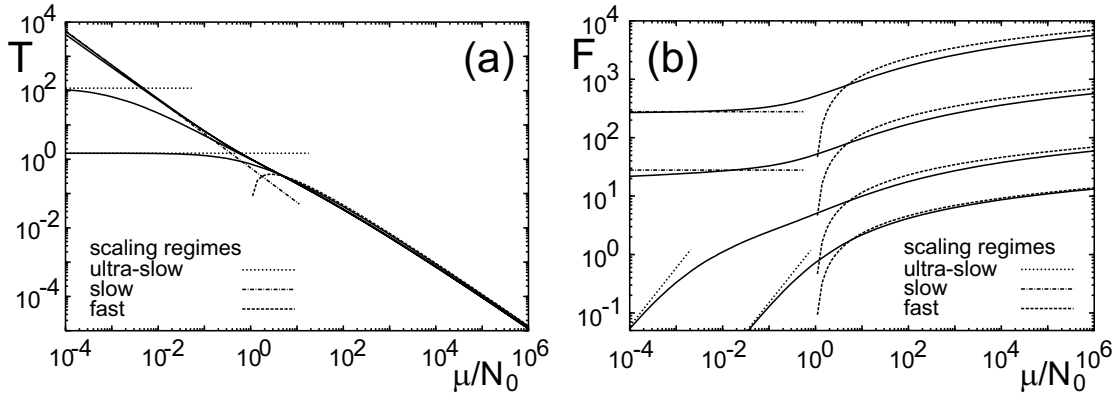

Figure 4.20: Solid lines: (a) mean cluster lifetime T and (b) mean rupture force $F = \mu T$ for the case $\gamma = 1$ as a function of μ/N_0 for $N_t = 2$, 10, 10^2 and 10^3. In (a) the curves for the two largest clusters are nearly identical. The initial condition is $N_0 = N_{eq} = N_t/2$. Dashed lines: Scaling expressions.

loading regime. For the smallest clusters, the numerical results can be described by the scaling results for ultra-slow and fast loading in the respective regions. The slow loading regime is absent here because the fluctuation-determined lifetime is small. For other on-rates $\gamma \neq 1$, the existence of the slow loading regime depends on the lifetime T_0 which has to be sufficiently large that $f_c/T_0 \ll N_{eq}$.

4.4 Summary

In this chapter, we analysed the cooperative decay of a cluster of adhesion bonds under linearly rising force. Moreover, non-cooperative loading of irreversible bonds was discussed. Significant differences between stochastic and deterministic treatment are found for small clusters or slow loading, when stochastic fluctuations are relevant. However, fluctuations do not affect the typical shape of rupture trajectories of single clusters but rather the time at which cluster dissociation occurs. For vanishing rebinding, $\gamma = 0$, our treatment applying numerical solutions of deterministic and master equation, nicely confirms the scaling analysis of the deterministic equation for cluster lifetime T as function of μ and N_0 [Seifert, 2000]. However, in contrast to the scaling analysis, the full treatment presented here allows for detailed comparison with experiments, e.g. in regard to typical unbinding trajectories or binding strength over a range of loading rates spanning different scaling regimes. Moreover, the stochastic analysis allows to determine the distribution of bond strengths and lifetimes, which allows detailed comparison with experimental results.

For non-cooperative linear loading it was possible to solve the time-dependent master equation by its equivalence to the linear equation for force free decay. The lacking cooperativity of the bonds induced an acceleration of the single bond dynamics without the instability against a reduction of closed bonds which is the signature of cooperativity expressed by the non-linearity of the transition rates. Exact results for the average lifetime of adhesion clusters confirm the results of the scaling analysis presented in Seifert [2000] also for this case. The comparison of the exact analytical solutions and numerical solutions with the Gillespie algorithm for time-dependent rates showed very good agreement which validates the numerical results.

For shared linear loading in the case of finite rebinding, $\gamma > 0$, the scaling analysis of the deterministic equation yields two different scaling regimes for T. The stochastic analysis reveals a

sequence of two loading regimes for slow loading $\mu \ll N_{eq}$. For ultra-slow loading, T is independent of μ and is determined by the adhesion clusters decay by stochastic fluctuations to the absorbing boundary and T is determined by the time-scale for stochastic fluctuations to the absorbing boundary. For larger loading (but still with $\mu \ll N_{eq}$) T scales inversely with μ because of the finite strength of adhesion clusters. The rupture force $F = \mu T$ is the critical force f_c identified for constant force in the previous chapter. In the fast loading regime, the results for $\gamma = 0$ apply. A distinct intermediate loading regime for $1 < \mu \ll N_t$ as proposed in Seifert [2000] could not be identified.

Our results for shared loading can be applied for example to rolling adhesion of leukocytes, when multiple L-selectin bonds are dynamically loaded in shear flow [Dwir et al., 2003]. Dynamic force spectroscopy has only recently been applied to clusters of adhesion bonds [Prechtel et al., 2002]. RGD-lipopeptides on a vesicle have been presented to $\alpha_\nu\beta_3$-integrins on a cell. The thermal membrane fluctuations can be disregarded on both sides, because the vesicle is under large tension and the integrins are rigidly connected to the cytoskeleton. Appreciable loading occurs only over a ring region along the rim of the contact disc, for which no inhomogeneities have been observed. If one neglects the subsequent peeling of the inner region, which presumably is much faster, our model can be applied. The parameter values can be estimated to be $N_t \approx 100$, $F_B \approx 40\,\mathrm{pN}$, $k_0 \approx 0.01\,\mathrm{Hz}$ and $\gamma \approx 1$. Loading rates have been varied from $r = 20 - 4 \times 10^3\,\mathrm{pN\,/\,s}$, that is $\mu/N_t = 0.5 - 100$. Therefore this experiment should correspond to the intermediate and fast loading regimes. Even more recently, dynamic force spectroscopy experiments are undertaken with the biomembrane force probe using small numbers of bonds ($N_t = 1 \ldots 10$) under fast loading. In these experiments, the exact number of molecules in each attempt is unknown and the force spectra for different numbers have to be superimposed. We expect that future improvements in experimentation will make it possible to probe also the slow loading regime, where rebinding and stochastic effects become relevant. In order to achieve a more complete understanding of the role of force in cell adhesion, future modelling should also address the detailed nature of the force transducer, non-homogeneous loading and more realistic scenarios for the rebinding process.

Chapter 5

Impact of receptor-ligand distance on adhesion cluster stability

In experimental and biological systems, receptor and ligand molecules can usually not be attached directly to a surface because the interference with the surface might disturb their function. Instead, they are usually tethered to the substrate via polymeric linker molecules. This allows the molecules to form adhesion bonds when two opposing surfaces are separated by a certain distance. Because stretching the linker molecules requires energy, the binding probability and the force exerted on the bonds then depend on the distance between the surfaces.

As explained in Chapter 2, this distance ℓ between the equilibrium positions of receptors and ligands is typically used in experiments to control the force exerted on an adhesion cluster. In this chapter, we use this distance explicitly as a parameter instead of the force and extend the model to include also a distance dependent rebinding rate. We derive transition rates for rupture and rebinding that can be used in the master equation and in the deterministic equation. We analyse the stability of adhesion clusters using a bifurcation analysis of the deterministic equation which is compared to the stationary probability distribution that follows from the master equation. In the main part of the chapter, we model the tethers as harmonic springs. Thereby, we discuss the case of general transducer stiffness. This allows the tethers that bind to the transducer to reduce the actual distance of the transducer from the ligands which increases the probability for rebinding. We also discuss the limits of soft and stiff transducers and introduce a model that takes into account the finite extensibility of real polymers.

5.1 Kinetic description in the harmonic spring model

The distance dependence of the binding process of tethered bonds has been investigated experimentally with the surface forces apparatus [Wong et al., 1997, Jeppesen et al., 2001]. One surface was coated with receptors while to the opposing surface ligands were tethered with linkers of varying length. The surfaces were approached slowly and a rapid increase of force corresponding to the formation of many bonds was observed when the surfaces had approached close to the radius of gyration of the polymers. The experimental situation has been analysed theoretically using a mean field approach [Moreira et al., 2003, Moreira and Marques, 2004]. The binding kinetics of a tethered ligand over a given distance was described by reaction-diffusion equations. The distance between the surfaces was given so that binding was non-cooperative and a mean field description for tether binding could be applied. In regard to cells adhesion, distance dependent binding is important for the forma-

tion of new adhesion contacts. Before firm contacts are established, cell membrane and substrates are typically separated by a distance in the range of $\mu\mathrm{m}$ which has to be bridged by the first adhesion bonds. After the first adhesion bonds have bridged this distance and contact is established, the distance decreases to the range of nm.

In this section, we derive expressions for the transition rates of the bonds in an adhesion cluster which include the spatial separation of receptors and ligands. These will be used to describe adhesion cluster dynamics within the framework of the master equation (2.24) and the deterministic approximation (2.36) for the average number of closed bonds. Thereby we include cooperative effects due to sharing of the force. To derive the transition rates, we use the spring model for the adhesion cluster that was presented in Chapter 2 and is shown in a similar form in Fig. 5.1. We denote the distance ℓ between the equilibrium position of the transducer and that of the ligands as the receptor-ligand distance. This is the extension that is necessary for the first tether to bind to the transducer. The actual distance of the transducer from the ligands will reduce upon binding of tethers to a value $x_b < \ell$.

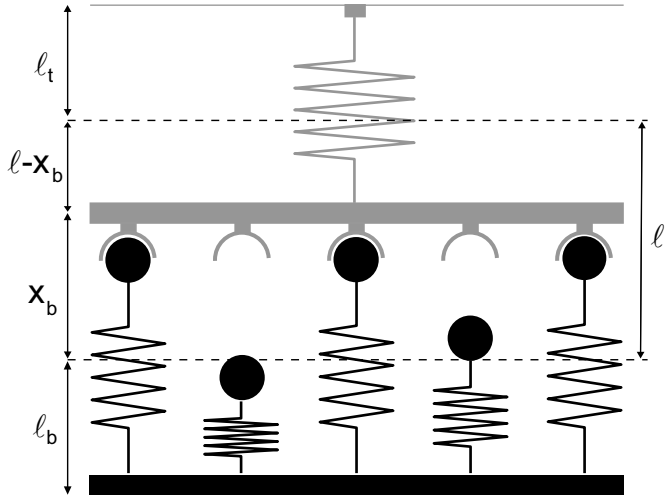

Figure 5.1: Simple spring model for adhesion clusters as introduced in Seifert [2000] and discussed before in Chapter 2. The rest lengths of tether and transducer springs are denoted by ℓ_b and ℓ_t, their spring constants by k_b and k_t, respectively. The equilibrium positions of the springs – marked by the dashed lines – are separated by the distance ℓ. The extension of the tether springs is x_b; that of the transducer spring is $\ell - x_b$. The position of the transducer follows from mechanical equilibrium $ik_bx_b = k_t(\ell - x_b)$, where i is the number of closed bonds.

In the derivation of the transition rates we assume that, for a given number of closed bonds i, the position of the transducer is determined by the condition of mechanical equilibrium between transducer and tether forces. This amounts to assuming that the relaxation of the transducer to its equilibrium position is fast compared to changes in i. In experiments on single bonds in the biomembrane force probe it has been found indeed that the relaxation time of the force transducer was much shorter that the typical time for rupture of the bonds [Nguyen-Duong et al., 2003]. There, the relaxation time of the transducer was estimated to be on the order of $10^{-3}\,\mathrm{s}$ so that with typical binding times in the range of seconds, the assumption of mechanical equilibrium is valid. In the same vein, we assume that the distribution of the ligands follows a stationary Boltzmann distribution for the potential. This requires that also the relaxation time of the polymer tethers, which is given by the Rouse time, is short compared to the time-scale for rupture and rebinding.

Another assumption we use to derive the transition rates is that the transducer has a fixed position and binding events are solely promoted by tether fluctuations. Fluctuations of the transducer can be neglected if one or more tethers are bound to the transducer. The variance of the position of the free transducer in its harmonic potential is proportional to the inverse force constant, $\sigma^2 = k_BT/k_t$. If i tethers are bound, the transducer moves in the potential of the transducer and the i tether springs with a variance of $\sigma^2 = k_BT/(k_t + ik_b)$ which should be small compared to that of the single, free tethers. For the free transducer, fluctuations cannot generally be neglected. Indeed, in the limit of a

soft transducer (and very stiff tethers) we have to take transducer fluctuations into account to allow binding of the tethers.

5.1.1 Rupture rate

The Bell-like off-rate (2.6) for single bonds depends on the force exerted on the individual molecule. In Chapter 2 we derived the expression for the extension of the bound tether springs (i.e. the distance of the transducer from the equilibrium position of the tethers) from the condition of mechanical equilibrium in the simple spring model which is shown in Fig. 5.1. The extensions of the bound tethers that are attached to the transducer by the i closed bonds is given in (2.8) as

$$x_b(i) = \frac{k_t \ell}{k_t + k_b i} \,. \tag{5.1}$$

Here, ℓ is the separation of the equilibrium positions of transducer and tethers. We non-dimensionalise all distances by writing them in units of the unstressed length of the tethers ℓ_b. Defining the dimensionless separation $\lambda := \ell/\ell_b$, the dimensionless tether extension $\xi_b := x_b/\ell_b$ as function of i reads

$$\xi_b(i) = \frac{\ell/\ell_b}{1 + \kappa i} = \frac{\lambda}{1 + \kappa i} \,. \tag{5.2}$$

The ratio $\kappa = k_b/k_t$ of the force constant of the tethers k_b and the transducer, k_t has been used before in Chapter 2. As in the previous chapters, force is measured in units of the intrinsic force scale for bond rupture, F_B. The dimensionless expression for the force per bond is

$$f_b(i) = k_b \xi_b(i) \frac{\ell_b}{F_B} = \frac{\lambda \phi}{1 + \kappa i} \,. \tag{5.3}$$

The dimensionless parameter $\phi := k_b \ell_b / F_B$ is the force in units of F_B that is necessary to extend a tether spring by ℓ_b, i.e., to its double rest length. The product $\lambda\phi = k_b \ell / F_B$ is the dimensionless tether force at the extension ℓ that is necessary to initiate the first binding event. This product replaces the force f which was used in the discussion of constant loading in Chapter 2. With Bell's equation (2.6), the dimensionless single bond off-rate is

$$k_{off}/k_0 = e^{f_b(i)} = e^{\frac{\lambda\phi}{1+\kappa i}} \,. \tag{5.4}$$

With i closed adhesion bonds in a cluster of N_t adhesion bonds, the reverse rate is given by

$$r(i) = i e^{f_b} = i e^{\frac{\lambda\phi}{1+\kappa i}} \,. \tag{5.5}$$

This is a non-linear function of i which, unlike the case of shared loading with a soft transducer, remains finite for $i = 0$.

5.1.2 Rebinding rate

Next we derive an expression for the dependence of the rebinding rate of tethered bonds in the cluster on the distance ξ_b of the receptors from the ligands. Using expression (5.2), this rebinding rate can then be written as a function of i so that it can be used in the master equation (2.24).

The ligands move in the one-dimensional harmonic potential of the tethers between two impenetrable and immobile walls: the substrate is at a distance $-\ell_b$ and the transducer at a distance x_b from

the resting position of the tethers which is chosen as the origin of a coordinate system (see Fig. 5.1). We assume that the ligands follow a stationary canonical distribution in the potential and that the transducer is fixed at the position given by mechanical equilibrium. This distribution yields the probability that the ligands are close to the transducer which is proportional to the effective binding rate of the adhesion bonds.

Substrate and transducer impose an infinite potential on the ligands which thus move in the potential

$$U(x) = \begin{cases} \frac{k_b}{2}x^2 & \text{if } -\ell_b \leqslant x \leqslant x_b, \\ \infty & \text{elsewhere.} \end{cases} \tag{5.6}$$

The canonical distribution $\rho(x)$ of the ligands embedded in a surrounding heat bath is given by the Boltzmann factor normalised with the partition function $Z(x_b) = \int_{-\ell_b}^{x_b} e^{-\frac{U(x)}{k_B T}}\, dx$:

$$\rho(x) = \frac{1}{Z} e^{-\frac{U(x)}{k_B T}} = \frac{1}{Z} e^{-\frac{k_b x^2}{2k_B T}}\,. \tag{5.7}$$

The partition function can be evaluated in terms of the error function $\mathrm{erf}\,(x) := (2/\sqrt{\pi}) \int_0^x e^{-t^2}\, dt$ as

$$Z(x_b) = \left[\frac{\pi k_B T}{2k_b}\right]^{\frac{1}{2}} \left\{ \mathrm{erf}\left(\left[\frac{k_b \ell_b}{2k_B T}\right]^{\frac{1}{2}}\right) + \mathrm{erf}\left(\left[\frac{k_b x_b^2}{2k_B T}\right]^{\frac{1}{2}}\right)\right\}. \tag{5.8}$$

The one-dimensional density has the dimension of an inverse length and is non-dimensionalised by multiplying with the tether rest length ℓ_b. In terms of the dimensionless lengths $\xi_b = x_b/\ell_b$ and $\xi := x/\ell_b$ and the newly introduced dimensionless parameter $\beta := k_b \ell_b^2 / 2k_B T$ the dimensionless form of the density (5.7) reads

$$\rho(\xi) = 2\left[\frac{\beta}{\pi}\right]^{\frac{1}{2}} \frac{e^{-\beta\xi^2}}{\mathrm{erf}\left(\beta^{\frac{1}{2}}\right) + \mathrm{erf}\left(\beta^{\frac{1}{2}}\xi_b\right)}\,. \tag{5.9}$$

It is a renormalised Gaussian which depends on temperature through β which is the energy of the tether spring at an extension ℓ_b measured in units of thermal energy $k_B T$.

Using the concept of the encounter complex formation, receptor-ligand binding occurs with a conditional binding rate $\hat{\gamma}$ if the ligand approaches the receptors to less than a 'capture distance' ℓ_c. Since interactions of biological adhesion bond are usually short ranged, ℓ_c will be small and $\rho(\xi)$ can be assumed to be approximately constant over the length ℓ_c. The probability for the ligand to be within the capture distance is approximately $(\ell_c/\ell_b)\rho(\xi_b)$, where the tether rest length was used for non-dimensionalisation. The effective binding rate is then given by $(\ell_c/\ell_b)\hat{\gamma}\rho(\xi_b) = \gamma\rho(\xi_b)$. The on-rate $(\ell_c/\ell_b)\hat{\gamma} := \gamma$ is the effective binding rate for a homogeneous distribution of ligands over the length ℓ_b. It is thus related to the on-rate γ used in the previous chapters and we will use similar numerical values for it in the following.

In state i of the adhesion cluster there are $N_t - i$ free tethers which all have the same distribution $\rho(\xi_b(i))$. The rebinding rate is given by

$$g(i) = \gamma(N_t - i)\rho(\xi_b(i)) = 2\gamma(N_t - i)\left[\frac{\beta}{\pi}\right]^{\frac{1}{2}} \frac{e^{-\beta\left[\frac{\lambda}{1+i\kappa}\right]^2}}{\mathrm{erf}\left(\beta^{\frac{1}{2}}\right) + \mathrm{erf}\left(\frac{\beta^{\frac{1}{2}}\lambda}{1+i\kappa}\right)}\,. \tag{5.10}$$

name		definition	typical value	meaning
β	:=	$k_b\ell_b^2/k_BT$	$0.1\ldots10$	tether energy in units of thermal energy
λ	:=	ℓ/ℓ_b	$0.1\ldots10$	transducer-tether distance
N_t	:=	N_t	$10\ldots25$	cluster size
ϕ	:=	$k_b\ell_b/F_B$	0.1	tether force in units of the force scale for bond rupture
κ	:=	k_b/k_t	1	ratio of tether and transducer stiffness
γ	:=	$\hat{\gamma}(\ell_c/\ell_b)$	1	conditional single bond on-rate

Table 5.1: The six parameters of the model, their definitions, typical values used and their meaning.

where the tether extension $\xi_b(i)$ from (5.2) as function of the number of bound tethers i has been inserted in the density (5.9). The rebinding rate is the probability that one of the ligands is inside the capture distance times the on-rate from within this capture distance. Due to the non-linear dependence of ρ on $\xi_b(i)$ and the non-linearity of $\xi_b(i)$ with i, the rebinding rate is a strongly non-linear function of the number of closed bonds i.

5.1.3 Transition rates and dynamic equations

Summarising, the distance dependent rupture and rebinding rates are given by

$$r(i) = ie^{f_b(\xi_b(i))} = ie^{\frac{\lambda\phi}{1+\kappa i}} \quad \text{and} \quad g(i) = \gamma(N_t - i)\rho(\xi_b(i))\,. \tag{5.11}$$

The reverse rate is the same as in the general case discussed in Chapter 2. Force is replaced by the parameter $\lambda\phi = k_b\ell/F_B$ which is the dimensionless force on the tether at an extension ℓ, the distance of the equilibrium positions of tether and transducer. In Chapter 2, loading was also induced by changing this distance. Here, we use ℓ (or λ in dimensionless form) explicitly as a parameter. The actual distance $\xi_b(i)$ between receptors and ligands reduces with the number of bound tethers i. This increases the binding rate $g(i)$ and at the same time decreases the reverse rate $r(i)$ so that cooperativity of ligand binding arises from the sharing of the force and the cooperative influence of the tethers on the distance ξ_b.

The master equation (2.24) with the transition rates (5.11) is non-linear because both, rupture *and* the rebinding rate, are non-linear functions of i. To allow formation of stable adhesion clusters we consider a reflecting boundary at the dissociated state $i = 0$. Since the reverse rate vanishes, $r(i = 0) = 0$, the system is enclosed between two natural, reflecting boundaries. The deterministic equation (2.36) now reads

$$\frac{d}{d\tau}N = g(N) - r(N) = 2\gamma(N_t - N)\left[\frac{\beta}{\pi}\right]^{\frac{1}{2}} \frac{e^{-\beta\left[\frac{\lambda}{1+N\kappa}\right]^2}}{\operatorname{erf}\left(\beta^{\frac{1}{2}}\right) + \operatorname{erf}\left(\frac{\beta^{\frac{1}{2}}\lambda}{1+N\kappa}\right)} - Ne^{\frac{\lambda\phi}{1+\kappa N}}\,. \tag{5.12}$$

Due to the non-linearity of the transition rate, it is not an accurate description of the stochastic average $N(\tau)$. Only in the limit of a stiff transducer, that is $\kappa = 0$, the distance $\xi_b = \lambda$ becomes independent of i and the transition rates are linear in i.

Our model now contains six parameters. The on-rate γ and the cluster size N_t have been used before in the previous chapters. The ratio $\kappa = k_b/k_t$ of the force constants has been introduced in the model chapter, however in Chapters 3 and 4, only the limits of $\kappa \to \infty$ (soft transducer) and $\kappa \to 0$

(stiff transducer) were discussed. Here it is taken into account explicitly; relevant values for it will be in the range between 1 and N_t, i.e., between the limits of soft and stiff transducer. In the following we will use $\kappa = 1$. The parameter $\phi = k_b\ell_b/F_B$ measures the force needed to stretch the tethers in units of the intrinsic force scale of the adhesion bonds $F_B = k_BT/x_B$. For an entropic spring, this essentially scales as the ratio of reactive compliance and size of the monomers of the polymer. It will thus be rather a small value. In the following we use $\phi = 0.1$. The force used to drive cluster dissociation is now replaced by the product $\phi\lambda = k_b\ell/F_b$. The distance $\lambda = \ell/\ell_b$ is the distance of the equilibrium positions of tethers and transducer. The energy of the tethers is measured in units of thermal energy by the parameter $\beta = k_b\ell_b^2/2k_BT$.

Experimentally it will be easiest to change the distance λ. The stiffness of the tethers may be changed by using different molecules in different assays, such as single or double stranded DNA. This would change β, but also the force constant expressed by ϕ. Changes in temperature would change β alone. However, experimentally, a change of the temperature might have badly controlled effects on the affinity of adhesion bonds. Moreover, the rest length ℓ_b might change which was used as the unit for lengths. In the following we will concentrate on the influence of a variable distance λ and also of changes in β on the solutions of the dynamical equations.

5.2 Deterministic analysis

To investigate formation and stability of adhesion clusters from a completely unbound state it will be particularly important to consider the behaviour of the deterministic equation in the vicinity of $N = 0$. The reverse rate $r(N)$ vanishes for $N \to 0$ and the time derivative $dN/d\tau$ at $N = 0$ is determined by the forward rate alone. The forward rate is always positive and at $N = 0$ we have

$$\left.\frac{d}{d\tau}N\right|_{N=0} = 2\gamma N_t \left[\frac{\beta}{\pi}\right]^{\frac{1}{2}} \frac{e^{-\beta\lambda^2}}{\mathrm{erf}\left(\beta^{\frac{1}{2}}\right) + \mathrm{erf}\left(\beta^{\frac{1}{2}}\lambda\right)} \geqslant 0\,. \tag{5.13}$$

Therefore, N increases from zero until it reaches a stable stationary state. The lowest steady state is always stable because the time derivative $dN/d\tau$ crosses zero from above.

The time derivative $dN/d\tau$ is plotted in Fig. 5.2 as function of N for different values of (a and b) λ and (c and d) β for a cluster size of $N_t = 10$ in (a and c) and $N_t = 25$ in (b and d). The other parameters are fixed at the values given in the figure caption. The figure shows that for small β and λ, the time derivative is positive and large at $N = 0$. It increases initially with increasing N, passes through a maximum and finally becomes negative. The zero corresponds to a stable steady state of the system. With increasing λ or β, the value of $dN/d\tau$ at $N = 0$ decreases, approaches zero but always remains positive. The slope $d(dN/dt)/dN$ is also positive for small parameters, decreases with increasing β or λ and becomes negative eventually. If this is the case, two additional fixed points appear: a stable one close to $N = 0$ and an unstable one in between the two stable fixed points at small and large N, respectively. The unstable one moves out to larger N as λ or β increase and finally merges with the upper stable fixed point. For larger parameters, only the single, globally stable fixed point at $0 \lessapprox N$ remains. In the bistable region where the system has two fixed points it depends on the initial condition – above or below the unstable fixed point – which of the stable fixed points attracts the solution for N.

Fig. 5.3 shows the bifurcation diagram following from the fixed points seen in Fig. 5.2. The positions of the fixed points are determined numerically and plotted as function of (a and b) λ for $\beta = 0.5, 1.0$ and 2.0 and as function of (c and d) β for $\lambda = 0.5, 1.0$ and 2.0. The cluster size is

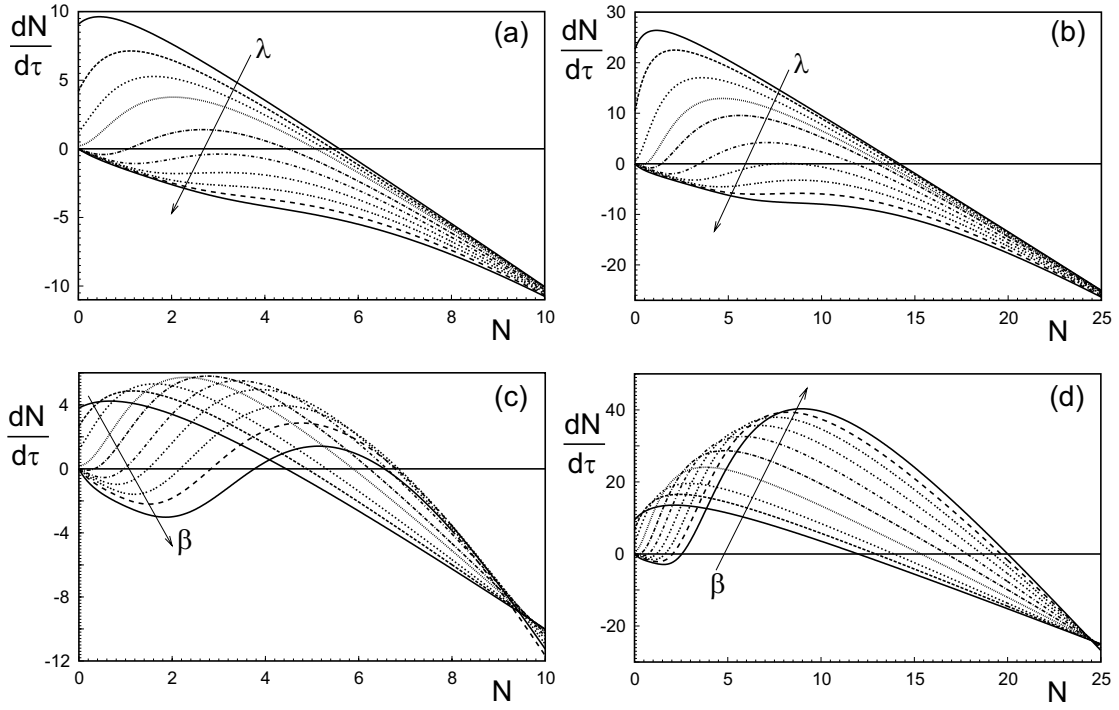

Figure 5.2: The derivative $dN/d\tau$ as function of the number of closed bonds N for (a and c) $N_t = 10$ and (b and d) $N_t = 25$ for the values (a and b) $\beta = 1.0$ and λ varying between $\lambda = 0.1$ and 16 and (c and d) for $\lambda = 1.5$ with β varying between $\beta = 0.1$ and 16. The other parameters are $\gamma = 1$, $\kappa = 1$ and $\phi = 0.1$.

$N_t = 10$ in (a and c) and $N_t = 25$ in (b and d), respectively. The system undergoes a sequence of two bifurcations in which, at small parameters, two additional fixed points appear. At large parameter values, two existing fixed points merge and vanish. The bifurcations correspond to the points where additional zeros of $dN/d\tau$ appear and dissappear in Fig. 5.2. For small parameters, there is a single, globally stable fixed point at a large number of closed bonds. This corresponds to a bound state of the adhesion cluster. With increasing λ the position of the bound state decreases steadily until is vanishes in the second bifurcation. For larger values of β, the decrease with λ is faster and the bifurcation occurs earlier. At small λ, the size of the stable cluster grows with β and is in the range of $N_t/2$ as found in Chapter 3 for $f = 0$ at the same value of $\gamma = 1$. The unstable fixed point appears in the first bifurcation, increases with increasing λ and vanishes in the second bifurcation. The stable fixed point at small N appears together with the unstable one. It decreases with increasing λ and approaches $N = 0$. Nevertheless, it exists for all values of λ although it is hardly visible in the plots. The position of the first bifurcation decreases with increasing β in a similar way as the second one and the width of the bistable region does not depend strongly on β. As function of β, the upper stable fixed point first increases from the value at $\beta = 0$ before is decreases again when approaching the second bifurcation. For small λ, the upper bifurcation point shifts to enormously large β while the first bifurcation hardly changes its position. In practical situations, either a single, large cluster or a bistable state will be observed for accessible β at small λ.

The existence of a stable cluster for small λ and β can be understood from the behaviour of the transition rates. For small enough receptor-ligand distances, the tethered ligands frequently encounter

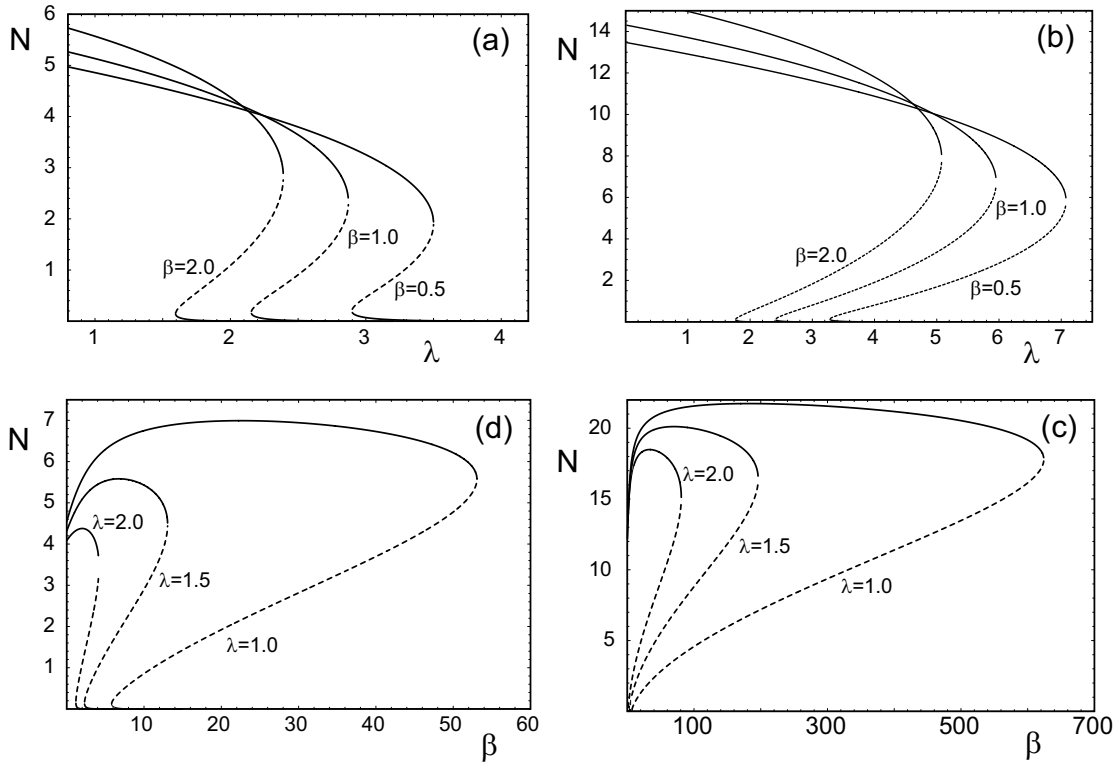

Figure 5.3: The fixed points as function of (a and b) λ for $\beta = 0.5, 1.0$ and 2.0 and (c and d) as function of β for $\lambda = 1.0, 1.5$ and 2.0. The total number of bonds is $N_t = 10$. The stable stationary states are the solid lines while the unstable state is shown as a dashed curve. The other parameters are $\gamma = 1$, $\kappa = 1$ and $\phi = 0.1$.

the receptors on the transducer and the effective rebinding rate will be large. On the other hand, the extension of the bound tethers is small so that the force which would accelerate bond rupture is small. For small β, the mechanism is similar. A small β corresponds to a large temperature or a small stiffness of the tethers. A large temperature increases the ligand density at the transducer and leads to an effectively large rebinding rate which stabilises the cluster. With increasing λ and β, density and rebinding rate decrease while the reverse rate increases and the bound state is not globally stable anymore. On the other hand, binding reduces the actual distance $\xi_b(i)$ according to (5.1). Thus, once a sufficient number of tethers is bound, a stable cluster can exist. In the deterministic description, however, this stable cluster cannot be reached from $N = 0$. In a stochastic description, as we have seen in the previous chapters, the unstable state will be a kinetic barrier for transitions between the stable states. Finally, for very large distances or very small temperatures, the reduction of the distance does not increase the binding rate sufficiently to compensate for the large unbinding rate. The bound steady state vanishes in another bifurcation and only the lower steady state which is practically identical to $N = 0$ exists.

The behaviour of the fixed points is reminiscent of a first order phase transitions in statistical physics at which two states can coexist because they are separated by an unstable region for N. In a deterministic dynamical system the steady state value of N undergoes hysteresis upon slow changes in the parameters λ or β. For small values of the parameters the system always enters the bound

steady state. Increasing either of the parameters slowly drives the system along the upper branch of the bifurcation diagram until the second bifurcation is reached and N changes discontinuously to the unbound state. The reverse process leads to a discontinuous transition at the lower bifurcation.

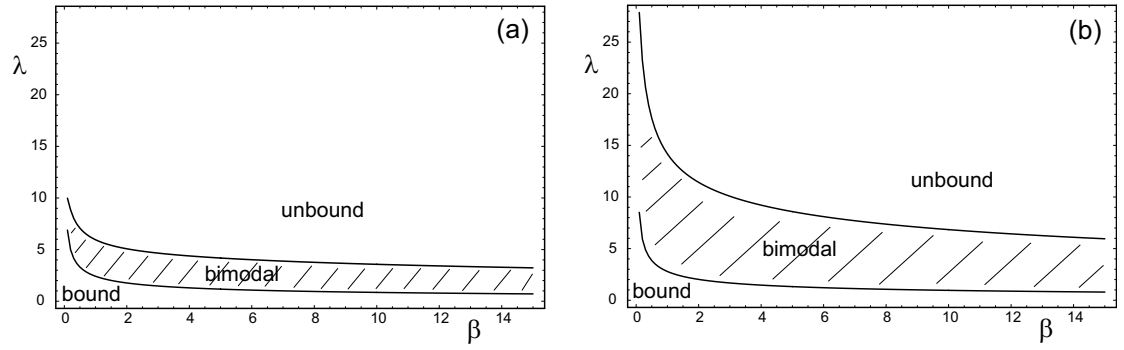

Figure 5.4: Stability diagram for adhesion clusters: solid lines are numerically determined positions of the lower and upper bifurcation as function of β and λ. The shaded region is the region of bistability, above the upper curve there is a single unbound state while below the lower curve there exists a single, bound cluster. The curves are derived for $N_t = 10$, $\phi = 0.1$, $\kappa = 1$ and the values (a) $\gamma = 1$ and (b) $\gamma = 5$.

The stability diagram in Fig. 5.4 plots the positions of the bifurcations as functions of the two parameters λ and β for (a) $\gamma = 1$ and (b) $\gamma = 5$. The other parameters are $N_t = 10$, $\phi = 0.1$, $\kappa = 1$. The dependence of the curves on β and λ is reciprocal as observed already in Fig. 5.3. For small λ, both curves decrease slowly with β and are almost parallel. This explains the large region of bistability for a given small λ as function of β. For very small β, the curves diverge and the region of bistability becomes narrow but exists also at large values of λ. The diagrams for different γ show that the upper bifurcation grows with γ while the lower curve is nearly independent on γ.

As an approximate criterion for the occurrence of the first bifurcation at small parameters we use that the slope $d(dN/d\tau)/dN = g'(N) - r'(N)$ of $dN/d\tau$ has to become negative just before the bifurcation. The derivative of the reverse rate at $N = 0$ is given by

$$\left.\frac{d}{dN} r(N)\right|_{N=0} = e^{\phi\lambda} \,. \tag{5.14}$$

The derivative of the forward rate $g(N)$ is

$$\left.\frac{d}{dN} g(N)\right|_{N=0} = \frac{2\gamma \left[\frac{\beta}{\pi}\right]^{\frac{1}{2}} e^{-\beta\lambda^2}}{\operatorname{erf}\left(\beta^{\frac{1}{2}}\right) + \operatorname{erf}\left(\beta^{\frac{1}{2}}\lambda\right)} \left(2\beta\lambda^2\kappa + \frac{\beta^{\frac{1}{2}}\lambda\kappa N_t e^{-\beta\lambda^2}}{\operatorname{erf}\left(\beta^{\frac{1}{2}}\right) + \operatorname{erf}\left(\beta^{\frac{1}{2}}\lambda\right)} - 1 \right) \tag{5.15}$$

For not too large λ we may neglect the derivative of the reverse rate and only discuss the second equation for the rebinding rate. For very large $\beta \gg 1$, the second term in parenthesis can also be neglected. Then, the relation

$$1 = 2\beta\lambda^2\kappa \Leftrightarrow \lambda^2 = \frac{1}{2\beta\kappa} \,, \tag{5.16}$$

for the parameters at the bifurcation results. The value of λ above which the system becomes bistable decreases as the inverse square root of β. On the other hand, for small $\beta \ll 1$, the first term in

parenthesis can be neglected and the error function becomes linear in its argument. This leads to

$$\beta = \frac{\ln\left(2\kappa N_t \lambda/\sqrt{\pi}(1+\lambda)\right)}{\lambda^2} \approx \frac{\ln\left(\kappa N_t\right)}{\lambda^2}\,. \tag{5.17}$$

where the last approximation is for large λ. For $\beta \to 0$, the value of λ at the bifurcation diverges, again with the inverse square root. These limiting cases qualitatively support reciprocal relation of λ and β of the numerical solutions in Fig. 5.4. Also the relative independence of the lower bifurcation point on the on-rate γ, which was observed in the Fig. 5.4, is retrieved.

5.3 Stochastic analysis

The stationary state $p_i(\infty) := \lim_{\tau\to\infty} p_i(\tau)$ can be calculated for any one-step master equation from the transition rates. This was done in Sec. 3.4 of Chapter 3 and the result is given in terms of the transition rates in (3.72). It is given by

$$p_i(\infty) = \frac{\prod_{j=0}^{i-1} \frac{g(j)}{r(j+1)}}{1+\sum_{k=1}^{N_t}\prod_{j=0}^{k-1}\frac{g(j)}{r(j+1)}}\,. \tag{5.18}$$

Fig. 5.5 shows a density plot of the stationary distribution $\{p_i(\infty)\}_{i=0}^{N_t}$ as function of the number of closed bond i and λ (a and b) and β (c and d), respectively and for the cluster sizes $N_t = 10$ in (a and c) and $N_t = 25$ in (b and d). The other parameters are chosen as $\gamma = 1$, $\kappa = 1$ and $\phi = 0.1$ as before. The plots confirm the results from the deterministic equation. For small parameter values the distribution is unimodal. The maximum corresponds to a single macrostate which is the bound state of the cluster. Around this maximum there is a wide distribution which becomes narrower with increasing N_t. In an intermediate range of parameters, the distribution becomes bimodal as a second, sharp maximum emerges close to the dissociated state. For large parameter values, the upper, bound macrostate disappears and only the unbound one remains.

For a bimodal distribution it is convenient to define the probability distribution and the averages around the different macrostates. A macrostate is defined by the deterministic number of closed bonds as it follows from the deterministic equation. A mesostate is the probability distribution over the whole set of states as a solution of the stochastic master equation. In general, it consists of more or less localised peaks around the macrostates. To identify these different macrostates states in the stochastic distribution, it is split in two parts at a minimum between the peaks[1]. Denoting the minimum of the distribution as N^* and adapting the normalisations leads to

$$p_i^u(\infty) = \frac{\prod_{j=0}^{i-1} \frac{g(j)}{r(j+1)}}{1+\sum_{i=1}^{N^*-1}\prod_{j=0}^{i-1}\frac{g(j)}{r(j+1)}} \quad \text{and} \quad p_i^b(\infty) = \frac{\prod_{j=0}^{i-1} \frac{g(j)}{r(j+1)}}{\sum_{i=N^*+1}^{N_t}\prod_{j=0}^{i-1}\frac{g(j)}{r(j+1)}}\,. \tag{5.19}$$

for the distribution $\{p^u(\infty)\}_{i=0}^{N^*-1}$ around the unbound and $\{p^b(\infty)\}_{i=N^*+1}^{N_t}$ around the bound state, respectively. The average number of closed bonds is given by

$$N(\infty) = \sum_{i=1}^{N_t} i p_i(\infty) \tag{5.20}$$

[1]Defining an effective energy landscape in analogy to a Boltzmann distribution as $E_i = -k_B T \ln p_i$, this minimum corresponds to a maximum in energy which separates two potential wells. In a deterministic description, it is determined by the initial condition, which of these two wells will be occupied. In a stochastic description, fluctuations allow equilibration between the wells.

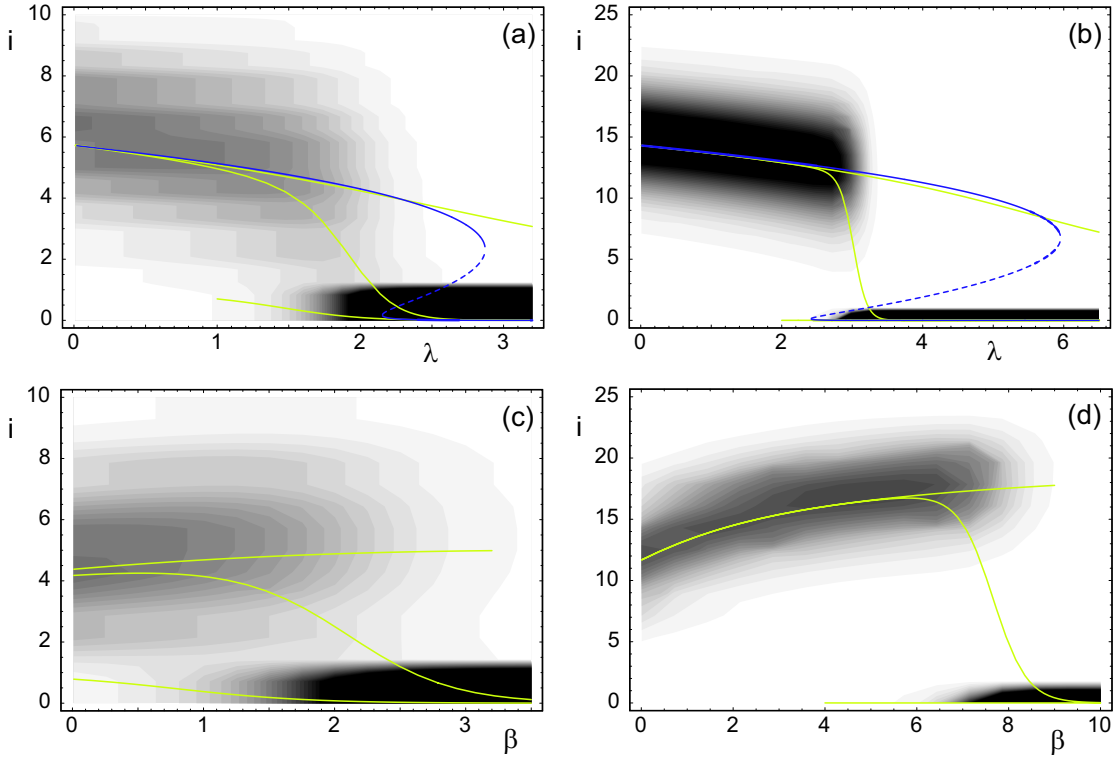

Figure 5.5: Density plot of the stationary distribution $\{p_i(\infty)\}_{i=0}^{N_t}$ as function λ for cluster sizes (a,c) $N_t = 10$ and (b,d) $N_t = 25$ and for (a,b) $\beta = 1.0$ as function of λ and for (c,d) $\lambda = 1.5$ as function of β. The other parameters are $\gamma = 1$, $\kappa = 1$ and $\phi = 0.1$. Dark regions indicate high probability. The yellow lines are the average number of closed bonds in the whole cluster and in the bound and the unbound state of the bimodal region, respectively. The blue curves in (a,b) are the stationary states of from the deterministic equation shown before in Fig. 5.3.

for the full distribution and by

$$N^u(\infty) = \sum_{i=1}^{N^*-1} i p_i^u(\infty) \quad \text{and} \quad N^b(\infty) = \sum_{i=N^*+1}^{N_t} i p_i^b(\infty) \tag{5.21}$$

for unbound and bound state, respectively. These averages $N(\infty), N^u(\infty)$ and $N^b(\infty)$ are plotted in Fig. 5.5 together with the probability distribution. For the plots, the minimum was set to $N^* \simeq 2$ which is usually a good approximation. The averages in the bound and unbound state follow closely the maxima of the distribution. In the bimodal region, the total average decreases quickly a soon as the absolute maximum of the occupancy changes from bound to unbound.

Fig. 5.5a,b also compares the stochastic stationary probability distribution and the average as function of λ to the deterministic steady states of Fig. 5.3. The deterministic steady state describes the stochastic averages in the bound state very well. The bistable region for the deterministic dynamical system corresponds to the bimodal distribution in the stochastic system. The point at which the bimodal distribution appears is underestimated by the deterministic bifurcation point for $N_t = 10$ but is well described for the larger $N_t = 25$. The stochastic transition between the different states becomes sharper for larger clusters. The position of this transition is close to the bifurcation at which

the unbound state first appears. For Fig. 5.5c,d, the deterministic steady states are not plotted. These extend to very large β which is not reflected by the stochastic distribution which shows a transition from bound to unbound close to the lower bifurcation.

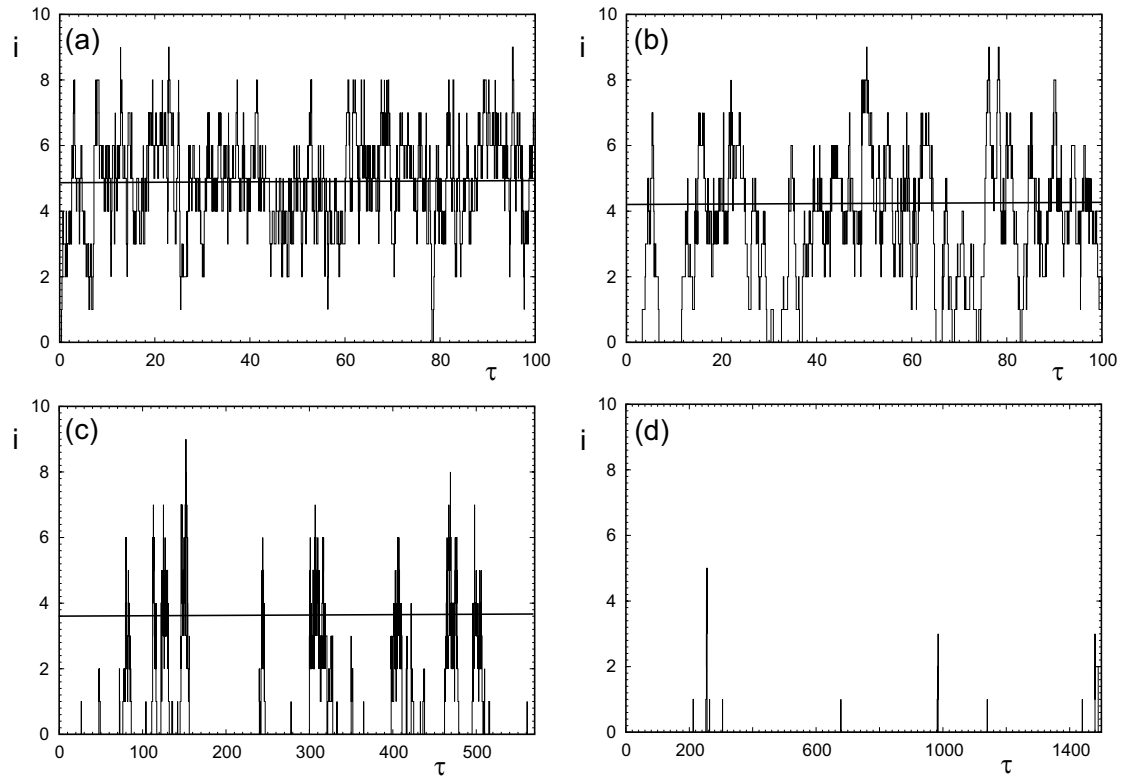

Figure 5.6: Single adhesion cluster trajectories for a cluster size $N_t = 10$ and $\beta = 0.5$, the other parameters are as in the previous figures. The time average over the trajectories should be identical to the stationary distribution. The parameter λ increases from (a) $\lambda = 1$ for which the stationary distribution is unimodal over (b) $\lambda = 2$ and (c) $\lambda = 3$ in the bimodal region to (d) $\lambda = 3.5$ for which there is only a single unbound macrostate. The horizontal lines indicate the position of the deterministic bound state taken from Fig. 5.3.

Fig. 5.6 plots single adhesion cluster trajectories generated with the Gillespie algorithm. The distribution of the i in a single trajectory, averaged over long times, would yield the stationary distribution $p_i(\infty)$. The trajectories are shown for $\beta = 0.5$ and increasing values of λ with $N_t = 10$, $\gamma = 1$, $\kappa = 1$ and $\phi = 0.1$. In (a) for $\lambda = 1$, the system is in the unimodal region with a single bound state of the cluster. The trajectory quickly reaches large numbers of closed bonds and fluctuates around the maximum of the distribution. Due to the small N_t, fluctuations are large and the reflecting boundary at $i = 0$ is occasionally encountered but the cluster quickly reassociates. In the bistable region in (b and c) for $\lambda = 2$ and $\lambda = 3$, it takes increasingly longer to reach the bound state from $i = 0$. Single bonds are formed frequently but are broken almost immediately and it takes several attempts to form a large cluster. Close to the second bifurcation as in (c), the bound state is still reached from $i = 0$ but the time to do so is very large and many single binding attempts are now necessary to reach a bound state. Once it was reached, the lifetime of the bound state is short. However, the actual transition from unbound to bound and vice versa is very fast. This leads to a minimum of occupancy between the

two maxima. Outside the bimodal region (d) even single binding events become rare. Formations of several bonds appear as a rare, short spikes in i.

To further quantify dynamic properties of the system we calculate the average first passage times between two different states μ and ν of the cluster. An expression for these times in terms of the transition rates can be found for arbitrary, constant transition rate as it was shown before in Sec. 3.4 for the transition between the initial and the detached state. The general expression for the first passage times from state μ to state $\nu > \mu$ can be calculated with the adjoint master equation approach [van Kampen, 2003] and is given by

$$T_{\mu,\nu} = \sum_{i=\mu}^{\nu-1} \sum_{j=0}^{i} \frac{\prod_{k=j+1}^{i} r(k)}{\prod_{k=j}^{i} g(k)} \,. \tag{5.22}$$

where a reflecting boundary at $i = 0$ is assumed and the reverse and forward rates (5.11) are used. For the reverse process, the role of reverse and forward rate is exchanged and the upper reflecting boundary at $i = N_t$ is now relevant instead of the lower boundary which cannot be encountered during the first passage process. The expression for the mean first passage time from ν to $\mu < \nu$ is

$$T_{\nu,\mu} = \sum_{i=\mu+1}^{\nu} \sum_{j=i}^{N_t} \frac{\prod_{k=i}^{j-1} g(k)}{\prod_{k=i}^{j} r(k)} \,. \tag{5.23}$$

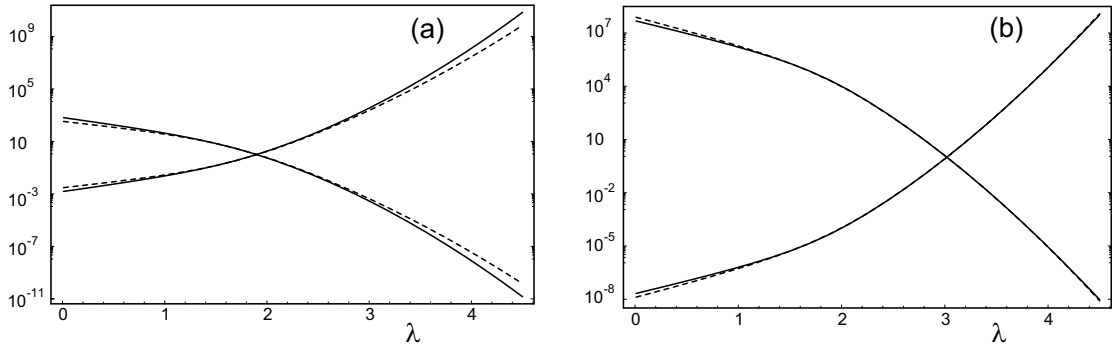

Figure 5.7: The ratio of mean first passage times from the upper bound state to the detached state $T_{\mu,0}/T_{0,\mu}$ and the inverse $T_{0,\mu}/T_{\mu,0}$ are plotted as function of λ for (a) $N_t = 10$ and for (b) $N_t = 25$. The parameter $\beta = 1$ was used and the other parameters are as in the previous figures. The ratio of occupancy of bound and unbound state $p^b(\infty)/p^u(\infty)$ and the inverse $p^u(\infty)/p^b(\infty)$ are plotted for comparison (dashed curves).

In the single bond trajectories it was observed that the actual transition times between bound and unbound state are small compared to the time the system spent in either of the states. We therefore expect that the mean first passage time from a bound state to the unbound state at $i = 0$ closely matches the average time spent in the bound state and vice versa. In Fig. 5.7 we plot the ratio $T_{\mu,0}/T_{0,\mu}$ of the first passage times between bound and unbound state in opposite directions, together with its inverse $T_{0,\mu}/T_{\mu,0}$ as function of λ. As a bound state we choose $\mu \simeq N_t/2$. As the occupancy of the bound state decreases with increasing λ, also the ratio decreases while the inverse increases. The curves closely match the ratios $p^b(\infty)/p^u(\infty)$ and $p^u(\infty)/p^b(\infty)$ for the relative occupancy probabilities

of bound and unbound state, respectively. This ratio is a measure for the relative time spent in the respective states since the time and ensemble average for the stationary state are equal. Expressions (5.22) and (5.23) give therefore an accurate approximation for the time spent in the macrostates.

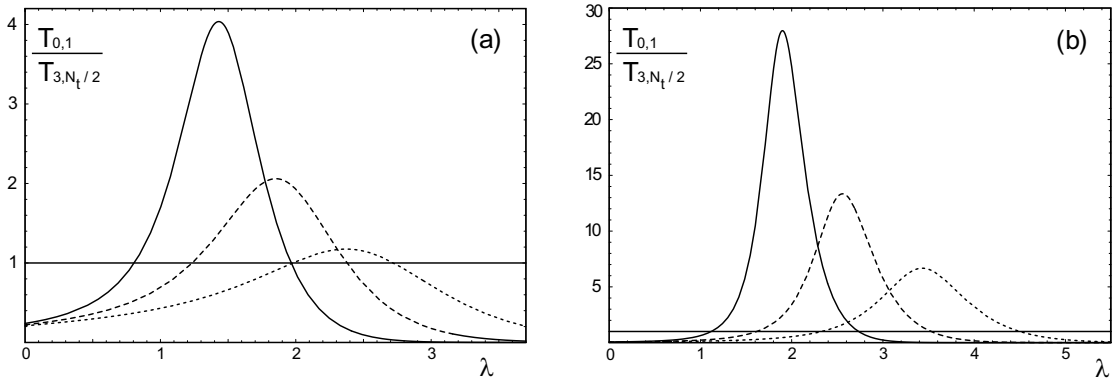

Figure 5.8: Ratio $T_{0,1}/T_{3,N_t/2}$ of the mean time for the formation of the first bond and the subsequent passage from $i = 3$ to a bound state with $i \simeq N_t/2$ for (a) $N_t = 10$ and (b) $N_t = 25$ as function of λ for $\beta = 0.5, 1.0$ and 2 (solid, dashed, dotted curves) and for the usual other parameters.

The mean first passage times also allow to demonstrate the existence of a kinetic barrier for binding and unbinding. The barrier is given by the unstable steady state in the deterministic description. The adhesion cluster trajectories in Fig. 5.6 have shown that also in the stochastic description the important steps are from $i = 0$ to $i = 1$ and from there to the bound state. Fig. 5.8 plots the ratio $T_{0,1}/T_{3,N_t/2}$ of the mean first passage times from $0 \to 1$ to the one from $3 \to N_t/2$. Again, we assumed that the bound state was reached when $i = N_t/2$. In the region of a unimodal distribution with a single bound state, the ratio is smaller than one. Each step between two states takes a similar amount of time so that the larger number of steps above $i = 1$ leads to a small value. In the region of bistability, the ratio grows dramatically. The rate limiting step for adhesion cluster formation is the first one. For larger λ outside the bistability region, the ratio becomes small again because transitions to the higher states take increasingly long.

5.4 Limiting cases: Soft and stiff transducer

In Chapters 3 and 4 two important limiting cases for the relative stiffness $\kappa = k_b/k_t$ of tethers and transducer were discussed, namely the soft and the stiff transducer [Seifert, 2000, 2002]. The main focus was thereby on the soft transducer because it leads to full cooperativity between the bonds whereas the stiff transducer rendered the bonds independent and non-cooperative. In the following we discuss implications of the two limits on the model for the distance dependent ligand binding.

5.4.1 Soft transducer

The soft transducer is characterised by a large stiffness of the tethers compared to the transducer so that $\kappa \to \infty$ in this limit. The consequence is that fluctuations of the transducer cannot be neglected anymore. On the contrary, while the ligands are rigidly attached to their stiff tethers, fluctuations of the transducer alone allow binding over the distance between the equilibrium positions of ligands and

receptors. However, once a tether binds, the transducer is arrested at the position of the tethers. This is the situation that was used in Chapters 3 and 4 to investigate adhesion cluster dissociation under shared loading. To discuss the possibility of the formation of stable clusters it is essential to take the first binding step into account.

Rupture rate

The reverse rate is non-zero only for $i > 0$. That means that the expressions derived in Chapter 2 for shared loading apply. The difference is now that the force which was used as a parameter there is replaced by the extension ℓ of the transducer spring when it is bound by a tether. However, with the extension of the transducer spring ℓ and the force constant k_t, the force exerted on the whole adhesion cluster is, in dimensionless form, $f = k_t\ell/F_B$ and can be used as a parameter. The force per bond is then given by $f_b = f/i$. According to Bell's equation (2.6) the single bond off-rate is $k_{off}/k_0 = e^{f_b} = e^{f/i}$ and the reverse rate $r(i) = ie^{f/i}$ is the same as in the case of shared loading.

Rebinding rate

The rebinding rate for the first step is determined by the probability for the transducer to be at the position of the ligand molecules. The transducer moves in a harmonic potential which on one side is bounded by the tethers and unbounded on the other side. The partition function is calculated in analogy to that for the tethers in (5.8). It is

$$Z = \left[\frac{\pi k_B T}{2k_t}\right]^{\frac{1}{2}} \left(1 + \mathrm{erf}\left(\left[\frac{k_t \ell^2}{2k_B T}\right]^{\frac{1}{2}}\right)\right) . \tag{5.24}$$

The arguments of the error functions are determined by the bounds at infinity (leading to $\mathrm{erf}\,(\infty) = 1$) and at $-\ell$. Apart from this, the only difference to (5.8) is the use of k_t instead of k_b. Non-dimensionalised with the transducer rest length ℓ_t, the probability density for the transducer to have an extension ℓ and to be close enough to the ligands to allow binding is given by (compare the analogous form of (5.9))

$$\rho = 2\left[\frac{\beta_t}{\pi}\right]^{\frac{1}{2}} \frac{e^{-\beta_t \lambda_t^2}}{1 + \mathrm{erf}\left(\beta_t^{\frac{1}{2}} \lambda_t\right)} . \tag{5.25}$$

In this expression we defined the dimensionless parameters $\lambda_t := \ell/\ell_t$ and $\beta_t := k_t \ell_t^2/2k_B T$ in analogy to λ and β for the case of general κ. The rebinding rate $g(0)$ for binding of a tether to the freely fluctuating transducer is given by $g(0) = \gamma N_t \rho$ where $\gamma = (\ell_c/\ell_t)\hat{\gamma}$ is the conditional binding rate times the dimensionless capture distance. The transducer with at least one tether bound is held in proximity of the tethers and the density on the capture distance can be assumed to be constant, that is, in dimensionless form $\rho = \ell_t/\ell_c$ so that the rebinding rate is given by $\hat{\gamma}$. The rebinding rate for $i > 0$ is thus $g(i) = \hat{\gamma}(N_t - i)$ as in the case of shared loading in Chapter 2.

Transition rates and dynamic equations

For the soft transducer the reverse rate is the same as for the case of shared loading,

$$r(i) = ie^{f/i} , \tag{5.26}$$

where the force scale $f = k_t\ell/F_B$ is the force at an extension ℓ of the transducer spring. The forward rate has to be split for the cases $i = 0$ and $i > 0$. We have

$$g(i) = \hat{\gamma}(N_t - i) \quad \text{for } i \geqslant 1 \quad \text{and} \quad g(0) = 2\gamma N_t \left[\frac{\beta_t}{\pi}\right]^{\frac{1}{2}} \frac{e^{-\beta_t \lambda_t^2}}{1 + \operatorname{erf}\left(\beta_t^{\frac{1}{2}} \lambda_t\right)} . \tag{5.27}$$

Only the binding rate for the initial step depends on the distance λ_t because the separation of ligands and transducer shrinks to zero upon the first binding event. For the following steps the binding rate is the same as found for shared loading in (2.25). As in the case of shared loading the boundary at $i = 0$ is an artificial boundary for the system because the rebinding rate is distinct from the other ones.

Deterministic analysis

In the deterministic differential equation (2.36) for $N(\tau)$ the deviation of the rebinding rate at $i = 0$ cannot be included in a simple way. Using the 'natural' rebinding rate, i.e. the definition of $g(i > 0)$ applied for $i = 0$, results in the exact same equation (2.42) as derived in Chapter 2 for shared loading. The only difference is that the parameter $\lambda\phi$ replaces the force f. The results, in particular the bifurcation analysis, would thus remain valid. A bistable region cannot be observed in the deterministic framework, because the alteration of the rebinding rate for the first step cannot be taken into account.

Stochastic analysis

For the stochastic description of the system in limit of the soft transducer, the results for the stationary distribution can be taken directly from the previous section. The only difference to the system that was discussed in Chapters 3 and 4 is in the forward rate $g(0)$ which can be significantly reduced for a density $\rho \ll 1$. The stationary probability distribution is given by (5.18) with the transition rates (5.26) and (5.27). If we rename these rates with a hat and use the original names for the transition rates from the model used in Chapters 3 and 4, the stationary state is given by

$$p_i(\infty) = \frac{(\hat{g}(0)/g(0)) \prod_{j=0}^{i-1} \frac{g(j)}{r(j+1)}}{1 + (\hat{g}(0)/g(0)) \sum_{k=0}^{N_t} \prod_{j=0}^{k-1} \frac{g(j)}{r(j+1)}} . \tag{5.28}$$

In this expression,

$$\frac{\hat{g}(0)}{g(0)} = \frac{\ell_t}{\ell_c} \frac{e^{-\beta_t \lambda^2}}{1 + \operatorname{erf}\left(\beta_t^{\frac{1}{2}} \lambda\right)} \tag{5.29}$$

is the ratio of the reverse rates. For small β and $\ell_t/\ell_c \to 1$ the expression for the stationary distribution approaches the one that was found in Chapter 3 for a force given by $f = \phi\lambda$ and a reflecting boundary. For larger β, the first binding step will become slow and a bimodal distribution as found in the case of general κ results. In the extreme limit of an absorbing boundary with $\hat{g}_0 = 0$, this distribution arises because the absorbing state accumulates realisations of the adhesion clusters.

5.4.2 Stiff transducer

In the limit $\kappa \to 0$ of the stiff transducer, fluctuations of the transducer can be neglected compared to those of the tethers. Owing to its large stiffness, the transducer has a fixed position at a distance

ℓ from the equilibrium positions of the tethers, that is, all tethers have to be stretched to the same extension ℓ. The force on each bound tethers is thus given by $F_b = k_b\ell$, irrespective of their number. In dimensionless units we have

$$f_b = \frac{k_b\ell_b}{F_B}\frac{\ell}{\ell_b} = \phi\lambda\,. \tag{5.30}$$

The force of i bound tethers on the transducer is $f_t = if_b = i\lambda\phi$. The dimensionless parameters $\phi = k_b\ell_B/F_B$ and $\lambda = \ell/\ell_b$ are defined as before. The reverse rate is a linear function of the number of bound tethers,

$$r(i) = ie^{\phi\lambda}\,. \tag{5.31}$$

The probability $\rho(\lambda)$ that a tether has an extension λ and is thus close to the transducer is constant because of the constant position of the transducer. It is given by (5.9) for $\xi = \xi_b = \lambda$. The rebinding rate is given by

$$g(i) = \gamma(N_t - i)\rho(\lambda) = 2\gamma(N_t - i)\left[\frac{\beta}{\pi}\right]^{\frac{1}{2}}\frac{e^{-\beta\lambda^2}}{\mathrm{erf}\left(\beta^{\frac{1}{2}}\right) + \mathrm{erf}\left(\beta^{\frac{1}{2}}\lambda\right)}\,, \tag{5.32}$$

where $\gamma = (\ell_c/\ell_b)\hat{\gamma}$ is the same as in the previous discussion of the general case.

The transition rates (5.31) and (5.32) are both linear functions of i. The linear deterministic and master equation have been solved in Chapter 3 and in Appendix A. The on-rate has to be replaced by $\gamma\rho(\lambda)$ and the force by $\phi\lambda$ which are both functions of λ. In the model of the stiff transducer, the bifurcations vanish completely because all cooperativity – expressed by the non-linearity of the transition rates – has been extinguished. However, because the of the strong dependence of the binding rate and the unbinding rate on λ, an approach of the transducer to the substrate will lead to a fast increase in the fraction of bound tethers as it was observed experimentally in Wong et al. [1997], Jeppesen et al. [2001] and investigated theoretically in Moreira and Marques [2004], Moreira et al. [2003].

5.5 Finite, non-linear extensibility of the polymer tethers

Real polymers are not infinitely extensible as it was assumed in the harmonic spring model, but have a finite contour length L. Real polymers consist of a finite number of monomers and it requires very large forces to stretch these monomers. On the other hand, we found that interesting dynamics occurs at fairly large extensions of the tethers. It will thus be interesting to investigate the influence of a finite extensibility of the tethers on the stability of adhesion clusters. To this end, we replace the harmonic tether springs by the more realistic worm-like chain model for biopolymers. The transducer is still modelled as a harmonic spring.

5.5.1 The worm-like chain model

A model that is often used for semiflexible biopolymers is the so-called worm-like chain or Kratky-Porod model [Doi and Edwards, 1986]. In this model, bending the segments of the chain relative to each other requires an energy which gives the polymer chain a certain stiffness. This model is thus often used for biopolymers that have a large persistence length due to their stiffness, as e.g. DNA molecules [Marko and Siggia, 1995] or the protein titin [Evans and Ritchie, 1999]. Particular effort has been invested in deriving the force extension relation, i.e., the dependence of the average extension of the chain on the applied force. In general, a worm-like chain behaves like a harmonic spring for

very small extensions, that is, the force increases linearly with extension. For large extensions close to the contour length the force diverges because the chain cannot be extended to lengths larger than L. For strands of DNA molecules, this behaviour could be described by an interpolation formula which approximates the actual behaviour at intermediate extensions fairly well [Marko and Siggia, 1995]. An extension of the worm-like chain model allows elastic stretching of the chain to values larger than the contour length [Kierfeld et al., 2004]. Using a continuous description of the chain several different scaling regimes of force with extension were identified. At large forces the divergence is levelled off by the transition to a linear regime where the chain is extended as an elastic rod.

In the following we will use the simple interpolation formula for the force extension relation. We assume that the polymer chains are tethered to the substrate as shown for the springs in Fig. 5.1. The ends are clamped at the substrate so that at zero extension of the chain, the polymer ends have a certain distance from the substrate. Because the polymers are relatively stiff, this allows to neglect the influence of the substrate on the distribution of the polymers above the substrate. On the other hand, the force extension relation is derived for freely rotating ends and will not be exact for small extensions. However, because we expect events with large extensions to be important for the binding process, this will be a minor assumption. The essential properties of the worm-like chain model that we incorporate in our model are the finite extensibility and the transition from linear elasticity for small extensions to the divergence at large extensions.

Force extension relation and reverse rate

The interpolation formula for the relation between force F and extension x is given by [Marko and Siggia, 1995]

$$F_{wlc}(x) = \frac{k_B T}{L_p}\left\{\frac{1}{4(1-(x/L))^2} + \frac{x}{L} - \frac{1}{4}\right\}. \tag{5.33}$$

Here, L_p is the persistence length of the polymer, L is its contour length and x denotes the average extension which is induced by the force F. The first term in curly brackets yields the divergence of the force upon approaching the contour length. The second term yields the harmonic behaviour at small extensions and the third, constant contribution is added to guarantee that the force vanishes at vanishing extension. The force constant for this harmonic behaviour is given by the ratio $k_B T/L_p$ of the thermal energy and persistence length.

We express the force in dimensionless quantities by measuring extension in units of the contour length, $\xi := x/L$ and force in units of the intrinsic force scale $F_B = k_B T/x_B$ for adhesion bond rupture, $f_{wlc} := F_{wlc}/F_B$. The force extension relation then reads

$$f_{wlc}(\xi) = \phi_{wlc}\left\{\frac{1}{4(1-\xi)^2} + \xi - \frac{1}{4}\right\} \tag{5.34}$$

The parameter $\phi_{wlc} := x_B/L_p$ is defined in analogy to ϕ in Tab. 5.1.3 and measures the ratio of the force scale for polymer extension and bond rupture. It is given by the ratio of the reactive compliance x_B of the adhesion bond and the persistence length L_p of the polymer. This is typically a small value; x_B is on the order of the size of a single molecule with typical values of $x_B \simeq 0.5\,\mathrm{nm}$ while the persistence length for semiflexible polymers can be large and on the order of $\mu\mathrm{m}$.

The extension $\xi_b(i)$ of tethers bound to the transducer is again determined by the condition of mechanical equilibrium at the transducer. This requires to solve

$$iF_{wlc}(x_b(i)) = i\frac{k_B T}{L_p}\left\{\frac{1}{4(1-(x_b(i)/L))^2} + \frac{x_b(i)}{L} - \frac{1}{4}\right\} = k_t(\ell - x_b(i)) = F_t \tag{5.35}$$

for the extension $x_b(i)$. The parameter ℓ is defined as in the rest of this chapter as the distance between positions of zero extension of the tethers and the transducer. To write (5.35) in dimensionless quantities we use the contour length to non-dimensionalise lengths. With the definition $\lambda_{wlc} := \ell/L$ in analogy to λ (see Tab. 5.1.3) the condition reads

$$i\kappa_{wlc}\left\{\frac{1}{4(1-\xi_b(i))^2}+\xi_b(i)-\frac{1}{4}\right\}=\lambda_{wlc}-\xi_b(i)\,. \tag{5.36}$$

Here, the parameter $\kappa_{wlc} := (k_BT/LL_p)/k_t$ is introduced which measures the ratio of the force constant of the polymer at small extensions and the force constant of the transducer. It is thus analogous to $\kappa = k_b/k_t$ for the simple spring model. Solution of (5.36) for $\xi_b(i)$ yields the tether extension and thus the force $f_{wlc}(\xi_b(i))$ as function of the number of bound tethers alone. Bell's equation for the off-rate $k_{off}/k_0 = e^{f_{wlc}(i)}$ leads to the reverse rate for the closed bonds in an adhesion cluster

$$r(i) = ie^{f_{wlc}(i)} \tag{5.37}$$

which can then be used in the master equation and in the deterministic equation. As a polynomial of third order, (5.36) can be solved for $\xi_b(i)$ but we will not write the solution down explicitly.

Rebinding rate

To calculate the on-rate for the bonds, we have to know the density of polymers on the transducer at a distance $x_b(i)$. With the force extension relation, stretching the polymer from zero extension to $x_b(i)$ requires the energy

$$V_{wlc}(x)=\int_0^{x_b(i)}F_{wlc}(x')\,dx'=k_BT\frac{L}{L_p}\left\{\frac{1}{4(1-(x_b(i)/L))}+\frac{(x_b(i)/L)^2}{2}-\frac{x_b(i)/L}{4}-\frac{1}{4}\right\} \tag{5.38}$$

In dimensionless units the ratio $V_{wlc}(\xi_b(i))/k_BT$ is

$$\frac{V_{wlc}(\xi_b(i))}{k_BT}=\frac{1}{\Lambda_p}\left\{\frac{1}{4(1-\xi_b(i))}+\frac{\xi_b^2(i)}{2}-\frac{\xi_b(i)}{4}-\frac{1}{4}\right\} \tag{5.39}$$

where the dimensionless persistence length is $\Lambda_p := L_p/L$. Using this energy in the Boltzmann factor $e^{-V_{wlc}(\xi_b)/k_BT}$ results in the density distribution of the ligands

$$\rho(\xi_b(i)) = e^{-V_{wlc}(\xi_b(i)))/k_BT}/Z(\xi_b(i)) \tag{5.40}$$

where $Z(\xi_b(i)) := \int_0^1 e^{-V(\xi)/k_BT}\,d\xi + \int_0^{\xi_b(i)} e^{-V(\xi)/k_BT}\,d\xi$ is the partition sum. In Z we included the possibility that the tethers can move back to the substrates to prevent that the partition function vanishes at an extension 0. The rationale is here that we assume that the polymer ends are clamped at the substrate as depicted in Fig. 5.1 for the springs. The other end of the polymer will thus have a certain average distance from the substrate. The exact limit of the integration (here we chose the contour length) will have little influence on the results because of the strong dependence of the Boltzmann factor on the extension. Inserting the distance as function of the number of closed bonds, leads to the rebinding rate as a function of i:

$$g(i) = \gamma(N_t - i)\rho(i) \tag{5.41}$$

The transition rates (5.37) and (5.41) can now be used in the deterministic equation and in the master equation to describe the adhesion cluster dynamics. The system has six parameters: on-rate γ and cluster size N_t are identical to those in the first sections. Defined in analogy to the parameters listed in Tab. 5.1.3 are κ_{wlc}, ϕ_{wlc} and λ_{wlc}. A new is the dimensionless persistence length Λ_p of the polymers which replaces β.

5.5.2 Deterministic results – Bifurcation analysis

The deterministic equation for adhesion cluster dynamics is given by

$$\frac{d}{d\tau}N = g(N) - r(N)\,. \tag{5.42}$$

A steady state analysis shows that this equation has a single, stable fixed point at relatively large numbers of closed bond for small receptor-ligand distances λ_{wlc}. A stable adhesion cluster can thus exist for sufficiently small distances. With increasing λ_{wlc} the system undergoes a bifurcation at which two additional fixed points appear very close to $N = 0$. The lower one is stable and practically identical to zero and the upper one is unstable and only marginally larger. For increasing λ_{wlc}, the unstable fixed point moves slightly outwards but stays close to zero. The position of the upper stable fixed point hardly decreases with increasing λ_{wlc}. The system thus remains bistable until the $\lambda_{wlc} = 1$ is reached. For larger distances binding is impossible because the tethers cannot be stretched to this distance.

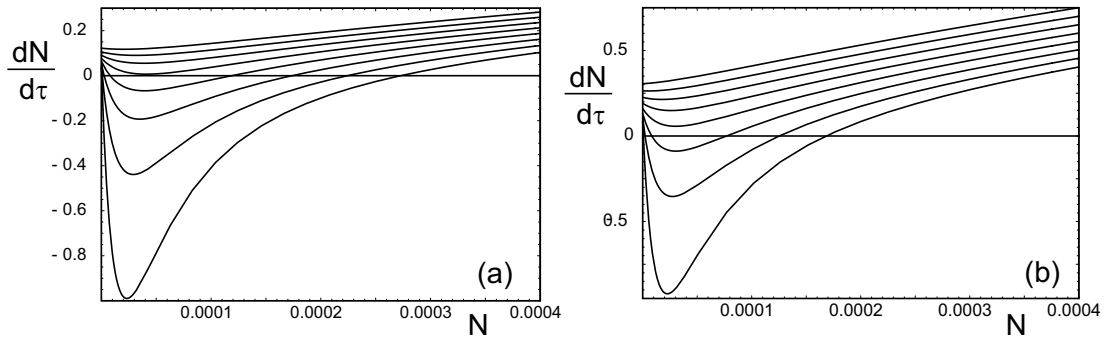

Figure 5.9: The deterministic time derivative $dN/d\tau$ of the number of closed bonds in the adhesion cluster in the vicinity of $N = 0$ for (a) $N_t = 10$ and (b) $N_t = 25$. The other parameters are given by $\kappa_{wlc} = 1, \phi_{wlc} = 0.1, \Lambda_p = 1$ and $\gamma = 1$. The distance λ_{wlc} varies for both N_t from $\lambda_{wlc} = 0.94$ in the upper curve in steps of 0.002 to $\lambda_{wlc} = 0.954$ in the lower curve.

The situation around the bifurcation is illustrated in Fig. 5.9. It shows the deterministic time derivative $dN/d\tau$ as function of N in the vicinity of $N = 0$. The cluster size was (a) $N_t = 10$ and (b) $N_t = 25$. The other parameters are given by $\kappa_{wlc} = 1, \phi_{wlc} = 0.1, \Lambda_p = 1$ and $\gamma = 1$. The receptor-ligand distance λ_{wlc} varies in both figures from $\lambda_{wlc} = 0.94$ in the upper curve in steps of 0.002 to $\lambda_{wlc} = 0.954$ in the lower curve. At $N = 0$, the time derivative $dN/d\tau$ is always positive. Similar to the situation for the harmonic springs, the slope of $dN/d\tau$ then becomes negative and a bifurcation appears. Unlike the case of harmonic springs, the position of the unstable, intermediate fixed point moves out to larger N very slowly so that is stays very close to zero until $\lambda_{wlc} = 1$ is reached.

5.5.3 Stochastic results – stationary probability distribution

Bistability of the deterministic solution corresponded to a bimodal stationary distribution $p_i(\infty)$ for the stochastic description. With the transition rates (5.37) and (5.41) derived in this section, the

stationary distribution can be calculated directly according to (5.18). It is shown in Fig. 5.10 for the cases $N_t = 10$ and $N_t = 25$ as function of λ_{wlc}. The other parameters are the same as in Fig. 5.9.

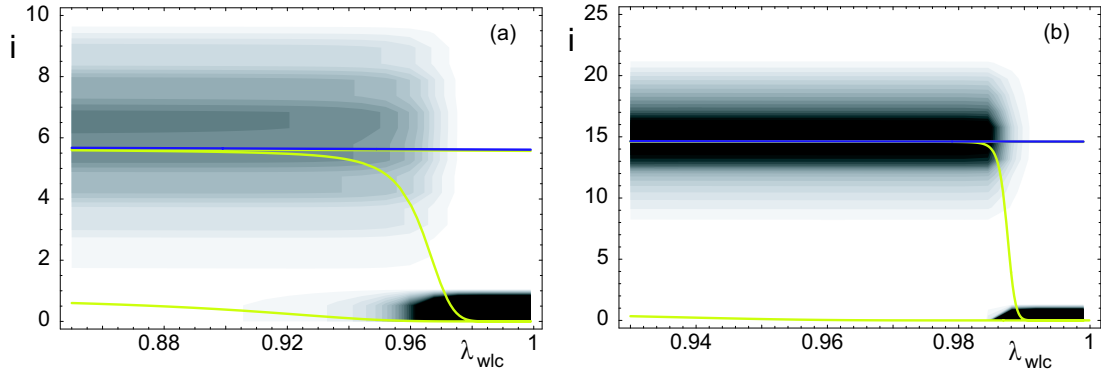

Figure 5.10: The stationary probability distribution $p_i(\infty)$ according to (5.18) with the transition rates (5.37) and (5.41) for the case (a) $N_t = 10$ and (b) $N_t = 25$ plotted as a function of λ_{wlc}. The other parameters are $\kappa_{wlc} = 1.0, \phi_{wlc} = 0.1, \Lambda_p = 1$ and $\gamma = 1$ as in Fig. 5.9. Together with the probability distribution, the average number of closed bonds $N(\infty)$ for the whole cluster and $N^b(\infty)$ in the bound and $N^u(\infty)$ in the unbound state as they are defined in (5.20) and (5.21) (yellow lines and the deterministic result for the upper, stable fixed point (blue) are plotted.

For small λ_{wlc}, the stationary distribution has a maximum at a large number of closed bonds. The distribution around this maximum becomes sharper for increasing cluster size. The position of the maximum shifts only very weakly to smaller values of i upon an increase of λ_{wlc}. For $N_t = 10$, a second maximum appears and the distribution becomes bimodal at a distance at which the bifurcation was observed in the deterministic description. For $N_t = 25$, this occurs at larger distances within the bistable region. The absolute maximum of the distribution switches quickly from the upper bound to the lower, unbound state. However, there still exists a shallow maximum of occupancy at the bound state which is not visible in the density plots but which is demonstrated by the behaviour of the average number of closed bonds. Plotted together with the probability are the averages in the whole cluster, $N(\infty)$ according to (5.20), in the bound state, $N^b(\infty)$, and in the unbound state, $N^u(\infty)$, which were defined in (5.21). The total average switches from bound to unbound state together with the absolute maximum of the distribution. The average in the bound state, however, remains large and hardly changes with λ_{wlc}. Moreover, it is almost identical to the bound, stable fixed point of the deterministic equation which is shown as the blue curve in the plots. This behaviour confirms that there will be no further bifurcation.

The reason for the minute changes of the maximum of the distribution and the absence of a second bifurcation is the super-linear increase of tether force f_{wlc} with extension ξ, in combination with the *linear* elasticity of the transducer. For large enough λ_{wlc}, strong stretching of the tethers to the super-linear regime is necessary to initiate the first binding event. The large force of the tether extends the relatively soft transducer spring strongly. Thereby the tether gets softer because the extension approaches the linear regime. Therefore, the dependence of $\xi_b(i)$ on i is weak once the first tethers are bound. The reverse rate $r(i) = ie^{f_{wlc}(\xi_b(i))}$ thus becomes almost linear for $i > 1$. Therefore, also the stable, bound fixed point persists until the maximum extension $\lambda_{wlc} = 1$ is reached; the diverging force extends the transducer sufficiently to induce further binding events. However, the binding probability vanishes as λ_{wlc} is approached so that the time it takes for a binding event to

occur diverges, while the time spent in the bound state decreases. The ratio of the lifetimes of bound and unbound state are given by the relative occupancy of bound and unbound state as shown for the harmonic spring model. Therfore, the unbound state is occupied almost exclusively for large enough λ_{wlc} above the bifurcation.

Finally we note that, had we also replaced the transducer spring by a worm like chain we expect a behaviour similar to the harmonic spring model. In particular, we expect a second bifurcation to occur in which the bound state disappears because the diverging force of the tethers is counteracted by the diverging transducer force.

5.6 Summary

In this chapter, we have discussed the influence of a distance dependent binding rate on the stability of adhesion clusters. Polymeric linker molecules that tether the ligand molecules to their substrate have been modelled as harmonic springs. The receptors were attached to the harmonic force transducer. The ligands bind to the receptors with a probability that decreases with the distance of the transducer from the equilibrium position of the ligands. The force that the bound tethers exert on the transducer increases with distance. An important point is that the tethers pull the transducer closer to the substrate. This leads to a positive feedback for tether binding and unbinding. Once a tether binds to the transducer it reduces the distance. This reduces the force on the closed bonds and thus reduces the reverse rate. On the other hand, the smaller distance leads to a higher probability for rebinding. Rupture of an adhesion bond in a cluster has the reverse effect: the distance increases which increases the rupture rate and decreases the rebinding rate which therefore induces rupture of further bonds.

A similar instability due to positive feedback was already observed in Chapters 3 and 4 where it resulted from the cooperativity of the bonds under shared loading. The non-linearity of the distance dependent rebinding rate gives rise to additional non-linear phenomena in the dynamic system. A stability analysis of the deterministic equation revealed the existence of a bistable region of receptor-ligand distances in which two stable fixed points, a bound and an unbound state, coexist. Corresponding to the bistability of the deterministic equation, the stochastic master equation revealed a bimodal stationary distribution of cluster sizes. Fluctuations allow the system to frequently switch between the bound and the unbound state. The rate for this switching is kinetically reduced by the unstable fixed point separating the stable ones. In the bimodal region, the binding of a single tether does not reduce the distance sufficiently to induce rebinding of further bonds and the formation of a stable cluster. The analysis of the first passage times and showed that the time the system spends in the bound state matches closely the relative stationary occupancy probability of this state. The time for the actual transition is thus small as has also been demonstrated with simulations of single cluster trajectories.

Initiation of the binding process, especially in the bimodal region, is very much dependent on extreme events where the tether springs are stretched to a multiple of their rest length. Replacing the infinitely extensible harmonic springs by the more realistic worm-like chain model for biopolymers with finite extensibility showed that the basic results for harmonic springs are conserved. A region with a bimodal probability distribution can be observed for receptor-ligand distances close to the maximal extension of the tethers. This region corresponds to the bistable region in the deterministic description. These regions are not bounded for large receptor-ligand distances (apart from the hard limit of the contour length of the polymers) because of diverging force of the tethers which extend the harmonic transducer strongly and induce further binding. The probability for the initial binding step, on the other hand vanishes for distances close to the contour length and the occupancy of the bound state vanishes.

The discussion of the limits for soft and stiff transducer showed that the soft transducer can still, due to the fluctuations of the transducer position itself, support the non-linear behaviour observed in the case of general stiffnesses of tether and transducer springs. For the stiff transducer, on the other hand, the feedback mechanism is fully lost because the force of the tethers does not suffice to reduce the distance of the transducer. This limit is the relevant limit for comparison with experiments on the surface forces apparatus as in Wong et al. [1997], Jeppesen et al. [2001]. Also in the theoretical studies of Moreira et al. [2003], Moreira and Marques [2004], the distance of the transducer was assumed to be fixed or moved at a constant velocity but independent of the number of bound tethers. The stochastic description in the master equation framework allowed to include the dependence of the distance on the number of bonds. Although a number of assumption were necessary, we expect that the instabilities could also be observed in an experimental system if sufficiently soft transducers are available. The binding probability of adhesion clusters then depends critically on the initial distance between tethers and transducer. Too large distances prevent formation of stable clusters completely. At small distances large, stable adhesions are readily formed. In the bistable region, the systems switches rapidly between bound and unbound state and the probability to find a bound cluster in one instance, is given by the relative occupancy in the bound state. In the context of cell adhesion small, initial adhesions might be formed and destructed frequently in the bimodal region. This would allow cells to probe a surface for favourable binding conditions. Once an appropriate binding site is found, the cell surface might yield and the distance is reduced so that stable adhesions form.

Appendices

Appendix A

Generating function

A.1 Generating function technique

A standard method to solve linear one-step master equations is the use of a generating function. This method is very successful for master equations with constant or linear transition rates and natural boundaries. Processes with artificial boundaries or non-linear rates are in general not solved this way.

The probability generating function of a distribution $\{p_i(t)\}_{i=-\infty}^{\infty}$ is defined as

$$G(s,t) := \sum_{i=-\infty}^{\infty} s^i p_i(t)\,. \tag{A.1}$$

For a one-step master equation with general forward rates $g(i)$ and reverse rates $r(i)$, the generating function satisfies the partial differential equation

$$\frac{\partial}{\partial t}G(s,t) = (s-1)g\left(s\frac{\partial}{\partial s}\right)G(s,t) + \left(\frac{1}{s}-1\right)r\left(s\frac{\partial}{\partial s}\right)G(s,t)\,, \tag{A.2}$$

in which the transition rates are formally written as a Taylor series in their argument $s(\partial/\partial s)$. Normalisation of the probability distribution and the initial condition $p_i(t=0) = \delta_{i,N_0}$ imply boundary and initial conditions for the generating function,

$$G(s,t)|_{s=1} = \sum_{i=-\infty}^{\infty} p_i(t) = 1 \quad \text{and} \quad G(s,t)|_{t=0} = s^{N_0}\,. \tag{A.3}$$

Moreover, we have

$$G(s,t)|_{s=0} = p_0(t)\,. \tag{A.4}$$

Solutions for (A.2) have been found for a number master equations, especially for random walks with constant transition rates and for linear master equations. Solutions for systems relevant in chemical and biological physics can be found, for example, in McQuarrie [1963], Goel and Richter-Dyn [1974].

The probability distribution functions are the coefficients of the polynomial $G(s,t)$. Once the generating function is known, the p_i are obtained immediately as derivatives of G:

$$p_i(t) = \frac{1}{i!}\,\frac{\partial^i}{\partial s^i}G(s,t)\bigg|_{s=0} \quad \text{for } i \geqslant 0 \text{ and} \quad p_i(t) = \frac{1}{i!}\,\frac{\partial^i}{\partial (1/s)^i}G(s,t)\bigg|_{\frac{1}{s}=0} \quad \text{for } i < 0\,. \tag{A.5}$$

The moments of the distribution can be calculated from the probability distribution but the generating function allows a more direct access. The n^{th} moment μ_n is given by the logarithmic derivative of G with respect to s:

$$\mu_n(t) = \frac{\partial^n}{\partial(\ln s)^n} G(s,t)\bigg|_{s=1} = \left[\left(s\frac{\partial}{\partial s}\right)^n G(s,t)\right]_{s=1} . \tag{A.6}$$

In particular, the average $N = \mu_1$ and the variance $\sigma_i^2 = \mu_2 - \mu_1^2$ are given by the first and second derivatives as

$$\begin{aligned} N(t) &= \mu_1(t) = \frac{\partial}{\partial s} G(s,t)\bigg|_{s=1} \\ \sigma_i^2(t) &= \mu_2(t) - \mu_1^2(t) = \frac{\partial}{\partial s} G(s,t)\bigg|_{s=1} + \frac{\partial^2}{\partial s^2} G(s,t)\bigg|_{s=1} - \left[\frac{\partial}{\partial s} G(s,t)\bigg|_{s=1}\right]^2 . \end{aligned} \tag{A.7}$$

With the two relations (A.5) and (A.6), knowledge of the generating function provides a complete solution of the master equation.

A.2 Application to adhesion cluster evolution for vanishing force

In Chapter 3 we use the solutions of the master equation for vanishing force, that is, of the linear one-step master equation

$$\frac{d}{dt} p_i = (i+1)p_{i+1} + \gamma(N_t - i + 1)p_{i-1} - \{i + \gamma(N_t - i)\}\, p_i \,. \tag{A.8}$$

with the transition rates $g(i) = \gamma(N_t - i)$ and $r(i) = i$. The master equation is defined for the finite set of states $0 \leqslant i \leqslant N_t$ but natural boundaries allow to treat the system as unrestricted and the partial differential equation for the generating function is given by

$$\frac{\partial}{\partial t} G(s,t) = \gamma N_t (s-1) G(s,t) - \left\{1 + \gamma(s-1) - \frac{1}{s}\right\} s \frac{\partial}{\partial s} G(s,t) \,. \tag{A.9}$$

The solution, with boundary and initial condition (A.3) for a general $0 \leqslant N_0 \leqslant N_t$, is given by [Goel and Richter-Dyn, 1974]

$$G_{N_0}(t,s) = \frac{\left[1 - e^{-(1+\gamma)t} + s\left(\gamma + e^{-(1+\gamma)t}\right)\right]^{N_0} \left[1 + \gamma e^{-(1+\gamma)t} + s\gamma\left(1 - e^{-(1+\gamma)t}\right)\right]^{N_t - N_0}}{(1+\gamma)^{N_t}} . \tag{A.10}$$

With relation (A.5) the general expression for the probability distribution follows as

$$\begin{aligned} p_i(t) = \left[\frac{1 + \gamma e^{-(1+\gamma)t}}{1+\gamma}\right]^{N_t} \sum_{k=0}^{\min\{N_0, i\}} & \frac{\gamma^{i-k}(N_t - N_0)!}{(i-k)!(N_t - N_0 - i + k)!} \cdot \\ & \times \binom{N_0}{k} \left[\frac{\gamma + e^{-(1+\gamma)t}}{1 - e^{-(1+\gamma)t}}\right]^k \left[\frac{1 - e^{-(1+\gamma)t}}{1 + \gamma e^{-(1+\gamma)t}}\right]^{N_0 + i - k} . \end{aligned} \tag{A.11}$$

The factorial $(N_t - N_0 - i + k)!$ in the denominator is 1 whenever the argument is negative. The stationary state of this distribution is independent of the initial condition. It is given by the binomial distribution

$$p_i(\infty) := \lim_{t\to\infty} p_i(t) = \binom{N_t}{i} \frac{\gamma^i}{(1+\gamma)^{N_t}} \,. \tag{A.12}$$

For $\gamma = 1$, this distribution is symmetric around the mean $N_t/2$.

The average and the variance of this distribution $\{p_i(t)\}_{i=0}^{N_t}$ in (A.11) are calculated from the generating function (A.10) using relation (A.6). The results are also listed in Goel and Richter-Dyn [1974]. For $N(0) = N_0$, the average is given by

$$N(t) = (N_0 - N_{eq})e^{-(1+\gamma)t} + N_{eq}\,, \tag{A.13}$$

where

$$N_{eq} := \lim_{t\to\infty} N(t) = \gamma N_t/(1+\gamma) \tag{A.14}$$

is the steady state value of the average number of closed bonds. To calculate the variance, also the second moment of (A.11) is needed, that is,

$$\mu_2 = \langle i^2\rangle = \frac{\partial^2}{\partial s^2}G(s,t)\bigg|_{s=1} + \frac{\partial}{\partial s}G(s,t)\bigg|_{s=1}\,, \tag{A.15}$$

and the variance is given by

$$\begin{aligned}\sigma_N^2 &= \frac{1+\gamma e^{-(1+\gamma)t}}{1+\gamma}N(t) - \frac{\gamma + e^{-(1+\gamma)t}}{1+\gamma}N_0 e^{-(1+\gamma)t} \\ &= \frac{1}{1+\gamma}\left\{N_{eq}\left(1-e^{-2(1+\gamma)t}\right) + (1-\gamma)(N_0-N_{eq})e^{-(1+\gamma)t}\left(1-e^{-(1+\gamma)t}\right)\right\}\,.\end{aligned} \tag{A.16}$$

The value of the variance in the stationary state scales linearly with cluster size $N_{eq} \propto N_t$

$$\sigma_N^2(\infty) := \lim_{t\to\infty}\sigma_N^2(t) = \frac{N_{eq}}{1+\gamma}\,. \tag{A.17}$$

The mean square deviation σ_N^2/N^2 thus scales as $1/N_{eq}(1+\gamma) = 1/\gamma N_t$ with rebinding rate and cluster size. A rebinding rate $\gamma > 1$ thus decreases the the width of the distribution.

A.3 Specific initial conditions

In Chapter 3 we use the distribution functions for the initial conditions $N_0 = N_t$ and $N_0 = 0$. For these choices the general expressions shorten considerably. For the initial condition $N_0 = N_t$, the generating function is

$$G_{N_t}(t,s) = \left[\frac{1-e^{-(1+\gamma)t} + s\left(\gamma + e^{-(1+\gamma)t}\right)}{1+\gamma}\right]^{N_t}\,. \tag{A.18}$$

The probability functions then take form of a time dependent binomial distribution

$$p_i(t) = \binom{N_t}{i}\frac{\left[\gamma + e^{-(1+\gamma)t}\right]^i\left[1-e^{-(1+\gamma)t}\right]^{N_t-i}}{(1+\gamma)^{N_t}}\,. \tag{A.19}$$

The average number of closed bonds in this distribution also follows the exponential decrease

$$N(t) = \frac{N_t}{1+\gamma}e^{-(1+\gamma)t} + N_{eq} = \frac{\gamma + e^{-(1+\gamma)t}}{1+\gamma}N_t\,. \tag{A.20}$$

The variance for $N_0 = N_t$ is

$$\sigma_N^2(t) = \frac{\gamma + e^{-(1+\gamma)t}}{1+\gamma} N_t \frac{1 - e^{-(1+\gamma)t}}{1+\gamma} = \frac{1}{1+\gamma} N(t) \left(1 - e^{-(1+\gamma)t}\right) . \tag{A.21}$$

For the initial condition $N_0 = 0$, the generating function is

$$G_0(t,s) = \left[\frac{1 + \gamma e^{-(1+\gamma)t} + s\gamma \left(1 - e^{-(1+\gamma)t}\right)}{1+\gamma} \right]^{N_t} \tag{A.22}$$

and the probability functions are given by

$$p_i(t) = \binom{N_t}{i} \frac{\gamma^i \left[1 - e^{-(1+\gamma)t}\right]^i \left[1 + \gamma e^{-(1+\gamma)t}\right]^{N_t - i}}{(1+\gamma)^{N_t}} . \tag{A.23}$$

If $\gamma = 1$, this distribution is identical to the one for $N_0 = N_t$ when the functions for i and $N_t - i$ are exchanged. The average

$$N(t) = N_{eq}(1 - e^{-(1+\gamma)t}) \tag{A.24}$$

increases exponentially towards the steady state. The variance also increases from zero towards the steady state. It is given by

$$\sigma_N^2(t) = \frac{1 + \gamma e^{-(1+\gamma)t}}{1+\gamma} N_{eq} \left(1 - e^{-(1+\gamma)t}\right) = \frac{1 + \gamma e^{-(1+\gamma)t}}{1+\gamma} N(t) . \tag{A.25}$$

A.4 Vanishing rebinding

If the rebinding rate vanishes, $\gamma = 0$, the expressions above become particularly simple. Since new bonds cannot be formed, the only reasonable initial condition is $N_0 = N_t$. In this case, the generating function (A.18) reads

$$G_{N_t}(t,s) = \left[1 - (1-s)e^{-t}\right]^{N_t} . \tag{A.26}$$

The probability distribution (A.19) takes the form of a time dependent binomial distribution:

$$p_i(t) = \binom{N_t}{i} e^{-it} \left[1 - e^{-t}\right]^{N_t - i} . \tag{A.27}$$

The average number of closed bonds shows an exponential decrease

$$N(t) = N_t e^{-t} \tag{A.28}$$

with constant rate from the initial number of closed bonds. The binomial distribution is the stochastic version of this 'radioactive decay'. The variance is given by

$$\sigma_N^2(t) = N(t)(1 - e^{-t}) = N_t e^{-t}(1 - e^{-t}) . \tag{A.29}$$

As the average it is linear in the total system size N_t. The relative mean square deviation σ_N^2/N^2 thus decreases as $1/N_t$. Because on the long time limit, the variance and the average decay in the same time-scale $\tau_r = 1$, the relative mean square deviation diverges for large times as $\sigma_N^2/N^2 \sim e^t$.

Appendix B

Gillespie algorithm

B.1 Basic idea of the algorithm

The Gillespie algorithm [Gillespie, 1976, 1977] is used for solving master equations with Monte Carlo methods. In Monte Carlo simulations of systems that follow a master equation, a large number of stochastic trajectories through the set of states has to be generated and cumulated into a histogram which is used as an approximation for the probability distribution. This way to generate stochastic trajectories was actually among the earliest applications of the Monte Carlo method [Metropolis and Ulam, 1949]. Depending on the properties of the master equation and the quantities one is interested in, the number of trajectories needed may be very large. For the system we have discussed, it is in the range of $10^4 \dots 10^7$. Therefore it is important to use an efficient algorithm to generate these trajectories which is provided by the Gillespie algorithm.

One standard way to generate the trajectories is to iterate the system by a discrete, finite time-step Δt and decide at each step whether one of the possible transitions takes place or if the system stays in the same state. This means, the probabilities on the right hand side of the Chapman-Kolmogorov equation (2.23) have to be calculated and the transition is selected randomly using this distribution. This procedure introduces an inaccuracy due to the finiteness of the time-step. To keep this small, the time-step has to be made small. This, on the other hand, can render the generation of the trajectories inefficient because during many time-steps, the state of the system may not change while the transition rates and random numbers have to be calculated anew in every time-step. The Gillespie algorithm takes a different approach. To avoid unnecessary computation of the transition rates in times where the system is idle, the distribution waiting times – the times between two subsequent changes of the state of the system – is applied. The waiting time distribution depends on the current state of the system and the transition rates (which may themselves be time-dependent). The Gillespie algorithm draws waiting times at random from the exact waiting time distribution and decides then, which of the reactions will take place.

In this way the time-steps are large if the system is relatively idle and unnecessary computations are avoided, while in situations where many reactions occur small steps are taken and inaccuracies due to the finite time-step are avoided. In this sense, the Gillespie algorithm is exact for the generation of the trajectories. The only source of inaccuracy lies in the finite number of trajectories and in the choice of the random number generator which are common to all Monte Carlo methods, in particular the iterative procedure. That method, however, has the advantage that it is more generally applicable, in particular for time dependent rates. As we will see in the following, the Gillespie algorithm might not be applicable for general time dependent rates without additional computational effort. Moreover,

the iterative algorithm requires a single random number per step, the Gillespie algorithm needs at least two. Nevertheless, it is an efficient and exact algorithm for stochastic simulations.

The Gillespie algorithm was originally derived for chemical reactions [Gillespie, 1977]. These occur randomly with constant transition rates which depend on the concentrations of the molecules converted in the reactions. In the following, we derive the waiting time distribution for a system in which a certain number M of reactions take place stochastically in parallel with general, time dependent transitions rates. Then, we describe the actual implementation of the algorithm for which two different flavours exist. We apply the algorithm to adhesion cluster dynamics in which two different reactions (rupture and rebinding) are possible with the rates given by (2.22) and give expressions for shared and non-collective loading in the cases of constant and linearly increasing force.

B.2 Waiting time distribution

For a stochastic reaction in isolation which takes place with a reaction rate $\alpha_\mu(t)$, we denote by $p_\mu^0(t)$ the probability that a reaction has *not* occurred up to time t, when the system entered the state χ at time t_0. Both functions depend on χ and $p_\mu^0(t)$ will also depend on the time t_0 but we will drop these dependences in the notation. It will always be assumed that the system is initially in state χ and the initial time is t_0. This probability decreases with the rate $\alpha_\mu(t)$ so that $p_\mu^0(t)$ is determined by the differential equation

$$\frac{d}{dt}p_\mu^0(t) = -\alpha_\mu(t)p_\mu^0(t)\,. \tag{B.1}$$

The initial condition for the probability is $p_\mu^0(t_0) = 1$ and (B.1) is solved by

$$p_\mu^0(t) = e^{-\int_{t_0}^t \alpha_\mu(t')\,dt'}\,. \tag{B.2}$$

The probability that the system stays in state χ during the interval $[t_0, t]$ decreases exponentially with the integral of the transition rate. The probability density, $w_\mu(t, t_0)$, that the next reaction occurs at time t and the time interval between two subsequent reactions is $t - t_0$, is the negative derivative of $p_\mu^0(t)$. With the right hand side of (B.1), it reads

$$w_\mu(t, t_0) = \alpha_\mu(t)p_\mu^0(t) = \alpha_\mu(t)e^{-\int_{t_0}^t \alpha_\mu(t')\,dt'}\,. \tag{B.3}$$

This is the distribution of waiting times between two subsequent reactions if only a single type of transition is possible.

If M different reactions can occur simultaneously, the probability $P_0(t)$ that neither of these occurred between in the time interval $[t_0, t]$ is the product

$$P_0(t) = \prod_{\mu=1}^{M} p_\mu^0(t) = e^{-\int_{t_0}^t \left\{\sum_{\mu=1}^M \alpha_\mu(t')\right\} dt'} \tag{B.4}$$

over the $p_\mu^0(t)$ for the single reactions. This expression does not assume independence of the reactions because, as long as no transition occurs, all reactions have identical initial conditions. From (B.4) it follows that the probability $P_0(t)$ satisfies the differential equation

$$\frac{d}{dt}P_0(t) = -\left\{\sum_{\mu=1}^{M}\alpha_\mu(t)\right\}P_0(t)\,. \tag{B.5}$$

It expresses that the state χ can be left through M parallel pathways with the reaction rates $\alpha_\mu(t)$. The right hand side of the differential equation (B.5) with P_0 from (B.4) gives the waiting time distribution $W(t, t_0)$ for M parallel transitions. It is

$$W(t, t_0) = \left\{ \sum_{\mu=1}^{M} \alpha_\mu(t) \right\} e^{-\int_{t_0}^{t} \left\{ \sum_{\mu=1}^{M} \alpha_\mu(t') \right\} dt'} . \tag{B.6}$$

It determines the probability distribution for the waiting times without specifying which reaction takes place. The probability q_μ that reaction μ occurs under the condition that the time of the transition is t, is given by the weight (the relative strength of the unbinding pathway) of the rate $\alpha_\mu(t)$ at time t, i.e.,

$$q_\mu(t) = \frac{\alpha_\mu(t)}{\sum_{\nu=1}^{M} \alpha_\nu(t)} . \tag{B.7}$$

It only depends on the time t of the reaction, because the history is contained in the integral over the rates in the exponential in the waiting time distribution (B.6). In the Gillespie algorithm, the type of the reaction thus has to be determined after the time of the reaction is determined.

B.3 Implementation

B.3.1 Gillespie's direct method

There are two different implementations of the Gillespie algorithm. The 'direct method' uses the full waiting time distribution (B.6) for M parallel reactions to determine the time between two subsequent reactions. Once this time is fixed, the type of reaction is selected according to the distribution (B.7).

Drawing waiting times To generate random numbers with the waiting time distribution (B.6), a transformation from uniformly distributed numbers, generated with a standard random number generator, is used. The transformation uses the 'cumulative' waiting time distribution

$$F(t) = \int_{t_0}^{t} W(t', t_0)\, dt' \tag{B.8}$$

which is the probability that at least one reaction takes place in the interval $[t_0, t]$. It is a strictly monotonic increasing function in t that can be inverted for $F^{-1}(p)$. This yields the time $t = F^{-1}(p)$ after which a reaction has occurred with probability p. For the waiting time distribution $W(t, t_0)$ in (B.6), the integral F is readily calculated since $W(t, t_0) = -\dot{P}_0(t)$, so that

$$F(t) = -\int_{t_0}^{t} \dot{P}_0(t')\, t' = -\left. P_0(t') \right|_{t'=t_0}^{t'=t} = P_0(t_0) - P_0(t) . \tag{B.9}$$

Since $P_0(t_0) = 1$,

$$F(t) = 1 - P_0(t) = 1 - e^{-\int_{t_0}^{t} \left\{ \sum_{\mu=1}^{M} \alpha_\mu(t') \right\} t'} . \tag{B.10}$$

Next, a uniformly distributed random number ξ is drawn from the range of probabilities $(0, 1)$ and inserted into $F^{-1}(\xi)$. This yields the random time at which the probability for the a reaction has reached ξ. An interval $\Delta\xi$ around ξ is transformed to an interval Δt around t with the weight

$$\Delta t = \left. \frac{d}{dp} F^{-1}(p) \right|_{p=\xi} \Delta\xi = \frac{\Delta\xi}{\left. \frac{d}{dt'} F(t') \right|_{t'=t}} \tag{B.11}$$

which leads to

$$\lim_{\Delta\xi\to 0}\frac{\Delta\xi}{\Delta t} = \frac{d}{dt'}F(t')\bigg|_{t'=t} = W(t,t_0)\,. \tag{B.12}$$

Thus, the uniform distribution of ξ on $(0,1)$ is transformed into the waiting time distribution (B.6) for $F^{-1}(\xi)$ [Gillespie, 1976, Allen and Tildesley, 1987]. We denote the random number by $1-\xi$ and write for the waiting time τ between two subsequent reactions:

$$\tau := t - t_0 = F^{-1}(1-\xi) - t_0\,. \tag{B.13}$$

The random number $1-\xi$ has the same distribution over the same interval as ξ and therfore yields the same distribution for τ. The time $F^{-1}(1-\xi)$ is the absolute time at which the transition takes place.

The crucial step in this procedure is the inversion of F. With (B.10) for F, one has to solve

$$-\ln\xi = \int_{t_0}^{t}\left\{\sum_{\mu=1}^{M}\alpha_\mu(t')\right\}dt' \tag{B.14}$$

for t. For constant rates, the right hand side is linear in $\tau = t - t_0$,

$$-\ln\xi = (t-t_0)\sum_{\mu=1}^{M}\alpha_\mu\,, \tag{B.15}$$

and the waiting time is given by

$$\tau = F^{-1}(\xi) - t_0 = -\frac{\ln\xi}{\sum_{\mu=1}^{M}\alpha_\mu}\,. \tag{B.16}$$

For time dependent rates, however, the inversion is not necessarily possible analytically. In these cases one can still implement the inversion numerically but this will reduce the efficiency of the algorithm. Another possible way to get around this difficulty is to use the next reaction method described in the next subsection which does not use the full distribution but only utilises the waiting time distribution for the single transitions in isolation.

Selecting the reaction type The reaction type μ is chosen after the waiting time has been determined with the conditional probability $q_\mu(t)$ from (B.7). To determine the type of reaction, the sum over the rates,

$$\alpha(t) := \sum_{\mu=1}^{M}\alpha_\mu(t)\,, \tag{B.17}$$

is calculated and a second random number ζ with a uniform distribution is drawn from the interval $[0,\alpha(t)]$. The reaction type μ is the one for which the random number is between

$$\alpha_{\mu-1} < \zeta \leqslant \alpha_\mu\,, \tag{B.18}$$

where $\alpha_0 = 0$ is assumed. This yields the correct distribution for the types.

B.3.2 Next-reaction method

The 'next reaction method' of the Gillespie algorithm does not use the full waiting time distribution (B.6) to determine the waiting time of the system. Instead, M waiting times $\tau_\mu = t_\mu - t_0$ – one for each of the reactions μ – are drawn from the distributions $w_\mu(t, t_0)$ in (B.3). Thereafter, the type of reaction is determined as the one with the shortest waiting time which is then chosen as the waiting time for the system.

The waiting times τ_μ are chosen in the same way as in the direct method. We have to calculate cumulative probability

$$F_\mu(t) = \int_{t_0}^{t} w_\mu(t', t_0)\, dt' = 1 - p_\mu^0(t) = 1 - e^{-\int_{t_0}^{t} \alpha_\mu\, dt'} \tag{B.19}$$

that at least one reaction of type μ takes place in the interval $[t_0, t]$ under the condition that all other reactions are impossible. Waiting times are determined by drawing M random numbers ξ_μ from a uniform distribution on the interval $(0, 1)$ which are inserted into the inverse $F_\mu^{-1}(1 - \xi_\mu)$ so that the waiting times are

$$\tau_\mu = F_\mu^{-1}(1 - \xi_\mu) - t_0\,. \tag{B.20}$$

The type of reaction is chosen as the one with the shortest waiting time, i.e., $\tau := \min_\mu\{\tau_\mu\}$. The inversion of the F_μ is slightly easier than for the direct method because one has to solve

$$-\ln \xi_\mu = \int_{t_0}^{t} \alpha_\mu(t')\, dt' \tag{B.21}$$

for t. For a constant rate the expression for the waiting time is

$$\tau_\mu = F_\mu^{-1}(1 - \xi_\mu) - t_0 = -\frac{\ln \xi_\mu}{a_\mu}\,. \tag{B.22}$$

When not all rates depend on time, this implementation of the Gillespie algorithm allows to calculate the waiting times with the simple rule (B.22) for the constant rates and use more complex expression or numerical inversion of F only for the time dependent rates.

The next reaction method generates the correct waiting time distribution $W(t, t_0)$ for the whole system. The probability $\omega_\nu(\tau)$ that the waiting time τ is selected for the reaction ν, is the the product of $w_\nu(t, t_0)$, the probability that reaction ν generates this waiting time, and the probability that all other times are larger than this time, i.e.,

$$\begin{aligned}\omega_\nu(\tau) = w_\nu(t, t_0) \prod_{\mu\neq\nu} \{1 - F_\mu(t)\} = w_\nu(t, t_0) \prod_{\mu\neq\nu} p_\mu^0(t) = \\ = \alpha_\nu(t) p_\nu^0(t) \prod_{\mu\neq\nu} p_\mu^0(t) = \alpha_\nu(t) \prod_{\mu=1}^{M} p_\mu^0(t) = \alpha_\nu(t) P_0(t)\,.\end{aligned} \tag{B.23}$$

The complete waiting time distribution is the sum over all these $\omega_\nu(t)$ since any of the M reaction might take place at time t. The waiting time distribution in the next reaction method is thus given by

$$\sum_{\nu=1}^{M} \omega_\nu(t) = \left\{ \sum_{\nu=1}^{M} \alpha_\nu(t) \right\} P_0(t) = W(t, t_0) \tag{B.24}$$

which is exactly the result (B.6) for the waiting time distribution of the whole system.

The next-reaction method requires to draw one random number for each of the M reactions. For large numbers of reactions it might therefore become less efficient than the direct method which requires only two random numbers, independent of the number of reactions. On the other hand, the calculation of the waiting times from the random numbers may be easier for the next-reaction method. Moreover, refined implementations of the next-reaction method have been derived [Gibson and Bruck, 2000] which allow to re-use the waiting times and thus increase efficiency. In the application to adhesion cluster dynamics we deal with only two different reactions and we prefer the next-reaction method.

B.4 Application to adhesion cluster dynamics

The dynamics of adhesion clusters is described by the one-step master equation (2.24). There are $M = 2$ different reaction, namely the unbinding and rebinding transition of a single bond in the cluster. The state of the cluster is determined by the number of closed bonds, i. Unbinding occurs with the reverse rate $r(i)$ and decreases i by one to $i-1$; rebinding occurs with the forward rate $g(i)$ and increases i to $i+1$. The forward and the reverse rates for adhesion cluster dynamics are

$$g(i) = \gamma(N_t - i) \quad \text{and} \quad r(i) = ie^{f(i)}\,, \tag{B.25}$$

where $f(i)$ is the force per bond which may depend on the number of closed bonds in the cluster.

In the simulations presented in the text, we use the next reaction version of the Gillespie algorithm. In the following, the explicit expressions for the generation of waiting times for unbinding and rebinding are collected. Thereby, we have to distinguish between constant loading, in which both rates are constant, and linear loading where the reverse rate is time dependent while the forward rate is still a constant.

B.4.1 Constant loading

For constant loading, the transition rates are also constant and expressions (B.22) can be applied to determine the waiting times. They are

$$\tau_- = -\frac{\ln \xi_1}{r(i)} \quad \text{and} \quad \tau_+ = -\frac{\ln \xi_2}{g(i)}\,, \tag{B.26}$$

for unbinding and rebinding, respectively. Both random numbers $\xi_{1,2}$ are uniformly distributed on $(0,1)$. If $\tau_- \leqslant \tau_+$, the waiting time is τ_-, a closed bond unbinds and a transition $i \to i-1$ takes place. If $\tau_+ < \tau_-$ the waiting time is τ_+, an open bond rebinds and the transition $i \to i+1$ occurs.

For the case of shared loading, the force per bond is $f(i) = f/i$ and the random waiting times for unbinding and binding are determined by

$$\tau_- = -\frac{\ln \xi_1}{ie^{f/i}} \quad \text{and} \quad \tau_+ = -\frac{\ln \xi_2}{\gamma(N_t - i)}\,, \tag{B.27}$$

respectively. For non-cooperative loading, the force per bond is the parameter of the system and $f(i) = f$ is independent of i. The waiting times are determined by

$$\tau_- = -\frac{\ln \xi_1}{ie^{f}} \quad \text{and} \quad \tau_+ = -\frac{\ln \xi_2}{\gamma(N_t - i)}\,. \tag{B.28}$$

In both expressions, the denominator depends linearly on the number of closed bonds.

B.4.2 Linear loading

For linear loading, the force per bond increases linearly in time, $f(i) = \mu(i)t$, where $\mu(i)$ is the constant loading rate per closed bond. The rupture rate $r(i) = ie^{\mu(i)t}$ increases exponentially with time. The time integral over the reverse rate is

$$\int_{t_0}^{t} r(i)\,dt' = i\int_{t_0}^{t} e^{\mu(i)t'}\,dt' = \left.\frac{ie^{\mu(i)t'}}{\mu(i)}\right|_{t_0}^{t} = \frac{ie^{\mu(i)t_0}}{\mu(i)}\left\{e^{\mu(i)(t-t_0)} - 1\right\}. \tag{B.29}$$

Determining the waiting times requires inversion of the cumulative probability

$$F(t) = 1 - \exp\left(\frac{ie^{\mu(i)t_0}}{\mu(i)}\left\{1 - e^{\frac{\mu(i)(t-t_0)}{i}}\right\}\right). \tag{B.30}$$

The inverse of $F(t)$ is given by

$$F^{-1}(1-\xi_1) - t_0 = \frac{1}{\mu(i)}\ln\left(1 - \frac{\mu(i)}{ie^{\mu(i)t_0}}\ln\xi\right). \tag{B.31}$$

It depends on the loading rate per bond $\mu(i)$ and the rupture rate at time t_0 of the last transition.

The waiting times for rupture and rebinding are thus determined in the following way. Two random numbers ξ_1 and ξ_2 uniformly distributed on the interval $(0, 1)$ are generated and inserted in the expressions for the waiting times,

$$\tau_- = F^{-1}(\xi_1) - t_0 = \frac{1}{\mu(i)}\ln\left(1 - \frac{\mu(i)}{ie^{\mu(i)t_0}}\ln\xi_1\right) \quad \text{and} \quad \tau_+ = F^{-1}(\xi_2) - t_0 = \frac{\ln\xi_2}{g(i)}. \tag{B.32}$$

As before, the actual transition is chosen as the one with the shortest transition time.

For shared loading the loading rate per bond is $\mu(i) = \mu/i$ so that the expressions for the waiting times become

$$\tau_- = F^{-1}(\xi_1) - t_0 = \frac{i}{\mu}\ln\left(1 - \frac{\mu/i}{ie^{\mu t_0/i}}\ln\xi_1\right) \quad \text{and} \quad \tau_+ = F^{-1}(\xi_2) - t_0 = \frac{\ln\xi_2}{\gamma(N_t - i)}. \tag{B.33}$$

For non-cooperative loading the loading rate per bond is replaced by μ itself and the waiting times are determined by

$$\tau_- = F^{-1}(\xi_1) - t_0 = \frac{1}{\mu}\ln\left(1 - \frac{\mu}{ie^{\mu t_0}}\ln\xi_1\right) \quad \text{and} \quad \tau_+ = F^{-1}(\xi_2) - t_0 = \frac{\ln\xi_2}{\gamma(N_t - i)} \tag{B.34}$$

for unbinding and rebinding, respectively.

Appendix C

Solution of a three state one-step master equation with constant rates

For small adhesion clusters with only a few molecular bonds, the master equation (2.24) can be solved in a closed analytical form for general, constant transition rates. In Chapter 3 we derived a solution for the two bond cluster ($N_t = 2$) under constant shared loading with an absorbing boundary. The transition rates were given by (2.25) for $i = 1, 2$ and $r_0 = 0$ and $g_0 = 0$. In the following, we give a detailed derivation of the general solution of a one-step master equation with three state for arbitrary transition rates and boundary conditions. The extension of this method to larger clusters is straightforward in principle, but the complexity of the solutions make numerical methods more preferable.

C.1 Matrix notation and eigenvector expansion

To solve the master equation (2.24) for constant transition rates we introduce matrix notation. The general one-step master equation for a three state system reads

$$\begin{aligned}
\frac{d}{d\tau}p_0 &= -g_0 p_0 + r_1 p_1 \\
\frac{d}{d\tau}p_1 &= g_0 p_0 - (r_1 + g_1) p_1 + r_2 p_2 \\
\frac{d}{d\tau}p_2 &= g_1 p_1 - r_2 p_2 \,.
\end{aligned} \tag{C.1}$$

The transition rates – g_i are the forward rates for an increase of i and r_i the reverse rate for a decrease in i – can be an arbitrary set of numbers. As a linear differential equation for the probability distribution $\{p_i(\tau)\}_{i=0}^{2}$, a master equation can be written in the form

$$\frac{d}{d\tau}\mathbf{p} = \mathbb{W} \cdot \mathbf{p} \,, \tag{C.2}$$

where the vector $\mathbf{p} := (p_0, p_1, p_2)^\dagger$ contains the probability distribution and the matrix

$$\mathbb{W} = \begin{pmatrix} -g_0 & r_1 & 0 \\ g_0 & -(r_1 + g_1) & r_2 \\ 0 & g_1 & -r_2 \end{pmatrix} \tag{C.3}$$

describes the possible transitions with their respective rates. The formal solution of (C.2) is

$$\mathbf{p}(\tau) = e^{\mathbb{W}\tau} \cdot \mathbf{p_0} \tag{C.4}$$

with the initial state $\mathbf{p_0}$. If the eigenstates of $\mathbb{W}$ are linearly independent, this can be written as an expansion in the eigenvectors,

$$\mathbf{p}(\tau) = \sum_{\lambda} c_\lambda \mathbf{p}_\lambda e^{\lambda\tau} \,. \tag{C.5}$$

The eigenvalues of $\mathbb{W}$ are denoted by λ and $\mathbf{p}_\lambda$ is the eigenstate with eigenvalue λ. The sum runs over all eigenvalues. The coefficients c_λ are determined by the initial condition

$$\mathbf{p_0} = \sum_{\lambda} c_\lambda \mathbf{p}_\lambda \,. \tag{C.6}$$

One eigenvalue of matrices of the type of (C.3) vanishes . The eigenstate belonging to $\lambda_0 = 0$ is the stationary state $\mathbf{p}_{\lambda_0} = \mathbf{p}_\infty$, which is unique for master equations that are not decomposable or of splitting type (in these cases multiple stationary states exist) [van Kampen, 2003]. All other eigenvalues are negative and the eigenstates are transient. Their contribution to the solution $\mathbf{p}(\tau)$ decreases exponentially. The stationary state has to be normalised, that is $\|\mathbf{p}_\infty\|_1 := \sum_i p_i = 1$, to guarantee normalisation of the probability distribution. The transient eigenstates do not contribute to the normalisation and their norm vanishes, $\|\mathbf{p}_{\lambda_i}\|_1 = 0$. The general solution of the master equation (C.1) is thus of the form

$$\mathbf{p}(\tau) = \mathbf{p}_\infty + \sum_{\lambda<0} c_\lambda \mathbf{p}_\lambda e^{\lambda\tau} \,. \tag{C.7}$$

Solving (C.1) amounts to determining the stationary state and the two negative eigenvalues of the $\mathbb{W}-$matrix (C.3) with their respective eigenstates and inserting them in (C.7) with the desired initial condition c_λ determined by (C.6).

C.2 Solutions for eigenstates and eigenvalues

For the master equation (C.2) described by the W-matrix (C.3) the general solution can be found in close analytical form for arbitrary, constant transition rates. The stationary state, the eigenstate of $\mathbb{W}$ with eigenvalue $\lambda_0 = 0$, is given by

$$\mathbf{p}_\infty = \frac{(r_1 r_2, g_0 r_2, g_0 g_1)^\dagger}{g_0(g_1 + r_2) + r_1 r_2} = \frac{1}{\Omega^2 - \omega^2} \begin{pmatrix} r_1 r_2 \\ g_0 r_2 \\ g_0 g_1 \end{pmatrix} \,. \tag{C.8}$$

The abbreviations Ω and ω are defined as

$$\Omega := \frac{1}{2}(g_0 + g_1 + r_1 + r_2) \quad \text{and} \quad \omega := \sqrt{\Omega^2 - (g_0 g_1 + g_0 r_2 + r_1 r_2)} \tag{C.9}$$

so that $\mathbf{p}_\infty$ is normalised. The negative eigenvalues are real and can be written as

$$\lambda_{1,2} = -(\Omega \pm \omega) \,, \tag{C.10}$$

while the corresponding transient eigenstates are

$$\mathbf{p_1} = \frac{1}{\Omega^2 - \omega^2} \begin{pmatrix} \lambda_2 + r_1 + g_0 \\ \lambda_1 + r_2 \\ g_1 \end{pmatrix} \quad \text{and} \quad \mathbf{p_2} = \frac{1}{\Omega^2 - \omega^2} \begin{pmatrix} \lambda_1 + r_1 + g_0 \\ \lambda_2 + r_2 \\ g_1 \end{pmatrix} \,. \tag{C.11}$$

The prefactor has been chosen for convenience. As required, the norm of the transient eigenstates vanishes.

The initial condition $\mathbf{p_0} = (0,0,1)^\dagger$ (that is $p_i(0) = \delta_{i,2}$) imposes the expansion coefficients $c_{\lambda_{1,2}}$ in the general solution (C.7)

$$\begin{aligned} c_1 &= \frac{1}{2g_1\omega}\left\{r_1r_2(\lambda_2+r_2) - r_2g_0(\lambda_1+r_1+g_0)\right\} \\ c_2 &= \frac{1}{2g_1\omega}\left\{r_2g_0(\lambda_2+r_1+g_0) - r_1r_2(\lambda_1+r_2)\right\} . \end{aligned} \tag{C.12}$$

With the form (C.10) of the eigenvalues, the time-dependent solution (C.7) of the master equation can be written as

$$\mathbf{p}(\tau) = \mathbf{p}_\infty + \left\{c_2\mathbf{p}_2 e^{\omega\tau} + c_1\mathbf{p_1}e^{-\omega\tau}\right\} e^{-\Omega\tau} . \tag{C.13}$$

The time-scale for cluster evolution is determined by the two eigenvalues $\lambda_1 = -\Omega-\omega < \lambda_2 = -\Omega+\omega < 0$. Depending on the relative size of Ω and ω, these time-scales may be strongly separated. The short term behaviour is then determined by λ_1 while the long term relaxation to the steady state is determined by λ_2.

Using the abbreviations Ω and ω, the solution for the probability distribution $\{p_i\}_{i=0}^2$ reads

$$p_0(\tau) = \frac{r_1r_2}{\Omega^2-\omega^2}\left\{1 - \left(\cosh(\omega\tau) + \frac{\Omega}{\omega}\sinh(\omega\tau)\right)e^{-\Omega\tau}\right\} \tag{C.14}$$

$$\begin{aligned} p_1(\tau) = {}& \frac{1}{\Omega^2-\omega^2} \\ & \left\{r_2g_0\left[1 - \left(\cosh(\omega\tau) - \frac{\Omega-g_0}{\omega}\sinh(\omega\tau)\right)e^{-\Omega\tau}\right] + r_1r_2\frac{r_2-g_0}{\omega}\sinh(\omega\tau)e^{-\Omega\tau}\right\} \end{aligned} \tag{C.15}$$

$$\begin{aligned} p_2(\tau) = {}& \frac{1}{\Omega^2-\omega^2}\Big\{g_0g_1\left[1 + \left(\frac{r_2}{g_1}\cosh(\omega\tau) - \frac{r_2(\Omega-r_1-g_0)}{g_1\omega}\sinh(\omega\tau)\right)e^{-\Omega\tau}\right] + \\ & + r_1r_2\left(\cosh(\omega\tau) + \frac{\Omega-r_2}{\omega}\sinh(\omega\tau)\right)e^{-\Omega\tau}\Big\} . \end{aligned} \tag{C.16}$$

The different time-scales are now hidden in the hyperbolic terms. The competition between increasing hyperbolic terms and decreasing exponentials eventually leads to an exponential decrease because $\Omega > \omega$. The solution thus approaches the steady state (C.8) exponentially fast.

The average number of closed bonds is

$$\begin{aligned} N(\tau) = \frac{1}{\Omega^2-\omega^2}\Big\{ & g_0(r_2+2g_1) + r_2(2r_1+g_0)\cosh(\omega\tau)e^{-\Omega\tau} + \\ & + \frac{r_2}{\omega}(r_1(r_1+g_1)+g_0(2r_1-g_0))\sinh(\omega\tau)e^{-\Omega\tau}\Big\} . \end{aligned} \tag{C.17}$$

The number of closed bonds reduces from the initial value $N(0) = 2$ to the steady state. As described above and also noted in Sec. 3.1 for vanishing rebinding, the relaxation is not described by a single exponential but, in this case, by two exponential time-scales. In the general case of N_t+1 states, there are N_t different eigenvalues and time-scales. The number of closed bonds in the stationary state is given by

$$N_{eq} = \frac{g_0r_2+2g_0g_1}{\Omega^2-\omega^2} = \frac{g_0(r_2+2g_1)}{r_2(r_1+g_0)+g_0g_1} . \tag{C.18}$$

It vanishes for $g_0 = 0$, that is for an absorbing boundary.

Dissociation rate and average lifetime are not defined for reflecting boundary conditions. The mean first passage time through the detached state and the probability distribution for the first detachment could be calculated from the solution above by Laplace techniques as they were used in Sec. 3.2. However, it is much simpler to calculate the distribution directly with an absorbing boundary in place that is by setting $g_0 = 0$.

C.3 Absorbing boundary

In Sec. 3.4 of Chapter 3 we derived the solutions for an absorbing boundary at $i = 0$. It is implemented by setting the rebinding rate $g_0 = 0$ in the master equation (C.2) or in the $\mathbb{W}$-matrix (C.3). With the general solution presented in this appendix, the special case for an absorbing boundary is achieved by setting $g_0 = 0$ in the above expressions (note that $\Omega^2 - \omega^2 = r_1 r_2$ in this case). The steady state then is $p_i(\infty) = \delta_{i,0}$ and the average number of closed bonds vanishes in the steady state. The dissociation rate is simply obtained as $D(\tau) = r_1 p_1 = \dot{p}_0$ and the average lifetime can be calculated by simple integration. The results are given in Sec. 3.4.

Bibliography

M. Aigner and G. M. Ziegler. *Proofs from THE BOOK*. Springer, Berlin-Heidelberg, 3rd edition, 2004.

B. Alberts, A. Johnson, J. Lewis, M. Raff, K. Roberts, and P. Walter. *Molecular biology of the cell*. Garland Science, New York, 4th edition, 2002.

M. Allen and D. J. Tildesley. *Computer Simulation of Liquids*. Clarendon, Oxford, 2nd edition, 1987.

R. Alon, S. Chen, K. D. Puri, E. B. Finger, and T. A. Springer. The kinetics of L-selectin tethers and the mechanics of selectin-mediated rolling. *Journal of Cell Biology*, 138:1169–1180, 1997.

R. Alon, D. A. Hammer, and T. A. Springer. Lifetime of the P-selection-carbohydrate bond and its response to tensile force in hydrodynamic flow. *Nature*, 374:539–542, 1995.

N. Q. Balaban, U. S. Schwarz, D. Riveline, P. Goichberg, G. Tzur, I. Sabanay, D. Mahalu, S. Safran, A. Bershadsky, L. Addadi, and B. Geiger. Force and focal adhesion assembly: a close relationship studied using elastic micro-patterned substrates. *Nature Cell Biology*, 3:466–472, 2001.

D. Bartolo, I. Derényi, and A. Ajdari. Dynamic response of adhesion complexes: Beyond the single-path picture. *Physical Review E*, 65:051910, 2002.

W. Baumgartner, P. Hinterdorfer, W. Ness, A. Raab, D. Vestweber, H. Schindler, and D. Drenckhahn. Cadherin interaction probed by atomic force microscopy. *Proceedings of the National Academy of Science of the U.S.A.*, 97:4005–4010, 2000.

G. I. Bell. Models for the specific adhesion of cells to cells. *Science*, 200:618–627, 1978.

G. I. Bell, M. Dembo, and P. Bongrand. Cell adhesion competition between nonspecific repulsion and specific bonding. *Biophysical Journal*, 52:1051–1064, 1984.

M. Benoit, D. Gabriel, G. Gerisch, and H. E. Gaub. Discrete interactions in cell adhesion measured by single-molecule force spectroscopy. *Nature Cell Biology*, 2:313–317, 2000.

U. Bockelmann, P. Thomen, B. Essavaz-Roulet, V. Viasnoff, and F. Heslot. Unzipping DNA with optical tweezers: High sequence sensitivity and force flips. *Biophysical Journal*, 82:1537–1553, 2002.

P. Bongrand. Ligand-receptor interactions. *Reports on Progress in Physics*, 62:921–968, 1999.

O. Braun, A. Hanke, and U. Seifert. Probing molecular free energy landscapes by periodic loading. *Physical Review Letters*, 93:158105, 2004.

O. Braun and U. Seifert. Periodically driven stochastic un- and refolding transitions of biopolymers. *Europhysics Letters*, 68:746–752, 2004.

F. Brochard-Wyart and P.-G. de Gennes. Adhesion induced by mobile binders: Dynamics. *Proceedings of the National Academy of Science of the U.S.A.*, 99:7854–7859, 2002.

F. Brochard-Wyart and P.-G. de Gennes. Unbinding of adhesive vesicles. *Comptes Rendus Physique*, 4:281–287, 2003.

G. A. Cecchi and M. O. Magnasco. Negative resistance and rectification in brownian transport. *Physical Review Letters*, 76:1968–1971, 1996.

D. Chandler. *Introduction to Modern Statictical Mechanics*. Oxford University Press, Oxford, 1987.

K.-C. Chang, D. F. J. Tees, and D. A. Hammer. The state diagram for cell adhesion under flow: leukocyte rolling and firm adhesion. *Proceedings of the National Academy of Science of the U.S.A.*, 97:11262–11267, 2000.

S. E. Chesla, P. Selvaraj, and C. Zhu. Measuring two-dimensional receptor-ligand binding kinetics by micropipette. *Biophysical Journal*, 75:1553–1572, 1998.

M. E. Chicurel, C. S. Chen, and D. E. Ingber. Cellular control lies in the balance of forces. *Current Opinion in Cell Biology*, 10:232–239, 1998.

C. Cozens-Roberts, D. Lauffenburger, and J. A. Quinn. Receptor-mediated cell attachment and detachment kinetics: I. probabilistic model and analysis. *Biophysical Journal*, 58:841–856, 1990a.

C. Cozens-Roberts, D. Lauffenburger, and J. A. Quinn. Receptor-mediated cell attachment and detachment kinetics: II. experimental model studies with the radial-flow detachment assay. *Biophysical Journal*, 58:857–872, 1990b.

M. Dembo, D. C. Torney, K. Saxman, and D. Hammer. The reaction limited kinetics of membrane-to-surface adhesion and detachment. *Proceedings of the Royal Society London B*, 234:55–83, 1988.

I. Derényi, D. Bartolo, and A. Ajdari. Effects of intermediate bound states in dynamic force spectroscopy. *Biophysical Journal*, 86:1263–1269, 2004.

M. Doi and S. F. Edwards. *The theory of polymer dynamics*. Clarendon, Oxford, 1986.

O. Dwir, A. Solomon, S. Mangan, G. S. Kansas, U. S. Schwarz, and R. Alon. Avidity enhancement of L-selectin bonds by flow: shear-promoted rotation of leukocytes turn labile bonds into functional tethers. *Journal of Cell Biology*, 163:1–11, 2003.

T. Erdmann and U. S. Schwarz. Adhesion clusters under shared linear loading: a stochastic analysis. *Europhysics Letters*, 66:603–609, 2004a.

T. Erdmann and U. S. Schwarz. Stability of adhesion clusters under constant force. *Physical Review Letters*, 92:108102, 2004b.

T. Erdmann and U. S. Schwarz. Stochastic dynamics of adhesion clusters under shared constant force and with rebinding. *Journal of Chemical Physics*, 121:8997–9017, 2004c.

E. Evans. Probing the relation between force – lifetime – and chemistry in single molecular bonds. *Annual Review of Biophysical Biomolecular Structures*, 30:105–128, 2001.

E. Evans and V. Heinrich. Dynamic strength of fluid membranes. *Comptes Rendus Physique*, 4: 265–274, 2003.

E. Evans, A. Leung, D. Hammer, and S. Simon. Chemically distinct transition states govern rapid dissociation of single L-selectin bonds under force. *Proceedings of the National Academy of Science of the U.S.A.*, 98:3784–3789, 2001.

E. Evans, A. Leung, V. Heinrich, and C. Zhu. Mechanical switching and coupling between two dissociation pathways in a P-selectin adhesion bond. *Proceedings of the National Academy of Science of the U.S.A.*, 101:11281–11286, 2004.

E. Evans and K. Ritchie. Dynamic strength of molecular adhesion bonds. *Biophysical Journal*, 72: 1541–1555, 1997.

E. Evans and K. Ritchie. Strength of a weak bond connecting flexible polymer chains. *Biophysical Journal*, 78:2439–2447, 1999.

A. E. Filipov, J. Klafter, and M. Urbakh. Friction through dynamical formation and rupture of molecular bonds. *Physical Review Letters*, 92:135503, 2004.

E.-L. Florin, V. T. Moy, and H. E. Gaub. Adhesion forces between individual ligand-receptor pairs. *Science*, 264:415–417, 1994.

J. Fritz, A. G. Katopodis, F. Kolbinger, and D. Anselmetti. Force-mediated kinetics of single P-selectin/ligand complexes observed by atomic force microscopy. *Proceedings of the National Academy of Science of the U.S.A.*, 95:12283–12288, 1998.

C. G. Galbraith, K. M. Yamada, and M. P. Sheetz. The relationship between force and focal adhesion development. *Journal of Cell Biology*, 159:695–705, 2002.

M. Gao, H. Lu, and K. Schulten. Simulated refolding of stretched titin immunoglobulin domains. *Biophysical Journal*, 81:2268–2277, 2001.

B. Geiger and A. Bershadsky. Assembly and mechanosensory function of focal contacts. *Current Opinion in Molecular Cell Biology*, 13:564–592, 2001.

B. Geiger, A. Bershadsky, R. Pankov, and K. M. Yamada. Transmembrane extracellular matrix-cytoskeleton crosstalk. *Nature Reviews Molecular Cell Biology*, 2:793–805, 2001.

M. A. Gibson and J. Bruck. Efficient exact stochastic simulation of chemical systems with many species and many channels. *Journal of Physical Chemistry*, 104:1876–1889, 2000.

D. T. Gillespie. A general method for numerically simulating the stochastic time evolution of coupled chemical reactions. *Journal of Computational Physics*, 22:403–434, 1976.

D. T. Gillespie. Exact stochastic simulation of coupled chemical reactions. *Journal of Physical Chemistry*, 81:2340–2361, 1977.

N. S. Goel and N. Richter-Dyn. *Stochastic Models in Biology*. Academic Press, London, 1974.

B. Goldstein and C. Wofsy. Why is it so hard to dissociate multivalent antigens from cell-surface antibodies ? *Immunology Today*, 17:77–80, 1996.

J. Gore, F. Ritort, and C. Bustamante. Bias and error in estimates of equilibrium free-energy differences from nonequilibrium measurements. *Proceedings of the National Academy of Science of the U.S.A.*, 100:12564–12569, 2003.

I. S. Gradshteyn and I. M. Ryzhik. *Table of Integrals, Series, and Products*. Academic Press, New York, 5th edition, 1994.

H. Grubmüller, B. Heymann, and P. Tavan. Ligand binding: Molecular mechanics calculations of the streptavidin-biotin rupture force. *Science*, 271:997–999, 1996.

D. A. Hammer and S. M. Apte. Simulation of cell rolling and adhesion on surfaces in shear flow: general results and analysis of selectin-mediated neutrophil adhesion. *Biophysical Journal*, 63: 35–57, 1992.

D. A. Hammer and D. A. Lauffenburger. A dynamical model for receptor-mediated cell adhesion to surfaces. *Biophysical Journal*, 52:475–487, 1987.

P. Hänggi, P. Talkner, and M. Borkovec. Reaction-rate theory: fifty years after kramers. *Reviews of Modern Physics*, 62:251–341, 1990.

A. K. Harris, P. Wild, and D. Stopak. Silicone rubber substrata: A new wrinkle in the study of cell locomotion. *Science*, 208:177–179, 1980.

B. Heymann and H. Grubmüller. Dynamic force spectroscopy of molecular adhesion bonds. *Physical Review Letters*, 84:6126–6129, 2000.

J. Honerkamp. *Stochastic Dynamical Systems*. VCH Verlagsgesellschaft, Weinheim, 1993.

G. Hummer and A. Szabo. Free energy reconstruction from nonequilibrium single-molecule pulling experiments. *Proceedings of the National Academy of Science of the U.S.A.*, 98:3658–3661, 2001.

R. O. Hynes. Integrins: Bidirectional, allosteric signaling machines. *Cell*, 110:673–687, 2002.

B. Isralewitz, M. Gao, and K. Schulten. Steered molecular dynamics and mechanical functions of proteins. *Current Opinion in Structural Biology*, 11:224–230, 2001.

S. Izrailev, S. Stepaniants, M. Balsera, Y. Oono, and K. Schulten. Molecular dynamics study of unbinding of the avidin-biotin complex. *Biophysical Journal*, 72:1568–1581, 1997.

C. Jarzynski. Equilibrium free-energy differences from nonequilibrium measurements: A master-equation approach. *Physical Review E*, 56:5018–5035, 1997a.

C. Jarzynski. Nonequilibrium equality for free energy differences. *Physical Review Letters*, 78:2690–2693, 1997b.

C. Jeppesen, J. Y. Wong, T. L. Kuhl, J. N. Israelachvili, N. Mullah, S. Zalipsky, and C. M. Marques. Impact of polymer tether length on multiple ligand-receptor bond formation. *Science*, 293:465–468, 2001.

M. S. Z. Kellermayer, S. B. Smith, H. L. Granzier, and C. Bustamante. Folding-unfolding transitions in single titin molecules characterized with laser tweezers. *Science*, 276:1112–1116, 1997.

J. Kierfeld, O. Niamploy, V. Sa-yakanit, and R. Lipowsky. Stretching of semi-flexible polymers with elastic bonds. *European Physical Journal E*, 14:17–34, 2004.

H. A. Kramers. Brownian motion in a field of force. *Physica*, 7:284, 1940.

F. Li, S. D. Redick, H. P. Ericksen, and V. T. Moy. Force measurements of the $\alpha_5\beta_1$ integrin-fibronectin interaction. *Biophysical Journal*, 84:1252–1262, 2003.

J. Liphardt, S. Dumont, S. B. Smith, I. T. Jr., and C. Bustamante. Equilibrium information from nonequilibrium measurements in an experimental test of Jarzynski's equality. *Science*, 296:1832–1835, 2002.

R. Lipowsky. Adhesion of membranes via anchored stickers. *Physical Review Letters*, 77:1652–1655, 1996.

J. F. Marko and E. D. Siggia. Stretching DNA. *Macromolecules*, 28:8759–8770, 1995.

B. T. Marshall, M. Long, J. W. Piper, T. Yago, R. P. McEver, and C. Zhu. Direct observation of catch bonds involving cell-adhesion molecules. *Nature*, 423:190–193, 2003.

P. E. Marszalek, H. Lu, H. Li, M. Carrion-Vazquez, A. F. Oberhauser, K. Schulten, and J. M. Fernandez. Mechanical unfolding intermediates in titin modules. *Nature*, 402:100–103, 1999.

D. A. McQuarrie. Kinetics of small systems I. *J. Chem. Phys.*, 38:433–436, 1963.

R. Merkel. Force spectroscopy on single passive biomolecules and single biomolecular bonds. *Physics Reports*, 346:343–385, 2001.

R. Merkel, P. Nassoy, A. Leung, K. Ritchie, and E. Evans. Energy landscapes of receptor-ligand bonds explored with dynamic force spectroscopy. *Nature*, 397:50–53, 1999.

N. Metropolis and S. Ulam. The monte carlo method. *Journal of the American Statistical Association*, 44:335–341, 1949.

A. G. Moreira, C. Jeppesen, F. Tanaka, and C. M. Marques. Irreversible vs. reversible bridging: When is kinetics relevant for adhesion? *Europhysics Letters*, 62:876–882, 2003.

A. G. Moreira and C. M. Marques. The role of polymer spacers in specific adhesion. *Journal of Chemical Physics*, 120:6229, 2004.

V. T. Moy, E.-L. Florin, and H. E. Gaub. Intermolecular forces and energies between ligands and receptors. *Science*, 266:257–259, 1994.

M. Nguyen-Duong, K. W. Koch, and R. Merkel. Surface anchoring reduces the lifetime of single specific bonds. *Europhysics Letters*, 61:845–851, 2003.

A. Nicolas, B. Geiger, and S. A. Safran. Cell mechanosensitivity controls the anisotropy of focal adhesions. *Proceedings of the National Academy of Science of the U.S.A.*, 101:12520–12525, 2004.

A. Nicolas and S. A. Safran. Cell mechanosensitivity controls the anisotropy of focal adhesions. *Physical Review E*, 69:051902, 2004.

C. E. Orsello, D. A. Lauffenburger, and D. A. Hammer. Molecular properties in cell adhesion: a physical and engineering perspective. *Trends Biotech.*, 19:310–316, 2001.

E. Perret, A.-M. Benoliel, P. Nassoy, A. Pierres, V. Delmas, P. Bongrand, and H. Feracci. Fast dissociation kinetics between individual E-cadherin fragments revealed by flow chamber analysis. *The EMBO Journal*, 21:2537–2546, 2002.

S. Pierrat, F. Brochard-Wyart, and P. Nassoy. Enforced detachment of red blood cells adhering to surfaces: Statistics and dynamics. *Biophysical Journal*, 87:2855–2869, 2004.

K. Prechtel, A. Bausch, V. Marchi-Artzner, M. Kantlehner, H. Kessler, and R. Merkel. Dynamic force spectroscopy to probe adhesion strength of living cells. *Physical Review Letters*, 89:028101, 2002.

W. H. Press, W. T. Vetterling, S. A. Teukolsky, and B. P. Flannery. *Numerical recipes in* $C++$. Cambridge University Press, Cambridge, 2nd edition, 2002.

M. Rief, M. Gautel, F. Oesterhelt, J. M. Fernandez, and H. E. Gaub. Reversible unfolding of individual titin immunoglobulin domains by AFM. *Science*, 276:1109–1112, 1997.

M. Rief and H. Grubmüller. Force spectroscopy of single biomolecules. *CHEMPHYSCHEM*, 3: 255–261, 2002.

D. Riveline, E. Zamir, N. Q. Balaban, U. S. Schwarz, T. Ishizaki, S. Narumiya, B. Geiger, and A. Bershadsky. Focal contacts as mechanosensors: Externally applied local mechanical forces induce growth of focal contacts by an mdia1-dependent and rock-independent mechanism. *Journal of Cell Biology*, 153:1175–1185, 2001.

A. Rohrbach, C. Tischer, D. Neumeyer, and E.-L. Florin. Trapping and tracking a local probe with a photonic force microscope. *Review of Scientific Instruments*, 75:2197–2210, 2004.

H. Rossiter, R. Alon, and T. S. Kupper. Selectins, t-cell rolling and inflammation. *Molecular Medicine Today*, 3:214–222, 1997.

U. S. Schwarz and R. Alon. L-selectin-mediated leukocyte tethering in shear flow is controlled by multiple contacts and cytoskeletal anchorage facilitating fast rebinding events. *Proceedings of the National Academy of Science of the U.S.A.*, 101:6940–6945, 2004.

U. S. Schwarz, N. Q. Balaban, D. Riveline, A. Bershadsky, B. Geiger, and S. A. Safran. Calculation of forces at focal adhesions from elastic substrate data: the effect of localized force and the need for regularization. *Biophysical Journal*, 83:1380–1394, 2002.

U. Seifert. Rupture of multiple parallel molecular bonds under dynamic loading. *Physical Review Letters*, 84:2750–2753, 2000.

U. Seifert. Dynamic strength of adhesion molecules: Role of rebinding and self consistent rates. *Europhysics Letters*, 58:792–798, 2002.

J. C. Shillcock and U. Seifert. Escape from a metastable well under a time-ramped force. *Physical Review E*, 57:7301–7304, 1998.

D. A. Simson, F. Ziemann, M. Strigl, and R. Merkel. Micropipet-based pico force transducer: In depth analysis and experimental verification. *Biophysical Journal*, 74:2080–2088, 1998.

S. B. Smith, L. Finzi, and C. Bustamante. Direct mechanical measurements of the elasticity of single DNA molecules by using magnetic beads. *Science*, 258:1122–1126, 1992.

T. Strunz, K. Oroszlan, I. Schumakovitch, H. J. Güntherodt, and M. Hegner. Model energy landscapes and the force-induced dissociation of ligand-receptor bonds. *Biophysical Journal*, 79:1206–1212, 2000.

J. L. Tan, J. Tien, D. M. Pirone, D. S. Gray, K. Bhadriraju, and C. S. Chen. Cells lying on a bed of microneedles: An approach to isolate mechanical force. *Proceedings of the National Academy of Science of the U.S.A.*, 100:1484–1489, 2003.

D. F. J. Tees, J. T. Woodward, and D. A. Hammer. Reliability theory for receptor-ligand bond dissociation. *Journal of Chemical Physics*, 114:7483–7496, 2001.

N. G. van Kampen. *Stochastic Processes in Physics and Chemistry*. Elsevier, Amsterdam, 2003.

T. R. Weikl, J. T. Groves, and R. Lipowsky. Pattern formation during adhesion of multicomponent membranes. *Europhysics Letters*, 59:916–922, 2002.

T. R. Weikl and R. Lipowsky. Adhesion-induced phase behavior of multicomponent membranes. *Physical Review E*, 64:011903, 2001.

T. R. Weikl, R. R. Netz, and R. Lipowsky. Unbinding transitions and phase separation of multicomponent membranes. *Physical Review E*, 62:R45–R48, 2000.

J. Y. Wong, T. L. Kuhl, J. N. Israelachvili, N. Mullah, and S. Zalipsky. Direct measurement of a tethered ligand receptor interaction potential. *Science*, 275:820–822, 1997.

E. Zamir, M. Katz, Y. Posen, N. Erez, K. M. Yamada, B. Z. Katz, S. Lin, A. Bershadsky, Z. Kam, and B. Geiger. Dynamics and segregation of cell-matrix adhesions in cultured fibroblasts. *Nature Cell Biology*, 2:191–196, 2000.

X. Zhang, E. Wojcikiewicz, and V. T. Moy. Force spectroscopy of the leukocyte function-associated antigen-1/intercellular adhesion molecule-1 interaction. *Biophysical Journal*, 83:2270–2279, 2002.

C. Zhu. Kinetics and mechanics of cell adhesion. *Journal of Biomechanics*, 33:23–33, 2000.

D. Zuckerman and R. Bruinsma. Statistical mechanics of membrane adhesion by reversible bonds. *Physical Review Letters*, 74:3900–3903, 1995.

R. Zwanzig. Simple model of protein folding. *Proceedings of the National Academy of Science of the U.S.A.*, 94:9801–9804, 1995.

Acknowledgments

Zum Schluss möchte ich noch all jenen meinen herzlichen Dank aussprechen, die in irgendeiner Form zu dieser Arbeit beigetragen haben.

Zuerst gilt mein Dank Prof. Lipowsky an dessen Institut ich diese Arbeit angefertigt habe und dabei die angenehmen Arbeitsbedingungen und das reichhaltige Angebot an Seminaren und Vorlesungen genossen habe.

Zuallerzweit danke ich besonders Ulrich Schwarz für die Gelegenheit dieses Thema zu bearbeiten, für die intensive Betreuung während dieser Arbeit und schließlich auch dafür, dass er mir nun die Gelegenheit geboten hat, Heidelberg kennenzulernen.

Zudem sollen jene erwähnt werden, die aufopferungsvoll Teile dieser Arbeit gelesen habe und durch ihre Kommentare wesentliches zur Verbesserung des Textes beigetragen haben, insbesondere Ilka Bischofs, Stefan Klumpp und Christian Korn.

Zuguterletzt danke ich all den Kollegen am Max-Planck-Institut für Kolloid- und Grenzflächenforschung, die dafür gesorgt haben, dass mit die Zeit in Golm in angenehmster Erinnerung bleiben wird. Insbesondere danke ich Ilka Bischofs, Stefan Klumpp, Gunnar Linke und Jan Kierfeld. Auch bedanken möchte ich mich bei Thomas Baumann und den Rest der IT-Gruppe für die zuverlässige Arbeit der Rechner.

Zuallerletzt sei auch meinen Eltern gedankt.